



The Structure and Function of Asphaltenes: An Organic Geochemical and Ultrasound Study

A thesis submitted to the Newcastle University in partial fulfilment of the requirements
for the award of the degree of Doctor of Philosophy in the Faculty of Science,
Agriculture and Engineering

by

Ishicheli Reuben Agbidi

School of Civil Engineering and Geosciences, Newcastle University,
Newcastle upon Tyne, UK

December 2015

DECLARATION

I hereby certify that this work is my own original research, except where contributions of others are involved, every effort is made to indicate this clearly, with due reference to the literature and acknowledgement. No part of this work has been submitted previously for a degree or other qualification in this, or any other University.

Ishicheli Reuben AGBIDI

ABSTRACT

A multidisciplinary approach is used in order to gain a deeper understanding of petroleum geochemistry and specifically the aggregation properties of the asphaltenes. Such knowledge is essential to solving problems caused by asphaltene deposition in both the downstream and upstream sectors of the oil industry.

In this thesis a thorough organic geochemical characterisation of a set of asphaltenes originating from a variety of non-degraded to biodegraded crude oils from locations distributed around the world including Nigeria, United Kingdom, Middle East, North America and Serbia have been performed. Several geochemical techniques including Iatroscan analysis and thin layer chromatography were used to describe the crude oils. Fourier transform infrared (FTIR), ultrasonic spectrometry and ruthenium ion catalysed oxidation (RICO) analysis in combination with gas chromatography-mass spectrometry (GC-MS) were used for the molecular characterisation of the asphaltenes.

The crude oils have been characterised to elucidate their level of degradation, source, depositional environment and thermal maturity by a variety of biomarker and non-biomarker parameters. The results reveal differences in the extent of biodegradation within the samples, ranging from level (1) to (6) using the Peters and Moldowan biodegradation scale (Peters *et al.*, 2005a). The samples are sourced from either terrigenous organic matter deposited under oxic-suboxic conditions, marine organic matter deposited under anoxic conditions or a mixed contribution of terrestrial and marine sources.

The processes to determine asphaltene concentrations in the oils were tested using Iatroscan and subsequently compared to gravimetric analysis. Results from both techniques show variations in asphaltene content in the whole oil.

Following RICO analysis, acids are generated and released covalently bound hopanoic acids that reveal the existence of carbon number shift in the hopanes. The chemically bound biomarkers are consistent with low maturity distributions amongst all oils.

Analysis of the FTIR spectra from the asphaltenes show that crude oil asphaltenes consist of aliphatic moieties bound to aromatic structures. Although, aliphatic moieties

are dominant, carboxyl groups and other oxygenated functionalities are significant components present. Carboxyl groups were detected in most of the asphaltenes analysed in this work from around the world, but were not detected in heavily biodegraded samples.

High-precision ultrasound resonance spectroscopy was used to elucidate the mechanism of asphaltene aggregation in toluene solution. A new method namely the attenuation of sound for detecting asphaltene aggregation was developed. This work has identified that asphaltenes exhibit a critical nanoaggregate concentration (CNAC) in toluene at approximately ~0.03 – 0.16 g/L, depending upon the nature and source of the asphaltene. The CNAC of asphaltenes from the non-biodegraded oils is ~0.03 – 0.10 g/L and from a biodegraded oil is ~0.16 g/L. The results confirm previous aggregation measurements in that asphaltenes can self-associate in solution to give rise to, more or less, extended aggregates. In general, CNAC is controlled by the effect of biodegradation and attenuation data has considerable potential to corroborate previous finds regarding CNAC.

ACKNOWLEDGEMENTS

I would like to foremost thank my supervisors Dr Geoffrey Abbott and Nick Parker not only for the supervisory role but for their continuous support, timely encouragement and excellent guidance over the last 4 years in my graduate studies at the Newcastle University. Their supervision of this research was quite comprehensive without which it would have been tough to successfully complete. I highly appreciated their patience and trust during my research program.

I will forever be indebted to Delta State Scholarship Board for the financial support as a postgraduate scholarship to do doctorate in the United Kingdom.

I am thankful to all members of school of civil engineering and geosciences, namely, Prof. Tom Wagner, David Manning, Dr. Martin Jones, Helen Talbot, Carolyn Aitken and Angela Sherry, for their co-operation and useful discussions. My special thanks and gratitude go to Bernie Bowler, Paul Donohue, Phil Green, Graham Patterson, Yvonne Hall and Margaret Wardley for the special help I received at one time or the other. I am also thankful to all members of Biogeochemistry Research group during my graduate studies for their co-operation and useful discussions.

I would like to thank Prof. M. J. Povey from School of Food Science and Nutrition at the University of Leeds for providing his Laboratory for the ultrasound study. I also acknowledge Dr. Nicholas Watson and M J Holmes for their technical support and advice at Leeds University. My colleagues, Onoriode Esegbue, Jasmin Black, Ida Shafiee Ismail, Victoria Oriuwa, Tom Charlton, Timi Oriaku, Mohammed Alaween, Eminue Oboho, Kauthar Al-Hadhrami, Davison Davis, Osarobo Ighodaro and Sani Makarfi are highly appreciated for all their contributions in one way or the other. I must also acknowledge the Department of Petroleum Resources of Nigeria for permission to release crude oil samples and the managements of the operating company (Chevron) for crude oil provision for this study. Thanks also to Dr. Ksenija Stojanović (University of Belgrade) and Dr. Jamie Burgess (Shell) for donation of some the crude oils for this study.

Finally, my deepest gratitude goes to my parents Peter and Martina Agbidi for their invaluable sacrifice and encouragement, all family members, including Azuka Agbidi, Gabriel Njokede, Daddi Amudo, Gladys Opone, Lizzy Agbidi, Jones Okonye, Izu Osakwe, Thelma Okonye, Chika Agbidi, Ifeoma Agbidi, Uche Erhunmwunse, Chioma Adams, Olise Agbidi, Cleopatra Agbidi, Bright Omenogor, Joy Omenogor, Ambrose Isibor, Bestman Edema and Mudia Ojo-Igbinoba for their tireless effort and continuous support in my entire life.

I also like to express my heartfelt thanks to my lovely wife, Gladys and my Kids, Eliora, Christa and Newton for their tremendous understanding and patience. Sorry I couldn't be there all the times, but you were always treasured to my heart.

DEDICATION

This research project is dedicated to Azuka Agbidi for all the support he has offered toward the successful completion of this study.

TABLE OF CONTENTS

Abstract.....	iii
Acknowledgements.....	v
Dedication.....	vii
Table of contents.....	viii
List of tables.....	xv
List of figures.....	xviii
List of symbols.....	xxvi
List of appendices.....	xxix
Chapter 1 Introduction.....	1
1.1 Introduction	1
1.2 Aim and objectives	2
1.3 Thesis structure.....	2
Chapter 2 Literature Review.....	5
2.1 Introduction	5
2.2 Petroleum characterisation	5
2.2.1 Saturated hydrocarbons.....	7
2.2.2 Aromatic hydrocarbons.....	8
2.2.3 Resins	9
2.2.4 Asphaltenes	10
2.3 Characterisation of asphaltenes	10

2.3.1	Elemental composition of asphaltenes	11
2.3.2	Asphaltene structure.....	11
2.3.3	Asphaltene molecular weights	12
2.4	Biomarkers	13
2.4.1	Asphaltene bound-biomarkers	17
2.5	Biodegradation scales.....	20
2.6	Asphaltenes and aggregation.....	22
2.6.1	Aggregation.....	22
2.6.2	Asphaltene precipitation and flocculation.....	24
2.7	Relevance	25
2.8	Scope and Delimitation	26
Chapter 3	Experimental Methods	27
3.1	Introduction	27
3.2	Description of samples	27
3.2.1	Nigerian oils	28
3.2.2	United Kingdom oils	30
3.2.3	Middle East oils	33
3.2.4	North American oils	33
3.2.5	Serbian oils.....	34
3.2.6	Coal samples	35
3.3	Methods and sample preparation.....	35

3.3.1	Iatroscan thin-layer chromatography (TLC-FID)	36
3.3.2	Precipitation and purification of asphaltenes	38
3.3.2.1	Asphaltene Recovery	38
3.3.2.2	Cleaning the Asphaltenes.....	38
3.3.3	Fractionation of oils	39
3.3.4	Fractionation of maltenes.....	40
3.3.5	Ruthenium ion catalysed oxidation (RICO) of asphaltenes	40
3.3.5.1	Esterification of acids.....	41
3.3.6	Preparation of samples for Fourier transform infrared spectroscopy (FTIR)	
	41	
3.3.7	Preparation of samples for ultrasonic spectroscopy.....	41
3.4	Analytical techniques	42
3.4.1	Gas chromatography (GC)	42
3.4.2	Gas chromatography-mass spectrometry (GC-MS).....	42
3.4.3	Fourier transform infrared spectroscopy (FTIR).....	43
3.4.4	Ultrasonic spectroscopy of asphaltenes in organic solvent.....	44
Chapter 4	Oil and coal characterisation using conventional molecular parameters ..	46
4.1	Introduction	46
4.2	Methods	46
4.3	Results and discussion.....	47
4.3.1	Molecular characteristics of oils	47
4.3.1.1	Normal alkanes and acyclic isoprenoids	47
4.3.1.2	Steranes	51

4.3.1.3	Tricyclic and tetracyclic terpanes.....	56
4.3.1.4	Aromatic hydrocarbons	58
4.3.1.5	Source facies and thermal maturity.....	63
4.3.1.6	Biodegradation level based on Peters and Moldowan classification scale	65
4.3.2	Molecular characterisation of North Sea Coals	67
4.3.2.1	Normal Alkanes and acyclic isoprenoids.....	67
4.3.2.2	Steranes	69
4.3.2.3	Tricyclic and tetracyclic terpanes.....	72
4.3.2.4	Aromatic hydrocarbons	74
4.3.2.5	Source facies and thermal maturity.....	76
4.3.3	Comparative biomarker analysis in the studied oils and coals.	76
4.4	Summary and conclusions.....	86
Chapter 5	Determination of asphaltene content in crude oil	87
5.1	Introduction	87
5.2	Methods	88
5.3	Data interpretation	88
5.4	Results and discussion.....	91
5.4.1	Iatroskan measurement of asphaltenes	91
5.4.1.1	Nigerian oil	91
5.4.1.2	United Kingdom oils.....	92
5.4.1.3	Middle East oils	93
5.4.1.4	North American oils	94
5.4.1.5	Serbian oils.....	95
5.4.2	Calibration measurement of asphaltenes.....	96
5.4.2.1	Nigeria oils.....	96
5.4.2.2	United Kingdom oils	97
5.4.2.3	Middle East oils	98

5.4.2.4	North American oils	99
5.4.2.5	Serbian oils.....	100
5.5	Summary and conclusions.....	101
Chapter 6 Structural characterisation of asphaltenes by FTIR		102
6.1	Introduction	102
6.2	Methods	103
6.2.1	Sample preparation.....	103
6.2.2	Analytical procedure	104
6.2.3	Infrared analysis	105
6.3	Results and discussion.....	107
6.3.1	Spectral analysis of asphaltene.....	107
6.3.2	Functional characteristics of asphaltenes	108
6.3.2.1	Nigerian oils	108
6.3.2.2	United Kingdom oils	109
6.3.2.3	Middle East oils	110
6.3.2.4	North American oils	110
6.3.2.5	Serbian oils.....	111
6.3.3	Structural characteristics of asphaltenes	112
6.3.3.1	Nigerian oils	112
6.3.3.2	United Kingdom oils	113
6.3.3.3	Middle East oils	113
6.3.3.4	North American oils	114
6.3.3.5	Serbian oils.....	114
6.3.4	Chemometric analysis of spectroscopic data	116
6.4	Summary and conclusions.....	120

Chapter 7 Characterisation of bound biomarkers of asphaltenes released by ruthenium ion catalysed oxidation (RICO)	121
7.1 Introduction	121
7.2 Methods	122
7.2.1 Sample preparation.....	122
7.2.2 Identification and quantification of acids.....	123
7.2.3 Chemometric multivariate analysis.....	124
7.3 Results and discussion.....	126
7.3.1 <i>n</i> -alkanoic acids.....	126
7.3.1.1 Mass spectral characteristics of n-alkanoic compounds	126
7.3.1.2 Distribution of n-alkanoic compounds.....	127
7.3.2 α - ω - <i>di-n</i> alkanoic acids	128
7.3.3 α -branched alkanoic acids	129
7.3.4 Cyclic acids	129
7.3.4.1 Hopanoic acids	129
7.3.4.2 Steranoic acid acids.....	133
7.3.5 Effect of thermal maturation on asphaltene biomarkers	135
7.3.6 Effect of biodegradation on asphaltene biomarkers.....	137
7.3.7 Effect of source parameters on asphaltene biomarker	137
7.3.8 Comparative biomarker analysis of the studied maltene and bound asphaltenes.	139
7.4 Summary and conclusions.....	144

Chapter 8	The ultrasonic characterisation of asphaltene nanoaggregation in petroleum	145
8.1	Introduction	145
8.2	Theory	147
8.2.1	Sound and ultrasonic sound wave	147
8.2.2	Speed of sound in homogenous liquid	148
8.2.3	Speed of sound in asphaltene solution	149
8.2.4	Attenuation of sound in asphaltene solution	152
8.3	Methods	153
8.3.1	Fitting to two straight lines and the mean CNAC	153
8.3.2	Error analysis	154
8.4	Results and discussion.....	156
8.4.1	The effects of asphaltene concentration on ultrasonic velocity of sound	156
8.4.2	The effects of asphaltene concentration on attenuation of sound	158
8.4.3	Comparative analysis of ultrasonic velocity and attenuation of sound to petroleum asphaltenes of different compositions.....	160
8.5	Summary and conclusions.....	163
Chapter 9	Conclusions and Future Work.....	164
9.1	General conclusions	164
9.2	Future work	166

LIST OF TABLES

Chapter 2

Table 2.1: Elemental composition of asphaltenes from various petroleum asphaltenes and coals.

Chapter 4

Table 4.1: Normal alkane and isoprenoid alkane distributions of the studied crude oil samples.

Table 4.2: Sterane and hopane peak assignment.

Table 4.3: Source and maturity parameters computed from steranes in the studied oils.

Table 4.4: Biomarker ratios based on terpanes (m/z 191) in the studied crude oils.

Table 4.5: Peak identification of biomarkers in aromatic hydrocarbons.

Table 4.6: Selected molecular parameter for thermal maturity and source indicators from aromatic hydrocarbon fractions in the oils.

Table 4.7: Summary of maturity and source facies biomarkers in the studied oils.

Table 4.8: Biodegradation level of the studied oils based on the presence and absence of molecular parameters.

Table 4.9: Normal alkane and isoprenoid alkane distributions of the studied coals.

Table 4.10: Source and maturity parameters computed from steranes in the studied coals

Table 4.11: Biomarker ratios based on terpanes (m/z 191) in the studied coals

Table 4.13: Selected molecular parameter for thermal maturity and source indicators from aromatic hydrocarbon fractions in the coals.

Table 4.13: Summary of maturity and source facies biomarkers in the studied coals.

Table 4.14: Molecular parameters in the PCA of the oils and coal extracts.

Table 4.15: Loading weightings and molecular parameters used within the oil and coal extract samples in terms of principal component analyses.

Table 4.16: Score weightings of studied samples in terms of PC1 – PC4.

Chapter 5

Table 5.1: Variation in gross composition (wt. %) for Nigerian crude oils calculated from Iatroscan analysis.

Table 5.2: Variation in gross composition (wt. %) for United Kingdom crude oils calculated from Iatroscan analysis.

Table 5.3: Variation in gross composition (wt. %) for Middle East crude oils calculated from Iatroscan analysis.

Table 5.4: Variation in gross composition (wt. %) for North American crude oils calculated from Iatroscan analysis.

Table 5.5: Variation in gross composition (wt. %) for Serbian crude oils calculated from Iatroscan analysis.

Table 5.6: Differences in the asphaltene values of the Nigerian crude oils in the gravimetric method versus Iatroscan method.

Table 5.7: Differences in the asphaltene values of the United Kingdom crude oils in the gravimetric method versus Iatroscan method.

Table 5.8: Differences in the asphaltene values of the United Kingdom crude oils in the gravimetric method versus Iatroscan method.

Table 5.9: Differences in the asphaltene values of the North American crude oils in the gravimetric method versus Iatroscan method.

Table 5.10: Differences in the asphaltene values of the Serbian crude oils in the gravimetric method versus Iatroscan method.

Chapter 6

Table 6.1: List of samples used for the FTIR study.

Table 6.2: General features of the infrared spectral bands from FTIR spectrum of asphaltenes.

Table 6.3: Band assignments from FTIR.

Table 6.4: Structural relationships derived from the analysis of the ATR-FTIR spectra.

Table 6.5: Ratios calculated from the ATR-FTIR spectra.

Table 6.6: Cluster analysis of observations for absorption spectra of quantitative ratios, standardised variables, squared Euclidean distance, linkage and amalgamated steps.

Table 6.7: Final partition of number of clusters.

Chapter 7

Table 7.1: List of the samples used in the RICO analysis of the asphaltenes.

Table 7.2: Structural assignments of steroid alkanoic and hopanoic acid biomarkers present in the asphaltene fraction.

Table 7.3: Parameters calculated on the basis of distribution and abundance of hopanoic, steranoic and *n*-alkanoic acids in the asphaltene fraction.

Table 7.4: Cluster Analysis of Observations for biomarkers from RICO analysis.

Table 7.5: Final partition of biomarkers from RICO analysis.

Chapter 8

Table 8.1: Experimentally determined CNAC with statistical uncertainties in velocity of sound for asphaltenes in toluene at 25 °C.

Table 8.2: Experimentally determined CNAC with statistical uncertainties in attenuation of sound for asphaltenes in toluene at 25 °C.

Table 8.3: Comparison of experimentally determined CNAC with statistical uncertainties in toluene using attenuation and velocity of sound for asphaltenes in toluene at 25 °C.

LIST OF FIGURES

Chapter 2

Figure 2.1: Separation of crude oil into four hydrocarbon group type.

Figure 2.2: Molecular structures of representative straight chain and acyclic isoprenoids compounds in crude oils.

Figure 2.3: Molecular structures of examples of five to six ring naphthalenes

Figure 2.4: Molecular structure of common aromatic hydrocarbons found in crude oil

Figure 2.5: Molecular structure of asphaltene from different origin.

Figure 2.6: Chemical structures of some acyclic isoprenoid and polycyclic classes built from isoprene subunits.

Figure 2.7: Configuration pathway for the formation of hopanes in source rocks and crude.

Figure 2.8: Configuration pathway for the formation of steranes in source rocks and crude oils.

Figure 2.9: Illustration of chemical degradation.

Figure 2.10: Biodegradation scale modified.

Figure 2.11: Yen-Mullins model of asphaltene.

Chapter 3

Figure 3.1: Geographical location of the study samples.

Figure 3.2: Location map of Niger Delta.

Figure 3.3: Niger Delta: stratigraphy and formation depobelts.

Figure 3.4: Location of Captain oil field.

Figure 3.5: Location of the Nelson oil field.

Figure 3.6: Location of the Flora oil field.

Figure 3.7: Area of study in Serbian part of the Pannonian Basin.

Figure 3.8: Research methodology flowchart.

Figure 3.9: High-precision ResoscanTM ultrasound spectrometer.

Chapter 4

Figure 4.1: Representative GC/FID chromatograms of saturated hydrocarbon fractions of selected non-degraded NE (O) and biodegraded NC (O) crude oils from Niger Delta.

Figure 4.2: Source rock anoxia inferred from the histogram of pristane/phytane ratios for the studied oils.

Figure 4.3: Relationship between Pr/ nC_{17} against Ph/ nC_{18} for the studied oils.

Figure 4.4: A cross plot of dibenzothiophene/phenanthrene ratio (DBT/PHEN) and the ratio of pristane to phytane for the studied oils.

Figure 4.5: Representative GC-MS mass chromatogram m/z 217 showing the distributions of C_{27} , C_{28} and C_{29} steranes from crude oil samples NC (O) and NE (O), Nigeria.

Figure 4.6: Ternary diagram showing the distribution of the C_{27} , C_{28} , and C_{29} -Steranes from GC-MS analyses of studied oils and coals interpreted in terms of likely depositional environment.

Figure 4.7: Ternary diagram showing the distribution of the C_{27} , C_{28} , and C_{29} -Steranes from GC-MS analyses of the studied oils interpreted in terms of likely source precursors.

Figure 4.8: Cross plot of C_{29} steranes I/R against C_{29} steranes S/R parameter defines oils into various zones of thermal maturity.

Figure 4.9: Representative partial m/z 191 mass chromatograms showing tricyclic and tetracyclic terpane distributions in NC (O) and NE (O) crude oils.

Figure 4.10: Correlation between Ts/Tm and 29Ts/29Tm ratios showing the maturity of the studied oils

Figure 4.11: Source rock anoxia inferred from extended hopanes (Hop (35/34) ratios of the studied oils.

Figure 4.12: GC-MS m/z 178 and 192 mass chromatograms showing the distributions of the phenanthrene and methylphenanthrenes in representative oil NC (O) from Nigeria.

Figure 4.13: GC-MS m/z 128 and 142 mass chromatograms showing the distributions of the naphthalene and methylnaphthalenes and also GC-MS m/z 156 and 170 mass chromatograms showing the distributions of dimethylnaphthalenes and trimethylnaphthalenes in the representative oil NC (O) from Nigeria.

Figure 4.14: Cross plots of maturity parameter computed from aromatic hydrocarbons of the oils.

Figure 4.15: Representative GC/FID chromatograms of saturated coal extracts of CA3 (C) and CA6 (C) from North Sea coals, United Kingdom.

Figure 4.16: Relationship between $\text{Pr}/n\text{C}_{17}$ against $\text{Ph}/n\text{C}_{18}$ for the North Sea coals from the United Kingdom.

Figure 4.17: Source rock anoxia inferred from the histogram of pristane/phytane ratios from the North Sea coals.

Figure 4.18: A cross plot of dibenzothiophene/phenanthrene ratio (DBT/PHEN) and the ratio of pristane to phytane from the North Sea coals.

Figure 4.19: Representative GC-MS mass chromatogram m/z 217 showing the distributions of C_{27} , C_{28} and C_{29} steranes from the coals, United Kingdom.

Figure 4.20: Ternary diagram showing the distribution of the C_{27} , C_{28} , and C_{29} -Steranes from GC-MS analyses of the studied coals interpreted in terms of likely source precursors.

Figure 4.21: Ternary diagram showing the distribution of the C_{27} , C_{28} , and C_{29} -Steranes from GC-MS analyses of studied coals interpreted in terms of likely depositional environment.

Figure 4.22: Cross plot of C_{29} steranes I/R against C_{29} steranes S/R parameter defines North Sea coals into various zones of thermal maturity.

Figure 4.23: Representative partial m/z 191 mass chromatograms showing tricyclic and tetracyclic terpane distributions in CA3 (C) and CA6 (C) coals.

Figure 4.24: Correlation between Ts/Tm and $29\text{Ts}/29\text{Tm}$ ratios showing the maturity of the studied coals.

Figure 4.25: Source rock anoxia inferred from extended hopanes ($\text{Hop} (35/34)$) ratios of the coals from United Kingdom (after IGI's p: 3.5 geochemical interpretation software).

Figure 4.26: GC-MS m/z 178 and 192 mass chromatograms showing the distributions of the phenanthrene and methylphenanthrenes in representative coal (CA3) from the North Sea, UK.

Figure 4.27: GC-MS m/z 128 and 142 mass chromatograms showing the distributions of the naphthalene and methylnaphthalenes and also GC-MS m/z 156 and 170 mass chromatograms showing the distributions of dimethylnaphthalenes and trimethylnaphthalenes in the representative oil CA3 (C) from the North Sea, UK.

Figure 4.28: Cross plots of maturity parameter computed from aromatic hydrocarbons of the coals.

Figure 4.29: A loadings plots showing the relationship between different biomarker parameters in terms of the principal component analysis of the oil and coal extract samples used in the study.

Figure 4.30: Principal component analysis (PC1 to PC2) results showing classification of the oils and coal extracts based on the score weightings of molecular parameters

Figure 4.31: Principal component analysis (PC2 to PC3) results showing classification of the oils and coal extracts based on the score weightings of molecular parameters.

Figure 4.32: Principal component analysis (PC3 to PC4) results showing classification of the oils and coal extracts based on the score weightings of molecular parameters.

Chapter 5

Figure 5.1: Percentage distribution of SARA fractions from the Nigerian oils with values.

Figure 5.2: Percentage distribution of SARA fractions for the United Kingdom crude oils.

Figure 5.3: Percentage distribution of SARA fractions from the Middle East oils with values.

Figure 5.4: Percentage distribution of SARA fractions from the North American oils with values.

Figure 5.5: Percentage distribution of SARA fractions from the Serbian oils with values.

Figure 5.7: Correlation of asphaltene content (mg/g) recovered from Iatroscan versus gravimetric method from the Nigerian oils.

Figure 5.8: Weight of asphaltene content (mg/g) recovered from the United Kingdom oils.

Figure 5.9: Correlation of asphaltene content (mg/g) recovered from Iatroscan versus gravimetric method from the United Kingdom oils.

Figure 5.10: Weight of asphaltene content (mg/g) recovered from the Middle East oils.

Figure 5.11: Weight of asphaltene content (mg/g) recovered from the North American oils.

Figure 5.12: Correlation of asphaltene content (mg/g) recovered from Iatroscan versus gravimetric method from the North American oils.

Figure 5.13: Weight of asphaltene content (mg/g) recovered from the Serbian oils.

Chapter 6

Figure 6.2: FTIR spectra obtained with FTIR-KBr compared with ATR-FTIR of the infrared spectra bands of asphaltene (NA61) from North America.

Figure 6.2: Infrared spectra of representative asphaltene fractions from Nigerian crude oils.

Figure 6.3: Infrared spectra of representative asphaltene fractions from United Kingdom crude oils.

Figure 6.4: Infrared spectra of ME39(A) and ME43(A) asphaltene fractions from Middle East crude oils.

Figure 6.5: Infrared spectra of representative asphaltene fractions from the North American crude oils.

Figure 6.6: Infrared spectra of SN1(A) and SN2(A) asphaltene fractions from Serbian crude oils.

Figure 6.7: Loading plots showing the relationship between studied asphaltene samples in terms of PC1 (56.67% of total variables) versus PC2 (20.37% of total variables) analysis of multivariate data analysis.

Figure 6.8: Score plots showing the relationship between studied asphaltene samples in terms of PC1 (56.67% of total variables) versus PC2 (20.37% of total variables) analysis of multivariate data analysis.

Figure 6.9: Dendrogram showing cluster analysis of Structural relationships derived from the analysis of the FTIR spectra.

Chapter 7

Figure 7.1: The mass spectrum of methyl hexadecanoate used to identify the *n*-alkanoic acids from the RICO products of the methyl esters.

Figure 7.2: GC of *n*-alkanoic acids methyl esters from RICO products of representative asphaltenes of biodegraded and non-biodegraded Nigerian oils (top) with correspondent *n*-alkanes on maltenes (bottom).

Figure 7.3: GC-MS m/z 98 ion chromatograms of α - ω -di-*n* alkanoic acids of RICO products of representative asphaltenes from Nigeria.

Figure 7.4: GC-MS chromatograms of *n*-alkanoic acid for asphaltene ND (A) from Nigeria. The numbers above the peaks are the carbon numbers on the acid portion of the esters.

Figure 7.5: Partial mass chromatograms of the C₃₀ (m/z = 235), C₃₁ (m/z = 249) and C₃₂ (m/z = 263) hopanoic acids on asphaltene sample from NB(A), NC (A) biodegraded oils and ND(A) of non-biodegraded oil from Nigeria.

Figure 7.6 Bar charts showing a comparison of 22S/(22S + 22R) C₃₂ $\alpha\beta$ maturity parameter values for maltene-derived hopanes and the asphaltene-derived hopanoic acid RICO products from biodegraded oils.

Figure 7.7 Bar charts showing a comparison of 22S/(22S + 22R) C₃₂ $\alpha\beta$ maturity parameter values for maltene-derived hopanes and the asphaltene-derived hopanoic acid RICO products from non-biodegraded oils.

Figure 7.8: Partial mass chromatograms of the m/z = 275 and m/z = 289 of the steranoic and 4-methylsteranoic acids methyl esters of RICO products of asphaltenes from NB(A), NC(A) biodegraded oils and ND(A) of non-biodegraded Nigeria oils.

Figure 7.9: Bar charts showing comparison of 20S/(20S + 20R) values for asphaltene-derived steranoic acid RICO products and the maltene-derived steranes from biodegraded oils.

Figure 7.10: Bar charts showing comparison of 20S/(20S + 20R) values for asphaltene-derived steranoic acid RICO products and the maltene-derived steranes from non-biodegraded oils.

Figure 7.11: Distributions in steranoic acids from asphaltene-derived acid RICO product of C₂₉ vs. C₃₀ 20S (20S/20S + 20R) maturity parameters

Figure 7.12: Distributions in steranoic acids from asphaltene-derived acids RICO product of C₂₉ vs. C₃₀ ($\alpha\beta\beta/\alpha\beta\beta + \alpha\alpha\alpha$) maturity parameters.

Figure 7.13: Ternary diagram of C₂₈ – C₃₀ $\alpha\alpha\alpha$ (R) of steranoic acid distributions from asphaltene fractions of asphaltene (a) corresponding to maltene (c), suggesting facies source of the oils.

Figure 7.14: Ternary diagram of C₂₈ – C₃₀ $\alpha\alpha\alpha$ (R) of steranoic acid distributions from asphaltene fractions of asphaltene (b) corresponding to maltene (d), suggesting of likely facies source.

Figure 7.15: A loadings plot showing the relationship between different biomarker parameters in terms of PC1 versus PC2 analysis of multivariate RICO data analysis.

Figure 7.16: A scores plot showing the relationship between studied oil and coal samples in terms of PC1 versus PC2 from a principal component analysis of biomarkers from RICO analysis.

Figure 7.17: Dendrogram showing clusters formed from cluster analysis using PC1 to PC5 from RICO treatment of asphaltene.

Chapter 8

Figure 8.1: Schematic diagram of longitudinal ultrasonic waves.

Figure 8.2: Schematic diagram of attenuation of sound.

Figure 8.3: Schematic illustration of the fitting of the data to two straight lines.

Figure 8.4: Measured velocity of sound versus concentration of asphaltene (NA61) in toluene at 25 °C.

Figure 8.5: Measured velocity of sound versus concentration of asphaltene (SN1) in toluene at 25 °C.

Figure 8.6: Measured velocity of sound versus concentration of asphaltene (SN1) in toluene at 25 °C.

Figure 8.7: Statistical uncertainties of CNAC's of studied asphaltenes in toluene at 25 °C calculated from ultrasonic velocity of sound.

Figure 8.8: Measured attenuation of sound versus concentration of asphaltene (NA61) in toluene at 25 °C.

Figure 8.9: Measured attenuation of sound versus concentration of asphaltene (SN1) in toluene at 25 °C.

Figure 8.10: Measured attenuation of sound versus concentration of asphaltene (SN2) in toluene at 25 °C.

Figure 8.11: Statistical uncertainties of CNAC's of studied asphaltenes in toluene at 25 °C calculated from attenuation of sound.

LIST OF SYMBOLS

IS = Internal standard

UCM = unresolved complex mixture

w_t = weight of oil used for Iatroskan

w = total weight of oil sample (mg)

v = volume of oil sample used for Iatroskan (μl)

V= total volume of oil (μl)

R_c = response component

R_f = response factor

w_w = weight of oil used

Pa = Peak area of the four components in oil sample generated from Iatroskan

Rc_(sat)= Components of saturates

Rc_(aro)= Components of aromatics

Rc_(resin)= Components of resins

Rc_(asp)= Components of asphaltenes

Pa_(Sat) = Peak areas of saturate

Pa_(Aro) = Peak areas of aromatics

Pa_(Resin) = Peak areas of resins

Pa_(Asp) = Peak areas of asphaltenes

Comp_(sat) = Percentage composition of saturates

Comp_(aro) = Percentage composition of aromatics

Comp_(Resin) = Percentage composition of resins

Comp_(Asp) = Percentage composition of asphaltenes

C_x = Calculated amount of ester yield

P_x = Peak area of the ester

P_s = Peak area of the internal standard

W_{Ta} = Weight of the asphaltene

W_{Ti} = Weight of the internal standard

C_n = Amount per 1000C

%C = Percentage weight of carbon in a given asphaltene

M_c = Molar mass of the analyte

u is the speed of sound

κ is the wavenumber

ω is the angular frequency of the wave

p_0 is the initial wave amplitude

α is the attenuation coefficient

k is the compressibility

V is the total volume of the solution

p is the pressure

k_s is the adiabatic compressibility of the solution

k_1 is the apparent adiabatic compressibility of the asphaltene monomer

k_{NA} is the apparent adiabatic compressibility of the asphaltene nanoaggregate

k_0 is the adiabatic compressibility of the solution

ρ_0 is the density of the solvent

ρ is the density of the asphaltene solution

c is the mass concentration of the asphaltene

c_1 is the mass concentration of the asphaltene in the monomeric form

c_{NA} is the mass concentration of the asphaltene in the nanoaggregate form

c_{NAC} is the numerical value of the CNAC

w_0 is the mass of the solvent

v_0 is the specific volume of the solvent

v_I is the apparent specific volume of asphaltene monomer

v_{NA} is the apparent specific volume of the asphaltene nanoaggregate

LIST OF APPENDICES

Appendix 1.0: Study samples and locations.

Appendix 2.0: Monitored ions (m/z) in selected ion and full scan modes.

Appendix 3.0: Selected biomarker data for principal components analysis for the oils and coals.

Appendix 4.0: Comparison of weight of asphaltene content (mg/g) recovered from Iatroscan and gravimetric.

Appendix 5.0: Calculated contents in mg/g of the asphaltene fraction recovered from gravimetric procedure of the oils as mean \pm one standard error.

Chapter 1 Introduction

1.1 Introduction

As the world population grows, considerable effort is being spent developing unconventional sources of liquid and gaseous hydrocarbons. Amongst these are heavy oils, bituminous sands, oil shales and coals. Notable is the fact that these heavier feedstocks are rich in asphaltenes, which are precipitated from petroleum fluids and extracts by natural processes or in the laboratory by addition of excess nonpolar aliphatic hydrocarbon solvent e.g. *n*-pentane, *n*-hexane, or *n*-heptane (Speight, 1984). However, significant changes in pressure, temperature and composition of the crude oil properties as well as of the thermodynamic conditions at production, transport and processing of crude oils can also induce asphaltene precipitation (Wilhelms and Larter, 1994; Buckley *et al.*, 1998; Sheu, 2002; Hammami and Ratulowski, 2007). In such cases, the remaining fraction is called maltenes consisting of saturated hydrocarbons, aromatic hydrocarbons and resins. Characterisation of asphaltenes has become increasingly important as several economic problems including formation damage, flow line blockages and catalyst fouling have been linked to asphaltene precipitation, flocculation and deposition in the oil industry (Gawrys and Kilpatrick, 2005; Mullins, 2010). Asphaltenes have also been found to be responsible for the facilitation of the formation of extremely stable water in-crude oil emulsions, which increase production problems (McLean and Kilpatrick, 1997b).

Asphaltene molecular weight is a subject of debate (Speight and Moschopedis, 1981; Yen *et al.*, 1984; Badre *et al.*, 2006; Herod, 2010). The molecular weight debate is whether asphaltenes are monomeric (one fused-ring system per molecule) or polymeric. Badre *et al.* (2006), for example, observed that asphaltenes are monomeric, while Strausz *et al.* (1992a), proposed a crossed linked network of aromatic ring system (polymeric). Although, several workers have investigated the structural features of asphaltenes and agree that they consist of aromatic rings and appendages composed of aliphatic rings which are not easily biodegraded and have been used in oil-oil and oil-source correlation especially for biodegraded oils (Behar *et al.*, 1984; Strausz *et al.*, 1992b; Xiong and Geng, 2000). Despite the rapidly growing literature on the properties and the behaviour of petroleum asphaltenes, there is still controversy on their

aggregation properties. However, a deeper understanding of the chemical composition of asphaltenes may help us gain a better understanding of their nanoaggregation properties, sources of precursor materials, environmental conditions of deposition, biodegradation and maturation processes.

1.2 Aim and objectives

This study is aimed at the molecular characterisation of asphaltenes in both non-degraded and degraded crude oils from various oilfields around the world and to ascertain how aggregation properties correlate with the molecular characteristics.

The following objectives were undertaken to achieve the above aims:

- a. To ascertain which oils are biodegraded or non-degraded and then assess the extent of biodegradation in oils using Peters and Moldowan scale (Peters and Moldowan, 2005).
- b. To assess biomarker distribution ratios of whole oils, maltenes and asphaltenes in terms of source facies input, maturation and depositional environment.
- c. To measure the content of asphaltenes using the Iatroscan method.
- d. To assess the structural composition of asphaltenes of crude oils using mid-infrared attenuated total reflectance spectra (FTIR-ATR).
- e. To assess the relationship of hopane and sterane distributions in maltenes with those of corresponding hopanoic and steranoic acids released during ruthenium-ion-catalysed oxidation (RICO) treatment of respective asphaltenes of petroleum from the biodegraded and non-degraded crude oils.
- f. To measure the changes in the properties of the velocity and attenuation of sound at different concentrations of asphaltene precipitates using a high-precision ultrasound resonance spectrometer, so as to gain more insights on asphaltene aggregation and build on an earlier high quality factor (high-Q) ultrasonics study that was used to demonstrate asphaltene nanoaggregation by Andreatta et al. (2005).

1.3 Thesis structure

This thesis consists of nine chapters in the following order:

The first chapter provides a general introduction of the study. Here crude oil and the economic significance of asphaltenes are briefly introduced. The aims of the study and how to achieve these, as well as the need for the study are also presented. Following the brief introduction, a comprehensive literature review of previous work related to this thesis is presented in Chapter 2; petroleum characterisation, characterisation of asphaltenes, biomarkers, biodegradation scale, asphaltene aggregation, research problems, the relevance of research, scope and delimitation of the research.

Chapter 3 describes experimental equipment, analytical methods, materials and procedures used in the present study. The issues of replicability and reproducibility are also discussed.

Chapter 4 focuses on the biological marker (biomarkers) and non-biomarkers compounds of the crude oils and coals, so as to ascertain the probable sources, depositional environments, and the degree of alteration of the study samples.

Chapter 5 focuses on the results obtained in measuring the amount of asphaltene content and the corresponding asphaltene precipitates from the oil samples. The results from Iatroscan runs are also presented and compared with gravimetric results.

Chapter 6 describes the characterisation of different asphaltenes from various regions of the world in terms of their molecular structure and relates the changes to develop a classification system using asphaltene FTIR spectra.

Chapter 7 provides a comparison study of corresponding biomarkers of the maltene fractions from conventional geochemical data and bound biomarkers of asphaltenes released by ruthenium ion catalysed oxidation.

Chapter 8 provides the characterisation of asphaltene nanoaggregate as a function of concentration in toluene solution and proposed a concentration range at which nanoaggregate particles are formed depending on varying geochemical properties; source and biodegradation level.

Finally, Chapter 9 provides the general conclusions and major contributions of this research study and attempts to relate the molecular chemistry of degraded and non-

degraded Serbian oils of same source with that of their ultrasound data and also compare the molecular chemistry of non-degraded North American oil with the non-degraded Serbian oil.

Chapter 2 Literature Review

2.1 Introduction

This chapter is aimed at providing a detailed overview of some significant work on petroleum fluids composition and properties: with significant interest on the molecular nature of the asphaltene fraction (e.g. asphaltene composition, chemical structure, molecular weight etc.), biomarkers, and biodegradation. The properties of asphaltenes in crude oils are also comprehensively reviewed.

2.2 Petroleum characterisation

Petroleum is a naturally occurring complex mixture, consisting of several thousands of hydrocarbon and non-hydrocarbon compounds which are derived from the thermal decay of buried organic matter over geological time (Hunt, 1996). The source of petroleum is a geopolymmer termed kerogen (Tissot and Welte, 1984; Killops and Killops, 1994; Hunt, 1996). Kerogen is operationally defined as the organic constituent of sedimentary rocks that is insoluble in both aqueous alkaline and common organic solvents (Tissot and Welte, 1984). There are three principal stages (diagenesis, catagenesis and metagenesis) during the evolution of organic matter (Tissot and Welte, 1984; Hunt, 1996). Catagenesis corresponds to the principal stage of oil and gas formation. During this stage, kerogen is heated from about 50 – 150 °C resulting in the generation of liquid and gaseous hydrocarbons (Tissot and Welte, 1984).

The major elemental constituents of kerogen are hydrogen and carbon with minor amounts of sulphur, nitrogen and oxygen (Welte, 1972; Dow, 1977; Tissot and Welte, 1984). As kerogen thermally matures, hydrogen-rich kerogen generates predominantly oil whilst hydrogen-poor kerogen generates predominantly gas (Hunt, 1996). Three major types of kerogen namely Types I, II and III have been identified (Tissot and Welte, 1984). Type I kerogen is mainly derived from lacustrine algae and deposited in reducing environments. H/C ratios are generally high and therefore have an elevated potential for oil and gas generation. Type II kerogen contains organic carbon derived from various sources including phytoplankton, zooplankton, higher plants and bacteria. This kerogen type has higher H/C and lower O/C ratios relatively to other types. Type

III kerogen is mainly derived from terrestrial higher plants and has a lower and a higher O/C ratio relatively to the other kerogen types.

Petroleum contains a broad range of molecular types from small, simple volatile compounds like methane to extremely large, complex non-volatile and colloidally dispersed macromolecules like asphaltenes. The hydrocarbon compounds, include molecules that comprise carbon and hydrogen atoms including acyclic alkanes (normal and isoalkanes), cycloalkanes (naphthenes), and aromatic hydrocarbons, while the non-hydrocarbons contain one or more heteroatoms such as nitrogen, sulphur, oxygen (NSO) as well as metallic constituents, particularly vanadium, nickel and iron, which have considerable influence on product quality of the crude oil (Boduszynski, 1988; Speight, 1991). Hydrocarbon content may be as much as 97% w/w (especially for a light oils) or as low as 50% w/w for heavy oils and bitumen (Speight, 1991). Furthermore, the major constituents of the naphthene series of hydrocarbons found in crude oils are defined by the number of rings (e.g. containing monocyclic, bicyclic, tricyclic rings). These constituents have great consequence on the quality of the oil, such that it determines the price of its products.

In general, crude oil can be classified on the basis of solubility and polarity of its compound fractions which can be easily distinguish from each other (Speight, 1991). The crude oils are separated into chemical class composition based on saturates (S), aromatics (A), resins (R), and the asphaltenes (A) i.e SARA contents as shown in Figure 2.2 (Speight, 1999; Jiang *et al.*, 2008). In this method, asphaltenes are initially precipitated from petroleum fluids and extracts by natural processes or in the laboratory by addition of excess non-polar aliphatic hydrocarbon solvent e.g. *n*-pentane, *n*-hexane, or *n*-heptane as shown in Figure 2.1. (Speight, 1984; Wilhelms and Larter, 1984; Speight, 1999). After the precipitation and isolation of the asphaltenes, the remaining soluble fraction in light *n*-alkanes, are maltenes consisting of saturated hydrocarbons, aromatic hydrocarbons and resins.

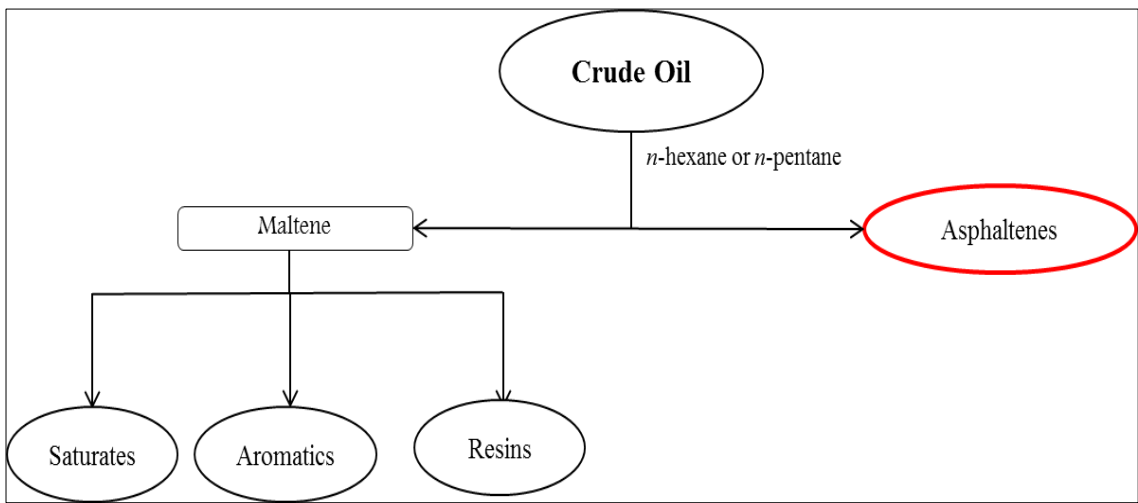


Figure 2.1: Separation of crude oil into four hydrocarbon group type.

The maltenes can be further fractionated into individual fractions by eluting the adsorbed sample on a chromatographic column using solvents with different polarities. However, both resins and asphaltenes are hetero compounds and form the most aromatic component of the crude oil (Groenzin and Mullins, 1999). SARA compositions have also been studied using Iatroskan TLC-FID (Karlsen and Larter, 1991; Lu *et al.*, 2008). However, the practicality and application of Iatroskan TLC-FID in the separation of extracts or crude oils is limited by calibration and standardisation of response factors.

2.2.1 Saturated hydrocarbons

Saturated hydrocarbons are often called aliphatic compounds composed entirely of straight chain alkanes and branched iso-alkanes with the general formula C_nH_{2n+2} (*where n* is an integer) and molecular structure as shown in Figure 2.2. Also included in this group are the acyclic alkanes (normal and branched) and cycloalkanes or naphthenes (Killops and Killops, 1994). The naphthenes have a general formula C_nH_{2n} (Selley, 1985). Like the straight chains they occur in a homologous series containing one or more rings, each of which may have one or more alkyl side chains attached to each of the rings e.g. cyclopentane (C_5H_{10}), cyclohexane (C_6H_{12}), cyclohexane (C_6H_{10}), and ethyl cyclohexane (C_8H_{16}) with a general molecular structure as shown in Figure 2.3. Among these naphthenes are also important biological markers called hopanes and steranes detected in crude oil (Stout *et al.*, 2007). In both light and heavy oils, naphthenes are liquid at normal temperature and pressure consisting of about 40% of

both oils (Selley, 1985). Saturated hydrocarbons have been the subject of numerous investigations, especially sterane and hopane compounds. These biomarkers have been successfully applied in geochemical characterisation of petroleum source rocks and crude oils (Philp and Gilbert, 1986; Peters and Moldowan, 1991).

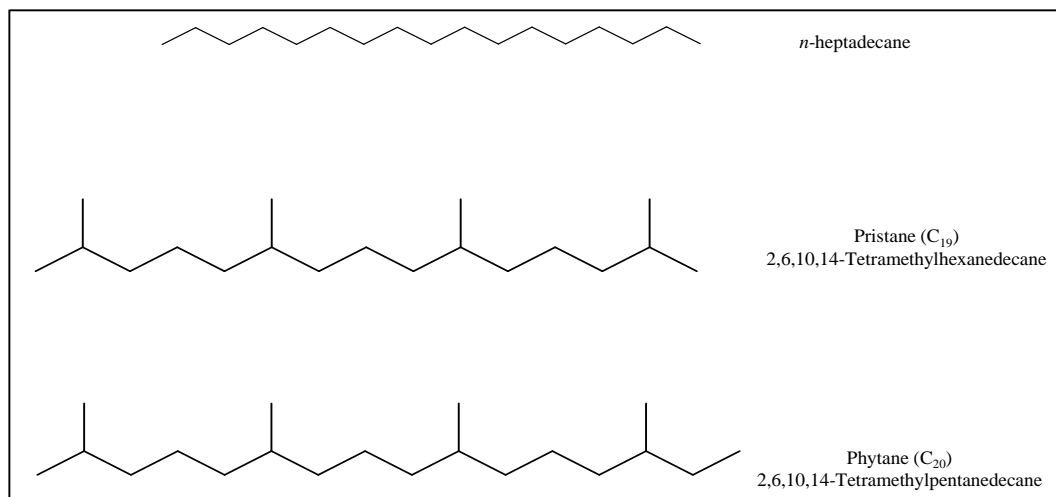


Figure 2.2: Molecular structures of representative straight chain and acyclic isoprenoids compounds in crude oils (Killops and Killops, 2005).

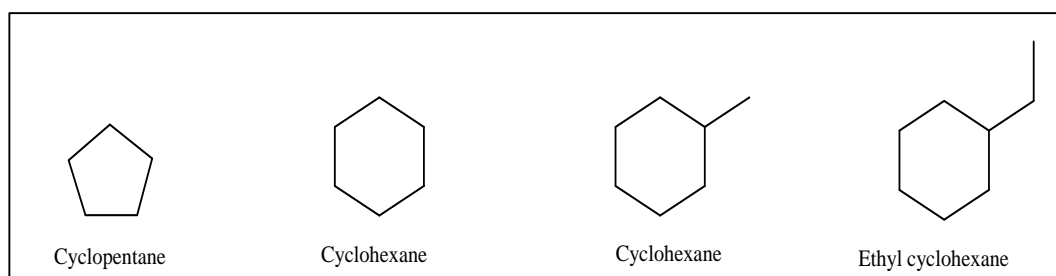


Figure 2.3: Molecular structures of examples of five to six ring naphthalenes redrawn from (Selley, 1985).

2.2.2 Aromatic hydrocarbons

Aromatic hydrocarbons are found in crude oils and most commonly compounds are benzene, benzene derivatives and fused benzene ring compounds (Selley, 1985). Their molecular structures generally consist of one or more benzene rings that contain alternating single and double bonds in its chemical structure such as benzene (C_6H_6) or naphthalene ($C_{10}H_8$) as shown in Figure 2.4.

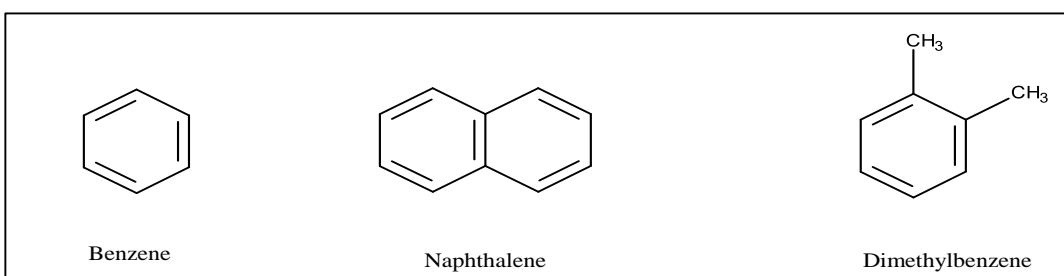


Figure 2.4: Molecular structure of common aromatic hydrocarbons found in crude oil redrawn from Speight (1991) and (Selley, 1985).

These hydrocarbons may be bonded to naphthenic rings and alkyl side chains. Aromatic hydrocarbons can be divided into monoaromatic, di- and tri-, aromatic hydrocarbons based on the number of aromatic rings and are known as polynuclear aromatic hydrocarbons (PAH) (Peters *et al.*, 2005a). Examples of monoaromatic including benzene, toluene, ethylbenzene and xylene (BTEX) while PAH's include naphthalene, phenanthrene, dibenzothiophene, anthracene and pyrene etc (Kanaly and Harayama, 2000). In crude oils and sediments, aromatics usually have other organic compounds of benzene derivatives that may contain other elements such as N, S, O and metals. Several studies applied aromatic hydrocarbons, especially the distributions and relative amounts of mono-, di- and PAH's from GC-MS, for assessing the maturity of organic matter in source rocks and crude oils (Mackenzie *et al.*, 1981; Welte *et al.*, 1982; Radke, 1988).

2.2.3 Resins

Resins are polar molecules in crude oils and solvent soluble sedimentary organic matter and contain heteroatoms such as nitrogen, oxygen or sulphur (Speight, 2004). The resin is defined operationally by the separation method (Speight, 1984; Andersen and Speight, 2001). Hence, different fractionation methods of crude oil will yield different quantity and resin composition (Andersen and Speight, 2001). Resins are composed of similar type of chemical structures as asphaltenes but with lower molecular weights (Murgich *et al.*, 2006). They co-precipitate and strongly absorb onto the asphaltenes during separation processes (Mullins and Sheu, 1998). The nature of resins in crude oils has been debated and there is a concept that resins play an important role in asphaltene flocculation in crude oils (Carnahan *et al.*, 1999; Mansoori *et al.*, 2007). Hence, the stability of asphaltenes increases linearly with the amount of resins (León *et al.*, 1999).

Despite the natural materials which stabilize asphaltenes in petroleum fluids, quite little is known due to limited research of resins.

2.2.4 Asphaltenes

The typical definition of asphaltenes is that they are the heaviest and most polar components present among the hydrocarbon fractions in bituminous sands, oil shales, heavy oils and coal. Asphaltenes can also be defined as a solubility class, insoluble in light alkanes such as *n*-hexane, *n*-pentane, or *n*-heptane (Speight, 1984; Pelet *et al.*, 1986). They are soluble in aromatic solvents such as toluene, and the nature and amount of an asphaltene fraction is strongly dependent on the source and method of separation (Speight and Moschopedis, 1981; Speight, 2004). However, different solvents and methods can yield different compositions and amounts of asphaltene. One long debate in the asphaltene study has been their tendency to self-associate to form molecular nanoaggregates over a broad range of sizes (Speight and Moschopedis, 1981; Yen *et al.*, 1984). Asphaltene particles are believed to exist in the form of nanoaggregates in crude oils and organic solvents such as toluene. However, small size asphaltenes may dissolve in a petroleum crude or relatively large asphaltenes may flocculate out of the solution, due to excess *n*-alkane content of the oil, forming random flocs (large molecular assemblage) as shown in Figure. 2.11. Asphaltenes have been widely used for different studies, including (i) pyrolysis and (ii) ruthenium ion catalysed oxidation studies where asphaltenes are chemically degraded to small fragments with distributions that could be used to differentiate the oils (Behar *et al.*, 1984; Ekweozor, 1984; Muhammad and Abbott, 2012). Such studies have been widely used, especially in oil-oil and oil-source rock correlation studies of severely altered biodegraded oils, or bitumen (Peng *et al.*, 1999b; Ma *et al.*, 2008).

2.3 Characterisation of asphaltenes

Over the past several years, there has been progress in the molecular characterisation of asphaltenes, focusing on revealing the true composition of asphaltene, chemical structure, and molecular weight. Several studies using different techniques have been extensively applied to unveil these characteristics.

2.3.1 Elemental composition of asphaltenes

Asphaltene elemental compositions have been found to be narrowly variable corresponding to H/C ratio of $1.15 \pm 0.05\%$. However, values outside this range are often found depending in the proportions of the heteroelements, such as proportion of oxygen and sulphur (Speight, 1999). Many studies have investigated the elemental composition toward understanding asphaltenes deposition problems (Yen *et al.*, 1961; Mullins and Sheu, 1998; Sarmah *et al.*, 2010). Asphaltenes are a mixture of carbon, hydrogen, nitrogen, oxygen, sulphur and traces of nickel and vanadium (Mullins and Sheu, 1998; Branco *et al.*, 2001; Sarmah *et al.*, 2010). The elemental analysis (Table 2.1), shows that asphaltenes are predominantly carbon ($\sim 80\%$ w/w) and hydrogen ($\sim 8\%$ w/w) with smaller amounts of nitrogen, oxygen, sulphur, nickel and vanadium (Speight and Moschopedis, 1981; Mullins and Sheu, 1998; Speight, 1999; Bada *et al.*, 2007). Furthermore, oxygen contents vary from 0.3 – 4.9% w/w, sulphur from 0.3 – 10.3% w/w and nitrogen from 0.6 – 3.3% w/w (Speight and Moschopedis, 1981; Speight, 1991). The H/C ratio of asphaltenes from different geological origins is about 1.1 – 1.2 (Speight and Moschopedis, 1981; Callejas and Martínez, 2000).

Table 2.1: Elemental composition of asphaltenes from various coal and bitumen (Badre *et al.*, 2006).

Asphaltene sample	C	H	N	O	S	C:H
UG8 ^P	81.07	7.11	1.02	1.60	8.94	1:1.045
Athabasca ^P	77.03	8.01	1.27	3.00	8.18	1:1.239
Ven20 ^P	84.75	7.81	1.75	1.72	4.57	1:1.098
Lino ^C	90.35	5.53	2.23	1.90	<0.23	1:0.729
BA ^C	79.23	6.19	1.49	1.36	0.39	1:0.931

^P Petroleum asphaltenes

^C Coal asphaltenes

2.3.2 Asphaltene structure

The structure of asphaltenes has been investigated by various methods; including physical techniques, (infrared spectroscopy, X-ray, electron microscopy, small-angle neutron scattering) and chemical methods (oxidation and hydrogenation). They appear to agree that asphaltenes are aromatic molecules surrounded and linked by network of

aromatic ring systems, essentially a polymer (e.g., carboxylic acid, carbonyl, phenol, pyrrole and pyridine) capable of donating or accepting protons inter- and intramolecularly (Calemma *et al.*, 1999; Gawrys and Kilpatrick, 2005). The physical methods suggest the fused system consists of aromatic rings and appendages made up of aliphatic rings, small aliphatic side chains and polar heteroatom-containing functional groups, such as hydroxyl, carboxyl, carbonyl groups (Mullins and Sheu, 1998). However, the application of chemical methods ($\text{H}_2\text{O}_2/\text{CH}_3\text{COOH}$ treatment and pyrolysis) to study the asphaltene aggregates from two Venezuelan crude oils have shown similar distributions of oxidation products, including terpanes and steranes (Liao *et al.*, 2006). These techniques have proposed structures of asphaltene molecules, which include the atoms carbon, hydrogen, oxygen, nitrogen and sulphur contained in both polar and non-polar groups as in Figure 2.5. Hence, two representative asphaltene structures arise for two different crude oil asphaltenes of different source. Asphaltenes have been reported to possess structural features of remnants of the kerogen from which these were derived over geological time, and have been used to correlate crude oils to their source rocks, and to evaluate their thermal and reservoir emplacement histories, especially for biodegraded oils (Behar *et al.*, 1984; Strausz *et al.*, 1992b; Xiong and Geng, 2000).

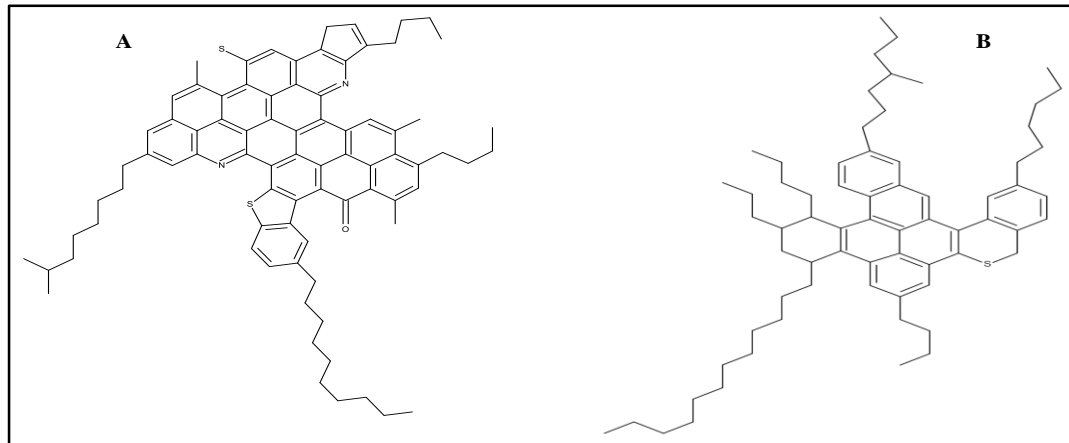


Figure 2.5: Molecular structure of asphaltene from different origin; (A) as proposed by Groenzin and Mullins (2000) and (B) Speight and Moschopedis (1981).

2.3.3 Asphaltene molecular weights

The molecular weights of asphaltenes are variable and there is debate as to whether they are monomeric or polymeric as different measurements from previous studies has revealed various values which differ by as much as a factor of 10 or more (Groenzin and

Mullins, 1999). The determination of molecular weights of asphaltenes has been difficult because of their tendency to associate with other fractions of hydrocarbons to form well-ordered crystalline structures. However, there is no general agreement to the problem as different measurements have given different molecular weights. The result of the molecular mass measurements of asphaltenes extracted from coal and petroleum using laser desorption/ionization (LDI) mass spectrometric measurements revealed that coal asphaltenes have a relatively narrow molecular weight distributions, typically within 600 - 800 amu, while petroleum asphaltenes show a broader molecular weight distributions, which falls rapidly above 1500 amu (Hortal *et al.*, 2007). As a result, these measurements are in good agreement with mass spectrometric and molecular diffusion studies of asphaltenes. However, time-resolved fluorescence depolarization (FD) measurements have revealed that asphaltenes are small molecules weights with mean molecular weights of roughly 750 amu with most of the population being between 500 and 1000 amu for petroleum asphaltene, and primarily monomeric and not polymeric (Groenzin and Mullins, 1999; Andreatta *et al.*, 2005a). We must be cautious with assigning mean values size to the heterogeneous population of asphaltene aggregates due to wide range of stability among the various aggregates. This might lead to conflicting interpretation of data from various techniques (Gawrys and Kilpatrick, 2005; Mostowfi *et al.*, 2008; Gray *et al.*, 2011). Thus, despite research on this subject, Sheu (2002) argued that the molecular weight is not suitable as a sole parameter to characterise asphaltene behavior in petroleum fluids.

2.4 Biomarkers

Biomarker or biological marker molecules are certain organic compounds occurring in crude oils, bitumen, coal, and source rocks that can be traced back to their biological molecular precursors in the contemporary or extinct biota. These complex molecular fossils possess a basic carbon skeleton that can be linked to a known natural product in the biosphere such as chlorophyll, sterols, and hopanoids (Peters *et al.*, 1992; Peters *et al.*, 2005b). Many biomarkers in crude oils are resistant to secondary processes, e.g. biodegradation. In the past three decades, these classes of organic compounds have provided an improved understanding of sources of organic matter, environmental conditions during deposition, maturity, age and degree of biodegradation, in petroleum

exploration and production (Behar *et al.*, 1984; Behar and Albrecht, 1984; Peters *et al.*, 2005b). Key common examples of biomarker classes include: branched and cyclic hydrocarbons. However, a whole variety of acyclic isoprenoid hydrocarbons like phytane, to polycyclic classes, such as the hopane and steranes have been reported in crude oils, bitumen, coal, and source rock extracts (Hunt, 1996; Peters *et al.*, 2005b). All these compounds, extending from C₅ – C₄₅, and are formed from the same building blocks of isoprene units that are linked together (Killops and Killops, 1994). Thus, based upon the number of isoprene units present, acyclic isoprenoids can be grouped into four classes (i) head-to-tail acyclic isoprenoids which have their methyl groups linked to the even carbon numbers on the chain (ii) tail-to-tail acyclic isoprenoids (iii) head-to-head isoprene units, and (iv) irregular acyclic isoprenoids. Figure 2.6 shows some examples of acyclic isoprenoids and polycyclic classes found in crude oils and coal extracts.

Numerous studies, including GC-MS have investigated biological markers, especially steranes and hopanes, which occur widely in petroleum and sediments. They are believed to be derived from the acyclic terpenoids, sterols and hopanoid terpenes biosynthesised by organisms present at the time of deposition (Mackenzie *et al.*, 1980; Petrov, 1984; Peters *et al.*, 2005b). These studies can hardly be overemphasized, as during diagenesis and catagenesis in sediments, biomarkers can undergo complex gradual structural modifications of a number of chiral centre as they achieve thermodynamic stability (Mackenzie *et al.*, 1980).

Below are the configuration pathways for the formation of hopanes from crude oils (Figure 2.7). Their structures can differ considerably between crude oils from different source facies and (Peters *et al.*, 2005a) via the configuration pathway. The origin of hopane biomarkers suggests they are associated with bacterial inputs. However, the change of various biomarker ratios present in the different organic compounds can be associated with certain characteristic differences which has occurred in the oils and sediments. These, provide geological information on source, maturity, biodegradation and correlation studies. The hopane group comprises of three diagenetic products, namely 17 α ,21 β -(H), 17 β ,21 β -(H), and 17 β ,21 α (H)- hopanes (Figure 2.7). Other triterpanes include pentacyclic oleananes, lupanes and gammacerane, which also exist in

the great family of triterpane structures. Oleanane is unambiguously linked with angiosperms (flowering plant), which have a terrestrial plant source (Ekweozor *et al.*, 1979; Peters and Moldowan, 1991; Peters *et al.*, 2005b). Thus, the abundance of $18\alpha(\text{H})$ - oleanane relative to $17\alpha(\text{H})$ - hopane (oleanane index), monitored using the characteristic *m/z* 191 fragment ion from GC-MS analysis can be used as a source indicator (Ekweozor and Udo, 1988; Peters *et al.*, 2005b). Thus, oleanane can be used to infer the age of source rock from which the oil has been generated and a ratio > 0.20 is characteristic of Tertiary source rocks while < 0.20 suggests Cretaceous or very early Tertiary source rocks (Peters *et al.*, 2005a; Peters *et al.*, 2005b). However, in GC-MS analysis, $18\alpha(\text{H})$ - oleanane has been reported to co-elute with less stable $18\beta(\text{H})$ - oleanane isomer, in most common gas chromatograph column conditions which makes interpretation difficult.

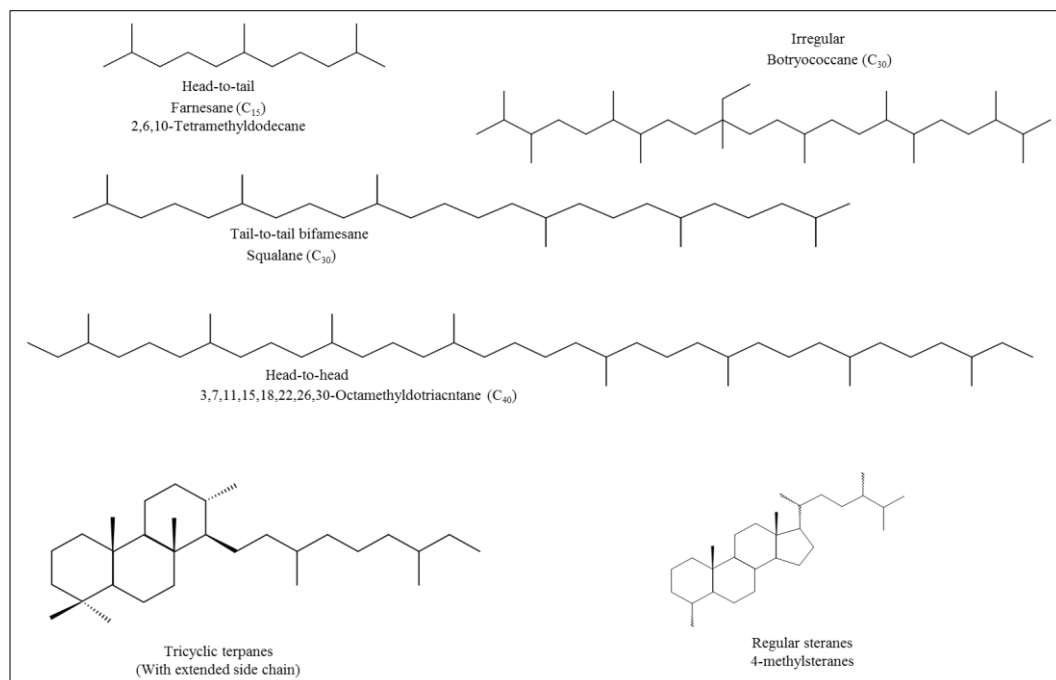


Figure 2.6: Chemical structures of some acyclic isoprenoid and polycyclic classes built from isoprene subunits (Hunt, 1996; IGI, 2004; Peters *et al.*, 2005a).

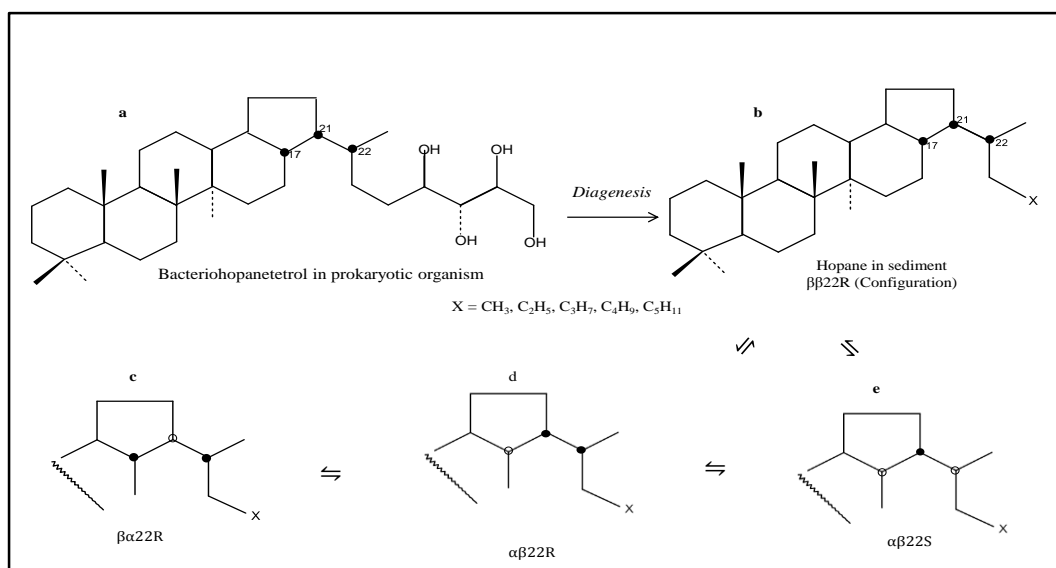


Figure 2.7: Configuration pathway for the formation of hopanes in source rocks and crude oils (Peters *et al.*, 2005a).

The sterane biomarkers have been widely reported and are believed to be derived from their biological steroids, which are linked to plant and animals. Hence during diagenesis, sterols undergo structural modifications by loss of 3β -hydroxyl group to form various regular steranes ($5\alpha(H),14\alpha(H),17\alpha(H)$) and rearranged steranes ($5\alpha(H),14\beta(H),17\beta(H)$) isomers (see Figure 2.8).

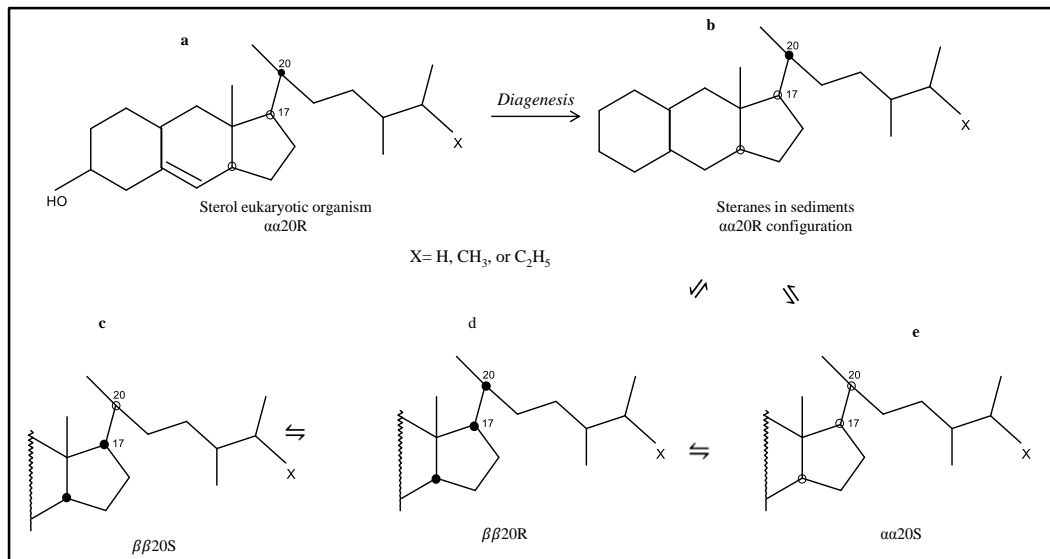


Figure 2.8: Configuration pathway for the formation of steranes in source rocks and crude oils (Peters *et al.*, 2005a).

However, other form of steranes including C_{21} and C_{22} consisting of $5\alpha(H),14\beta(H),17\beta(H)$ stereomers could also arise from the bacterial modification of the regular steranes (Moldowan *et al.*, 1991). Sterane distributions are usually determined

from m/z 217 chromatogram during GC-MS analysis. Huang and Meinschein (1979), suggested that the relative abundance of C₂₇, C₂₈ and C₂₉ sterane members in the rocks could be used to differentiate organic matter source (terrestrial or marine source). Consequently, the relative abundance of C₂₇-C₂₈-C₂₉ plotted on the ternary diagram established differences in the biological source contribution of the oils (Hu, 1991; Peters *et al.*, 2005a; Peters *et al.*, 2005b; Hakimi *et al.*, 2011). Also, maturity is also thought to play a role in sterane configuration where the relative abundance of 5 α (H),14 β (H),17 β (H) steranes are more stable and increases with increasing thermal stress (Peters and Moldowan, 1991; Killops and Killops, 2005; Peters *et al.*, 2005a).

Studies of the absolute abundance of the various isomers of steranes and hopanes during hydrocarbon generation from source rocks have provided evidence that the changes in ratios of isomers may not only be the result of isomerisation in the bitumen. Differences between the isomers in generation rates from kerogen and thermal stabilities may also be important as shown during hydrous pyrolysis (Abbott *et al.*, 1990) and in sediments thermally altered both by igneous intrusions (Bishop and Abbott, 1993) and burial maturation (Requejo, 1994). There is also evidence from thermochemolysis experiments in the presence of tetramethylammonium hydroxide (TMAH) that isomerisation takes place on the bound fraction (Abbott *et al.*, 2001; Sugden and Abbott, 2002).

2.4.1 Asphaltene bound-biomarkers

Asphaltenes are rich in biomarker compounds (see Figure 2.7 and 2.8), which are chemically bound or trapped within the macromolecular asphaltene network (Tissot and Welte, 1984; Pelet *et al.*, 1986). Furthermore, asphaltene bound-biomarkers have been reported to be found in sediments, coals and petroleum over geological time, and can provide information on the source and maturity of the asphaltenes and therefore on the oils (or bitumens) that contain them, especially for biodegraded oils (Ekweozor and Strausz, 1982; Behar *et al.*, 1984; Strausz *et al.*, 1992b; Xiong and Geng, 2000). They are considered as polycyclic aromatic structural units with aliphatic moieties (homologous series of alkyl moieties up to C₄₀) which are covalently bonded to the aromatic rings (Calemma *et al.*, 1998; Calemma *et al.*, 1999; Strausz *et al.*, 1999b). These polycyclic aromatic asphaltene structures have been characterised to be microporous and very weak, which permit it to adsorb and occlude other organic hydrocarbon species (Liao

and Geng, 2002; Liao *et al.*, 2006). Hence, they may be encapsulated within the core of asphaltenes and could represent remnants of the original oil (Acevedo *et al.*, 1997). Asphaltene biomarker compounds can be classified into two groups: (i) the adsorbed compounds and (ii) the occluded compounds. In the packed periphery inside the asphaltene aggregates, the adsorbed compounds may be exchanged within the bulk phase while occluded compounds can be adsorbed inside the asphaltene core (Liao and Geng, 2002; Liao *et al.*, 2006).

Previous studies, such as chemical degradation techniques, typically pyrolysis and ruthenium ion catalysed oxidation techniques have been extensively applied in geochemical studies of various forms of sedimentary organic matter including asphaltenes to release covalently bound biomarkers of asphaltenes (Rubinstein *et al.*, 1979; Ekweozor, 1984; Cassani and Eglinton, 1986; Mojelsky *et al.*, 1992; Peng *et al.*, 1999c; Strausz *et al.*, 1999b) and kerogen (Peng *et al.*, 1998; Abbott *et al.*, 2001; Sonibare *et al.*, 2009; Barakat *et al.*, 2012) as well as coal (Kidena *et al.*, 2008; Muhammad and Abbott, 2012). However, these techniques are tedious, time consuming and different chemical methods can selectively release biomarkers with different compositions. The RICO technique using ruthenium tetroxide (RuO_4) as oxidation reagent can release aromatic carbons in high yields to carbon dioxide (CO_2) without interference from other moieties that are covalent-bonded to the asphaltene molecular structures (Mojelsky *et al.*, 1992; Strausz *et al.*, 1992a). Hence, minimises alteration to their isomeric distributions of aromatic units connected by an alkyl bridge into typically products of asphaltene bound-biomarker (Figure 2.9). Furthermore, Figure 2.9 illustrates the selective oxidation of aromatic carbons to form to major products of carboxylic group.

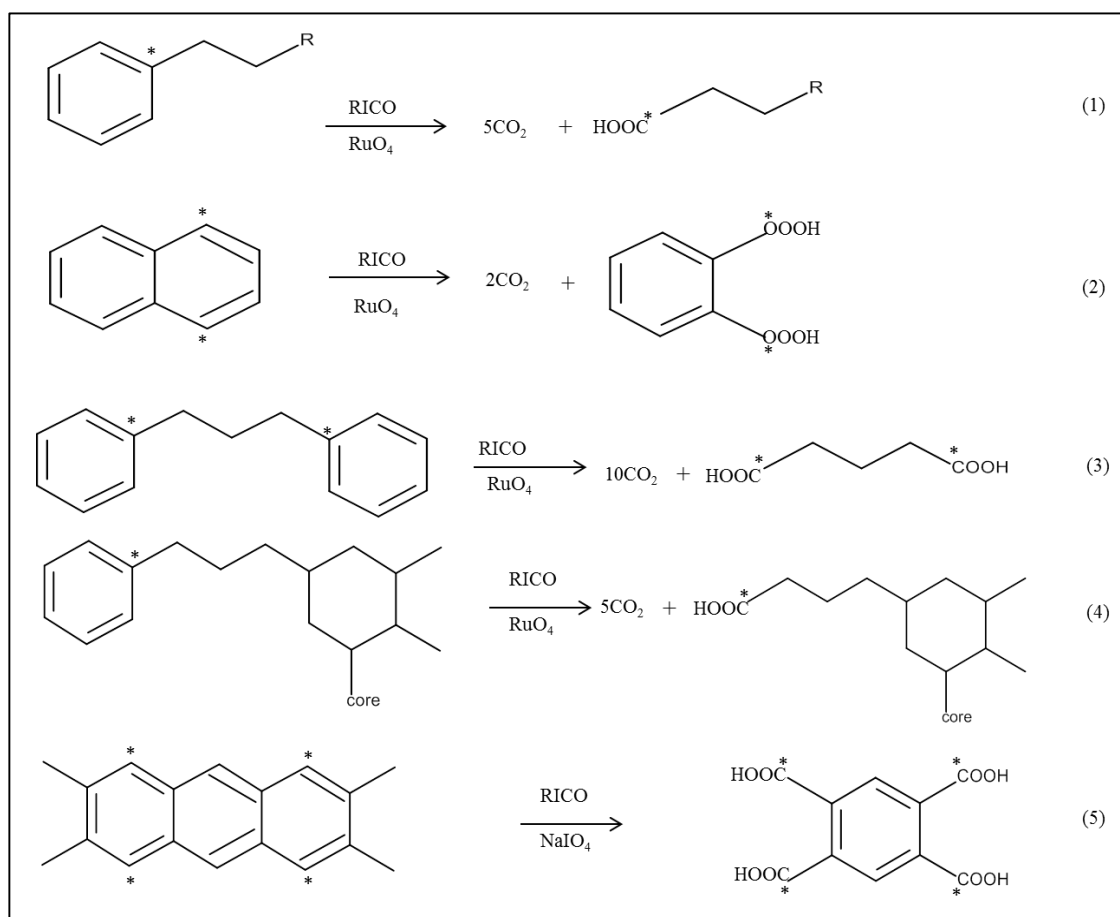


Figure 2.9: Illustration of chemical degradation (Mojelsky *et al.*, 1992).

There have been reports of the major products analysed from the RICO reactions of asphaltenes in petroleum and the distinguished asphaltene bound-biomarkers were the carboxylic acids: series of *n*-alkanoic, α,ω -di-*n*-alkanoic acids, isoprenoid acids, hopanoic acids and steranoic acids etc, in asphaltenes (Mojelsky *et al.*, 1992; Peng *et al.*, 1997; Peng *et al.*, 1999c). The occurrence of these biomarker compounds is similar to the biomarkers in the maltenes but show slight characteristic differences in the thermal maturity status (Peng *et al.*, 1999c). The *n*-alkanoic acids resulting from the RICO oxidation products of asphaltenes show a distinctive characteristic of abnormally high abundance of monoacids with distributions covering the C₁ – C₃₂ range and a clear even-to-odd preference feature, while the hopanoic acids can occur also and are best detected using *m/z* 191 mass chromatograms. These hopanoic acids ranged from C₂₈ – C₃₅, with the following configurations at the C₁₇ and C₂₁ chiral centres, 17 β ,21 β (H) (abbreviated to $\beta\beta$); 17 β ,21 β (H) (abbreviated to $\alpha\beta$) and 17 β ,21 α (H) which is abbreviated to $\beta\alpha$ (Bishop and Abbott, 1993). The $\beta\beta$ stereochemistry is believed to

have been inherited from the precursors of bacteriohopanetetrol and related tetrafunctional biohopanoids (Rohmer *et al.*, 1992).

Furthermore, steranoic acid (steranoic carboxylic acid) distributions of asphaltene have characteristics similar to those of their parent hydrocarbons. The m/z 217 Mass chromatograms reveals carbon number distribution ranges from C₂₇ – C₂₉, while m/z 275 shows C₂₈, C₂₉, and C₃₀ members and those of the C₂₈ members dominate the series of acids and are equivalent to regular sterane C₂₇, C₂₈, and C₂₉ members in oil. Similar carbon number offsets have been reported in that sterane isomerization is more advanced in the oil fractions compared to the bound biomarker fractions and therefore there is steric protection afforded to the bound biomarkers by their covalent binding within macromolecular host networks (Peters *et al.*, 1990; Love *et al.*, 1995). Furthermore, m/z 289 mass chromatograms reveals the C₂₉, C₃₀, and C₃₁ members equivalent to regular sterane C₂₈, C₂₉, and C₃₀ members in oil (Peng *et al.*, 1999c). These biomarkers from RICO have been widely used to explore oil-oil and oil-source correlations.

2.5 Biodegradation scales

Biodegradation of crude oil in subsurface petroleum reservoirs is an important geochemical alteration process that can significantly alter the quality of crude oil. The alteration process can lead to the modification of oil properties and its chemical composition, inducing the decrease of lighter compounds and an increase in sulphur content, acidity, metal content and decrease in API gravity, with severe economic consequences on oil recovery and quality (Head *et al.*, 2003; Bennett and Larter, 2008; Ross *et al.*, 2010). An increase in the content of resins, asphaltenes, metals (like vanadium and nickel) and sulphur in crude oil relative to their saturated and aromatic content is a feature of biodegradation in hydrocarbons (Peters *et al.*, 2005a; Peters *et al.*, 2005b). Thus, new compounds such as acyclic and cyclic, saturated and aromatic carboxylic acids, phenols and a complex variety of acidic compounds are formed. These compounds may be responsible for corrosion problems during processing of heavy and degraded oils (Head *et al.*, 2003).

Seifert and Michael Moldowan (1979) reported biodegradation of several of compounds in crude oils caused by the sequence of bacterial attack and water washing where less resistant compounds classes are removed prior to the most resistant ones. Notable is the sequence, most susceptible *n*-alkanes > acyclic isoprenoids (norpristane, pristane, phytane, etc...) > hopanes (25-norhopanes present) \geq steranes > hopanes (no 25-norhopanes) \sim diasteranes > aromatic steroids > porphyrins: least susceptible. The alteration of the molecular fingerprints and parameters of oils can affect source or maturity identification where partially biodegraded mature oils often resemble low maturity oils in composition from GC-MS analysis (Peters and Moldowan, 1991; Silva *et al.*, 2008). Hence, Peters *et al.* (2005a) proposed a classification system of 10 point biodegradation scale using the presence and absence of certain compounds in petroleum oils to comprehensively assess biodegradation.

Based on the approach, the general order-of-preference for biodegradation of Peters and Moldowan level 1 (abbreviated to PM 1) corresponds to early degradation (partial loss of *n*-alkanes), which are the most readily degraded, and Peters and Moldowan level 10 (abbreviated to PM 10) severely degraded oil with complete removal of acyclic isoprenoids, steranes, terpanes and aromatic steroids and altered C₂₆–C₂₉ aromatic steroids (Figure 2.10). The pathway to various levels of crude oil degradation has been well documented in the literature (Volkman *et al.*, 1984; Peters *et al.*, 1996; Head *et al.*, 2003; Peters *et al.*, 2005b; Bennett and Larter, 2008; Larter *et al.*, 2012).

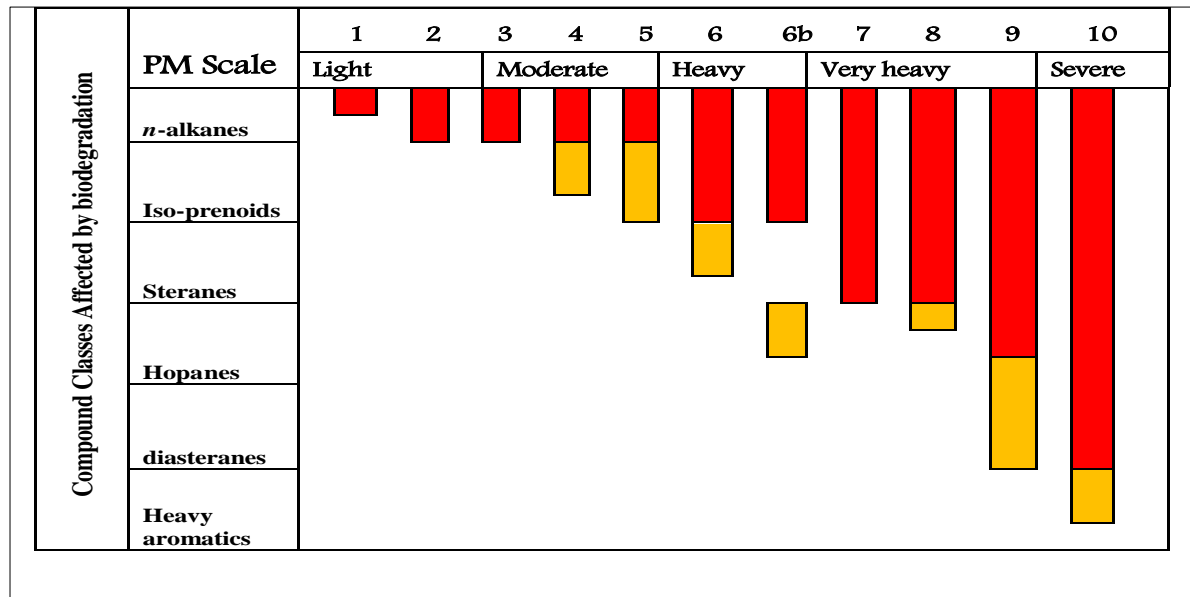


Figure 2.10: Biodegradation scale modified after Peters *et al.* (2005a).

Furthermore, caution is needed when using the PM scale, since biodegradation is a complex “quasi stepwise” process with synchronous elimination of many components at different rates rather than a qualitative assessment of a generalized pattern of compositional alteration. The PM scale focussed on compositional changes (detailed assessment) during moderate to severe alteration stages, although the most significant decrease in oil quality (e.g. API gravity) takes place during depletion of volumetrically relevant compounds during the early stages of biodegradation (Head *et al.*, 2003).

2.6 Asphaltenes and aggregation

Asphaltene aggregations are encountered both in the oil reservoirs and during transport and processing of oils. However, understanding asphaltene aggregation is a complex multicomponent process that involves a great diversity of interactions, at molecular and colloidal scales (Brandt *et al.*, 1995). Hence, two distinct properties are usually recognised: (a) aggregation and intermolecular forces and (b) asphaltene precipitation and flocculation.

2.6.1 Aggregation

The tendency of asphaltene molecules to aggregate is closely related to their molecular structure, since more or less extended aggregates can form by tacking planar aromatic parts of the molecules through π - π association or hydrogen bonds (Brandt *et al.*, 1995).

Generally, aggregation is the initial step towards precipitation and it depends on the state of solvent, temperature, pressure and concentration. However, there are two fundamental approaches currently debated in determining the morphologies of asphaltene-aggregated systems. One is the Island or Yen-Mullins model which was based on a pioneering work using X-ray diffraction (XRD) measurements for powdered asphaltenes samples from Kuwait tar oil, while the second is the archipelago model which consists of several aromatic moieties that are connected by alkyl bridges (Strausz *et al.*, 1999a).

In the Yen-Mullins model (Figure 2.11), there is a presumption that the asphaltene molecule is the key with a single fused (PAH) ring system. The second stage of the asphaltene hierarchical structure is the formation of asphaltene nanoaggregates with a single molecule (disordered stack of PAHs and with aggregation numbers ~6) into micelles and then the final stage is when nanoaggregates can form clusters of nanoaggregates and the aggregation numbers are estimated to be eight nanoaggregates (Mullins, 2010). Modelling for this system has been carried out on the asphaltene colloidal state by assuming simplified representations of crude oil containing functional groups that can form attached groups in the liquid phase such as carboxylic acids, nitrogen bases, aromatic rings, carboxylic esters, and porphyrins (Andreatta *et al.*, 2005a; Mullins, 2010; Mullins, 2011). It is recalled that the formation of asphaltenes is similar to that of surfactants and as such they self-associate in solution to give rise to more or less extended aggregates.

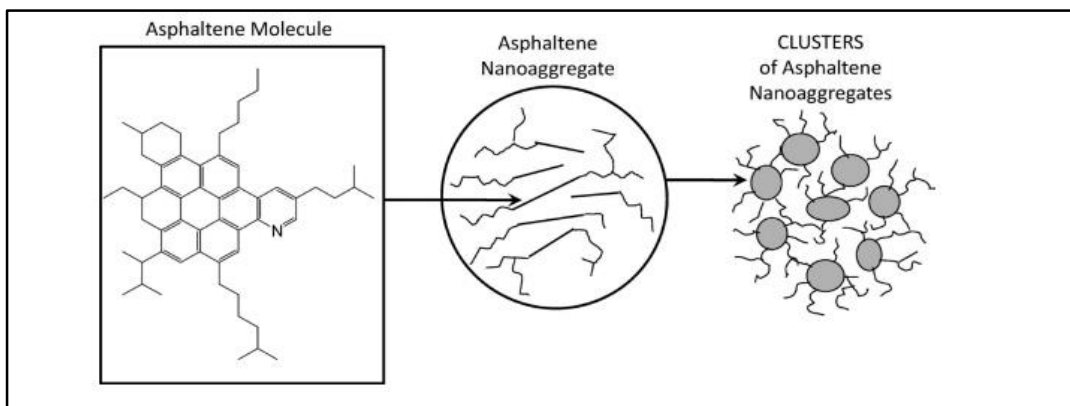


Figure 2.11: Yen-Mullins model of asphaltene Mullins (2010); (Mullins, 2011).

Mullins *et al.* (2012b), also pointed out that asphaltene monomers initially occur as dimers and trimers, followed by nanoaggregate growth at fairly low concentrations, and

the intermolecular binding energies are significant to proceed unhindered, yielding low observed solubilities. In fact, asphaltene particles can exist in the form of nanoaggregates in crude oils and organic solvents such as toluene. For example, at room temperature in toluene using high quality factor (high- Q) ultrasonics: a study detected that asphaltenes starts to associates at a CNAC of 50 - 150 mg/L and proceed to form nanoaggregates at above 150 mg/L (Andreatta *et al.*, 2005a; Andreatta *et al.*, 2005b; Mullins, 2010). Furthermore, it has been shown that CNAC varies depending on the source of the oil.

The archipelago model structurally classify asphaltenes as several aromatic moieties that are covalently linked together by aliphatic chains (Murgich *et al.*, 1999; Strausz *et al.*, 1999a). However, there is uncertainty to the number of aromatic rings present in the planar aromatic cores and the actual structure of the asphaltene molecules (Speight, 1999).

2.6.2 Asphaltene precipitation and flocculation

The aggregation of asphaltene molecules is believed to be the initial stage to asphaltene precipitation. However, it has long been confirmed that precipitation can occur due to changes in a petroleum system, among these including (i) changes in temperature and/or pressure as during oil production (ii) changes in fluid compositions as a mixture of several types of oils or injection of CO₂ fluids into the oil reservoir during recovery, and (iii) changes in the compositions of asphaltenes (Speight, 1991; Wilhelms and Larter, 1994). Knowledge of the mechanism of asphaltene aggregation may help to improve many problems associated to asphaltene deposition that are encountered by many industrial processes. These problems including oil pipeline blockage, plugging of wells and formation of tar mats in petroleum reservoirs and would result in less economic waste in the oil industry (Wilhelms and Larter, 1984; Buckley, 1999; Andreatta *et al.*, 2005b). Therefore, it is critical to know when and how asphaltenes will separate out of solution in the form of a heavier phase under a given set of operating conditions.

In the last three decades, a number of studies have been dedicated to characterise precipitation, flocculation and deposition of asphaltene molecules in a petroleum system, These employ two general fundamental approaches: (a) the solubility approach

and (b) the colloidal approach (Leontaritis and Ali Mansoori, 1988; Ali Mansoori, 1997; Andersen and Christensen, 1999; Wang and Buckley, 2001).

The first “solubility model” approach proposed that asphaltene molecules are formed when a large non-soluble particle (asphaltene) is stabilized in the solution by adsorption of resin on its surface as a function of the thermodynamic system, whereas relatively large aggregates may flocculate out of the solution and form micelles due to addition of excess *n*-alkanes. Studies, using surface tension and interfacial tension measurements, accurately detected the onset of asphaltene precipitation in crude oil (Vazquez and Mansoori, 2000; Priyanto *et al.*, 2001). However, flocculation of asphaltene in *n*-alkanes is known to be irreversible, having a hysteresis when the conditions are returned to preflocculation point (Acevedo *et al.*, 1995). As a result of their adsorption affinity to solid surfaces, asphaltene flocs (random nanoaggregates) forming clusters or quite stable deposits.

The second “colloidal model” approach suggests that asphaltenes would aggregate to form micelle-like aggregates or flocs of asphaltenes above a certain concentration resembling that of surfactants (Andersen and Birdi, 1991; Andreatta *et al.*, 2005a; Mullins, 2010). The “colloidal model” is completely accepted by Yen-Mullins model with the observation of CNAC of asphaltene in solution. However, primary asphaltene aggregation in crude oil occurs when different aromatic ring geometric (disks, spheres, cylinders) shapes and become suspended in the solution when the concentration of the system exceeds the CNAC (Andreatta *et al.*, 2005a; Mullins, 2010; Mullins *et al.*, 2012a). Furthermore, surface tension measurements of asphaltene/toluene systems have confirmed the CNAC of asphaltenes in different solvents with respect to asphaltic compounds are closely related. Hence, it is shown that asphaltene/toluene system has a hierarchy of aggregation, at which at a concentration below the CNAC, the asphaltenes in solution are in a molecular stage, whereas at above CNAC, asphaltenes exist as nanoaggregates which are much more uniform in their structure and less polydisperse.

2.7 Relevance

Chemical oxidation of isolated asphaltenes from crude oils and coals have been reported to provide acid products that contain biomarker compounds, which are chemically

bound or trapped within the macromolecular asphaltene network (Mojelsky *et al.*, 1992; Strausz *et al.*, 1992a). Their relative biomarker distributions have been reported to have the potential to reveal detailed information concerning thermal maturity, depositional environment and source of the asphaltenes, and evaluate crude oils and likely sources that contain the asphaltene (Rubinstein *et al.*, 1979; Liao and Geng, 2002; Liao *et al.*, 2006). Hence, when oils are biodegraded or lack source rock data, biomarkers generated from oxidation products of asphaltenes can provide vital information. Furthermore, understanding the chemical compositions, structures of asphaltenes with formation of critical nanoaggregate would provide us with an improved understanding of the uncertainties in their aggregation properties and hence provide a clue to the origin of thick deposits that can reduce flow line permeabilities causing wellbore plugging, pipeline fouling and solid build-up in petroleum industries.

2.8 Scope and Delimitation

This study is generally limited to studying how the molecular characteristics correlate with colloidal aggregation of asphaltenes in crude oils, for the purpose of providing a better understanding of the nanoaggregation properties. Consequently, crude oil and coal asphaltenes of various sources, precursor materials, environmental conditions of deposition, biodegradation and maturation processes will be used in this study. The molecular weights and sizes of asphaltenes will not be assessed.

The study will focus on asphaltenes, which are considered as the *n*-hexane isolated solids precipitated from crude oil and coal, then purified over 72 hours with precipitating solvent using Soxhlet extraction to remove co-precipitated resins.

Characterisation of the asphaltenes has been limited to RICO, FTIR and high precision ultrasound spectroscopy measurements.

Chapter 3 Experimental Methods

3.1 Introduction

This chapter discusses the samples and various procedures used in preparing the samples into a form amenable for analysis in this study, as well as discussing the analytical techniques used to characterise the samples. Three major sections were utilised to achieve the objectives of this study:

- a. The first major section briefly describes the total of 44 samples and petroleum geology of the locations; including a spectrum of petroleum compositions from non-biodegraded oils to biodegraded heavy crude oils and 3 coals.
- b. The second section provides the description of the various methods and analyses procedures adopted for the study.
- c. The final section describes the geochemical applications and analytical techniques used to characterise the set of oil and coal samples from the various locations.

3.2 Description of samples

A total of 44 samples (Appendix 3.1), including 41 crude oils and 3 coals were used in this study. The crude oils were obtained from different locations around the world including Niger Delta (Nigeria), United Kingdom, Middle East, North America and Serbia (Figure 3.1). Among the total oil samples are six crude oil samples obtained from Chevron Nigeria limited exploration site located in offshore Niger Delta, Nigeria. The two crude oils from Serbia were donated by Dr. Ksenija Stojanović (University of Belgrade) and the remaining oil and coal samples were provided by Dr G. D. Abbott, Newcastle University, United Kingdom.

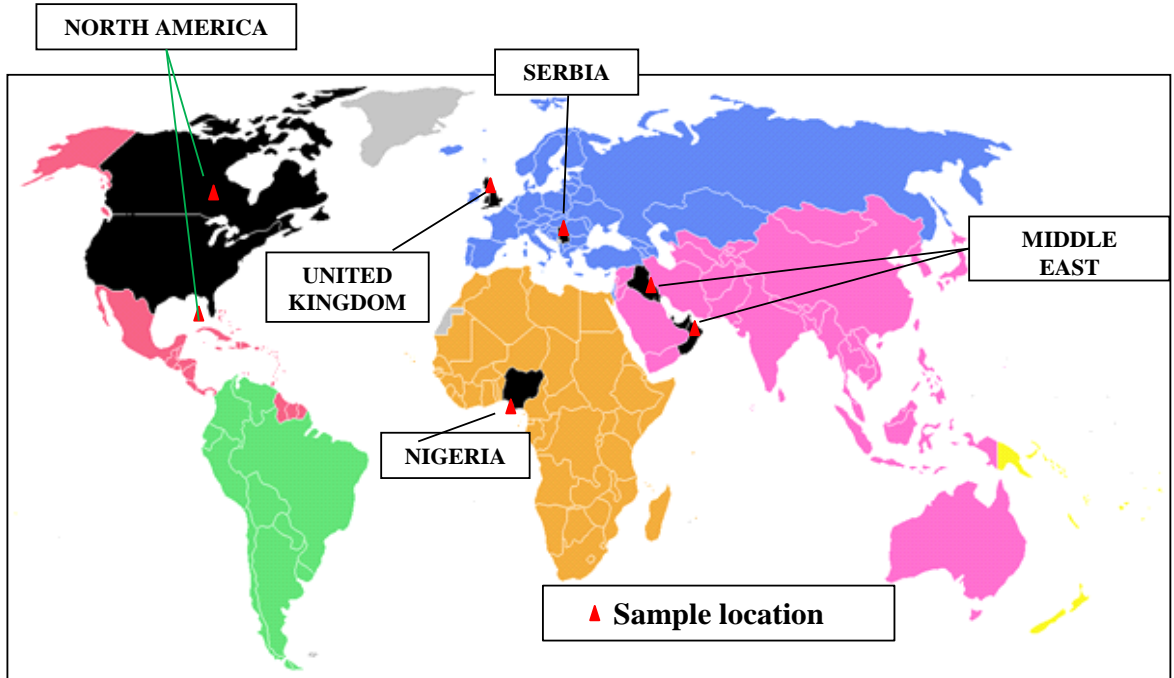


Figure 3.1: Geographical location of the study samples

3.2.1 Nigerian oils

A total of 12 Nigerian crude oils, including non-degraded and biodegraded oils, were used in this study. The samples; NA1, NB2, NC3, NA, ND, NE, NF, NO, NN, N25, N18 and NN1 (Appendix 3.1) were collected from onshore and offshore oil fields located in the Niger Delta, Nigeria. The field names and other details were not disclosed as requested by the providers.

The Niger Delta basin (Figure. 3.2) is located at the seaward part of the Benue trough and is an important oil-producing province in the world. Hence, several studies have been carried out on the petroleum system and basin evolution of the area (Dewey and Burke, 1974; Reijers, 2011). The Niger Delta has been described as consisting of Cretaceous sediments of Albian to Maastrichian age, which builds through pulses of sedimentation over an oceanward dipping continental basement into the Gulf of Guinea on the Atlantic Ocean of West Africa, thereafter progradation took place over a landward-dipping oceanic basement, as shown in the schematic map (Figure 3.3).

In the Niger Delta, three major lithographic units of sedimentary sequence of over 12 km thickness from shallowest to deepest exist, namely:

- a. The Benin Formation is the youngest and is composed of predominantly massive, highly porous sandstones that was deposited mainly in the continental and delta plain settings (~ 2000 m thick in the depocenter),
- b. The Agbada Formation is overlain by the Benin Formation, composed of alternating interbedded sandstones and shales deposits (~ 4000 m thick in the depocenter and thinning seaward towards the delta margin), and
- c. The Akata Formation, is composed of massive marine shales (~ 6000 m thick) deposited during the Palaeocene and through the Recent (Sonibare *et al.*, 2008).

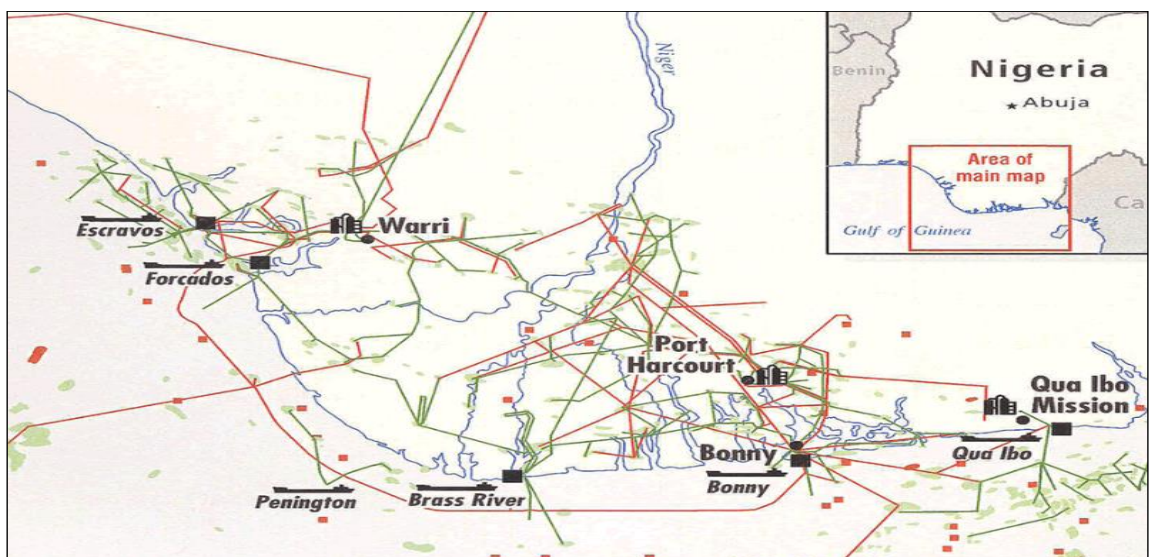


Figure 3.2: Location map of Niger Delta (EIA, 2012).

The lithographic units of sedimentary subsurface sequence of the Niger Delta is made up of superimposed lithofacies; continental, transitional between continental and marine, and marine environments of deposition (Ekweozor *et al.*, 1979). However, since oil was first discovered in commercial quantities in 1956, the region has becomes one of the most prolific hydrocarbon provinces in the world with over 5,000 wells and 100 oil fields discovered and an initial oil in place estimated at 30+ Billion barrels (bbls) of oil and 180 Trillion cubic feet (Tcf) of gas. Though, recently oil and gas exploration has shifted gradually focused on the deep and ultra-deep offshore part of the Niger Delta. A variety of criteria can be used to define deep & ultra-deep, deep water sometimes defined as water depth greater than or equal to 500m. The ultra-deep water is defined as depths greater than or equal to 1500m (TOTAL, 2006).

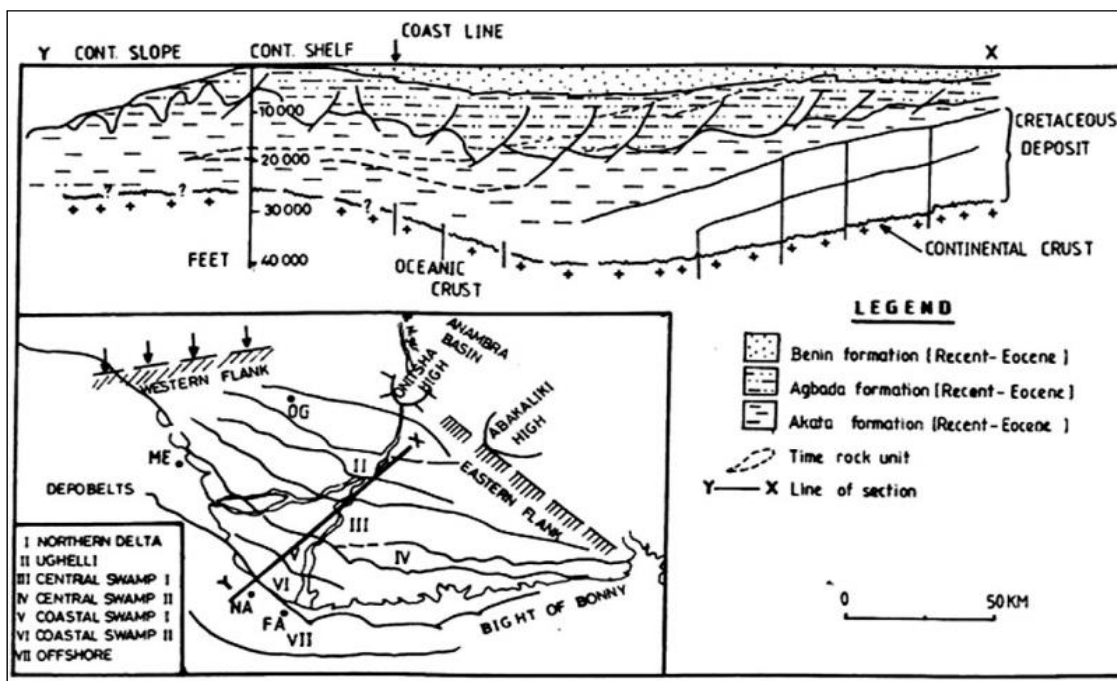


Figure 3.3: Niger Delta: stratigraphy and formation depobelts (Ekweozor and Daukoru, 1994).

Studies have shown that the principal sources of oil and gas accumulations in the region are type II, II-III and type III kerogen which exist mainly in the lower parts of the paralic sequence (Agbada Formation) and the topmost strata of the continuous marine shale (Akata Formation) deposited in marine deltaic environments (Sonibare *et al.*, 2008; Lehne and Dieckmann, 2010). Recent study has proposed the possibility of three source rock organofacies in the Niger Delta (Samuel *et al.*, 2009). These organofacies are of a more marine organofacies that dominates the deep water accumulations, a terrigenous intra-delta organofacies that is passive over the entire delta and the shallow water accumulations comprising mixed source rock facies.

3.2.2 United Kingdom oils

In this study, eleven crude oil samples were investigated; UKB, UK88, UK85, UK66, UK65, UK80, UK12, UK34, UK11, UK01, UK05, and UKV (Appendix 3.1) collected from oil fields located across the United Kingdom and the United Kingdom sector of the Northsea. These fields include Captain, Nelson and Flora oil fields (Figure 3.4).

The **Captain Field** (Figure 3.4) lies at approximately 145 km northeast of Aberdeen on Block 13/22a, which is on the western margin of the Halibut Horst (Captain Ridge) in the Western Moray Firth region of the UK North Sea (Pinnock and Clitheroe, 1997). In

the field, the oil sources are from the matured organic-rich shales of the Kimmeridge Clay Formation and the reservoir rocks are characterised by two main distinctive stratigraphic units, namely,

- The Upper Captain Sandstones and
- The Lower Captain Sandstones (thick-bedded fine to medium grained sandstones with very little interbedded silt or claystone).

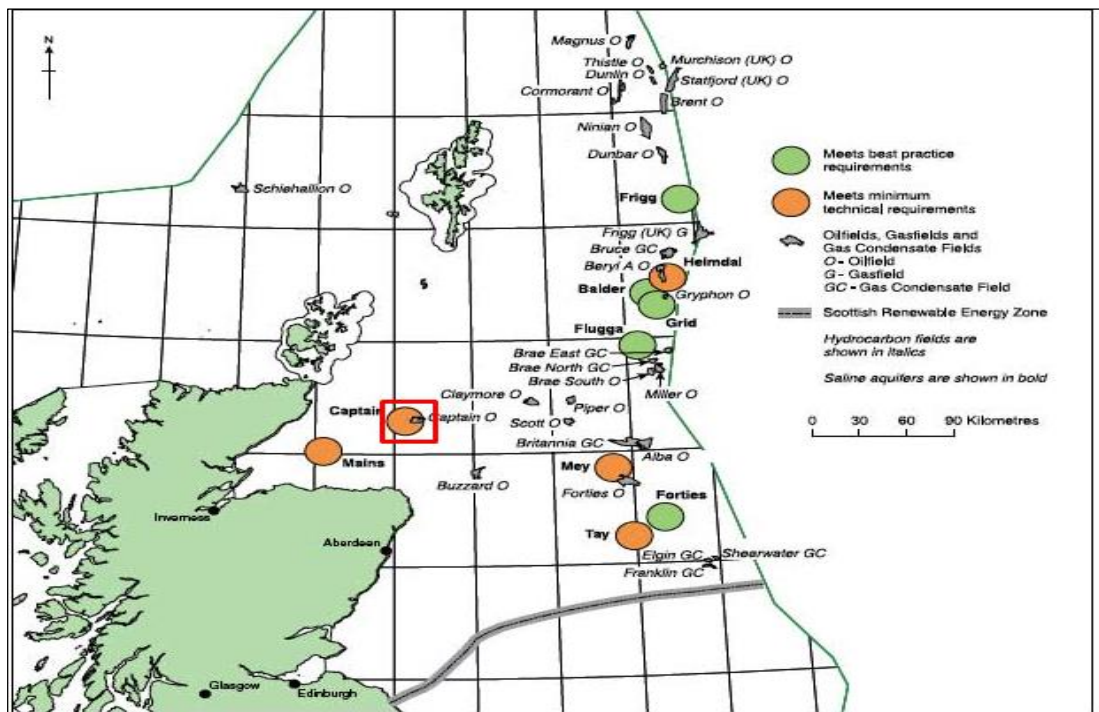


Figure 3.4: Location of Captain oil field (The Scottish Government, 2009).

The reservoir quality is generally good with average permeability of 7 darcys and porosity between 28 and 34% in the Lower Cretaceous in-situ rocks (Pinnock *et al.*, 2003). However, the oil quality is heavy with oil gravity ranging from 19° to 21° API and the oil reserve is estimated to be a total of 1000 million bbls (oil-in-place) and associated gas of 16 bcf (gas-in-place).

The **Nelson Field** (Figure 3.5) lies at approximately 180 km east of Aberdeen and comprises of four blocks; 22/11, 22/6a, 22/7 and 22/12a situated in the UK sector of the Central North Sea.

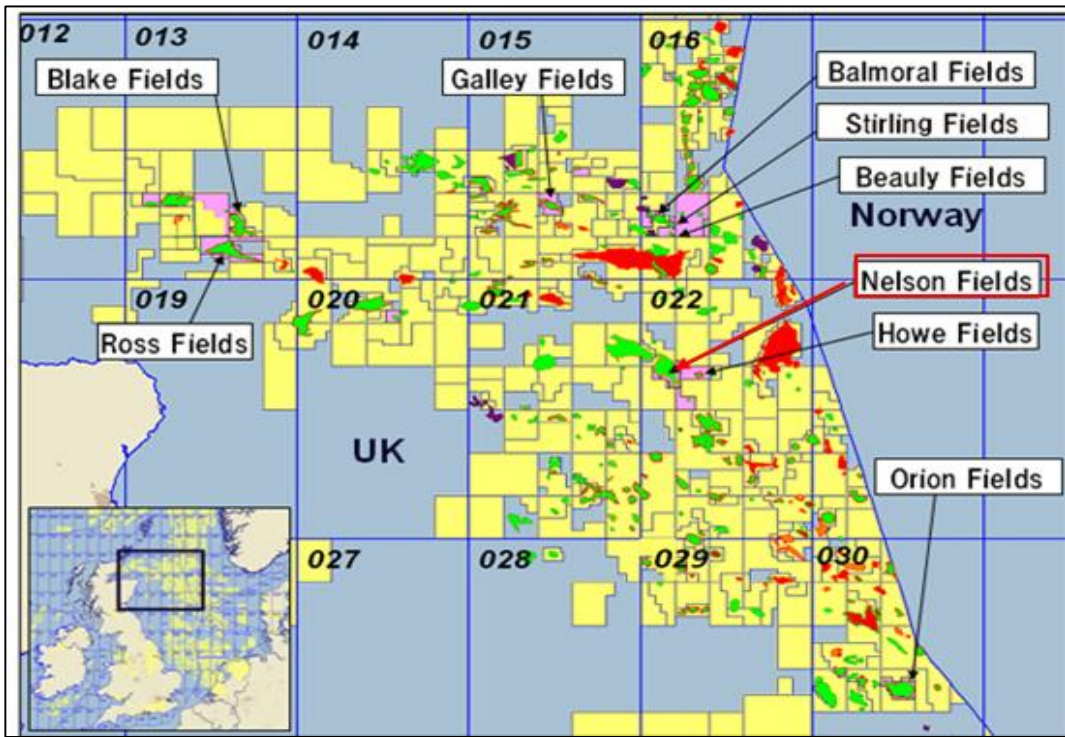


Figure 3.5: Location of the Nelson oil field (Sumitomo Corporation, 2009).

Hydrocarbon accumulations were first discovered in the Nelson oil field in 1988 and are believed to be sourced from the matured Jurassic Kimmeridge Clay Formation of the Forties Sandstone Member (Kunka *et al.*, 2003). The reservoir oil quality is light with gravity of 40.6° API and estimated recoverable reserve of a total 300 million bbls (oil-in-place) with some 100 bcf of gas (Whyatt *et al.*, 1992).

The Flora field (Figure 3.6) is located approximately 325 km southeast of Aberdeen and 9 km North of the Fife Field on the southern margin of the Central Graben and lies between Blocks 31/26a and 31/26c of the UK sector of the North Sea. (Hayward *et al.*, 2003). The field was discovered in August 1997 and is believed to be sourced mainly from the Kimmeridge Clay Formation of the Central Graben and is sealed by overlying Lower Cretaceous marls and Upper Cretaceous Chalk Group. The Flora Sandstone (an Upper Carboniferous fluvial deposit) and a thin Upper Jurassic veneer, trapped within a tilted fault block serve as the oil accumulation and have good reservoir quality with average porosity of 21%. Although, the reservoir suffers both sub-horizontal (floodplain shales) and vertical (faults) compartmentalization with 245 ft undersaturated oil column stacked within the fluvial channel sandbodies thought to be of Carboniferous or early

Permian age. The recoverable reserve is estimated at 13 million bbls (oil-in-place) and the field can produce 30000 BOPD at peak oil production (Hayward *et al.*, 2003).

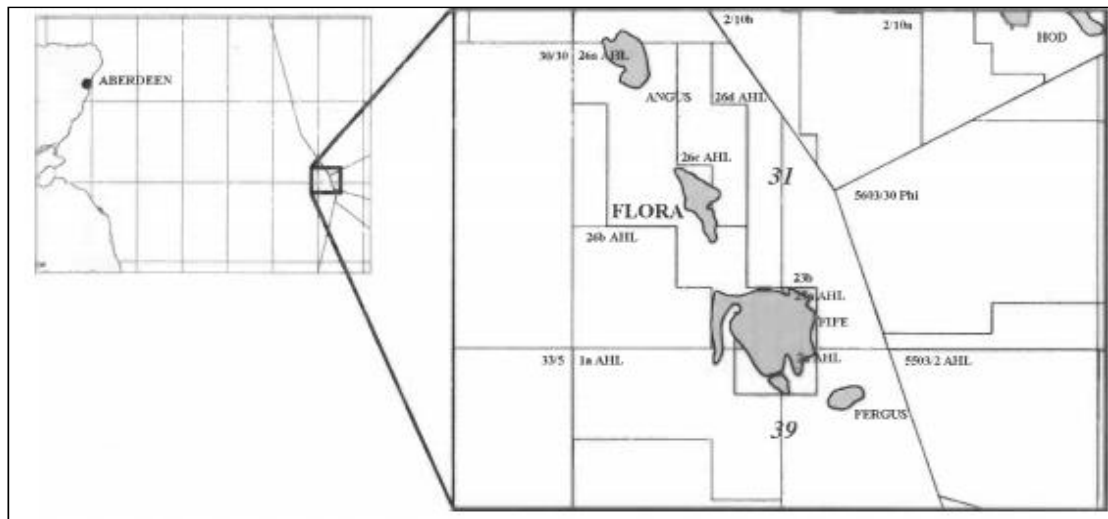


Figure 3.6: Location of the Flora oil field (Hayward *et al.*, 2003).

3.2.3 Middle East oils

A total of five crude oil samples ME12, ME43, ME39, ME77 and ME78 from different oil fields in the Middle East were investigated. The sample set includes;

- a. Two Qatar oils (ME12 & ME43) were collected from offshore fields of Al Shaheen and Bul Hanine respectively.
 - b. One Abu Dhabi oil (ME39) and
 - c. Two crude oil samples (ME77 & ME78) were collected from oil fields of Raudhatain and Sabriyah situated in the northern region of Kuwait.

3.2.4 North American oils

A total of 8 crude oils samples were obtained from the North America sector, among which are

- a. One sample (NAC) collected from an oil field in Canada and
 - b. Seven samples; including NA61, NA72, NA73, NA74, NA75, NA76, and NA79 were collected from oil fields located across different oil fields in Gulf of Mexico Basin at the North America region.

The Gulf of Mexico Basin is the largest petroleum producing basin in the North America show in Figure in 3.1, accounting for ~ 31% oil and ~ 48% gas production (Fails, 1990). Hence, many studies have substantially investigated the source rocks, migration and generation of petroleum in the northern Gulf of Mexico Basin. However, there are disagreements on the petroleum systems due to the variations in the organic source facies, hydrocarbon generation potential, different maturation history and mixing of fluids from multiple sources of the basin (Kennicutt II *et al.*, 1992; Whelan *et al.*, 1994; White *et al.*, 2003). In the offshore area, many petroleum accumulations and source rocks of nearly all ages have been proposed, including the three main models of hydrocarbon for the source of hydrocarbons in the Gulf of Mexico basin; the associated Cenozoic source (Marine deltaic shales), the disassociated Neogene source (Neogene organic rich source bed deposits and derived from salt dome dissolution) and the dis-associated pre-Neogene source (Mesozoic and Palaeogene sources). However, regionally consistent correlations may be recognized (Bissada *et al.*, 1988).

3.2.5 Serbian oils

The Serbian oils, including two oil samples (SN1 & SN2) were collected from oil fields located at the Pannonian Basin (Figure 3.7), in Serbia (Stojanović *et al.*, 2009). The Pannonian Basin is referred to as a typical continental Neogene back arc basin that is associated with a continental collision formed by processes of extension and subsidence and bordered by the Alps to the west and by the Carpathian Mountains to the east and north (Mrkić *et al.*, 2011). However, the basin was formed due to processes of extension and subsidence during the late Miocene and a continuous tectonic activity resulting to subsidence, uplifting and young faulting of the basin during the Neogene and Quaternary (Šolević *et al.*, 2008). The Serbian part of the Pannonian basin is the youngest sedimentary basin in the Alpine folded belt and belongs to the largest sub-basin; consist of a system of unique deep troughs of its own subsidence and separated by basement highs.

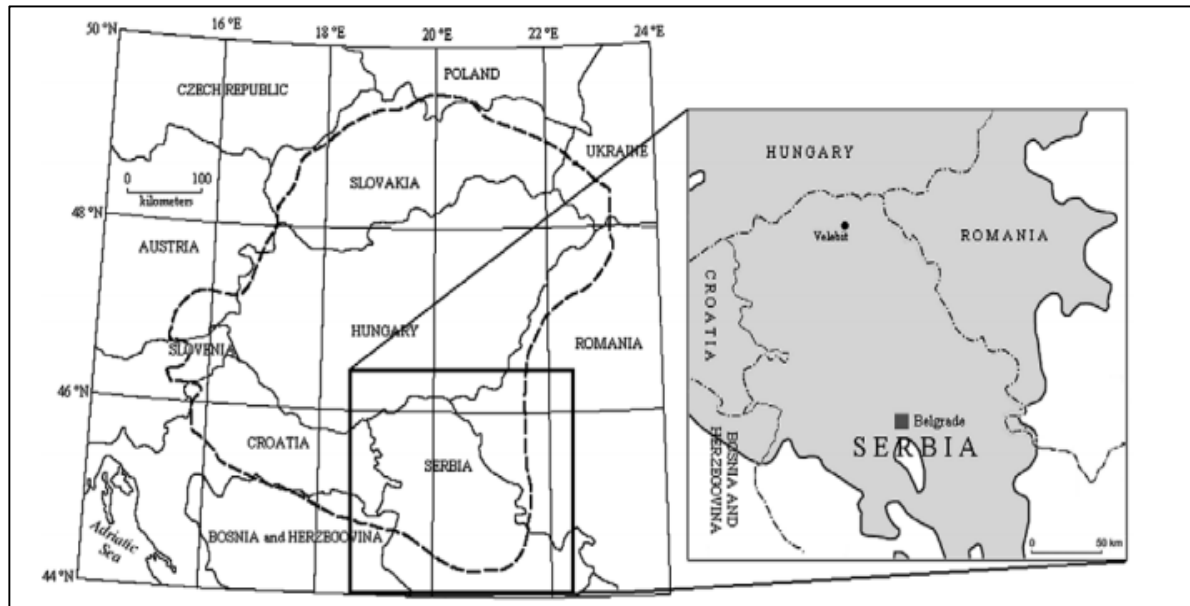


Figure 3.7: Area of study in Serbian part of the Pannonian Basin (Šolević *et al.*, 2008).

Most hydrocarbon plays exist in the basin of Neogene and Palaeogene basin-fill, and in the Mesozoic and Palaeozoic basement located within the north and central parts of Serbia in the Banat Depression, characterized by high thermal history here the studied samples were collected (Figure. 3.7). The oil and gas fields are in close proximity to areas of mature source rocks, found in immature sediments stratigraphically overlying the mature ones (Šolević *et al.*, 2008).

3.2.6 Coal samples

In this study, 3 North Sea coals namely; CA3, CA4 and CA6 from the United Kingdom were investigated. The samples were provided by Dr. Geoff Abbott and collected from different depths of the North Sea coal deposits, UK. Vitrinite reflectance investigations have been carried out on the samples.

3.3 Methods and sample preparation

This section describes and provides the description of the various methods and analyses procedures (Figure 3.8), used in this study.

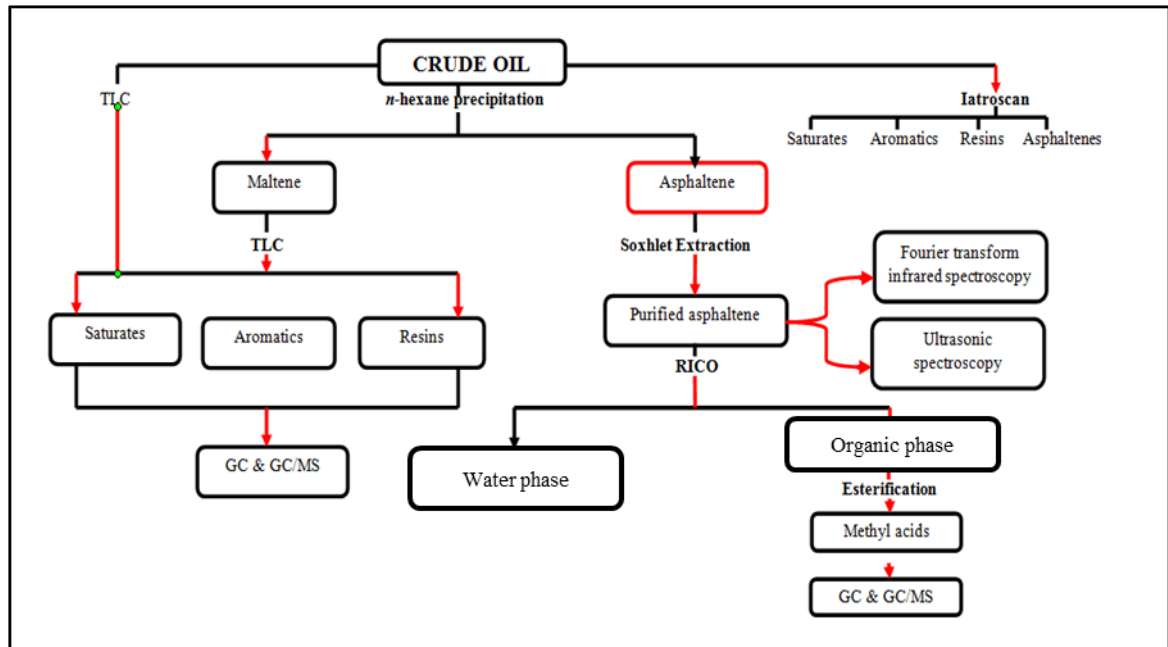


Figure 3.8: Research methodology flowchart.

3.3.1 Iatroscan thin-layer chromatography (TLC-FID)

Iatroscan analysis combines the resolution efficiency of thin-layer chromatography (TLC) with the detection sensitivity of the flame ionization detector (FID) for fraction quantification of crude oils (Karlsen and Larter, 1991). It provides for good precision and accurate information on the yield and relative proportions of the four major fractions of petroleum: saturates, aromatics, resins and asphaltenes (SARA). This technique is efficient, fast, cost-effective and uses small amounts of sample (Karlsen and Larter, 1991; Fan and Buckley, 2002). This study uses the Iatroscan to ascertain asphaltene concentrations. It is noteworthy that careful calibration need to be taken as the FID response factor (response area count per unit w/v% concentration), scan rate, hydrogen detector flow rate to the instrument and the size of the sample application spot can affect the results (Karlsen and Larter, 1991). Thus, the importance of accurate instrument setup and the fixing of operating variables for quantitative accuracy and reproducibility (Karlsen and Larter, 1991).

In this study, the three-step solvent development procedure was applied to achieve clear and reproducible separation of the four fractions; saturates, aromatics, polar and asphaltenes using *n*-hexane, toluene and DCM/ MeOH (93/7; vol/vol) respectively (Karlsen and Larter, 1991). First, a standard sample from a North Sea crude

oil (\sim 10 mg) was prepared in a glass vial and diluted in DCM (\sim 1 mL) to reduce viscosity prior to spotting on the chromarods. Then, each of the oil samples (\sim 10 mg) from the sample set were weighed and diluted with DCM (\sim 1 mL). In this analysis, chromarods S-III sintered silica gel phase, 0.9mm diameter by 15 cm long quartz rods was used. The set of ten chromarods were held in a single rack allowing all to be processed and simultaneously detected in a quick succession. Using micro syringe, oil sample (\sim 3 μ L of \sim 10 mg/mL) of the freshly prepared sample solution was spotted in triplicate onto the rod base of each chromarods and developed according to increasing order of polarity using *n*-hexane, toluene and DCM/MeOH as eluent. After spotting, the rack containing the chromarods was air dried for a minute and then placed in the first development tank to elute in hexane for \sim 30 minutes which separates the saturated hydrocarbons for \sim 10 cm up the chromarods. The chromarods were then air dried for 3 minutes. Further development takes place for \sim 15 minutes in toluene to separate the aromatics \sim 5 cm up the rods. The chromarods were then air dried for \sim 6 minutes and a final development takes place in 97:3 DCM/MeOH to separate the resins and asphaltenes for \sim 2 minutes. The chromarods were then dried in an oven at \sim 60 °C (90 seconds). As soon as the set of chromarods have passed through all the development tanks and are dried they are placed in the Iatroskan for analysis. The chromarods were then scanned in an Iatroskan machine TH-10, Mk 5 (Iatron Lab Inc., Tokyo), equipped with a flame ionization detector (FID), interfaced with an electronic integrator (Perkin-Elmer LCI-100) at a scan speed of 30 s per rod, effectively analysing 10 samples in 7.6 minutes.

The organic components separated on the chromarods were ionised and the ion currents were measured proportional to the organic mass of components being ionised in the flame and a response is recorded (data). The data were acquired, processed and stored on a Thermo-Atlas Chromatography Data system and the crude oil fractions represented by peaks in the form of chromatogram. The quantitative results were obtained by integrating the peak area for the four distinct components, including saturates, aromatics, resins and asphaltenes, assuming that each SARA fraction has an identical FID response factor.

3.3.2 Precipitation and purification of asphaltenes

The asphaltenes used in this study were isolated by consecutive precipitation steps as described by Alboudwarej *et al.* (2002). Here, the solvent *n*-hexane was used to isolate the asphaltenes from the crude oil samples. Hence, in this study a known weight of crude oil was weighed into a conical flask and dispersed with DCM (~1 – 2 mL) to reduce viscosity prior to the incremental introduction of 40-fold (w/v) of *n*-hexane; then the solution was followed by regular agitation to efficient mixing. The whole mixture was then stirred for 2 h in a ultrasonic bath and subsequently allowed to equilibrate overnight for 24 h in the dark.

3.3.2.1 Asphaltene Recovery

The equilibrated mixture was then weighed into several centrifugation vials and separated by centrifugal sedimentation at a speed of 3500 rev/minutes for 15 minutes using a Centrifuge 5810 model from Scientific Laboratory Supplies. Centrifugation of the mixture enables sedimentation of water and solid mixture. The asphaltenes were recovered by decanting the resulting supernatant (maltene; saturates, aromatics and resins) from the solid (asphaltene precipitate) into a round bottom flask. The recovered asphaltene precipitates were then re-dissolved in DCM (~1 mL) and re-precipitated with 40-fold (w/v) of *n*-hexane before stirring for 30 minutes in an ultrasonic bath and allowed to equilibrate for 3 h and then asphaltenes were recovered by centrifugation. This procedure was repeated for two or three more times until the mixture becomes colourless, so as to remove any occluded resins and aromatics from the precipitated asphaltenes. Using a minimum volume of DCM (1 – 2 mL) needed, the asphaltenes were transferred into a pre-weighed glass vial and then the excess solvent in the glass vial was removed under a gentle stream of nitrogen gas and then stood overnight at ambient temperature until it evaporates completely.

3.3.2.2 Cleaning the Asphaltenes

Co-precipitated resins and possible adsorbed compounds can be removed from dried asphaltenes using Soxhlet extraction technique for 72 h with *n*-hexane (Alboudwarej *et al.*, 2002), thought this treatment can only be necessary if the asphaltene is required for compositional or bound biomarker studies (Muhammad and Abbott, 2012). Hence, the

dried asphaltene precipitates were crushed with a spatula, weighed and transferred into pre-extracted Whatman cellulose thimbles (1 x 10 cm). This thimble containing the asphaltene sample was then plugged with pre-extracted cotton wool and place into the Soxhlet extracting apparatus. Then was extracted using re-distilled *n*-hexane for 72 h (at 24 h cycle each) and at the beginning of each cycle, fresh *n*-hexane solvent was used for extraction until the last cycle when the solvent becomes colourless. After the extraction, the extracts at each cycle were fractionated into aliphatic and aromatic hydrocarbons to ascertain asphaltene purity. Finally, the purified asphaltenes were transferred into a glass vial, air dried and weighed prior to further analyses.

3.3.3 Fractionation of oils

The crude oil samples were fractionated using thin layer chromatography (TLC plate) technique to obtain aliphatic hydrocarbon and aromatic hydrocarbon fractions from which different biomarkers were investigated. The TLC plates were prepared using aqueous slurry of 0.5 mm thick Keiselgel 60 G silica gel activated for 24 h at 100 – 120 °C. Each crude oil sample (~ 20 mg) was weighed in a glass vial and dissolved with DCM (~ 0.2 mL) to reduce the viscosity prior to TLC analysis. Then two internal standards (squalane and 1,1-binaphthyl) were prepared at different concentration and added for quantification of the aliphatic and aromatic hydrocarbon fractions respectively. The mixture of samples was then loaded onto the TLC plate at about 2 cm from the bottom of the plates.

Two standards (*n*-eicosane and phenanthrene) were also prepared and spotted along the side of the plate to visually identify the different hydrocarbon bands; aliphatic and aromatic fractions on the TLC plate. The plate was then run in a developing chamber filled with 200 mL of re-distilled petroleum ether until the fractions reach the top of the plate. The plate was dried and sprayed with rhodamine-6G dye. The different hydrocarbon fractions were then, identified under UV light and the aid of the standards along the side of the plate. The identified bands, each corresponding to aliphatic, aromatic hydrocarbons and the remaining polar fractions were scraped off with the spatula. The aliphatic fraction was then eluted with 10 mL of dichloromethane and 30 mL of petroleum ether while the aromatic fraction was eluted with 30 mL of dichloromethane and 10 mL of petroleum ether using short glass column (12.5 cm) into

a round bottom flask. This was followed by the evaporation of the fractions to about 1 mL using a rotary evaporator and then concentrated under stream of nitrogen gas to about 0.5 mL and then transferred into a GC vials for GC and GC-MS analyses for biomarkers study. On each batch of 10 samples, a triplicate and a blank were prepared.

3.3.4 Fractionation of maltenes

The resulting maltene fraction from the collection of the supernatant (aliphatic hydrocarbons, aromatic hydrocarbons and resins), during asphaltene isolation and the cleaning of the asphaltenes were separated into aliphatic and aromatic fractions using the TLC technique as described in section 3.3.3 prior to GC and GC-MS analyses.

3.3.5 Ruthenium ion catalysed oxidation (RICO) of asphaltenes

Ruthenium ion catalysed oxidation technique has had a very significant role in characterizing biomarkers bound on asphaltenes from the aromatic-attached aliphatic appendages (Peng *et al.*, 1999a; Peng *et al.*, 1999b; Muhammad and Abbott, 2012). This technique allows the degradation of aromatic rings which results in the release of the acyclic and cyclic aliphatic substituents to which the aromatics are bound, as carboxylic acids (acyclic and cyclic acids) (Strausz *et al.*, 1999b; Xu *et al.*, 2003; Anlai *et al.*, 2008; Ma *et al.*, 2008). The technique has been tested using model compounds for identifying oxidation products (Mojelsky *et al.*, 1992).

In this study, the procedure adopted involves adding purified asphaltenes (~50 mg) to a 100 mL conical flask and DCM (~4 mL) and stirring until it dissolved completely. Then acetonitrile (~4 ml) was added to the mixture, followed by (~5 mL) of 12% aqueous sodium periodate (NaIO_4) and RuCl_3 (~5 mg). This was mixed in orbital shaker for 24 h at room temperature and during the course of chemical reaction the solution turned yellow. Then DCM (~10 mL) and methanol (~10mL) were added to destroy excess oxidising agent and then the mixture was transferred to centrifuge tubes and these were centrifuged (3500 rpm, 15 minutes). After the initial centrifugation, the supernatant was carefully decanted and the residue washed with DCM and water (~10 mL each). This process was again repeated for two more times. The recovered washings were combined with the supernatant and the organic phase, containing free carboxylic acids. The

solvent in the organic phase was removed by rotary evaporation (25 °C, 25 mmHg), following the addition of acetone (~5 mL) and re-evaporation to remove traces of water.

3.3.5.1 Esterification of acids

About 1mL of DCM was used to transfer the acid fraction into a boiling tube before adding 25 µL of internal standard (1 mg/mL C₁₅D₃₁COOH) and 5 mL of 2% concentrated sulphuric acid in methanol. This mixture was then added with 3 - 4 anti-bumping granules and placed in a test tube heater for 3 hrs. These granules avoiding the sudden production of large gas bubbles which can lead to 'bumping' in the boiling tube. After boiling the mixture was allowed cooling before adding 10 mL of deionised water and extracted with 10 mL DCM repeatedly for three different times. The DCM extract was then washed with 4 mL of 2% NaHCO₃. This extract was extracted again with DCM (10 mL, x 3) before drying over anhydrous Na₂SO₄ and excess solvent was removed using a rotary evaporator at room temperature to about 1 mL and the esters transferred into a GC vial for GC and GC-MS analysis.

3.3.6 Preparation of samples for Fourier transform infrared spectroscopy (FTIR)

To prepare the sample for FTIR measurement, the isolated and purified *n*-hexane asphaltenes from the crude oils were ground into fine powder with an agate mortar and pestle until the grains were not visible. The powdered asphaltenes were then stored in glass vial ready for FTIR measurements on diamond Smart Orbit - Nicolet 6700 FT-IR spectrometer.

3.3.7 Preparation of samples for ultrasonic spectroscopy

The *n*-hexane isolated and purified asphaltenes used for the study were powdered and weighed using Mettler Toledo (Model MT5) 6 figure balance that was internally calibrated before use. Samples were prepared by mixing the weighed asphaltene powder with a known amount of toluene solvent (VWR Prolabo, purity of 99.5% Analar grade - Rampur) from the highest concentration to the lowest concentration of 2.3 g/L, with a stepwise reduction using volumetric flask and pipette with an error (± 0.06) as described by Andreatta *et al.* (2005a). The diluted asphaltene solutions was stirred and allow to

equilibrate for 15 – 20 minutes before applying per test from the lowest concentration to the highest concentration.

3.4 Analytical techniques

3.4.1 Gas chromatography (GC)

Gas chromatography was performed on the aliphatic and aromatic hydrocarbon fractions of the whole oils, maltenes and RICO products in order to determine that the concentration were right for GC-MS analysis. The compounds were analysed using Hewlett-Packard 5890 Series II gas chromatography equipped with a fused silica capillary column (30 m x 0.25 mm i.d) coated with 0.25 µm dimethyl polysiloxane (HP-5 phase). The GC oven temperature was initially programmed from 50 °C – 310 °C at 5 °C min and then held at final temperature for 26 minutes with helium as the carrier gas (flow 1 mL/min, pressure of 52.76 kPa, split at 32 mL/min). The sample (1 µL) in hexane/DCM was injected by an HP7673/7683 auto sampler and the split opened after 1 minute. After the solvent peak had passed the GC temperature programme and data acquisition commenced. The acquisition was stored on an Atlas laboratory data system on a desktop computer.

3.4.2 Gas chromatography-mass spectrometry (GC-MS)

The saturated hydrocarbon fractions of the whole oils, maltenes and RICO products of the acids were analysed by gas chromatography-mass spectrometry analyses on a Agilent 6890 GC equipped with splitless mode injector at (280 °C) linked to a Agilent 5975C MSD (electron voltage 70 eV, source temperature 230 °C, quadruple temperature 150 °C multiplier voltage 1800V, interface temperature 310 °C). The acquisition was controlled by MSD Chemstation software. The samples were analysed initially in full scan mode 50 - 600 atomic mass units/second (amu/sec) or in selected ion mode (SIM) for 35 ions dwell time per ion for greater sensitivity. The sample (1µL) in hexane was injected by an HP 7673 auto sampler and the split opened after 1 minute. After the solvent peak had passed the GC temperature programme and data acquisition commenced.

Separation of the aliphatic and aromatic hydrocarbon fractions and RICO products of the acids were performed on an Agilent fused silica capillary column (30 m x 250 μ m x 0.25 μ m) coated with 5% phenyl methyl siloxane (HP-5) phase. The GC was temperature programmed from 50 - 310 °C at 5 °C min and held at final temperature for 26 minutes with helium as the carrier gas (flow rate of 1ml/min, initial pressure of 52.76 kPa, split at 30 ml/min).

The acquired ions for the aliphatics, aromatics and acid fractions were monitored in the selected ion modes (SIM) and full scan modes (Appendix 3.2). Some of the ions for the aliphatic hydrocarbon fractions were; m/z 85 for the *n*-alkanes and isoprenoids, m/z 109 (diterpanes), m/z 123 (tetracyclic terpanes), m/z 149 (trisnorhopanes), m/z 163 (bisnorhopane), m/z 177 (demethylated hopanes), m/z 183 (acyclic isoprenoids), m/z 191 (triterpanes), m/z 205 (methylhopanes), m/z 217 (steranes), m/z 218 (steranes), m/z 219 (steranes), m/z 231 (methyl steranes). Compounds were identified from mass chromatograms of diagnostic ions and mass spectra by comparison with published literature (Peters *et al.*, 2005b).

3.4.3 Fourier transform infrared spectroscopy (FTIR)

The FTIR measurements were performed using Thermo Scientific Nicolet 6700 FTIR spectrometer in absorbance mode and a diamond smart orbit accessory. The precipitated *n*-hexane asphaltene samples were finely powdered in an agate mortar. About 5 - 10 mg of asphaltene was carefully placed with a spatula on the attenuated total reflectance (ATR) crystal (Diamond MIRacle) with an approximate diameter of 100 μ m and the spring-loaded ATR accessory was carefully lowered to make contact with the surface of the asphaltene sample at an incidence angle of 45° prior to the ATR-FTIR measurements. This was done gently as the asphaltene surface could be damaged by forceful contact with the internal reflection element. Consequently, ART-FTIR involves the collection of radiation reflected from the interface between the sample and a Zinc Selenide crystal (ZnSe), by which an evanescent wave penetrates from the crystal into the powder asphaltenes to obtain absorbance information as an interferogram signal. This interferogram signal permits sampling to generate an infrared spectrum while penetrating only a short distance (~1 – 4 micrometres) into the sample. However, prior to sample analysis, air was obtained under same sample condition through the relevant

ATR element when it was not in contact with the sample as background reference for each sample spectrum to enable direct comparison against absorbance libraries using OMNIC spectra software. Hence, all sample measurements resulted from an accumulation of 32 scans with a spectral resolution of 4 cm^{-1} in the $4000 - 500\text{ cm}^{-1}$ spectral domain and spectral calculations were performed using OMNIC software (version 6.1, Nicolet 6700 instrument Corp.). In order to evaluate the reproducibility of the method, each sample was based on replicate analysis. The total analysis time for each asphaltene sample by ATR was less than 1 minute.

3.4.4 Ultrasonic spectroscopy of asphaltenes in organic solvent

In this study, a high-precision ultrasound resonance spectroscopy (ResoScanTM, 2007) from TF Instruments GmbH, Germany (Figure 3.9) was used, which is specifically designed for the characterization of longitudinal (compressions and rarefactions) properties in the material (ResoScanTM, 2007). The acoustic ResoscanTM is similar to the instrument used by Andreatta *et al.* (2005a), but with several modifications that significantly improve precision. Both instruments are based on the “transmission” principle for measuring the speed of sound; however attenuation of sound was also used. The instrument has a resonance cavity with two channel-resonators Unit (RU) with built in resonator cells and Peltier thermostat (ResoscanTM – Research System from TF Instruments GmbH, Germany (Figure 3.9). The system has four main units: (I) 2-Channel-Resonator unit (RU), (II) Cell temperature measurement unit (CTM), (III) Peltier thermostat control unit (PTC), (IV) Resonator unit lid and metal block for the resonator unit. It measures the speed and attenuation of acoustic waves at high ultrasonic frequency propagating through liquid samples as a function of time or temperature.

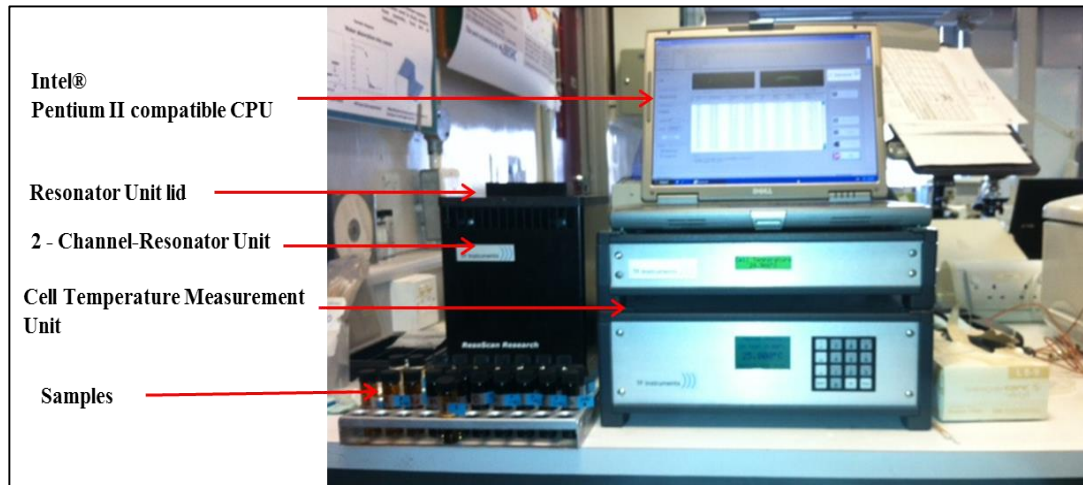


Figure 3.9: High-precision Resoscan™ ultrasound spectrometer.

The instrument is equipped with temperature measurement, set-up together in a regular block surface and connected to an internal thermometer. The instrument is then thermostated at atmospheric temperature of $25\text{ }^{\circ}\text{C} \pm 0.005\text{ }^{\circ}\text{C}$, so as to provide a stable temperature of measurement of the ultrasound resonance instrument. In this study, $\sim 2.3\text{ g}$ of asphaltene powder in 1 L of toluene was used as the sample. Aliquots of this stock sample were diluted further on a mass basis to prepare asphaltene solutions in the $\sim 0.06 - 2.3\text{ g/L}$ concentration range. The measurement, involves the simultaneous determination of the ultrasonic attenuation and ultrasonic speed of sound with high accuracy and reproducibility in two identical cells, each containing a given volume of $170 - 250\text{ }\mu\text{L}$ pure toluene solvent and analytic (asphaltenes) solution in the frequency range of $7 - 12\text{ MHz}$ and signal strength of 12 dB . The sound speed and attenuation frequency spectra are parameters of interest and are temperature dependent. Measurements were performed at several different concentrations ranging from $\sim 0.06 - 2.3\text{ g/L}$. At least 10 measurements were made at each concentration of interest at $\sim 25\text{ }^{\circ}\text{C}$ and after each test; the cells were properly cleaned with toluene to avoid contamination. The interpretation of the formation of asphaltene aggregation is calculated by plotting either average sound velocity or sound attenuation as a function of asphaltene concentration as described in Section 8.3.1 and Figure 8.3.

Chapter 4 Oil and coal characterisation using conventional molecular parameters

4.1 Introduction

Biomarkers provide valuable information that are used for source/depositional environment/thermal maturity/correlation of oil and their source rocks, as well as the degree of alteration for the oil (Peters and Fowler, 2002; Gürgey, 2003; Peters *et al.*, 2005b). Therefore, using the biomarker concept, oil fractions, in the absence of source rock samples, can give significant clues about the nature of their source rocks (Hughes *et al.*, 1995).

The objectives of this chapter are to use conventional organic geochemical molecular tools to broadly characterise the oils and coals in this study in terms of source facies input, thermal maturation and extent of biodegradation of the oils. This information will be used for ruthenium ion catalysed oxidation and ultrasonics study of the asphaltenes presented in the subsequent chapters of this thesis.

4.2 Methods

All samples (oils and coal extracts) were fractionated into aliphatic, aromatic and resin fractions as described in Chapter three, Section 3.3.3. The aliphatic and aromatic fractions were then analysed by gas chromatography (GC) experimental conditions as discussed in section 3.4.1 to produce normal and isoprenoid alkanes data. In addition, hopanes (tricyclic, tetracyclic and pentacyclic terpanes) were generated from the m/z 191; steranes using m/z 217, polymethyl aromatic compounds from m/z 142 for methylnaphthalenes; m/z 156 for dimethylnaphthalenes; m/z 178 for phenanthrene and m/z 192 for methylnaphthalenes were analysed by gas chromatography-mass spectrometry (GC-MS) analyses as discussed in section 3.4.2. The detailed results obtained from all these analyses are tabulated in Table 4.1 – 4.13 of this thesis. Furthermore, biomarker data and principal component analysis (PCA) for the oil and coal samples has been statistically examined by IGI's p: 3.5. The PCA reduce the dimensionality of the data by extracting latent variables to a few important groups to confirm the groupings established earlier.

4.3 Results and discussion

4.3.1 Molecular characteristics of oils

4.3.1.1 *Normal alkanes and acyclic isoprenoids*

Gas chromatograms of selected non-degraded (NE (O)) and biodegraded (NC (O)) crude oils are presented in Figure 4.1. Generally, the analysed non-degraded samples are dominated by *n*-alkane distributions of $n\text{C}_{11} - n\text{C}_{34}$ and isoprenoids pristane (Pr) and phytane (Ph). However, there is evidence of biodegradation in some of the samples as in sample NC (O) shown in Figure 4.1, (unresolved complex mixture (UCM) due to possible significant microbial attack). The biodegraded oils show depletion of *n*-alkanes. The geochemical ratios based on the *n*-alkanes distribution are presented in Table 4.1. The Pr and Ph were identified in the GC of all studied oils, with exception of NB (O), NC (O) UK80 (O) and UKV (O). The pristane/phytane (Pr/Ph) ratio is commonly used in organic geochemistry as an indicator of redox conditions in the depositional environment and source rock attributes of the oil (Didyk et al., 1978; Tissot and Welte, 1984; Powell, 1988). The interpretation infers that oils derived from mainly land plants would be expected to have $\text{Pr}/\text{Ph} > 3.0$ (oxidizing conditions), low values of (Pr/Ph) ratio (< 0.6) are indicative of marine (anoxic conditions) and values between 0.6 and 3.0 suggest intermediate conditions (dysoxic conditions). However, care has to be taken in drawing conclusions on the redox conditions derive from Pr/Ph ratios, as they are influenced by other complicating factors (Didyk et al., 1978; Peters et al., 2005a).

The (Pr/Ph) ratios for the studied oils range from 0.35 – 4.59 (Table 4.1 & Figure 4.2) suggesting oils derived from marine to terrigenous organic matter deposited in environmental conditions that transcend anoxic to oxic conditions (IGI, 2004) with oil samples from Nigeria showing more oxic condition. The oils were further classified based on associated source rock by plotting the ratio of $\text{Pr}/n\text{C}_{17}$ against $\text{Ph}/n\text{C}_{18}$ in Figure 4.3. In general, the diagram infers that the studied oils derived probably from terrigenous higher plant and or rich in marine organic matter. The ratio of dibenzothiophene/phenanthrene (DBT/PHEN) and the ratio of pristane to phytane have been used to infer source rock and depositional environment (Hughes et al., 1995). Therefore, using the criteria proposed by these authors, $(\text{DBT}/\text{PHEN})/(\text{Pr}/\text{Ph})$, the oils

are derived from marine + lacustrine (sulphate rich), lacustrine (sulphate poor), marine (+ lacustrine) shale and fluvio/deltaic (carbonaceous shale, coal) influence (Figure 4.4).

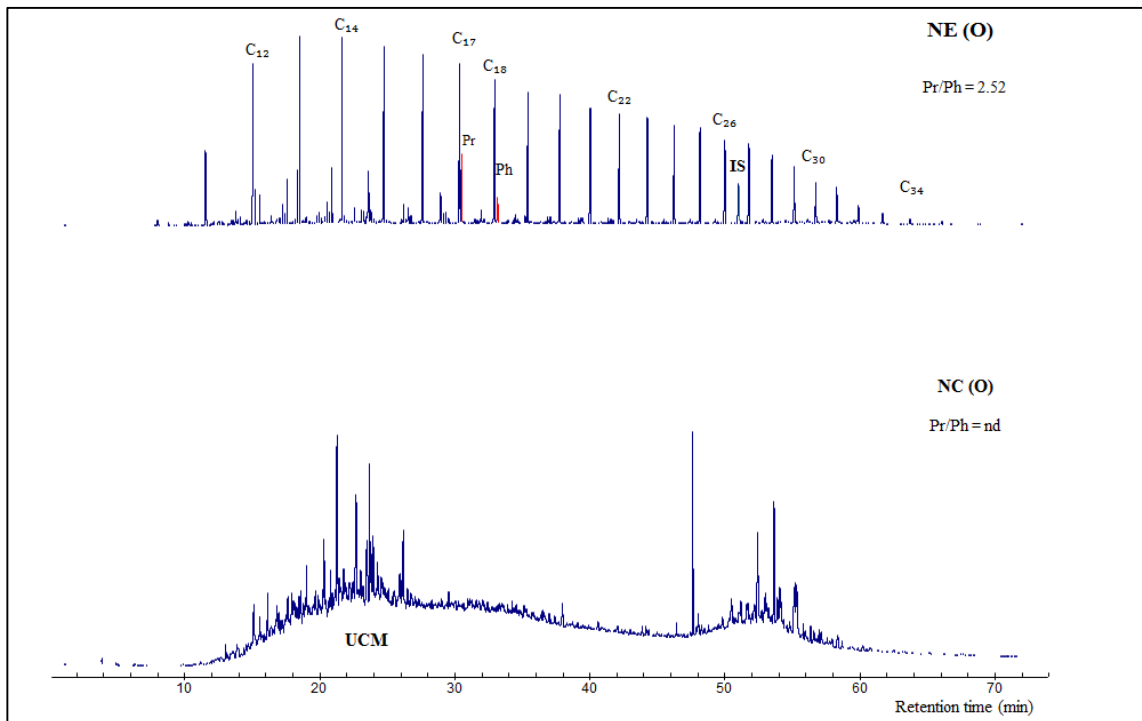


Figure 4.1: Representative GC/FID chromatograms of saturated hydrocarbon fractions of selected non-degraded NE (O) and biodegraded NC (O) crude oils from Nigeria.
IS = Internal standard, UCM = unresolved complex mixture.

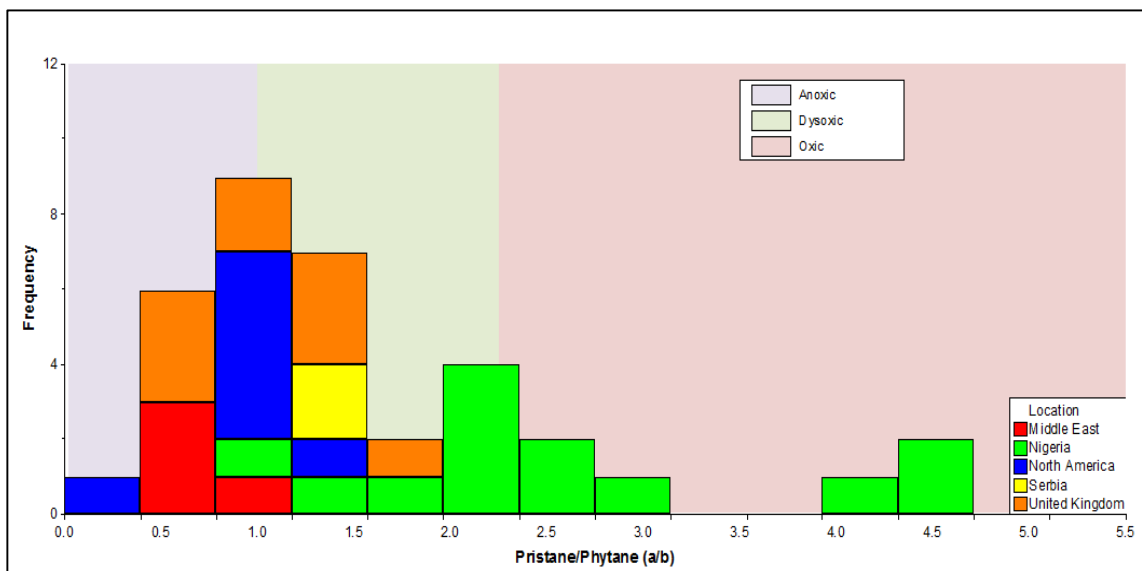


Figure 4.2: Source rock anoxia inferred from the histogram of pristane/phytane ratios for the studied oils (After IGI's p3.5 geochemical interpretation software).

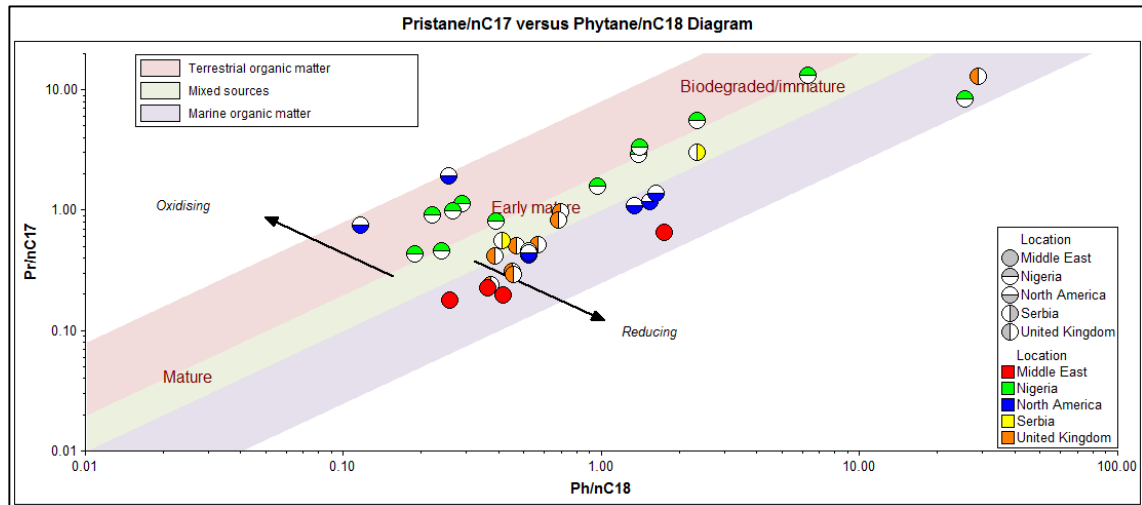


Figure 4.3: Relationship between Pr/nC₁₇ against Ph/nC₁₈ for the studied oils (After IGI's p:3.5 geochemical interpretation software).

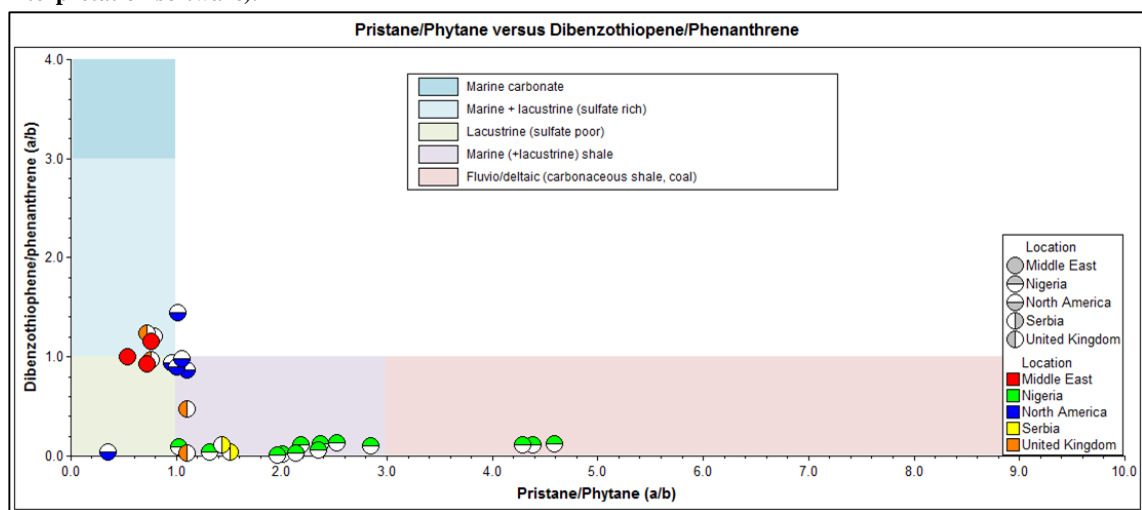


Figure 4.4: A cross plot of dibenzothiophene/phenanthrene ratio (DBT/PHEN) and the ratio of pristane to phytane for the studied oils (After IGI's p: 3.5 geochemical interpretation software).

Table 4.1: Normal alkane and isoprenoid alkane distribution of the studied crude oil samples.

Sample	Type	Location	Pr/Ph	NorPr/Ph	Pr/nC ₁₇	Ph/nC ₁₈	nC ₁₇ /nC ₁₈	CPI
NA1 (O)	Oil	Nigeria	4.59	0.33	0.92	0.22	1.80	1.13
NB2 (O)	Oil	Nigeria	4.38	0.33	1.14	0.29	2.58	0.95
NC3 (O)	Oil	Nigeria	4.29	0.34	1.00	0.26	2.14	1.12
NA (O)	Oil	Nigeria	1.02	nd	1.57	0.97	nd	nd
NB (O)	Oil	Nigeria	nd	nd	nd	Nd	nd	nd
NC (O)	Oil	Nigeria	nd	nd	nd	Nd	nd	nd
ND (O)	Oil	Nigeria	2.36	0.52	0.81	0.39	2.03	1.16
NE (O)	Oil	Nigeria	2.52	0.51	0.44	0.19	1.92	1.09
NF (O)	Oil	Nigeria	2.18	0.56	0.46	0.24	2.02	0.78
NO (O)	Oil	Nigeria	1.32	0.62	8.47	25.55	nd	nd
NN (O)	Oil	Nigeria	2.35	nd	2.92	1.40	1.95	nd
N25 (O)	Oil	Nigeria	2.01	0.41	13.14	6.31	1.13	nd
N18 (O)	Oil	Nigeria	1.96	0.37	27.89	11.79	0.44	nd
NNI (O)	Oil	Nigeria	2.84	0.37	3.32	1.41	1.90	nd
NN41 (O)	Oil	Nigeria	2.13	0.43	5.60	2.35	0.65	1.04
UKB (O)	Oil	United Kingdom	1.11	0.69	13.08	28.85	nd	nd
UK88 (O)	Oil	United Kingdom	1.10	0.76	0.52	0.57	4.24	0.95
UK85 (O)	Oil	United Kingdom	1.58	0.44	0.96	0.70	3.02	1.05
UK66 (O)	Oil	United Kingdom	1.25	0.87	0.42	0.39	5.30	0.99
UK65 (O)	Oil	United Kingdom	1.27	0.76	0.50	0.47	4.53	1.00
UK80 (O)	Oil	United Kingdom	nd	nd	nd	Nd	nd	nd
UK34 (O)	Oil	United Kingdom	1.33	0.60	0.82	0.68	3.25	1.06
UK11 (O)	Oil	United Kingdom	0.76	0.88	0.24	0.37	5.39	0.97
UK01 (O)	Oil	United Kingdom	0.78	0.95	0.31	0.45	4.76	0.93
UK05 (O)	Oil	United Kingdom	0.72	0.86	0.30	0.46	4.14	0.94
UKV (O)	Oil	United Kingdom	nd	nd	nd	Nd	nd	nd
NA72 (O)	Oil	North America	0.95	0.91	1.09	1.34	5.91	nd
NA73 (O)	Oil	North America	1.10	0.81	0.75	0.12	5.91	1.01
NA74 (O)	Oil	North America	1.10	0.92	0.46	0.52	6.12	1.00
NA75 (O)	Oil	North America	1.01	0.87	1.18	1.54	5.49	nd
NA79 (O)	Oil	North America	1.24	0.82	1.39	1.62	10.26	nd
NA61 (O)	Oil	North America	1.02	1.01	0.43	0.52	8.50	nd
NA76 (O)	Oil	North America	1.05	0.91	0.44	0.52	5.85	1.16
NAC (O)	Oil	North America	0.35	nd	1.91	0.25	nd	nd
ME77 (O)	Oil	Middle East	0.54	1.26	0.2	0.42	5.34	1.08
ME39 (O)	Oil	Middle East	0.76	0.82	0.18	0.26	4.56	0.97
ME43 (O)	Oil	Middle East	0.72	0.69	0.23	0.36	5.36	1.01
ME12 (O)	Oil	Middle East	0.89	0.6	0.66	1.74	7.45	1.04
SN1 (O)	Oil	Serbia	1.51	nd	3.04	2.34	nd	nd
SN2 (O)	Oil	Serbia	1.44	0.50	0.56	0.41	1.95	1.47

Pr/Ph = pristane/phytane ratio; Didyk *et al.* (1978); (Peters *et al.*, 2005b). Nor Pr: nor pristane (C₁₈ isoprenoid); Pr/nC₁₇ and Ph/ nC₁₈; nC₁₇ and nC₂₇ are n-alkanes with the 17, 18 and 25 carbon chain lengths (Peters *et al.*, 2005a); CPI = 0.5 x (((nC₂₅+2nC₂₇+nC₂₉+nC₃₁+nC₃₃)/(nC₂₄+nC₂₆+nC₂₈+nC₃₀+nC₃₂)) + ((nC₂₅+nC₂₇+nC₃₁+nC₃₃)/(nC₂₆+nC₂₈+nC₃₀+nC₃₂+nC₃₄))); Bray and Evans (1961). nd: not determined due to low concentration in the parameter.

4.3.1.2 Steranes

The measured ratios from the sterane distributions are listed in Table 4.3 and the C₂₇ – C₂₉ $\alpha\alpha\alpha$ steranes in the oils show mixed kerogen types (terrestrial and marine) characteristics with results in the range of 14% – 53%, 8% – 31% and 27% – 65% for the C₂₇, C₂₈ and C₂₉ $\alpha\alpha\alpha$ steranes respectively. However, the abundance of C₂₉ regular steranes, is higher compared to the C₂₇ and C₂₈ regular steranes (Figure 4.7) suggests a terrigenous contribution in the oils. The Nigerian oils (NO and NN), United Kingdom oils (UK85 and UK88), North American oils (NAC), and Middle East oils (ME77, ME39 and ME12) are comparatively richer in cholestane (C₂₇), suggesting a greater input in marine organic matter (Huang and Meinschein, 1979).

Generally, diasteranes and regular steranes are included in the biomarkers commonly used for maturity assessment (Seifert and Moldowan, 1978; Peters and Fowler, 2002). In the oils, sterane (C₂₉ $\alpha\alpha\alpha$) 20S/(20S + 20R) and $\alpha\beta\beta/\alpha\beta\beta + \alpha\alpha\alpha$ ratios range from 0.28 – 0.57 and 0.36 – 0.60 respectively (Table 4.3). These values are consistent with oils generated from immature to mature source rocks (Peters *et al.*, 2005a), which is further supported by Figure 4.8 that shows low to mid maturity status of the oils.

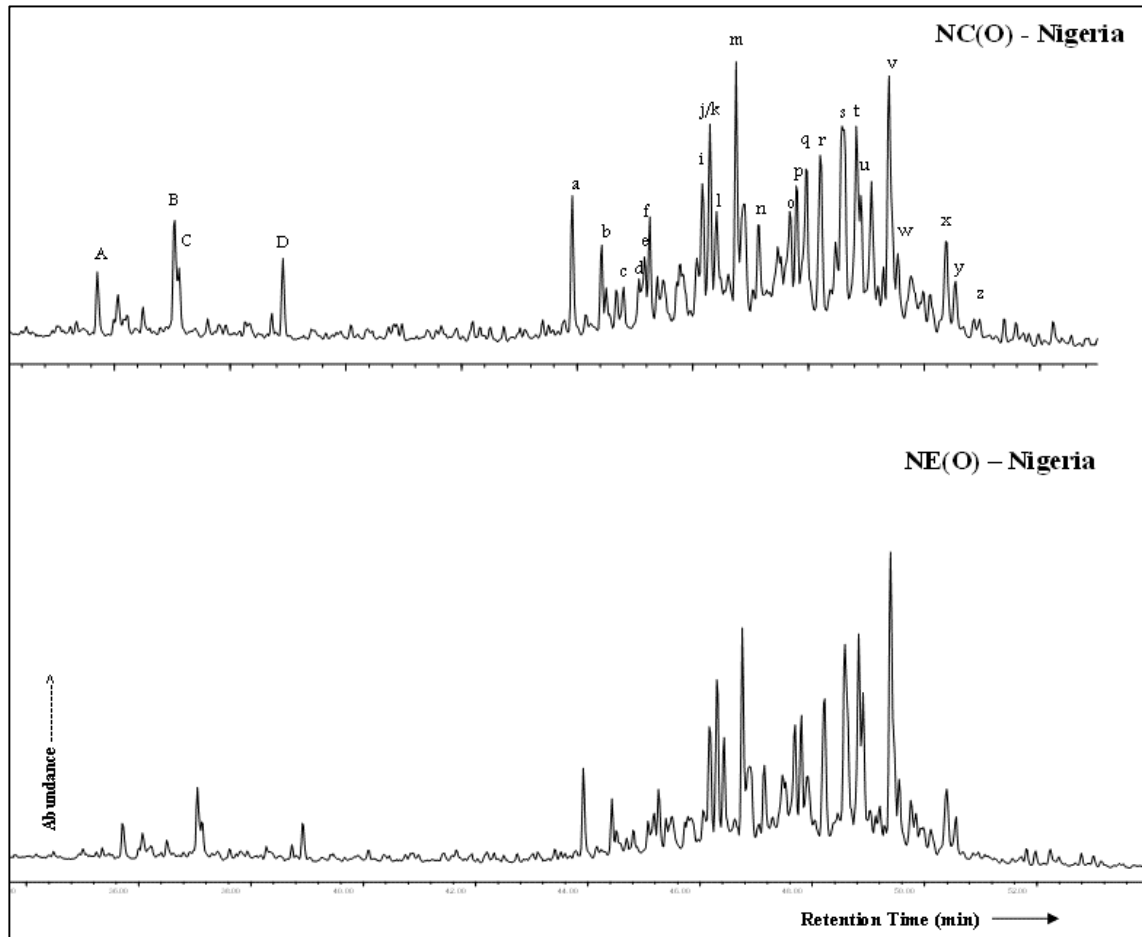


Figure 4.5: Representative GC-MS mass chromatogram m/z 217 showing the distributions of C₂₇, C₂₈ and C₂₉ steranes from crude oil samples NC (O) and NE (O) from Nigeria. See Table 4.2 for peaks identification.

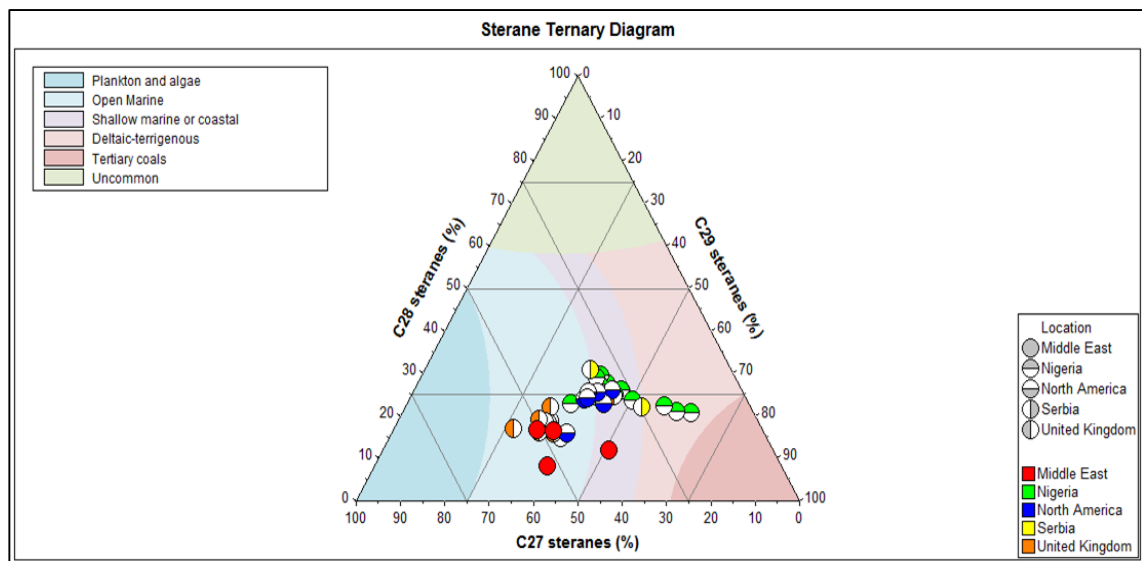


Figure 4.6: Ternary diagram showing the distribution of the C₂₇, C₂₈, and C₂₉-Steranes from GC-MS analyses of studied oils interpreted in terms of likely depositional environment. (After IGI's p: 3.5 geochemical interpretation software).

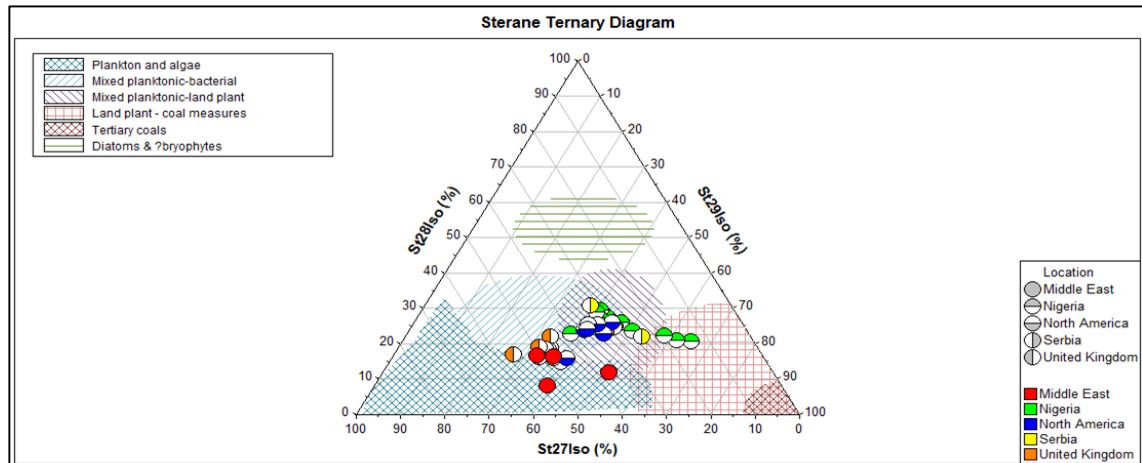


Figure 4.7: Ternary diagram showing the distribution of the C₂₇, C₂₈, and C₂₉-Steranes from GC-MS analyses of the studied oils interpreted in terms of likely source precursors. (After IGI's p: 3.5 geochemical interpretation software).

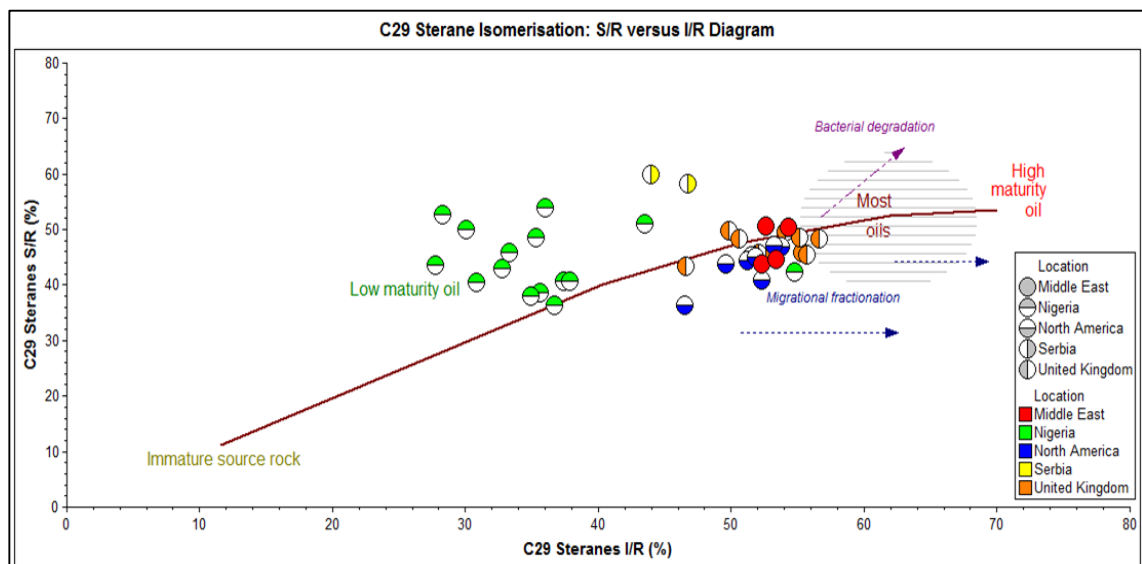


Figure 4.8: Cross plot of C₂₉ steranes I/R against C₂₉ steranes S/R parameter defines oils into various zones of thermal maturity (After IGI's p: 3.5 geochemical interpretation software).

Table 4.2: Sterane and hopane peak assignment (IGI, 2004).

Peak	Sterane compound name	Peak	Hopane compound name
A	Diapregnane	19T	C ₁₉ -tricyclic terpane
B	Pregnane	20T	C ₂₀ -tricyclic terpane
C	Homodiapregnane	21T	C ₂₁ -tricyclic terpane
D	Methylpregnane	22T	C ₂₂ -tricyclic terpane
a	C ₂₇ 13β(H), 17α(H),20S- diacholestane	23T	13β(H),14α(H)-18,19-dinorcheilanthane
b	C ₂₇ 13β(H), 17α(H),20R- diachlestane	24T	13β(H),14α(H)-19-norcheilanthane
c	C ₂₇ 13α(H), 17β(H),20S- diachlestane	T25S-T25- T25R	13β(H),14α(H)- cheilanthane (25S+25R)
d	C ₂₇ 13α(H), 17β(H),20R- diachlestane	24T (H)	18β(H)-de-E-hopane
e	C ₂₈ 13β(H), 17α(H),20S-24-methyldiachlestane	T26 S) + (T26 R)	13β(H),14α(H)-19-methylcheilanthane (25S+25R)
f	C ₂₈ 13β(H), 17α(H),20S-24-methyldiachlestane	T28S	13β(H),14α(H),25S-19-n-propylcheilanthane
g	C ₂₈ 13β(H), 17α(H),20R-24-methyldiachlestane	T28R	13β(H),14α(H),25R-19-n-propylcheilanthane
h	C ₂₈ 13β(H), 17α(H),20R-24-methyldiachlestane	T29S	13β(H),14α(H),25S-19-i-butylcheilanthane
i	C ₂₇ 5α(H), 14α(H), 17α(H),20S-cholestane	T29R	13β(H),14α(H),25R-19-i-butylcheilanthane
j/k	C ₂₇ 5α(H),14β(H),17β(H),20R-cholestane+C ₂₉ 13β(H),17α(H),20Sdiasterane	Ts	18α(H)-22-29,30-trisnorhopane (Ts)
l	C ₂₇ 5α(H), 14β(H), 17β(H),20S-cholestane	Tm	17α(H)-22,29,30-trisnorhopane (Tm)
m	C ₂₇ 5α(H), 14α(H), 17α(H),20R-cholestane	28H	17α(H), 18α(H)-28,30-bisnorhopane (+) 17β(H), 18α(H)-28,30-bisnormorethane
n	C ₂₉ 13β(H), 17α(H)-20R-24-ethyldiachlestane	29H	17α(H)-25norhopane
o	C ₂₈ 5α(H), 14α(H),17α(H),20S-24-methylcholestane	29Ts	17α(H)-norhopane
p	C ₂₈ 5α(H), 14β(H), 17β(H),20R-24-methylcholestane	29M	17β(H)-normorethane
q	C ₂₈ 5α(H), 14β(H), 17β(H),20S-24-methylcholestane	OL	18α(H)-oleanane
r	C ₂₈ 5α(H), 14α(H), 17α(H),20R-24-methylcholestane	30H	17α(H)-hopane
s	C ₂₉ 5α(H), 14α(H), 17α(H),20S-24-ethylcholestane	30M	17β(H), 21β(H)-morethane
t	C ₂₉ 5α(H), 14β(H), 17β(H),20R-24-ethylcholestane	31S	17α(H)-22S-homohopane
u	C ₂₉ 5α(H), 14β(H), 17β(H),20S-24-ethylcholestane	31R	17α(H)-22R-homohopane
v	C ₂₉ 5α(H), 14α(H), 17α(H),20R-24-ethylcholestane	Ga	gammacerane
w	C ₃₀ 5α(H), 14α(H), 17α(H),20S-24-propylcholestane	31S, R Mor	17β(H)-homomorethane (22S+22R)
x	C ₃₀ 5α(H), 14β(H), 17β(H),20R-24-propylcholestane	32S	17α(H)-22S-dihomohopane
y	C ₃₀ 5α(H), 14β(H), 17β(H),20S-24-propylcholestane	32R	17α(H)-22R-dihomohopane
z	C ₃₀ 5α(H), 14α(H), 17α(H),20R-24-propylcholestane	33S	17α(H)-22S-trihomohopane 33R 34S 34R 35S 35R
			17α(H)-22R-trihomohopane 17α(H)-22S-tetrahomohopane 17α(H)-22R-tetrahomohopane 17α(H)-22S-pentahomohopane 17α(H)-22R-pentahomohopane

Table 4.3: Source and maturity parameters computed from steranes in the studied oils.

New Name	Preg	20S(20S+20R)		20S(20S+20R)		20S(20S+20R)		20S(20S+20R)		Sterane (%)		
		C ₂₉ ααα	C ₂₉ αββ	C ₂₇ ααα	C ₂₈ ααα	C ₂₇ ααα	C ₂₈ ααα	C ₂₉ ααα				
NA1 (O)	7.01	0.28	0.44	0.13	0.19	14	21	65				
NB2 (O)	8.94	0.30	0.50	0.15	0.18	17	21	62				
NC3 (O)	8.58	0.28	0.53	0.17	0.19	19	22	58				
NA (O)	12.89	0.36	0.54	0.27	0.23	31	26	43				
NB (O)	11.00	0.35	0.48	0.27	0.24	30	26	44				
NC (O)	14.51	0.43	0.51	0.25	0.23	30	28	43				
ND (O)	13.84	0.33	0.46	0.24	0.23	27	26	47				
NE (O)	9.98	0.33	0.43	0.22	0.21	26	24	50				
NF (O)	9.02	0.31	0.41	0.27	0.23	29	25	46				
NO (O)	19.59	0.55	0.42	0.42	0.14	47	15	39				
NN (O)	15.20	0.37	0.36	0.37	0.21	40	23	37				
N25 (O)	11.69	0.36	0.39	0.29	0.24	32	26	42				
N18 (O)	12.97	0.37	0.41	0.28	0.27	30	30	40				
NNI (O)	11.87	0.38	0.41	0.29	0.25	31	28	41				
NN41 (O)	12.64	0.35	0.38	0.29	0.27	31	29	40				
UKB (O)	17.20	0.55	0.46	0.43	0.14	48	16	36				
UK88 (O)	18.24	0.50	0.50	0.30	0.22	34	25	41				
UK85 (O)	8.59	0.47	0.43	0.26	0.22	29	25	46				
UK66 (O)	22.69	0.52	0.46	0.51	0.15	56	17	27				
UK65 (O)	20.11	0.54	0.50	0.39	0.16	47	19	34				
UK80 (O)	18.97	0.53	0.46	0.40	0.19	45	22	33				
UK34 (O)	23.00	0.51	0.48	0.42	0.16	48	18	34				
UK11 (O)	15.24	0.52	0.45	0.43	0.15	48	17	36				
UK01 (O)	18.47	0.57	0.48	0.45	0.17	48	19	33				
UK05 (O)	21.78	0.55	0.49	0.47	0.15	51	16	33				
UKV (O)	18.22	0.56	0.45	0.45	0.17	49	19	32				
NA72 (O)	20.20	0.50	0.44	0.35	0.23	37	24	39				
NA73 (O)	20.23	0.52	0.45	0.31	0.23	33	25	42				
NA74 (O)	20.14	0.51	0.44	0.27	0.24	29	26	45				
NA75 (O)	20.25	0.52	0.45	0.30	0.21	33	23	44				
NA79 (O)	22.67	0.54	0.47	0.31	0.24	33	26	42				
NA61 (O)	17.16	0.52	0.41	0.32	0.23	35	26	39				
NA76 (O)	19.33	0.53	0.47	0.34	0.23	36	24	40				
NAC (O)	29.03	0.46	0.36	0.41	0.15	44	16	39				
ME77 (O)	29.59	0.52	0.44	0.45	0.16	47	17	36				
ME39 (O)	28.55	0.54	0.50	0.50	0.08	53	8	39				
ME43 (O)	12.84	0.53	0.45	0.35	0.11	37	12	51				
ME12 (O)	7.25	0.53	0.51	0.50	0.17	51	17	32				
SN1 (O)	5.01	0.44	0.60	0.23	0.21	24	22	53				
SN2 (O)	16.82	0.47	0.58	0.29	0.29	32	31	37				

Preg = diginane + 5α-pregnane + 20-methyldiginane + 5α methylpregnane/ same + C₂₉ 5α, 14α, 17α 20R + C₂₉ 5α, 14α, 17α 20S + C₂₉ 5α, 14β, 17β 20R + C₂₉ 5α, 14β, 17β 20S (Mackenzie, 1984). % C₂₇ααα, C₂₈ααα and C₂₉ααα = C₂₇, C₂₈, C₂₉ as percentage of sum 27-29 for 5α(H), 14α(H), 17α(H)-20R sterane (Peters *et al.*, 2005a); C₂₉ααα Sterane = 5α(H), 14α(H), 17α(H)-C₂₉ 20S/(20S+20R) sterane; C₂₉αββ Sterane = 5α(H), 14β(H), 17β(H), C₂₉ 20S/(20S+20R) sterane; C₂₇ααα Sterane = 5α(H), 14α(H), 17α(H)-C₂₇ 20S/(20S+20R) sterane; C₂₈ααα Sterane = 5α(H), 14α(H), 17α(H)-C₂₈ 20S/(20S+20R) sterane measured in *m/z* 217 mass chromatograms (Huang and Meinschein, 1979; Peters *et al.*, 2005a).

4.3.1.3 Tricyclic and tetracyclic terpanes

Tricyclic and tetracyclic terpanes are widely occurring biomarker constituents of many sediments and crude oils (Neto *et al.*, 1982). The Nigerian oils contain a notable higher oleanane index than gammacerane index (Table 4.4) and the presence of oleanane is an indicator of terrigenous input, for samples mainly deposited in a deltaic environment (Ekweozor *et al.*, 1979; Peters *et al.*, 2005b). The oleanane index calculated from the Nigerian oils range from 0.03 – 0.53 and the Serbian oils from 0.03 – 0.07 (Table 4.4) and this reflects a high contribution of angiosperms in the source rocks that generated the oils. Generally, oleanane was detected only in the Nigerian and Serbian oils, whilst gammacerane occurs in low abundances in all oil samples. Gammacerane is an indicator of stratified water column and high abundance is often seen in saline lacustrine oils (Sinninghe Damsté *et al.*, 1995). The studied oils have relatively low gammacerane index values ranging from 0.02 – 0.27 for the Nigerian oils, 0.02 – 0.34 for the United Kingdom oils, 0.03 – 0.78 for the American oils, 0.11 – 0.33 for the Middle East oils and 0.16 -0.27 for the Serbian oils.

The Ts/(Ts+Tm) ratio is generally used as a maturity parameter for oils of similar source and can also be used to infer source depositional environment of oils of similar maturity. However, it appears to be sensitive to clay-catalysed reactions (Seifert and Moldowan, 1978). The Ts/(Ts+Tm) values for the studied oils range from 0.08 - 0.86 and those for C₂₉Ts index range from 0.02 – 0.82 (Table 4.4), indicating different maturity levels between the oil samples. Hence, the correlation between plots of Ts/Tm and 29Ts/29Tm ratios (Figure 4.10), shows early - late maturity for all the oils. The C₃₅ versus C₃₄22(S + R)-17α (H), 21β (H)-extended hopanes may be used as indicative of source rock conditions during deposition, although it is affected by thermal maturity (Peters and Moldowan, 1991). The studied oils are most likely to be derived from organic matter deposited in dysoxic to anoxic depositional condition (Figure 4.11).

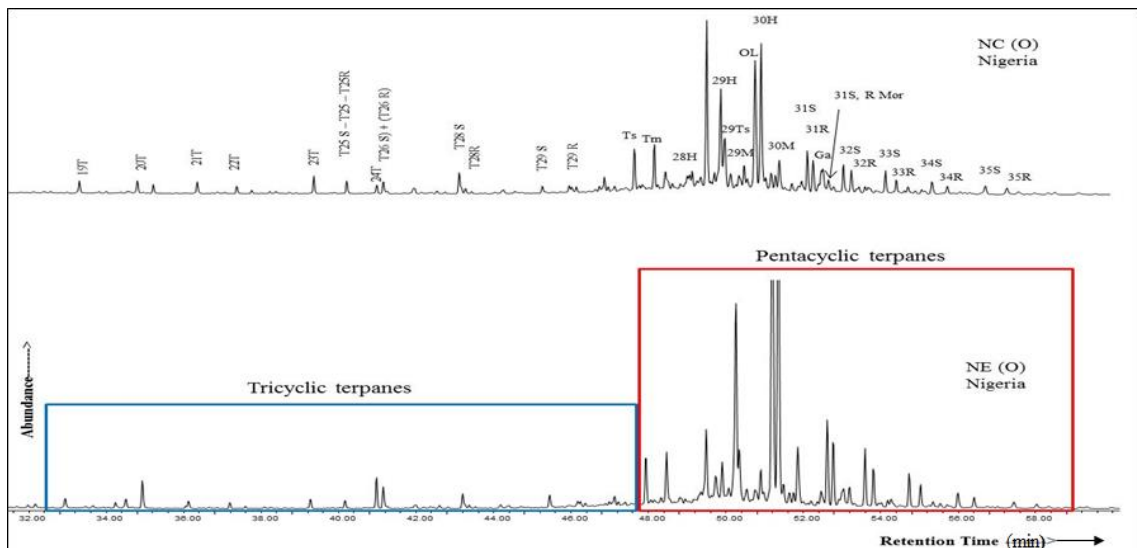


Figure 4.9: Representative partial m/z 191 mass chromatograms showing tricyclic and tetracyclic terpane distributions in NC (O) and NE (O) crude oil. Peak assignments are in Table 4.2

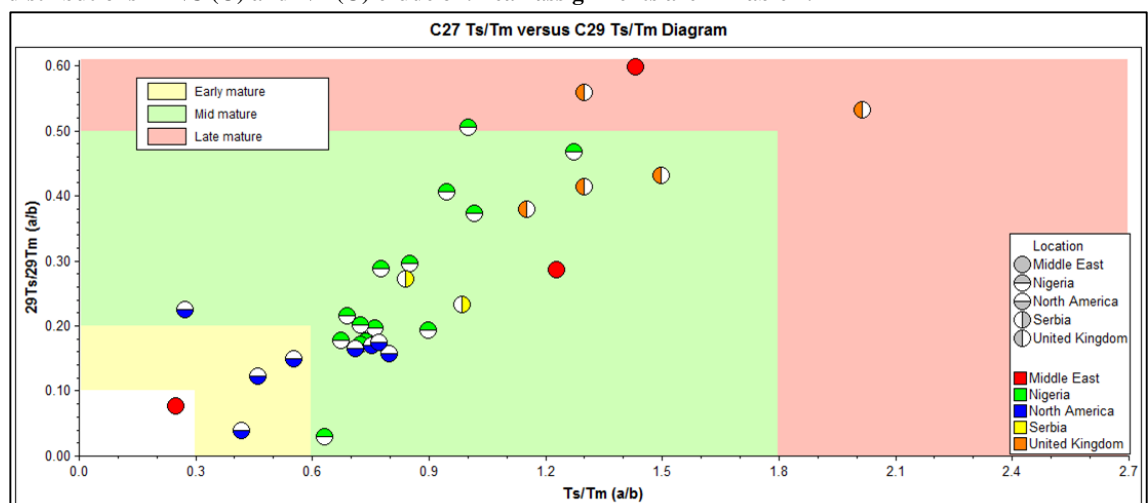


Figure 4.10: Correlation between Ts/Tm and 29Ts/29Tm ratios showing the maturity of the studied oils (after IGI's p: 3.5 geochemical interpretation software).

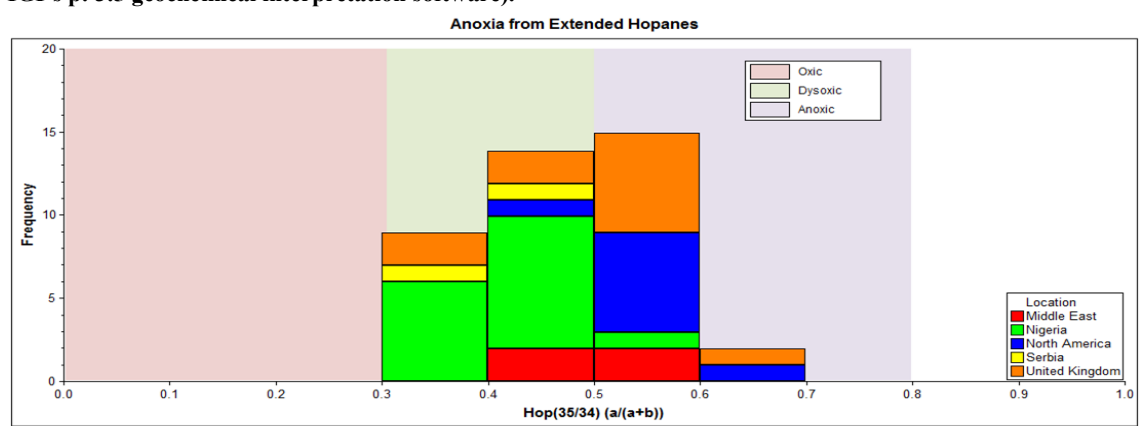


Figure 4.11: Source rock anoxia inferred from extended hopanes (Hop (35/34)) ratios of the studied oils (after IGI's p: 3.5 geochemical interpretation software).

Table 4.4: Biomarker ratios based on terpane (*m/z* 191) in the studied crude oils.

Sample Name	Ts/(Ts+Tm)	29Ts/29Tm	29Hops	30Hops	31Hops	HomoHop	Hop(35/34)	GI	OI
NA1 (O)	0.40	0.15	0.33	0.50	0.17	0.29	0.40	0.05	0.31
NB2 (O)	0.43	0.16	0.33	0.49	0.18	0.30	0.41	0.05	0.34
NC3 (O)	0.42	0.15	0.31	0.52	0.18	0.29	0.37	0.05	0.32
NA (O)	0.49	0.29	0.30	0.49	0.22	0.40	0.43	0.17	0.34
NB (O)	0.50	0.27	0.29	0.49	0.23	0.42	0.39	0.16	0.28
NC (O)	0.50	0.34	0.36	0.42	0.21	0.41	0.49	0.27	0.53
ND (O)	0.46	0.23	0.35	0.44	0.21	0.36	0.40	0.16	0.42
NE (O)	0.47	0.16	0.34	0.46	0.20	0.34	0.40	0.09	0.50
NF (O)	0.43	0.16	0.33	0.46	0.20	0.34	0.37	0.10	0.30
NO (O)	0.56	0.32	0.22	0.43	0.34	0.62	0.55	0.16	0.03
NN (O)	0.44	0.22	0.32	0.50	0.18	0.31	0.44	0.05	0.42
N25 (O)	0.42	0.17	0.33	0.48	0.19	0.34	0.42	0.08	0.37
N18 (O)	0.42	0.15	0.30	0.50	0.20	0.35	0.41	0.08	0.36
NN1 (O)	0.41	0.18	0.35	0.45	0.20	0.35	0.41	0.06	0.46
NN41 (O)	0.39	0.03	0.36	0.48	0.16	0.32	0.37	0.02	0.34
UKB (O)	0.57	0.29	0.23	0.43	0.34	0.61	0.56	0.15	nd
UK88 (O)	0.53	0.28	0.21	0.43	0.36	0.60	0.55	0.11	nd
UK85 (O)	0.86	0.22	0.21	0.48	0.31	0.56	0.48	0.08	nd
UK66 (O)	0.67	0.35	0.20	0.46	0.33	0.57	0.48	0.16	nd
UK65 (O)	0.50	0.53	0.18	0.45	0.37	0.56	0.35	0.07	nd
UK80 (O)	0.66	0.82	0.04	0.53	0.43	0.70	0.56	0.07	nd
UK34 (O)	0.51	0.40	0.19	0.45	0.36	0.57	0.58	0.02	nd
UK11 (O)	0.60	0.30	0.18	0.43	0.39	0.64	0.55	0.12	nd
UK01 (O)	0.73	0.49	0.18	0.41	0.42	0.69	0.61	0.16	nd
UK05 (O)	0.76	0.51	0.17	0.41	0.42	0.70	0.51	0.23	nd
UKV (O)	0.56	0.36	0.24	0.47	0.29	0.53	0.38	0.34	nd
NA72 (O)	0.42	0.14	0.30	0.35	0.35	0.52	0.51	0.13	nd
NA73 (O)	0.43	0.15	0.30	0.35	0.35	0.54	0.57	0.08	nd
NA74 (O)	0.44	0.14	0.32	0.35	0.32	0.49	0.50	0.08	nd
NA75 (O)	0.43	0.15	0.31	0.35	0.34	0.53	0.67	0.14	nd
NA79 (O)	0.36	0.13	0.47	0.06	0.47	0.63	0.52	0.32	nd
NA61 (O)	0.31	0.11	0.32	0.33	0.35	0.53	0.58	0.03	nd
NA76 (O)	0.29	0.04	0.64	0.05	0.31	0.49	0.53	0.78	nd
NAC (O)	0.21	0.18	0.28	0.41	0.32	0.50	0.58	0.15	nd
ME77 (O)	0.20	0.07	0.41	0.30	0.28	0.44	0.57	0.19	nd
ME39 (O)	0.91	0.60	0.30	0.34	0.36	0.61	0.55	0.13	nd
ME43 (O)	0.55	0.22	0.30	0.31	0.39	0.64	0.49	0.11	nd
ME12 (O)	0.59	0.37	0.23	0.48	0.29	0.53	0.47	0.33	nd
SN1 (O)	0.50	0.19	0.24	0.55	0.20	0.37	0.39	0.25	0.07
SN2 (O)	0.46	0.21	0.22	0.48	0.30	0.53	0.41	0.16	0.03

Ts/(Ts+Tm) = 18α (H)-trisnorhopane/ 17α (H)-trisnorhopane ratio; Moldowan *et al.* (1986). C₂₉Hops = C₂₉ Hopane/ (C₂₉ + C₃₀ + C₃₁ 22S and C₃₁ 22R); Killops *et al.* (1998). C₃₀Hops = C₃₀ Hopane/ (C₂₉ + C₃₀ + C₃₁ 22S and C₃₁ 22R); Killops *et al.* (1998). C₃₁Hops = (C₃₁ 22S and SSR Hopane)/ (C₂₉ + C₃₀ + C₃₁ 22S and C₃₁ 22R); Killops *et al.* (1998). HomoHop = $\alpha\beta$ C₃₅homohopane (22S+22R)/ \sum C₃₁. Hops C₃₅ /C₃₄ 17 α (H), 21 β (H)- pentakishomohopane (22S+22R)/ 17 α (H), 21 β (H)- tetrakishomohopane (22S + 22R); ten Haven *et al.* (1987). GI (Gammacerane index) = gammacerane/ gammacerane + C₃₀ 17 β (H), 21 β (H)-Hopane; (ten Haven *et al.*, 1987). OI (Oleanane index) = 18 α (H)-oleanane/oleanane 17 α (H), 21 β (H)-Hopane; measured in *m/z* 191.(Ekweozor and Telhaes, 1990).

nd: not determined due to low concentration in the parameter

4.3.1.4 Aromatic hydrocarbons

The major aromatic compounds studied includes methyl-, dimethyl-, and trimethylnaphthalenes, phenanthrene, methyl- and dimethylphenanthrenes, dibenzothiophene and benzothiophene, which were analysed by GC-MS for thermal maturity and organic source assessments. The distributions of the representative oil NC (O) are shown in Figures 4.12 and 4.13, with assignments of the peaks in Table 4.5.

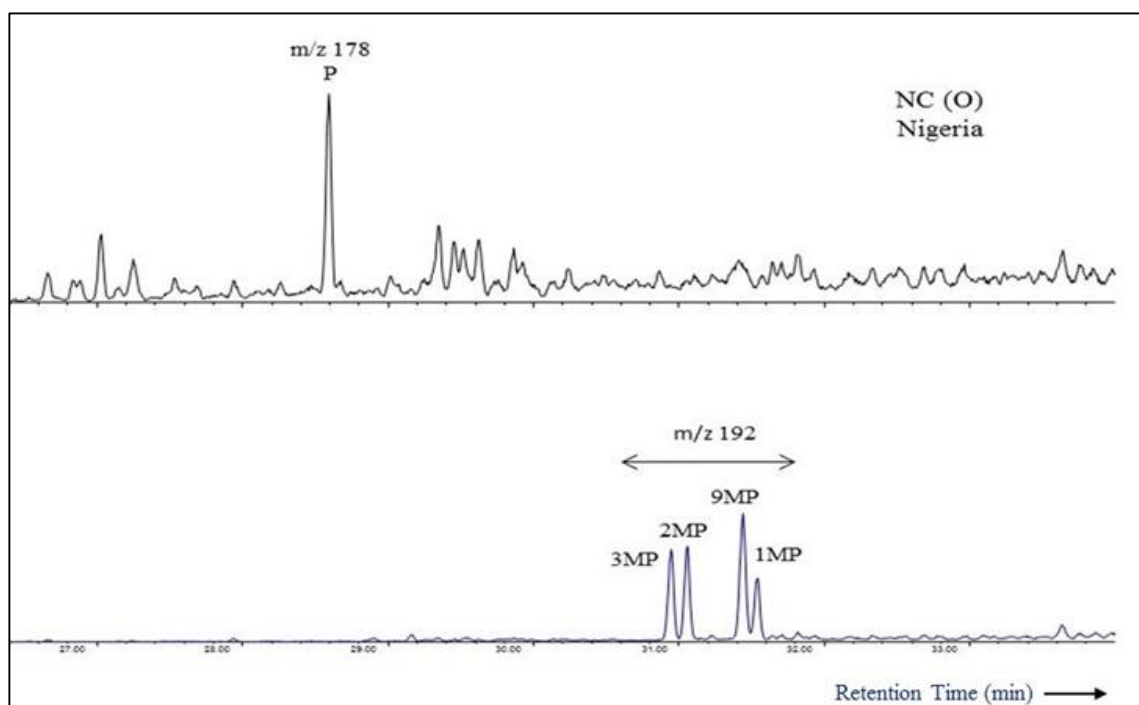


Figure 4.12: GC-MS m/z 178 and 192 mass chromatograms showing the distributions of the phenanthrene and methylphenanthrenes in representative oil NC (O) from Nigeria.

(P: phenanthrene; 3MP: 3-methyl phenanthrene; 2MP: 2-methyl phenanthrene; 9MP: 9-methyl phenanthrene, 1MP: 1-methyl phenanthrene)

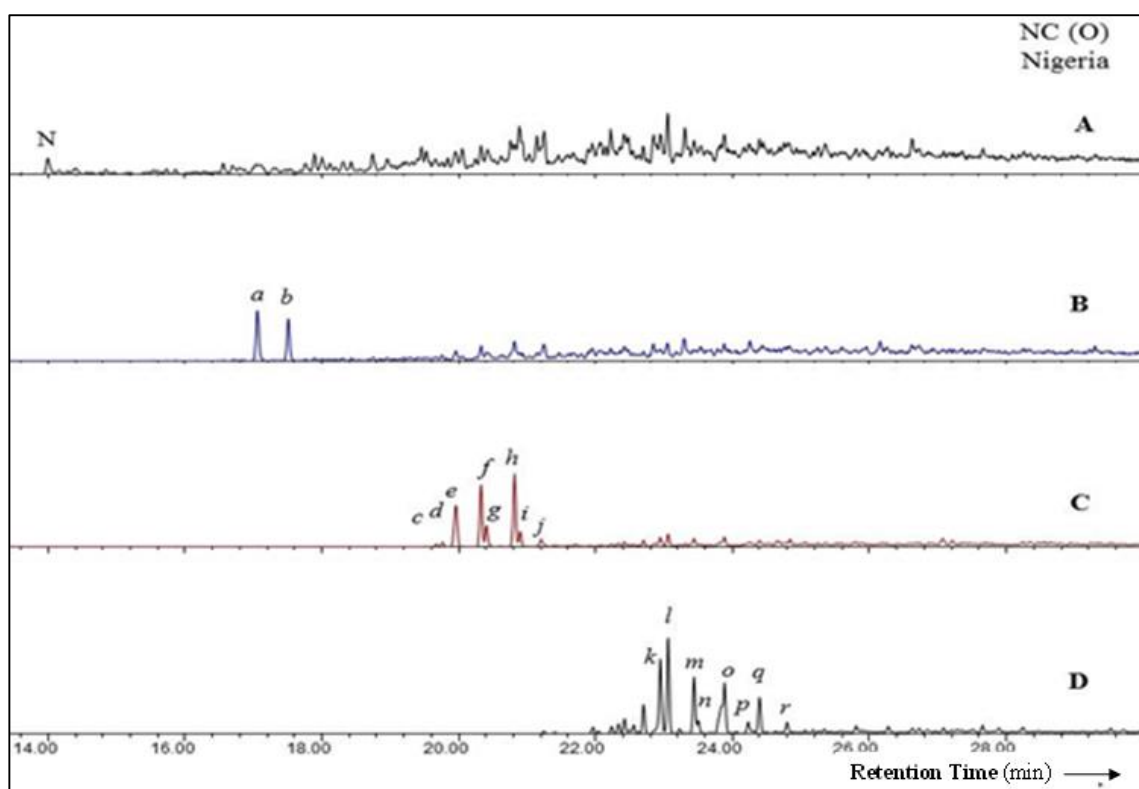


Figure 4.13: GC-MS m/z 128 and 142 mass chromatograms showing the distributions of the naphthalene and methylnaphthalenes and also GC-MS m/z 156 and 170 mass chromatograms showing the distributions of dimethylnaphthalenes and trimethylnaphthalenes in the representative oil NC (O) from Nigeria. Assignments of the peaks labelled in table 4.5.

Table 4.5: Peak identification of biomarkers in aromatic hydrocarbons.

Ions	Peak	Compound
<i>m/z</i> 178	P	Phenanthrene
<i>m/z</i> 192	3 MP	3-Methylphenanthrene
	2 MP	2-Methylphenanthrene
	9 MP	9-Methylphenanthrene
	1 MP	1-Methylphenanthrene
<i>m/z</i> 128	N	Naphthalene
<i>m/z</i> 142	a	2-Methylnaphthalene
	b	1-Methylnaphthalene
<i>m/z</i> 156	c	2-Dimethylnaphthalenes
	d	1- Dimethylnaphthalenes
	e	2,6+2,7- Dimethylnaphthalenes
	f	1,3+1,7- Dimethylnaphthalenes
	g	1,6- Dimethylnaphthalenes
	h	1,4+2,3- Dimethylnaphthalenes
	i	1,5- Dimethylnaphthalenes
	j	1,2- Dimethylnaphthalenes
	k	1,3,7- Trimethylnaphthalenes
	l	1,3,6- Trimethylnaphthalenes
<i>m/z</i> 170	m	1,3,5- Trimethylnaphthalenes
	n	1,4,6- Trimethylnaphthalenes
	o	1,4,7+1,2,6+1,6,9- Trimethylnaphthalenes
	p	1,2,4- Trimethylnaphthalenes
	q	1,2,5- Trimethylnaphthalenes
	r	1,2,3- Trimethylnaphthalenes

The Methylphenanthrene Index (MPI-1) is a commonly used molecular thermal maturity parameter and is sensitive to maturity increase (Radke, 1988) but facies dependent (Radke *et al.*, 1982a). MPI-1 can also be used to calculate the vitrinite reflectance equivalent (% VR_c) for crude oils with MPI-1 increasing from ca. 0.4 at VR_c of 0.6 % up to ca. 1.6 at the end of oil window (VR_c 1.3%) and decreases to ca. 0.5 at VR_c 2.0% at the end of gas window. The ratios of MPI-1 (0.08 – 1.00) and MPI-2 (0.11 – 1.01) calculated from the distributions of methylphenanthrenes in the oils (Table 4.5 & Figure 4.14) shows a consistent increase. There is a good positive correlation between the calculated MPI-1 and MPI-2. These maturity parameters have variable thermal maturity from immature to late thermally maturity of the oils.

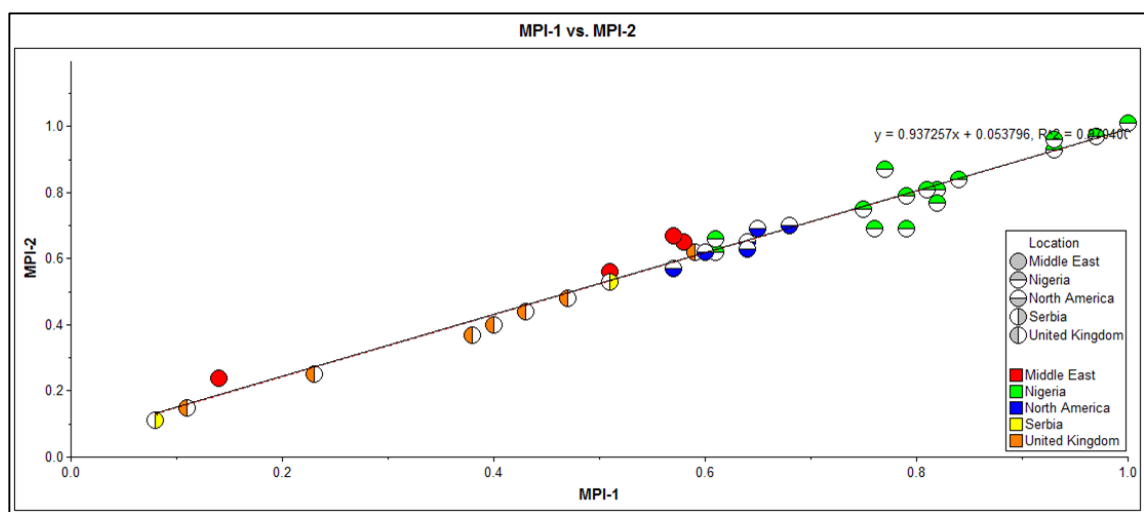


Figure 4.14: Cross plots of maturity parameter computed from aromatic hydrocarbons (MPI-1 and MPI-2) of the oils (After IGI's p: 3.5 geochemical interpretation software).

Table 4.6: Selected molecular parameter for thermal maturity and source indicators from aromatic hydrocarbon fractions in the oils.

Sample Name	MPI-1	MPI-2	MNR	4/1 MDT	3/2MDBT	DBT/PHEN	%R (MDBT)
NA1 (O)	0.61	0.62	0.59	5.35	3.41	0.12	1.34
NB2 (O)	0.82	0.81	0.61	5.03	3.79	0.11	1.33
NC3 (O)	0.75	0.75	0.62	4.96	4.07	0.11	1.32
NA (O)	0.77	0.87	0.55	3.49	2.51	0.09	1.23
NB (O)	0.79	0.79	0.50	3.79	2.57	0.07	1.25
NC (O)	0.93	0.93	0.57	3.34	2.43	0.10	1.22
ND (O)	0.93	0.96	0.60	3.78	2.59	0.12	1.25
NE (O)	0.81	0.81	0.62	4.15	2.64	0.13	1.28
NF (O)	0.84	0.84	0.62	4.13	2.75	0.12	1.28
NO (O)	0.61	0.66	0.49	2.00	1.19	0.04	1.09
NN (O)	1.00	1.01	0.65	3.79	4.80	0.07	1.25
N25 (O)	0.76	0.69	0.48	2.91	1.89	0.02	1.18
N18 (O)	0.79	0.69	0.53	3.19	1.97	0.01	1.21
NNI (O)	0.97	0.97	0.66	4.63	3.21	0.11	1.31
NN41 (O)	0.82	0.77	0.35	2.92	3.33	0.03	1.18
UKB (O)	0.64	0.65	0.42	2.09	1.10	0.03	1.10
UK88 (O)	0.47	0.48	0.48	2.16	1.06	0.47	1.11
UK85 (O)	0.23	0.25	0.52	nd	nd	Nd	nd
UK66 (O)	nd	nd	0.63	7.91	0.55	Nd	1.45
UK65 (O)	0.11	0.15	0.55	nd	nd	Nd	nd
UK80 (O)	nd	nd	0.58	1.72	0.83	Nd	1.05
UK34 (O)	nd	nd	0.65	5.00	0.61	Nd	1.33
UK11 (O)	0.43	0.44	0.47	1.81	0.99	0.97	1.06
UK01 (O)	0.38	0.37	0.41	2.47	1.11	1.21	1.14
UK05 (O)	0.40	0.40	0.42	2.58	1.12	1.24	1.15
UKV (O)	0.59	0.62	0.56	2.59	1.96	0.03	1.15
NA72 (O)	0.68	0.70	0.52	2.51	1.44	0.94	1.15
NA73 (O)	0.64	0.65	0.55	2.77	1.63	0.85	1.17
NA74 (O)	0.64	0.65	0.54	2.83	1.67	0.87	1.18
NA75 (O)	0.65	0.69	0.52	2.42	1.40	0.90	1.14
NA79 (O)	nd	nd	0.49	2.58	1.59	Nd	1.15
NA61 (O)	0.57	0.57	0.49	1.65	1.07	1.45	1.03
NA76 (O)	0.60	0.62	0.50	1.96	1.27	0.98	1.08
NAC (O)	0.64	0.63	0.60	0.99	1.68	0.04	0.90
ME77 (O)	0.58	0.65	0.50	2.32	1.62	1.00	1.12
ME39 (O)	0.57	0.67	0.50	3.74	2.44	1.16	1.25
ME43 (O)	0.51	0.56	0.53	2.08	1.51	0.93	1.10
ME12 (O)	0.14	0.24	0.55	nd	nd	Nd	nd
SN1 (O)	0.08	0.11	0.55	2.24	2.49	0.04	1.11
SN2 (O)	0.51	0.53	0.46	2.33	1.25	0.11	1.13

MPI-1 = $1.5(2\text{MP}+3\text{MP})/(P+1\text{MP}+9\text{MP})$; Radke *et al.* (1982b). MPI-2 = $3(2\text{MP})/(P+1\text{MP}+9\text{MP})$; (Radke *et al.*, 1982b). MNR = $(2\text{-MN}/1\text{MN})$; DBT/PHEN; Hughes *et al.* (1995); MPR = $(2\text{MP}) / (1\text{MP})$; (Radke *et al.*, 1984).

4.3.1.5 *Source facies and thermal maturity*

Based on the molecular properties, the oils exhibit two likely source facies i.e. terrigenous and marine source facies. These two distinct source rocks are typical of the oils from Nigeria as previously observed by Sonibare *et al.* (2008). The presence of $18\alpha(\text{H})$ -oleanane in the oils is also a good indicator of terrestrial organic input into the deltaic shale oil source rocks and it has been suggested as biomarker for angiosperm (flowering) plants (Ekweozor *et al.*, 1979). Hence, the abundance of oleanane permits the grouping of the likely source rocks that generated the oils into two families of terrigenous/deltaic and marine shale (Table 4.7). The maturity parameters based on aromatic compounds; MPI-1 and MPI-2 were generally well-correlated and allowed maturity trends to be established.

Table 4.7: Summary of maturity and source facies biomarkers in the studied oils.

Sample	Pr/Ph	CPI	Sterane (%)			Maturity	Likely source
			C ₂₇ ααα	C ₂₈ ααα	C ₂₉ ααα		
NA1 (O)	4.59	1.13	14.05	20.90	65.05	mid/mid	Terrigenous/Deltaic shale
NB2 (O)	4.38	0.95	17.15	21.12	61.73	mid/mid	Terrigenous/Deltaic shale
NC3 (O)	4.29	1.12	19.33	22.37	58.31	mid/mid	Terrigenous/Deltaic shale
NA (O)	1.02	nd	30.98	26.45	42.58	low---	Terrigenous/Marine shale
NB (O)	nd	nd	29.94	26.12	43.95	mid/mid	Terrigenous/Marine shale
NC (O)	nd	nd	29.52	27.77	42.71	high/mid	Terrigenous/Marine shale
ND (O)	2.36	1.16	27.16	26.13	46.71	high/mid	Terrigenous/Marine shale
NE (O)	2.52	1.09	25.75	23.80	50.44	mid/mid	Terrigenous/Marine shale
NF (O)	2.18	0.78	29.11	25.07	45.82	mid/mid	Terrigenous/Marine shale
NO (O)	1.32	nd	46.51	14.86	38.63	low---	Marine/Marine shale
NN (O)	2.35	nd	40.19	22.90	36.92	mid/mid	Marine/Marine shale
N25 (O)	2.01	nd	32.26	26.11	41.63	mid/mid	Terrigenous/Marine shale
N18 (O)	1.96	nd	29.93	29.69	40.38	mid/mid	Terrigenous/Marine shale
NNI (O)	2.84	nd	31.44	27.53	41.02	high/mid	Terrigenous/Marine shale
NN41 (O)	2.13	1.04	31.16	29.20	39.64	mid/mid	Terrigenous/Marine shale
UKB (O)	1.11	nd	47.53	16.13	36.33	high/mid	Open marine/Marine shale
UK88 (O)	1.10	0.95	34.12	24.83	41.05	mid/mid	Terrigenous /Marine shale
UK85 (O)	1.58	1.05	29.49	24.95	45.57	low---	Terrigenous/Marine + lacustrine shale
UK66 (O)	1.25	0.99	56.05	17.10	26.85	high/mid	Open marine/Marine shale
UK65 (O)	1.27	1.00	46.73	18.94	34.33	?	Open marine/Marine shale
UK80 (O)	nd	nd	45.18	22.05	32.76	?	Open marine/Marine shale
UK34 (O)	1.33	1.06	47.53	18.45	34.01	?	Open marine/Marine shale
UK11 (O)	0.76	0.97	47.58	16.73	35.69	mid/mid	Open marine/Marine shale
UK01 (O)	0.78	0.93	48.06	18.65	33.29	?	Open marine/Marine shale
UK05 (O)	0.72	0.94	50.65	16.36	32.99	?	Open marine/Marine shale
UKV (O)	nd	nd	49.16	19.21	31.62	?	Open marine/Marine shale
NA72 (O)	0.95	nd	36.64	23.91	39.45	high/mid	Open marine/Marine shale
NA73 (O)	1.10	1.01	32.79	25.03	42.17	?/mid	Open marine/Marine shale
NA74 (O)	1.10	1.00	29.34	26.12	44.54	mid/mid	Open marine/Marine shale
NA75 (O)	1.01	nd	32.71	23.05	44.24	mid/mid	Open marine/Marine shale
NA79 (O)	1.24	nd	32.82	25.61	41.58	low/low	Open marine/Marine shale
NA61 (O)	1.02	nd	34.96	25.62	39.43	low/low	Open marine/Marine shale
NA76 (O)	1.05	1.16	35.78	24.42	39.80	mid/mid	Shallow marine/Marine shale
NAC (O)	0.35	nd	44.49	16.02	39.49	mid/mid	Shallow marine/Lacustrine shale
ME77 (O)	0.54	1.08	47.19	16.56	36.26	low/high	Marine/Marine + lacustrine shale
ME39 (O)	0.76	0.97	52.82	8.34	38.85	mid/low	Marine/Marine + lacustrine shale
ME43 (O)	0.72	1.01	37.10	12.04	50.87	mid/?	Marine/Marine + lacustrine shale
ME12 (O)	0.89	1.04	50.82	16.76	32.42	mid/mid	Shallow marine/Lacustrine shale
SN1 (O)	1.51	nd	24.44	22.16	53.40	low/mid	Shallow marine/Marine shale
SN2 (O)	1.44	1.47	31.64	31.05	37.31	mid/mid	Shallow marine/Marine shale

4.3.1.6 Biodegradation level based on Peters and Moldowan classification scale

The varying degrees of alteration of the crude oils were ranked on the scale of Peter and Moldowan (PM) based on molecular composition, visual inspection of GC and GC-MS data from distributions, e.g. *n*-alkanes and isoprenoids, triterpanes, steranes as presented in Table 4.8. As revealed in the table, the oils from Nigeria (NA (O), NB (O), NC (O), NO (O), NN (O), N25 (O) N18 (O), NN1(O) and NA41 (O)), United Kingdom (UKB (O), UK66(O), UK65(O), UK80(O), North America (NA79 and NAC), Middle East (ME77) and Serbia (SN1) are characterised by complete or partial removal of *n*-alkanes and isoprenoid alkanes and the other oil samples are relatively unbiodegraded. Thus, these oils have undergone different level of biodegradation as shown in Table 4.8, with biodegradation ranking from PM level 1 to PM level 6.

Table 4.8: Biodegradation level of the studied oils based on the presence and absence of molecular parameters by Peters and Moldowan (1993).

Sample	<i>n</i> -alkanes	Isoprenoids	Steranes	Hopanes	Diasteranes	Aromatics	PM Scale	Biodegradation
NA1 (O)	✓	✓	✓	✓	✓	✓	1	Non-degraded
NB2 (O)	✓	✓	✓	✓	✓	✓	1	Non-degraded
NC3 (O)	✓	✓	✓	✓	✓	✓	1	Non-degraded
NA (O)	—	—	✓	✓	✓	✓	6	Biodegraded
NB (O)	—	✓—	✓	✓	✓	✓	5	Biodegraded
NC (O)	—	✓—	✓	✓	✓	✓	5	Biodegraded
ND (O)	✓	✓	✓	✓	✓	✓	1	Non-degraded
NE (O)	✓	✓	✓	✓	✓	✓	1	Non-degraded
NF (O)	✓	✓	✓	✓	✓	✓	1	Non-degraded
NO (O)	—	✓—	✓	✓	✓	✓	5	Biodegraded
NN (O)	✓—	✓—	✓	✓	✓	✓	3	Biodegraded
N25 (O)	✓—	✓—	✓	✓	✓	✓	3	Biodegraded
N18 (O)	✓—	✓—	✓	✓	✓	✓	3	Biodegraded
NNI (O)	✓—	✓	✓	✓	✓	✓	2	Biodegraded
NN41 (O)	✓—	✓—	✓	✓	✓	✓	3	Biodegraded
UKB (O)	—	✓—	✓	✓	✓	✓	5	Biodegraded
UK88 (O)	✓	✓	✓	✓	✓	✓	1	Non-degraded
UK85 (O)	✓	✓	✓	✓	✓	✓	1	Non-degraded
UK66 (O)	—	—	✓	✓	✓	✓	6	Biodegraded
UK65 (O)	—	—	✓	✓	✓	✓	6	Biodegraded
UK80 (O)	—	—	✓	✓	✓	✓	6	Biodegraded
UK34 (O)	✓	✓	✓	✓	✓	✓	1	Non-degraded
UK11 (O)	✓	✓	✓	✓	✓	✓	1	Non-degraded
UK01 (O)	✓	✓	✓	✓	✓	✓	1	Non-degraded
UK05 (O)	✓	✓	✓	✓	✓	✓	1	Non-degraded
UKV (O)	✓	✓	✓	✓	✓	✓	1	Non-degraded
NA72 (O)	✓	✓	✓	✓	✓	✓	1	Non-degraded
NA73 (O)	✓	✓	✓	✓	✓	✓	1	Non-degraded
NA74 (O)	✓	✓	✓	✓	✓	✓	1	Non-degraded
NA75 (O)	✓	✓	✓	✓	✓	✓	1	Non-degraded
NA79 (O)	✓—	✓—	✓	✓	✓	✓	3	Biodegraded
NA61 (O)	✓	✓	✓	✓	✓	✓	1	Non-degraded
NA76 (O)	✓	✓	✓	✓	✓	✓	1	Non-degraded
NAC (O)	—	—	✓	✓	✓	✓	6	Biodegraded
MET7 (O)	✓—	✓	✓	✓	✓	✓	3	Biodegraded
ME39 (O)	✓	✓	✓	✓	✓	✓	1	Non-degraded
ME43 (O)	✓	✓	✓	✓	✓	✓	1	Non-degraded
ME12 (O)	✓	✓	✓	✓	✓	✓	1	Non-degraded
SN1 (O)	—	✓—	✓	✓	✓	✓	5	Biodegraded
SN2 (O)	✓	✓	✓	✓	✓	✓	1	Non-degraded

✓ = present; — = complete removal; ✓— = minor removal.

4.3.2 Molecular characterisation of North Sea Coals

4.3.2.1 Normal Alkanes and acyclic isoprenoids

The analysed coals are dominated by *n*-alkanes distributions of *nC*₁₂ - *nC*₃₆, maximizing at *nC*₁₃ – *nC*₁₅ (Figure 4.15). The Pr/Ph ratios for the coals range from 2.44 – 4.36 (Table 4.9) and this suggests that the coals are derived from source rock with significant terrestrial organic matter contribution, deposited in an oxic environment (Figure 4.17). Based on the plot of (DBT/PHEN) versus (Pr/Ph) (Figure 4.18) it can be concluded that the coals were deposited in fluvial-deltaic setting with possible input of marine shale (Hughes *et al.*, 1995).

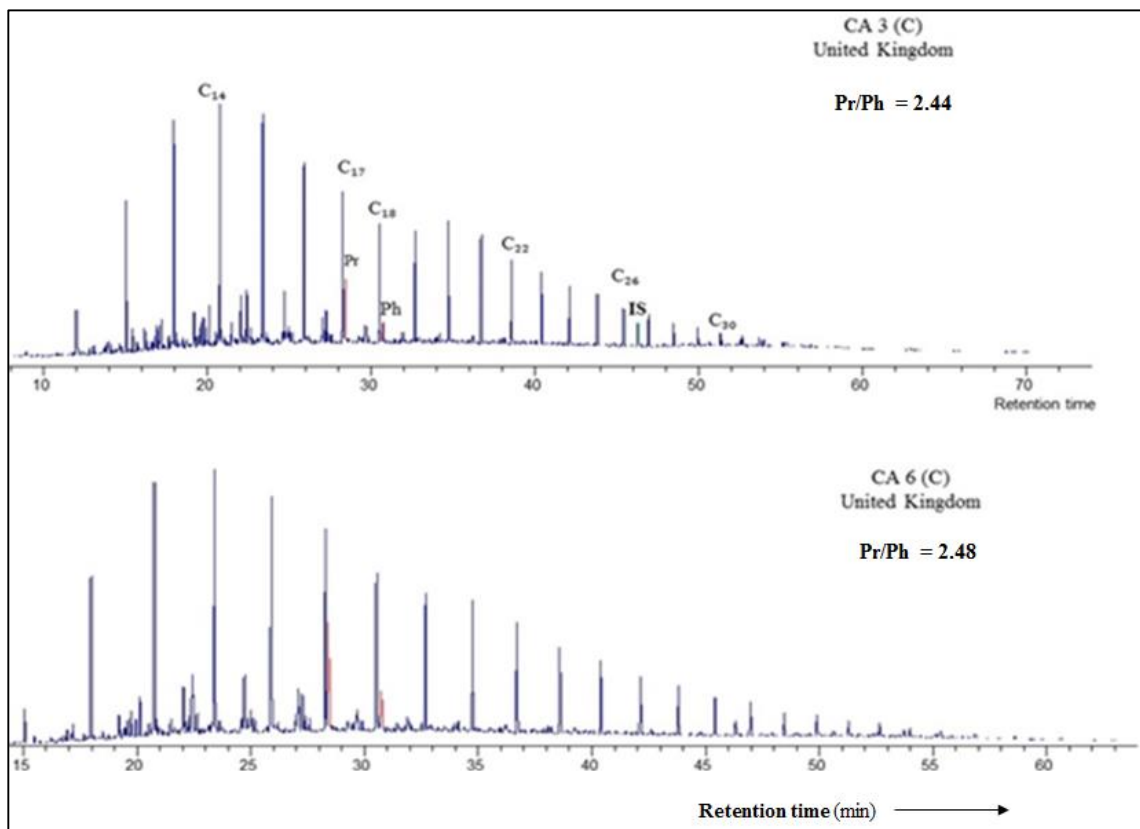


Figure 4.15: Representative GC/FID chromatograms of saturated coal extracts of CA3 (C) and CA6 (C) from North Sea coals, United Kingdom.

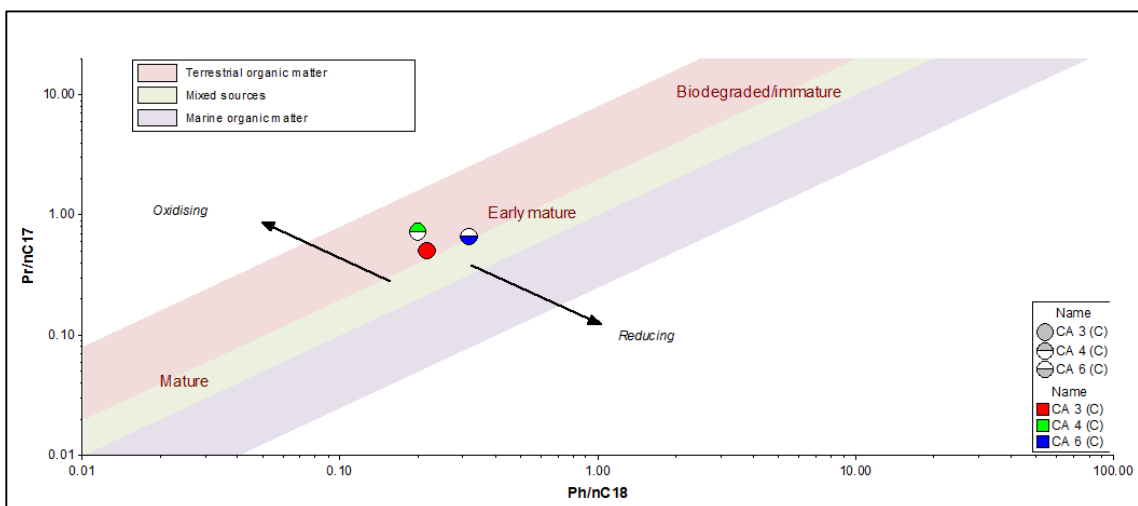


Figure 4.16: Relationship between Pr/nC_{17} against Ph/nC_{18} for the North Sea coals from the United Kingdom (Interpretation from geochemical software IGI's p: 3.5).

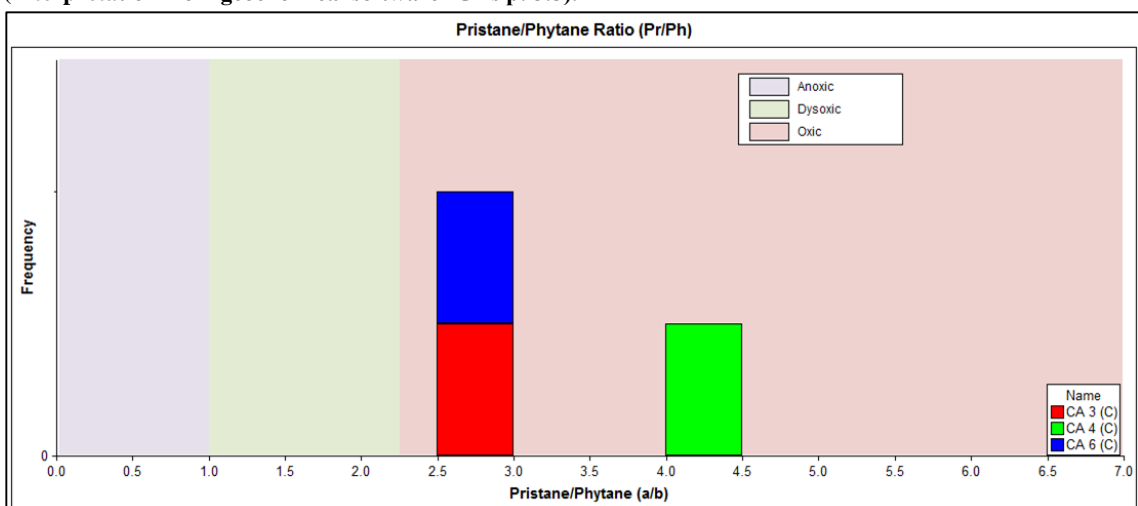


Figure 4.17: Source rock anoxia inferred from the histogram of pristane/phytane ratios from the North Sea coals (Interpretation from geochemical software IGI's p: 3.5).

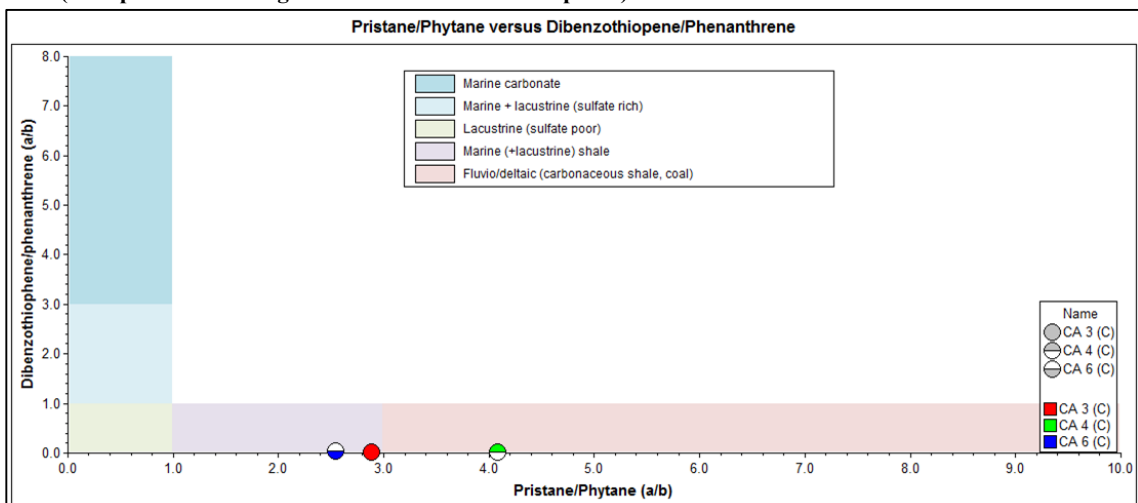


Figure 4.18: A cross plot of dibenzothiophene/phenanthrene ratio (DBT/PHEN) and the ratio of pristane to phytane for the studied coals (Interpretation from geochemical software IGI's p: 3.5).

Table 4.9: Normal alkane and isoprenoid alkane distribution of the studied coals.

Sample	Type	Location	Pr/Ph	NorPr/Ph	Pr/nC ₁₇	Ph/nC ₁₈	nC ₁₇ /nC ₁₈	CPI
CA 3 (C)	Coal	North Sea- UK	2.44	0.49	0.53	0.27	3.64	nd
CA 4 (C)	Coal	North Sea- UK	4.36	0.31	0.74	0.20	3.79	1.01
CA 6 (C)	Coal	North Sea- UK	2.48	0.36	0.64	0.33	6.17	nd

Pr/Ph = pristane/phytane ratio; Didyk *et al.* (1978); (Peters *et al.*, 2005b). Nor Pr: nor pristane (C₁₈ isoprenoid); Pr/nC₁₇ and Ph/ nC₁₈; nC₁₇ and nC₂₇ are *n*-alkanes with the 17, 18 and 25 carbon chain lengths; CPI = 0.5 x (((nC₂₅+2nC₂₇+nC₂₉+nC₃₁+nC₃₃)/(nC₂₄+nC₂₆+nC₂₈+nC₃₀+nC₃₂)) + ((nC₂₅+nC₂₇+nC₃₁+nC₃₃)/(nC₂₆+nC₂₈+nC₃₀+nC₃₂+nC₃₄))); Bray and Evans (1961).

4.3.2.2 Steranes

The sterane mass chromatograms *m/z* 217 of representative North Sea coals CA3(C) and CA6(C) are shown in Figure 4.19. In general, the measured ratios from the C₂₇ – C₂₉ $\alpha\alpha\alpha$ sterane distributions (Table 4.10) indicates the origin of the coals from land plants (Figure 4.20) with results in the range of 31 – 41%, 14 – 20% and 44 – 50 %, for the C₂₇, C₂₈, C₂₉ $\alpha\alpha\alpha$ steranes respectively.

The ratios of (C₂₉ $\alpha\alpha\alpha$ 20S/(20S + 20R) and $\alpha\beta\beta$ /($\alpha\beta\beta$ + $\alpha\alpha\alpha$) sterane range from 0.35 – 0.39 and 0.36 – 0.47 respectively (Table 4.10), which indicates that the coal samples are early mature (Figure 4.22) and this supports the previous interpretations based on *n*-alkanes/isoprenoids.

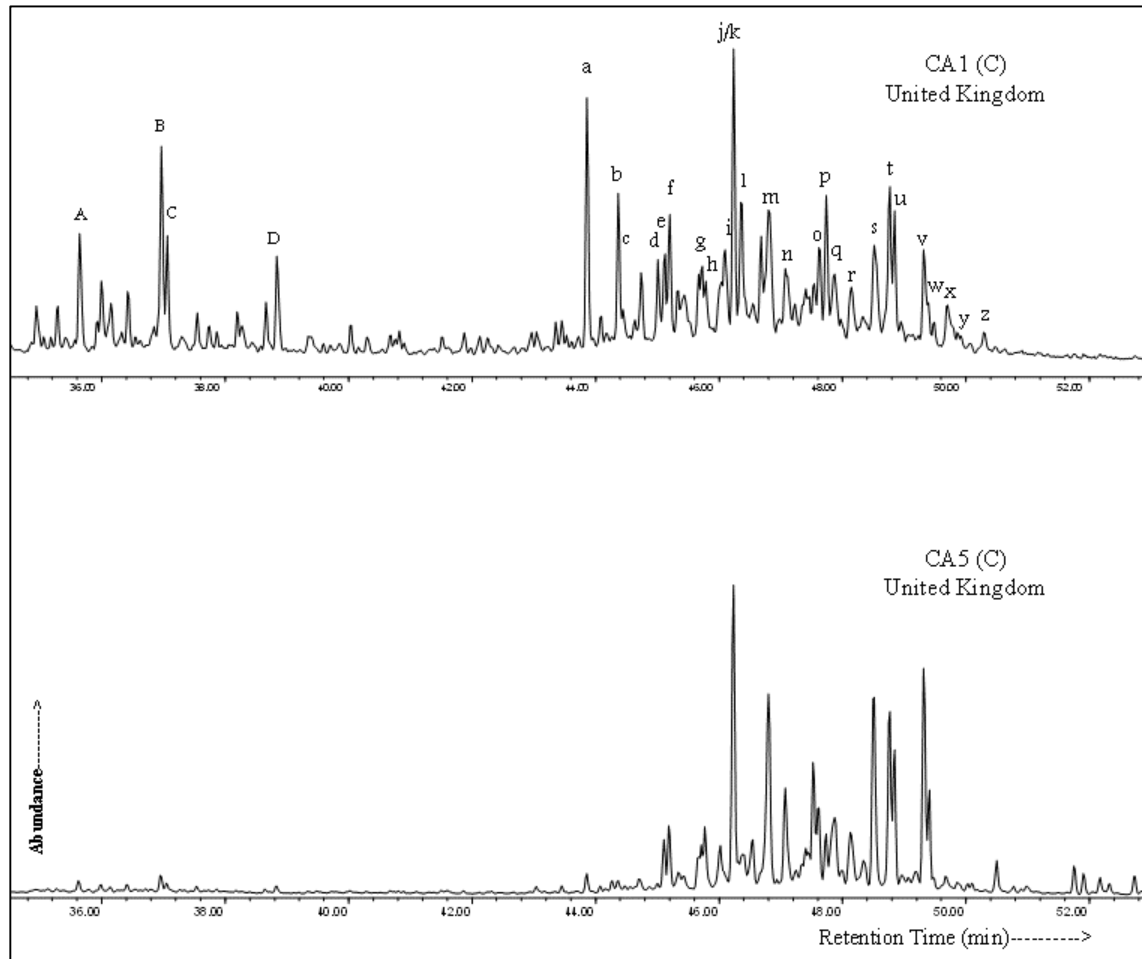


Figure 4.19: Representative GC-MS mass chromatogram m/z 217 showing the distributions of C_{27} , C_{28} and C_{29} steranes from the coals, United Kingdom.

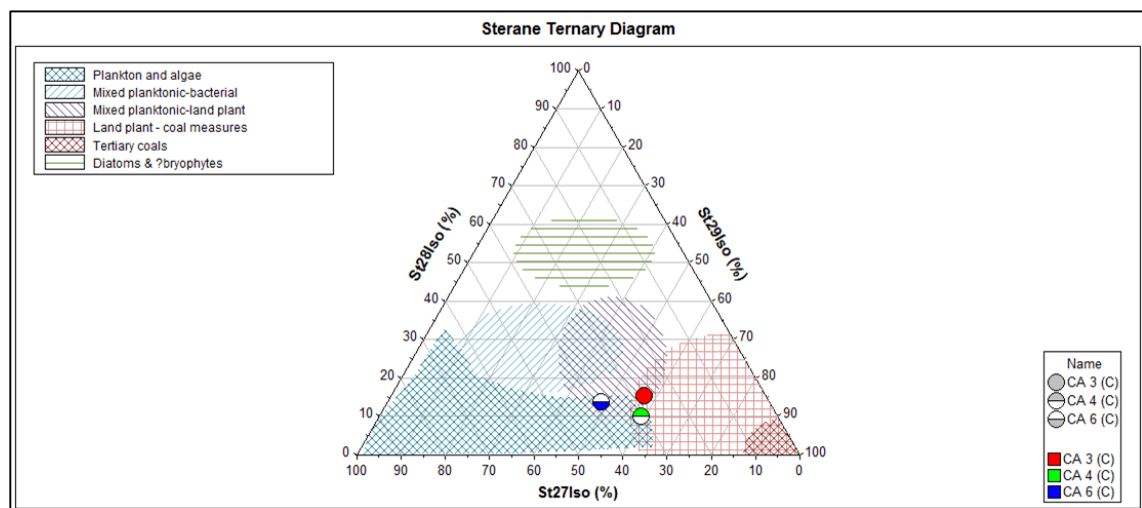


Figure 4.20: Ternary diagram showing the distribution of the C_{27} , C_{28} , and C_{29} -Steranes from GC-MS analyses of the studied coals interpreted in terms of likely source precursors. (After IGI's p: 3.5 geochemical interpretation software).

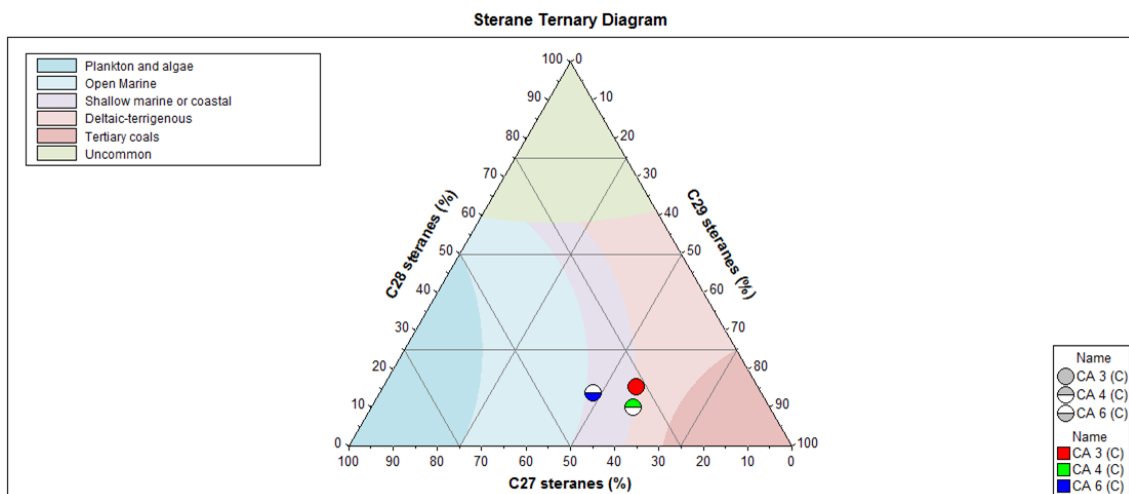


Figure 4.21: Ternary diagram showing the distribution of the C₂₇, C₂₈, and C₂₉-Steranes from GC-MS analyses of studied coals interpreted in terms of likely depositional environment. (After IGI's p: 3.5 geochemical interpretation software).

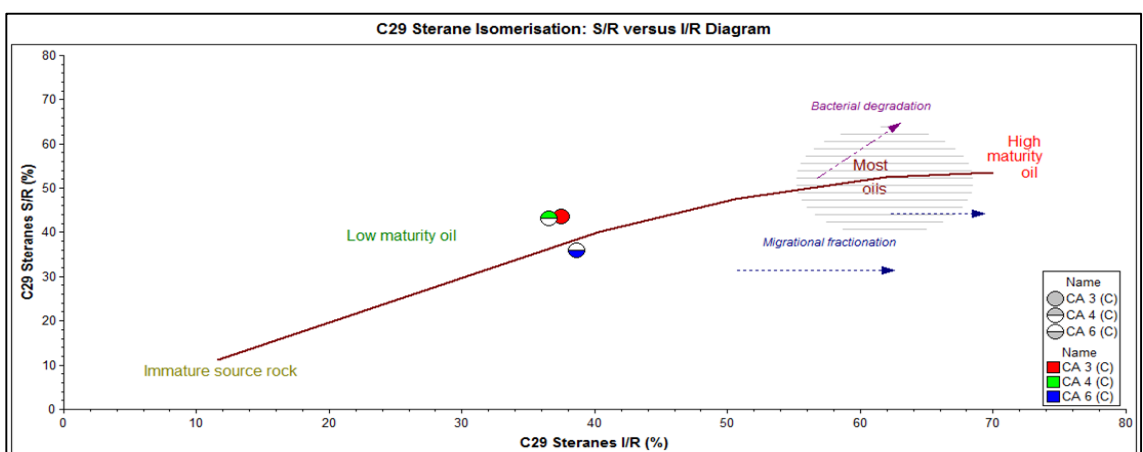


Figure 4.22: Cross plot of C₂₉ steranes I/R against C₂₉ steranes S/R parameter defines North Sea coals into various zones of thermal maturity. (After IGI's p: 3.5 geochemical interpretation software).

Table 4.10: Source and maturity parameters computed from steranes in the studied coals.

New Name	Preg	20S(20S+20R)	20S(20S+20R)	20S(20S+20R)	20S(20S+20R)	Sterane (%)		
		C ₂₉ ααα	C ₂₉ αββ	C ₂₇ ααα	C ₂₈ ααα	C ₂₇ ααα	C ₂₈ ααα	C ₂₉ ααα
CA 3 (C)	23.72	0.35	0.43	0.30	0.19	31	20	50
CA 4 (C)	6.99	0.38	0.47	0.39	0.14	41	14	45
CA 6 (C)	22.55	0.39	0.36	0.36	0.16	38	17	44

Preg = diginane + 5 α -pregnane + 20-methyldiginane + 5 α methylpregnane/ same + C₂₉ 5 α , 14 α , 17 α 20R + C₂₉ 5 α , 14 α , 17 α 20S + C₂₉ 5 α , 14 β , 17 β 20R + C₂₉ 5 α , 14 β , 17 β 20S (Mackenzie, 1984). % C₂₇ααα, C₂₈ααα and C₂₉ααα = C₂₇, C₂₈, C₂₉ as percentage of sum 27-29 for 5 α (H), 14 α (H), 17 α (H)-20R sterane; C₂₉ααα Sterane = 5 α (H), 14 α (H), 17 α (H)-C₂₉ 20S/(20S+20R) sterane; C₂₉αββ Sterane = 5 α (H), 14 β (H), 17 β (H), C₂₉ 20S/(20S+20R) sterane; C₂₇ααα Sterane = 5 α (H), 14 α (H), 17 α (H)-C₂₇ 20S/(20S+20R) sterane; C₂₈ααα Sterane = 5 α (H), 14 α (H), 17 α (H)-C₂₈ 20S/(20S+20R) sterane measured in m/z 217 mass chromatograms (Huang and Meinschein, 1979; Peters *et al.*, 2005a).

4.3.2.3 Tricyclic and tetracyclic terpanes

The distribution of terpanes obtained from m/z 191 mass chromatograms of representative North Sea coals CA3(C) and CA4(C) for this study are shown in Figure 4.23 and they are dominated by pentacyclic triterpanes. The calculated biomarker ratios are shown in Table 4.11. The values of Ts/(Ts+Tm) ratios from the coals range from 0.08 - 0.37 and those of C₂₉Ts index range between 0.04 and 0.20 (Table 4.11), indicating low thermal maturity level for the samples. Hence, the correlation between plots of Ts/Tm and 29Ts/29Tm ratios (Figure 4.24), shows early – mid maturity for the coals. The hopane C₃₀ $\beta\alpha/\alpha\beta + \alpha\beta$ and homohopanes 22S/(22S + 22R) isomerisation ratios of C₃₂ values range from 0.37 – 0.44 and 0.56 – 0.60 respectively (Table 4.11). These values indicates that the coals were deposited in an oxic/dysoxic environment based on Hop (35/34) ratio and are thermally mature based on Figure 4.27, however their Ts/Tm values are generally lower than 0.6 and this shows that they are early mature.

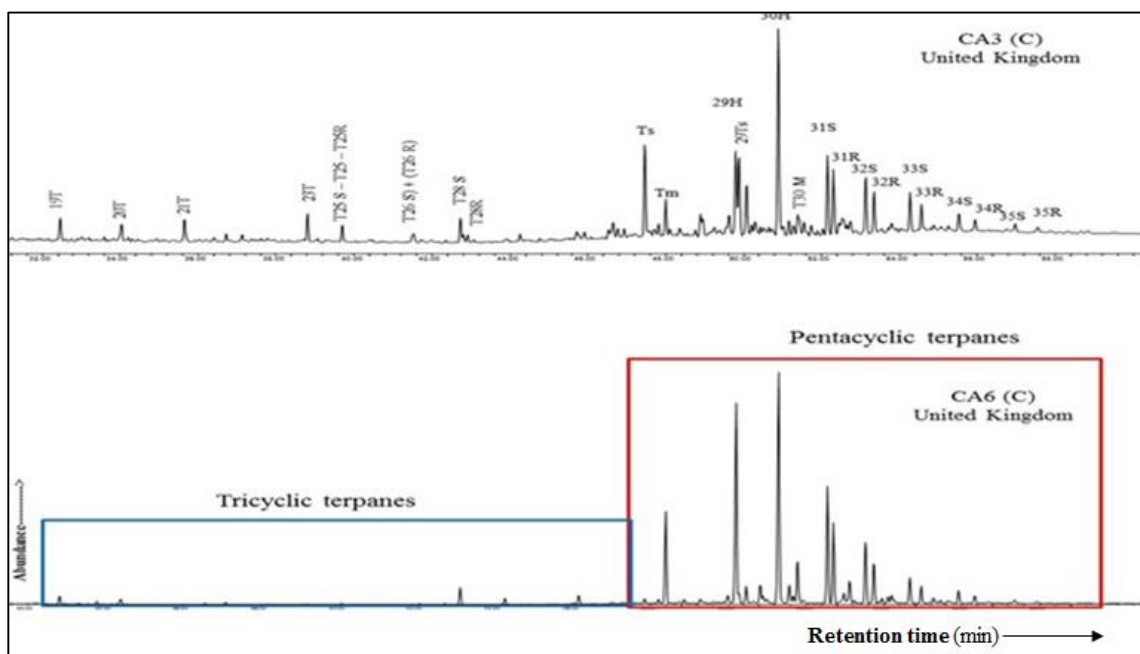


Figure 4.23: Representative partial m/z 191 mass chromatograms showing tricyclic and tetracyclic terpane distributions in CA3 (C) and CA6 (C) coals.

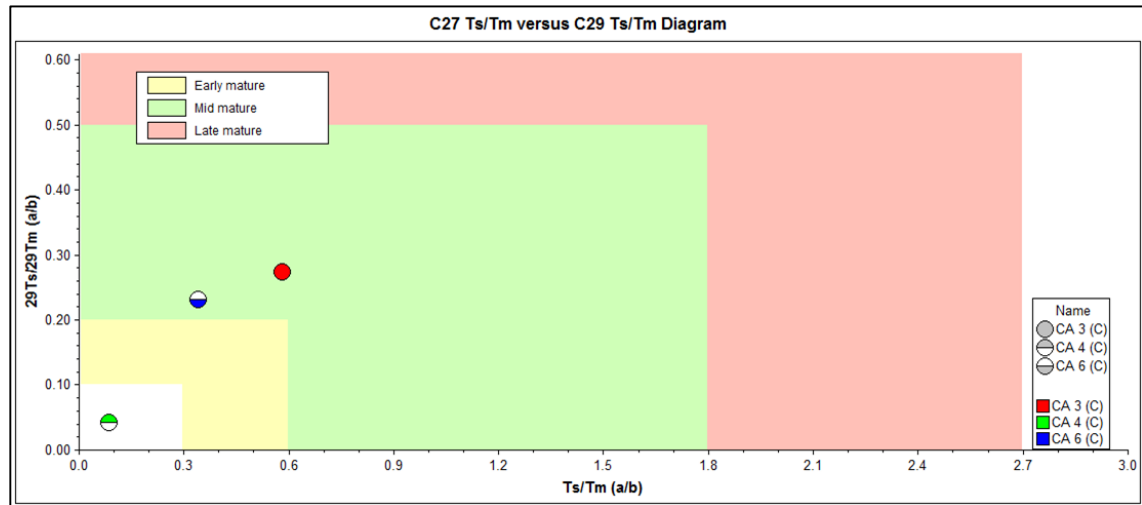


Figure 4.24: Correlation between Ts/Tm and $^{29}\text{Ts}/^{29}\text{Tm}$ ratios showing the maturity of the studied coals (After IGI's p: 3.5 geochemical interpretation software).

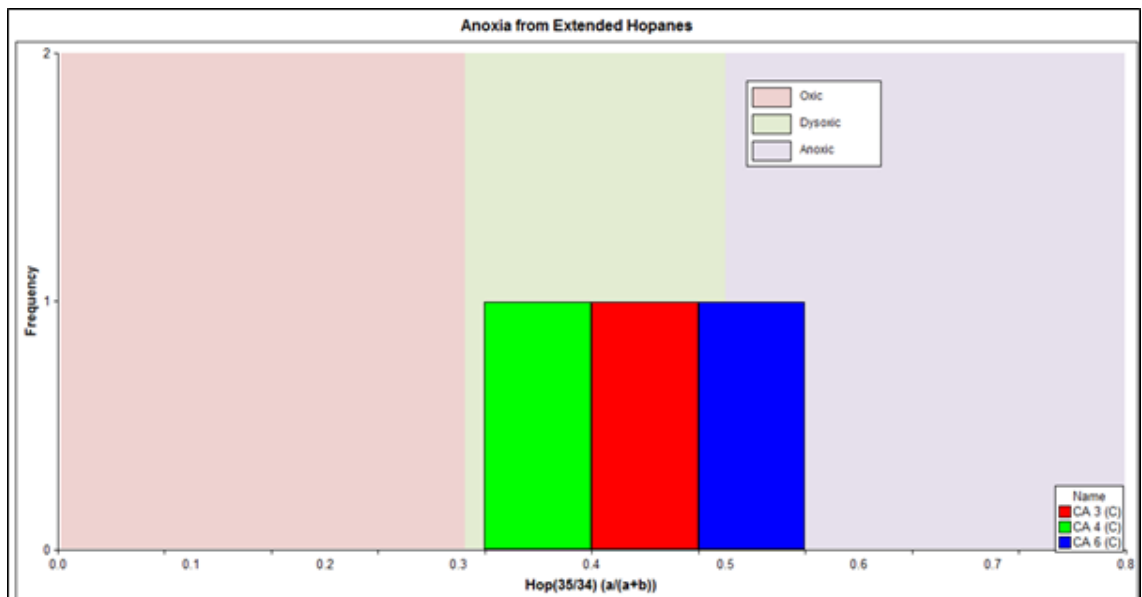


Figure 4.25: Source rock anoxia inferred from extended hopanes ($\text{Hop}(35/34)$) ratios of the coals from the North Sea, UK (After IGI's p: 3.5 geochemical interpretation software).

Table 4.11: Biomarker ratios based on terpane (m/z 191) in the studied coals

Sample Name	$\text{Ts}/(\text{Ts}+\text{Tm})$	$^{29}\text{Ts}/^{29}\text{Tm}$	$^{29}\text{Hops}$	$^{30}\text{Hops}$	$^{31}\text{Hops}$	$\text{Hop}32$	$\text{Hop}(35/34)$	GI	OI
CA 3 (C)	0.37	0.20	0.26	0.44	0.30	0.58	0.35	0.08	nd
CA 4 (C)	0.08	0.04	0.29	0.37	0.34	0.60	0.33	0.04	nd
CA 6 (C)	0.27	0.19	0.23	0.45	0.32	0.56	0.44	0.09	nd

$\text{Ts}/(\text{Ts}+\text{Tm}) = 18\alpha(\text{H})\text{-trisnorneohopane}/17\alpha(\text{H})\text{-trisnorhopane}$ ratio; Moldowan *et al.* (1986). $\text{C}_{29}\text{Hops} = \text{C}_{29}\text{ Hopane}/(\text{C}_{29} + \text{C}_{30} + \text{C}_{31} 22\text{S}$ and $\text{C}_{31} 22\text{R}$); Killops *et al.* (1998). $\text{C}_{30}\text{Hops} = \text{C}_{30}\text{ Hopane}/(\text{C}_{29} + \text{C}_{30} + \text{C}_{31} 22\text{S}$ and $\text{C}_{31} 22\text{R}$); Killops *et al.* (1998). $\text{C}_{31}\text{Hops} = (\text{C}_{31} 22\text{S}$ and SSR Hopane)/($\text{C}_{29} + \text{C}_{30} + \text{C}_{31} 22\text{S}$ and $\text{C}_{31} 22\text{R}$); Killops *et al.* (1998). HomoHop = $\alpha\beta\text{C}_{35}\text{homohopane}$ ($22\text{S}+22\text{R}$)/ $\sum\text{C}_{31}$. Hops $\text{C}_{35}/\text{C}_{34} 17\alpha(\text{H})$, $21\beta(\text{H})$ - pentakishomohopane ($22\text{S}+22\text{R}$)/ $17\alpha(\text{H})$, $21\beta(\text{H})$ - tetrakishomohopane ($22\text{S}+22\text{R}$); ten Haven *et al.* (1987). GI (Gammacerane index) = gammacerane/gammacerane + $\text{C}_{30} 17\beta(\text{H})$, $21\beta(\text{H})$ -Hopane; (ten Haven *et al.*, 1987). OI (Oleanane index) = $18\alpha(\text{H})$ -oleanane/oleanane $17\alpha(\text{H})$, $21\beta(\text{H})$ -Hopane; measured in m/z 191 (Ekweozor and Telhaes, 1990).

4.3.2.4 Aromatic hydrocarbons

The aromatic fractions obtained from the North Sea coals contain many compounds and the distributions of the representative coal CA3(3) are shown in Figure 4.26 and 4.27. The molecular parameters calculated from the aromatic compounds are presented in Table 4.13. The MPI-1 and MPI-2 ratios derived from the distributions of methylphenanthrenes in the coals range from 0.52 – 0.65 and 0.56 – 0.70 respectively (Table 4.13). The ratios of MPI-1 (0.52 – 0.65) and MPI-2 (0.56 – 0.70) calculated from the distributions of methylphenanthrenes in the coals (Table 4.13 & Figure 4.28) shows a consistent increase. There is a good positive correlation between the calculated MPI-1 and MPI-2 ratios. These thermal maturity parameters indicate thermally mature coals.

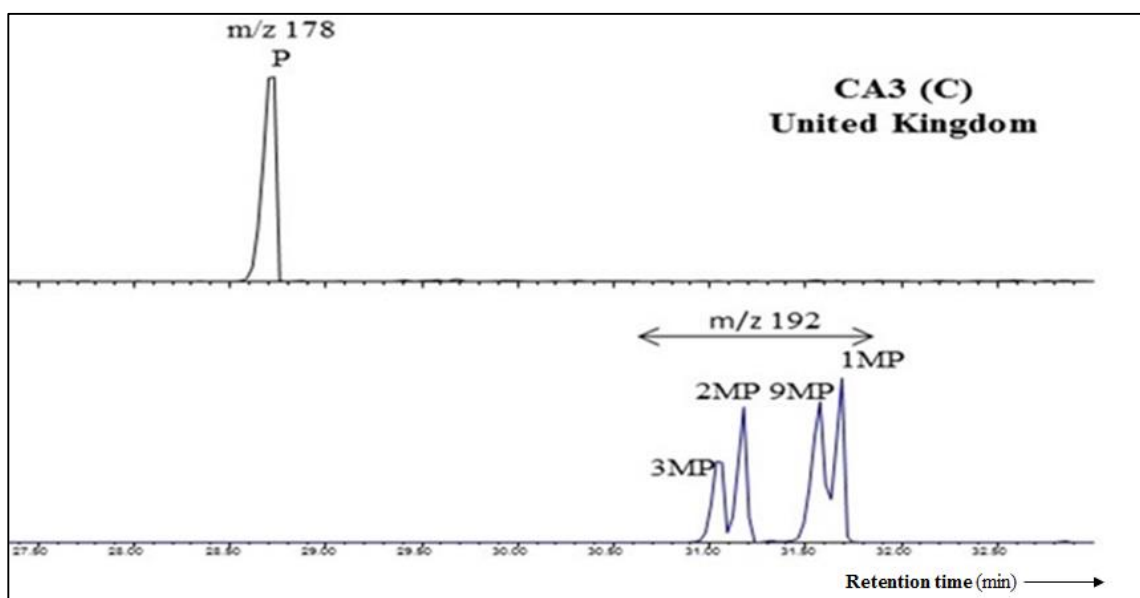


Figure 4.26: GC-MS m/z 178 and 192 mass chromatograms showing the distributions of the phenanthrene and methylphenanthrenes in representative coal (CA3) from the North Sea, UK.

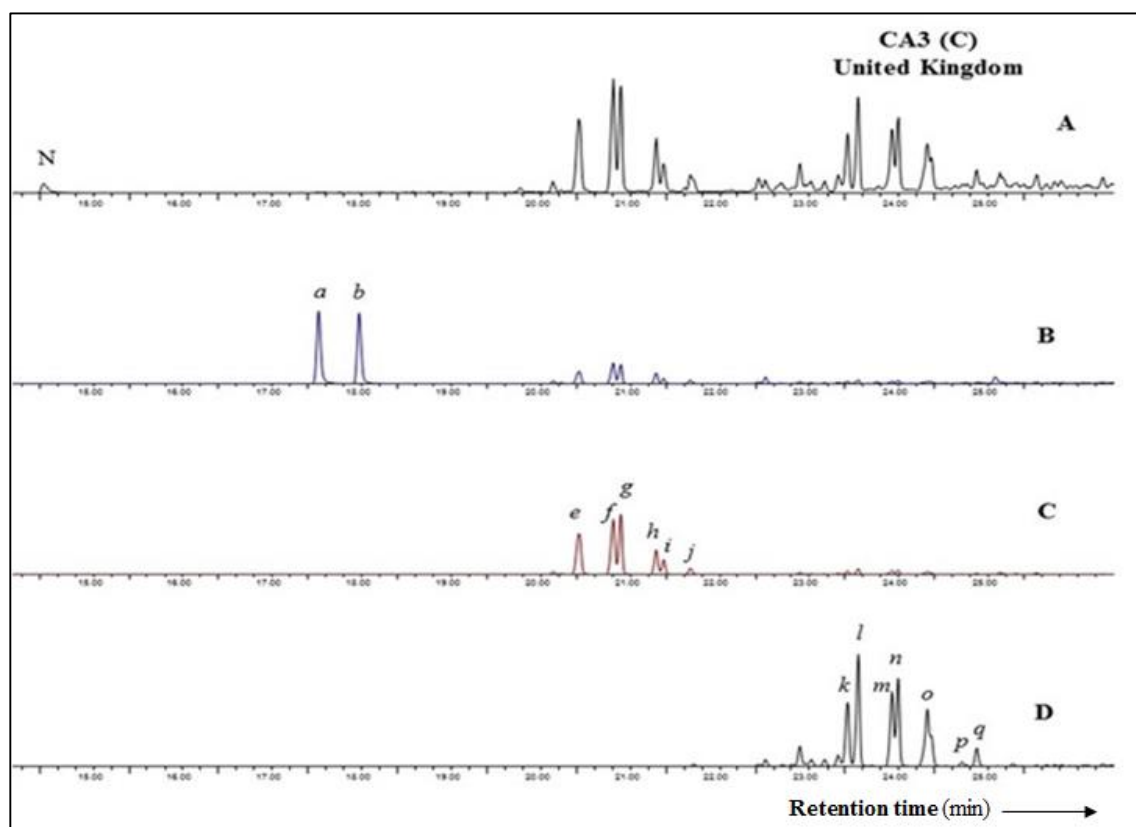


Figure 4.27: GC-MS m/z 128 and 142 mass chromatograms showing the distributions of the naphthalene and methylnaphthalenes and also GC-MS m/z 156 and 170 mass chromatograms showing the distributions of dimethylnaphthalenes and trimethylnaphthalenes in the representative oil CA3 (C) from the North Sea, UK.

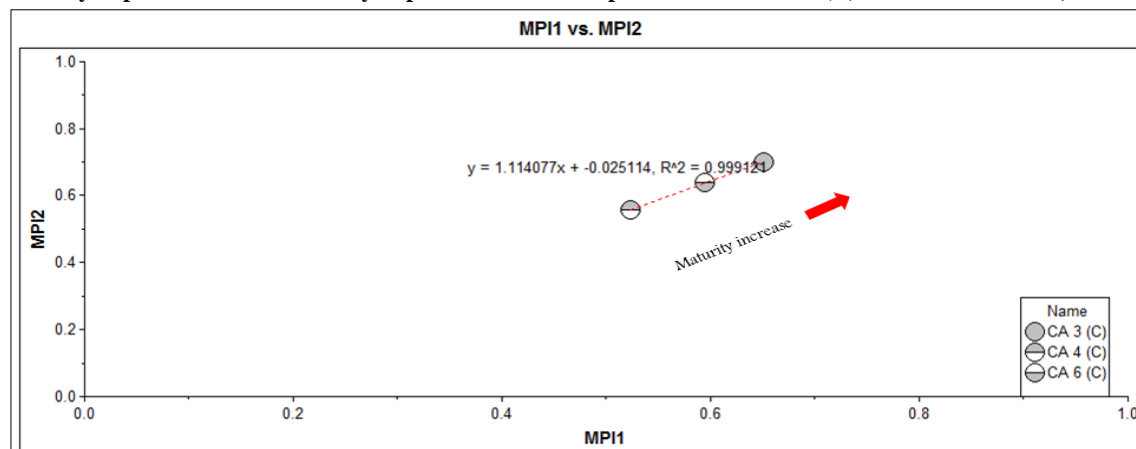


Figure 4.28: Cross plots of maturity parameter computed from aromatic hydrocarbons of the coals.

Table 4.13: Selected molecular parameter for thermal maturity and source indicators from aromatic hydrocarbon fractions in the coals.

Sample Name	MPI-1	MPI-2	MNR	4/1 MDT	3/2MDBT	DBT/PHEN	%R (MDBT)
CA 3 (C)	0.65	0.70	0.63	6.67	2.90	0.01	1.40
CA 4 (C)	0.52	0.56	0.66	4.77	2.00	0.01	1.31
CA 6 (C)	0.60	0.64	0.64	4.79	2.21	0.05	1.31

MPI-1 = $1.5(2MP+3MP)/(P+1MP+9MP)$; Radke *et al.* (1982b). MPI-2 = $3(2MP)/(P+1MP+9MP)$; (Radke *et al.*, 1982b). MNR = $(2-MN/1MN)$; DBT/PHEN; Hughes *et al.* (1995); MPR = $(2MP) / (1MP)$; (Radke *et al.*, 1984).

4.3.2.5 Source facies and thermal maturity

Based on the molecular properties of the studied coals from the North Sea, they exhibit overwhelmingly terrigenous organofacies and are believed to have been sourced from land-plants (Table 4.13). The high Pr/Ph ratios and the minor presence of gammacerane in the coals, may suggest hypersaline conditions. The coals are thermally immature – early mature as evident in the thermal maturity parameters calculated for the coals (Table 4.9, 4.10 and 4.13).

Table 4.13: Summary of maturity and source facies biomarkers in the studied coals.

Sample	Pr/Ph	CPI	Sterane (%)			Maturity	Likely source
			C ₂₇ aaa	C ₂₈ aaa	C ₂₉ aaa		
CA 3 (C)	2.44	nd	30.79	19.70	49.51	mid/mid	Land plant/coal measures
CA 4 (C)	4.36	1.01	40.98	14.15	44.87	mid/low	Land plant/coal measures
CA 6 (C)	2.48	nd	38.28	17.47	44.25	mid/mid	Planktonic/land plant

4.3.3 Comparative biomarker analysis in the studied oils and coals.

This section aims to integrate the results obtained from various biomarker parameters and provides a better understanding with regards to source facies, maturity and levels of biodegradation on the studied oil samples from different locations around the world. Principal component analysis (PCA) was applied to the data set (Appendix 3.0) to reduce the dimensionality of the data (PC1 – PC4) and account for the variation within the data (Zumberge, 1987). Thus, the resulting data is plotted in a two dimensional graph, whilst the two significant components still retain the relationships among the samples within the dataset.

The PCA performed here uses the 33 biomarker parameters (see Table 4.14). The loading weightings for each principal component are given in Table 4.15. The loading weightings for (PC1 and PC2) account for 53.75 % of the total variance in the dataset, distinctly separating the samples amongst related biomarkers. The loadings for PC1 show strong positive values for pregnanes (Mackenzie, 1984), C₂₉aaa, C₂₇aaa regular steranes (Peters *et al.*, 2005a), DBT/PHEN (Hughes *et al.*, 1995) and the 31Hops (Killops and Killops, 2005), homohopanes (Peters *et al.*, 2005a), Hop (35/34) (ten Haven *et al.*, 1987; Peters *et al.*, 2005a), Pr/nC₁₇ and Ph/nC₁₈ (Peters *et al.*, 2005a), while most of the aromatics and C₂₈aaa regular steranes (Peters *et al.*, 2005a) have

relatively strong negative loadings. The loading and score plots constructed on the basis of the PC1, (38.23 %) versus PC2, (15.52 %) shows the contribution of each variable related to PC1 and PC2 (Figure 4.29) and the relationships among the samples are also displayed in the plane of the PC1 and PC2 (Figure 4.30). Although, the score plot of PC1 against PC2 shows a meaningful pattern that can be attributed to the common characteristics of the oils and coals, the positive axis of PC1 is characterised by marine organic matter input whilst the negative axis is characterised by increasing terrestrial input. The Nigerian oils and North Sea coals are influenced by the terrestrial organic matter input.

The second principal component (PC2), which account for 15.52 % of the total variance in the dataset, grouped all Nigerian oils including (NA1, NA2, NA3, NE, NF, NA, NB, NC, N18, N25, ND & NN1) with the coals (CA3, CA4 & CA6) in the cluster (Figure 4.30). The loadings plots for the PC2 (Figure 4.29) show positive weightings for hopanes, tricyclic terpanes, steranes, aromatics (MNR & DMNR) whilst the aromatics (4/1 MDT, 3/2MDBT, %R (MDBT) (Radke *et al.*, 1982a), DBT/PHEN (Hughes *et al.*, 1995), MPI-1, MPI-2, MP(3+2)/9+1) (Radke *et al.*, 1986) and *n*-alkanes (Peters *et al.*, 2005a) have negative loadings.

The third principal component (PC3) accounts for 7.97% of the variance in the dataset. The loadings of the variables on the third component are shown in Figure 4.29. As observed previously, the PC3 show sterane variability, with pregnanes and C₂₇ααα regular steranes having strong positive loadings whilst the C₂₉αββ (Peakman *et al.*, 1989; Peters *et al.*, 2005a), C₂₈ααα, and C₂₉ααα steranes (Peters *et al.*, 2005a) have negative loadings.

The fourth principal component (PC4) accounts for only 6.97% of the variance in the dataset. The loadings of the variables show that it has positive loading for C₂₉αββ and % C₂₉ααα (Huang and Meinschein, 1979; Peters *et al.*, 2005a), MNR (Radke *et al.*, 1982b), 31Hops (Killops *et al.*, 1998), t29/t23, t26/t25 (Seifert and Moldowan, 1978) and the *n*-alkane parameters. However, negative loading were observed the parameters of hopanes, aromatics and steranes. The scores on PC4 (Figure 4.29) appear to have random setting of the samples within the plot of the dataset.

Furthermore, to improve the potential of identifying similarities and differences of the samples, hierarchical cluster analysis (HCA) from the principal components generated from PCA (Figure 4.32) was used to remove the negative influence of the multicollinearity of the dataset in the analysis (Hair, 2006). The classification is however more clearly shown in the dendrogram (Figure 4.30) from the hierarchical cluster analysis of the PC1 and PC2 from the PCA. There is a meaningful pattern attributed to the common source characteristic of the samples (marine and terrestrial organic matter input). Note the proximity of the samples in the plot indicates similarity in their molecular characteristics, and therefore many oils generated from the same source rocks are classified in the same cluster.

In general, however the oils from Nigeria and North Sea coals seem to be grouped together compared to the other oils. Other clusters are mixture of oils from different geographical locations (e.g. the United Kingdom and Middle East oils) consist exclusively of cluster 2 with similarity amongst them of 84 to 97%. Similarly, cluster 3 is a combination of oils from the Middle East (ME77) and most of the North American oils with exception of NAC oil from North America that are grouped in this cluster with similarity of over 99%.

It is also clear from Figure 4.30 that biodegradation does not seem to influence classification of the oils. Since, the biodegraded (e.g. NAC & UK88) and non-biodegraded (e.g. ME39 & ME43) oils are grouped in the same cluster.

Table 4.14: Molecular parameters in the PCA of the oils and coal extracts.

Number	Compound	Parameter	Explanation
1	Preg		C_{29} as percentage of sum 27-29 for $5\alpha(H)$, $14\alpha(H)$, $17\alpha(H)$ -20R sterane diginane + 5α -pregnane + 20 -methylgiginane + 5α methylpregnane/ same + C_{29} , 5α , 14α , 17α 20R + C_{29} , 5α , 14α , 17α 20S + C_{29} , 5α , 14β , 17β 20R + C_{29} , 5α , 14β , 17β 20S
2		$C_{29}\alpha\alpha\alpha$	C_{29} ster. S/(S + R)
3		$C_{29}\alpha\beta\beta$	C_{29} ster. $\alpha\beta\beta$ / $(\alpha\beta\beta + \alpha\alpha\alpha)$
4	Steranes	$C_{27}\alpha\alpha\alpha$	C_{27} ster. S/(S + R)
5		$C_{28}\alpha\alpha\alpha$	C_{28} ster. S/(S + R)
6		% $C_{27}\alpha\alpha\alpha$	C_{27} ster. as percentage of sum 27-29 for $5\alpha(H)$, $14\alpha(H)$, $17\alpha(H)$ -20R sterane
7		% $C_{28}\alpha\alpha\alpha$	C_{28} ster. as percentage of sum 27-29 for $5\alpha(H)$, $14\alpha(H)$, $17\alpha(H)$ -20R sterane
8		% $C_{29}\alpha\alpha\alpha$	C_{29} ster. as percentage of sum 27-29 for $5\alpha(H)$, $14\alpha(H)$, $17\alpha(H)$ -20R sterane
9		4/1 MDT	4-methyldibenzothiophene/1-methyldibenzothiophene
10		3/2MDBT	3- and 2-methyldibenzothiophene
11		DBT/PHEN	dibenzothiophene/phenanthrene
12		% R (MDBT)	mean vitrinite reflectance (% R_m) from of 4-methyldibenzothiophene relative to 1-methyldibenzothiophene
13	Aromatics	MPI-1	3- + 2-methylphenanthrene/phenanthrene and 9- + 1-methylphenanthrene
14		MPI-2	2-methylphenanthrene/phenanthrene and 9- + 1-methylphenanthrene
15		MP(3+2)/9+1	3- + 2-methylphenanthrene/9- + 1-methylphenanthrene
16		MNR	methylnaphthalene ratio (2-MN/1-MN)
17		DMNR	2,6- + 2,7-dimethylnaphthalene/1,5-dimethylnaphthalene
18		Ts/(Ts+Tm)	$18\alpha(H)$ -trisnorneohopane/ $17\alpha(H)$ -trisnorhopane ratio
19		29Ts/29Tm	$18\alpha(H)$ -norneohopane/ $17\alpha(H)$ -norhopane
20		29Hops	C_{29} Hops = C_{29} Hopane/ (C_{29} + C_{30} + C_{31} 22S and C_{31} 22R
21		30Hops	C_{30} Hops = C_{30} Hopane/ (C_{29} + C_{30} + C_{31} 22S and C_{31} 22R
22	Hopanes	31Hops	C_{31} Hops = C_{31} Hopane/ (C_{29} + C_{30} + C_{31} 22S and C_{31} 22R
23		HomoHop	$\alpha\beta$ C_{35} homohopane (22S+22R)/? C_{31}
24		Hop(35/34)	$C_{35}\alpha\beta S/C_{34}\alpha\beta S$
25		OI	$18\alpha(H)$ -oleanane/oleanane $17\alpha(H)$, $21\beta(H)$ -Hopane
26		Hop/Mor	$17\alpha(H)$ -norhopane/ $17\beta(H)$ -moretane
27		Hop(30/29)	$17\alpha(H)$ -hopane/ $17\alpha(H)$ -norhopane
28		t29/t23	C_{29} $17\alpha(H)$ -hopane/ C_{23} cheilhanthes
29	Tri- & Tetracyclic	t26/t25	C_{26} to C_{25} / $17\alpha(H)$ -hopane
30		t20-t26/T30	C_{28} to C_{26} cheilhanthes/ $17\alpha(H)$ -hopane
31		Pr/Ph	pristane/phytane
32	n-alkanes	NorPr	norpristane/pristane
33		nC_{17}/nC_{18}	nC_{17}/nC_{18} -alkane using GC data

Ratios were calculated from Pr = pristane; hop.= hopanes; ster.=steranes; hopane $\alpha\beta$ and $\beta\alpha$ refers to $17\alpha(H), 21\beta(H)$ and $17\beta(H), 21\alpha(H)$; hopane S/(S+R) refers to stereochemistry at C-22; sterane S/(S+R) refers to stereochemistry at C-20 ($\alpha\alpha\alpha$ configuration); sterane $\alpha\beta\beta$ and $\alpha\alpha\alpha$ refers to $5\alpha(H), 14\beta(H), 17\beta(H)$ and $5\alpha(H), 14\alpha(H), 17\alpha(H)$. Preg = pregnane.

Table 4.15: Loading weightings and molecular parameters used within the oil and coal extract samples in terms of principal component analyses (see table 4.14 for parameter explanation).

	Preg	C _{29aaa}	C _{29αββ}	C _{27aaa}	C _{28aaa}	%C _{27aaa}	%C _{28aaa}	%C _{29aaa}	4/1 MDT	3/2MDBT	DBT/PHEN
Loading 1	0.1797	0.2571	-0.0112	0.2214	-0.1444	0.2225	-0.1497	-0.2038	-0.1611	-0.2433	0.1267
Loading 2	-0.1491	0.0516	0.2207	0.0828	-0.0001	0.1071	0.0213	0.0425	-0.0289	-0.0434	-0.2044
Loading 3	0.1471	-0.1641	-0.1840	0.1119	-0.4394	0.1012	-0.4355	-0.0295	0.3813	0.1121	-0.0501
Loading 4	-0.2478	-0.0056	0.3031	-0.2285	0.0293	-0.2428	0.0177	0.3213	0.0134	-0.1046	-0.0070
	%R (MDBT)	MPI-1	MPI-2	MP(3+2)/9+1	MNR	DMNR	Ts/(Ts+Tm)	29Ts/29Tm	29Hops	30Hops	31Hops
Loading 1	-0.1352	-0.2112	-0.2054	-0.2243	-0.1427	-0.1170	0.0982	0.1445	-0.1291	-0.1162	0.2560
Loading 2	-0.0954	-0.1060	-0.1037	-0.0251	0.1500	0.0309	0.2570	0.2749	-0.3083	0.3752	0.0125
Loading 3	0.2406	-0.0650	-0.0482	-0.0566	0.1758	-0.1796	-0.1374	0.0590	-0.1804	-0.0233	0.0287
Loading 4	-0.1439	-0.3292	-0.3178	-0.2176	0.1396	-0.0948	-0.0091	-0.1055	0.0453	-0.0634	0.1083
	HomoHop	Hop(35/34)	OI	Hop/Mor	Hop(30/29)	t29/t23	t26/t25	t20-t26/T30	Pr/Ph	NorPr/Ph	nC ₁₇ /nC ₁₈
Loading 1	0.2561	0.1874	-0.2375	-0.0200	0.0003	-0.1480	-0.1219	0.2045	-0.1560	0.1506	0.1347
Loading 2	0.1000	-0.0279	0.0329	0.3301	0.4103	0.1153	0.0691	-0.1558	-0.0514	-0.2126	-0.2218
Loading 3	-0.0524	-0.1624	-0.1088	-0.0696	0.0290	0.2899	-0.0327	-0.0941	0.1464	-0.0374	0.0142
Loading 4	0.0287	-0.0827	-0.1713	-0.0691	-0.0635	0.2041	0.1341	-0.0711	0.2461	0.1363	0.3090

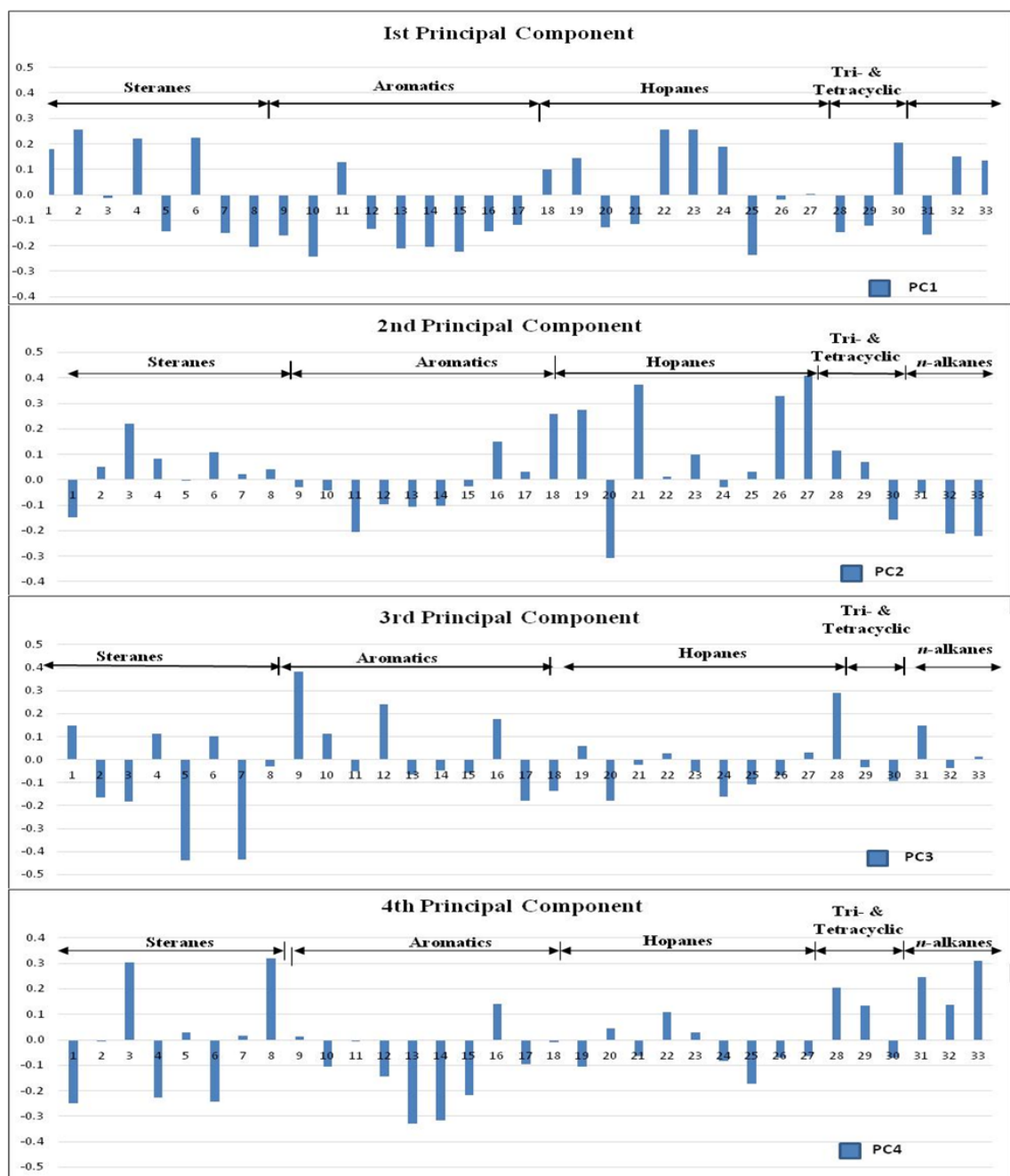


Figure 4.29: A loadings plots showing the relationship between different biomarker parameters in terms of the principal component analysis of the oil and coal extract samples used in the study (see table 4.14 for Molecular parameters).

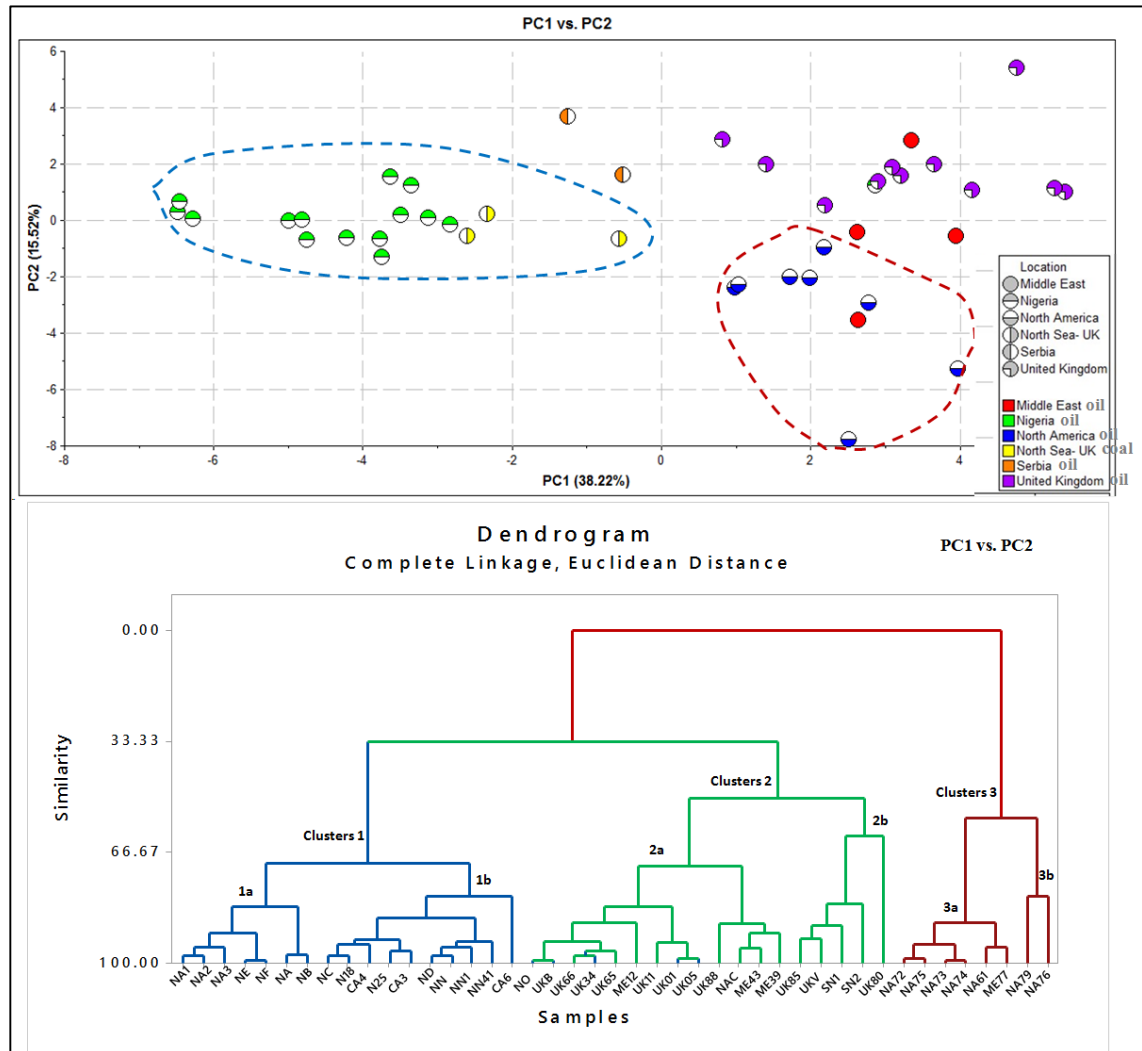


Figure 4.30: Principal component analysis (PC1 to PC2) results showing classification of the oils and coal extracts based on the score weightings of molecular parameters (see Table 4.16 for Score weightings).

The score plot of PC2 and PC3 is presented in Figure 4.31 and results of the PCA show that PC2 and PC3 cumulatively account for 23.49% of the variables within the dataset. As observed in the previous sections, the samples were grouped in a total of three clusters on the PC2 against PC3 (Figure 4.31). Nevertheless, it is interesting to note that this principal component grouped the Nigerian oils (NA1, NA2 & NA3), United Kingdom oils (UK66 & UK34), Middle East oil (ME39) and North Sea coals (CA3, CA4 & CA6) in same cluster (Cluster 1) with similarity amongst them of 97 - 100% indicating very similar biomarker compounds with respect to their scores on the PCs. Cluster 2 consist of mixture of oils from Nigeria (NA, NB, NC, N25, NN41, NE, NF, NO & N18), United Kingdom (UKB, UK66, UK34, UK65, UK11, UK01, UK05, UK88, UK85, UKV & UK80), North America (NAC), Middle East (ME12 & ME43)

and Serbia (SN1 & SN2). Cluster 3, on the other hand, consists mainly of North American oils (NA72, NA73, NA74, NA75, NA61, NA79 & NA76) all of which are source from marine shale.

The principal components PC3 and PC4 only account for less than 16% of the total variation within the dataset and there is no grouping into identifiable clusters (Figure 4.32).

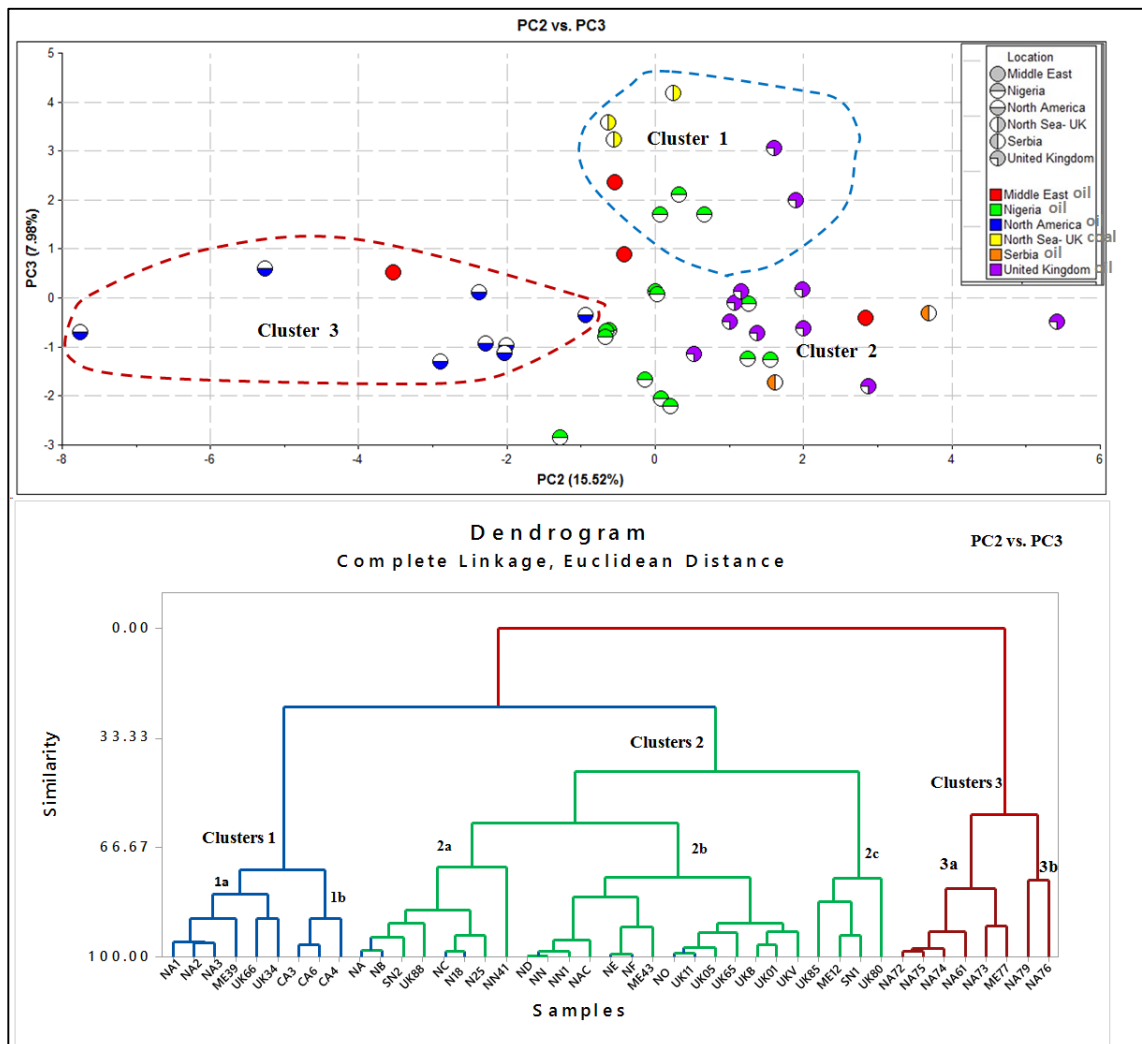


Figure 4.31: Principal component analysis (PC2 to PC3) results showing classification of the oils and coal extracts based on the score weightings of molecular parameters (see Table 4.16 for Score weightings).

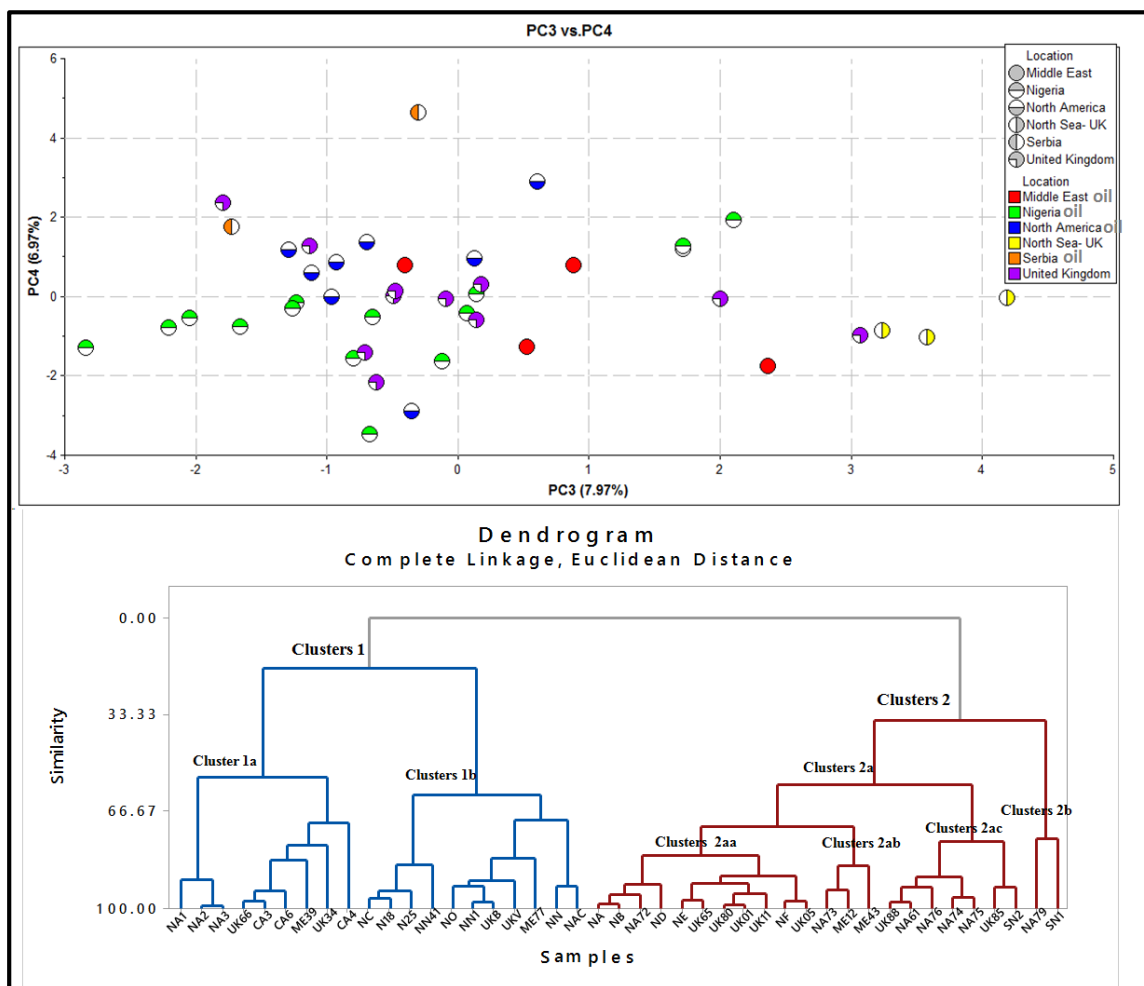


Figure 4.32: Principal component analysis (PC3 to PC4) results showing classification of the oils and coal extracts based on the score weightings of molecular parameters (see Table 4.16 for Score weightings).

Table 4.16: Score weightings of studied samples in terms of PC1 – PC4

Score 1	Score 2	Score 3	Score 4
-6.484	0.316	2.105	1.931
-6.277	0.069	1.714	1.202
-6.460	0.664	1.713	1.288
-3.352	1.242	-1.234	-0.153
-3.639	1.550	-1.266	-0.297
-3.132	0.082	-2.046	-0.549
-4.227	-0.629	-0.649	-0.517
-5.004	-0.004	0.139	0.074
-4.820	0.021	0.069	-0.408
2.861	1.252	-0.125	-1.638
-3.774	-0.657	-0.675	-3.463
-2.842	-0.142	-1.665	-0.756
-3.500	0.205	-2.206	-0.771
-4.756	-0.670	-0.801	-1.550
-3.755	-1.287	-2.843	-1.283
2.896	1.373	-0.714	-1.405
2.186	0.525	-1.135	1.288
0.817	2.876	-1.792	2.356
3.210	1.597	3.065	-0.982
3.650	1.989	0.177	0.311
4.750	5.417	-0.491	0.013
3.087	1.900	1.999	-0.058
4.159	1.071	-0.092	-0.052
5.399	1.007	-0.478	0.134
5.260	1.152	0.141	-0.598
1.398	1.995	-0.625	-2.162
1.715	-2.014	-0.963	-0.018
0.980	-2.382	0.122	0.962
1.024	-2.290	-0.930	0.871
1.985	-2.038	-1.120	0.606
3.971	-5.264	0.605	2.903
2.767	-2.905	-1.293	1.178
2.509	-7.756	-0.693	1.384
2.175	-0.947	-0.354	-2.894
2.628	-3.540	0.525	-1.267
3.935	-0.551	2.364	-1.740
2.614	-0.419	0.882	0.795
3.345	2.836	-0.404	0.784
-1.254	3.681	-0.301	4.639
-0.523	1.613	-1.725	1.763
-2.610	-0.554	3.235	-0.857
-2.340	0.245	4.185	-0.034
-0.571	-0.633	3.579	-1.029

4.4 Summary and conclusions

- a. The extent of biodegradation within the oils, ranges from level (1) to (6) using the Peters and Moldowan biodegradation scale.
- b. The non-biomarker and biomarker analyses of the samples predict their source facies as being any one of terrigenous organic matter deposited under oxic-suboxic conditions, marine organic matter deposited under anoxic or mixed contribution of terrestrial and marine sources.
- c. The oils and coals studied in this work show a broad range of maturity from immature to late mature.
- d. The results of the principal components analysis permitted an independent grouping of the studied samples and as such source facies influence is thought to be the dominant control on the groupings.

Chapter 5 Determination of asphaltene content in crude oil

5.1 Introduction

It is now routine to separate crude oils into different group-type fractions using Iatroscan (Karlsen and Larter, 1991). This is a thin-layer chromatography with flame ionisation detector (TLC-FID). TLC-FID thus reveals the percentage distribution of the crude oil classes: saturated hydrocarbons, aromatic hydrocarbons, resins and asphaltene fractions (Karlsen and Larter, 1991; Pollard *et al.*, 1992). The technique, depends on differences in the polarity of crude oil components and has become worthwhile as it is fast, efficient and cost effective for screening complex mixtures, such as crude oil (Karlsen and Larter, 1991; Bharati *et al.*, 1994; Jiang *et al.*, 2008). The practical application of this technique in the petroleum industry has been investigated (Karlsen and Larter, 1991; Bharati *et al.*, 1997). Hence, using Iatroscan in this study has relied upon natural standard (North Sea oil) for quantification of the crude oils and calibrating the instrument.

In this chapter, gravimetric results from consecutive precipitation of asphaltene as described by Alboudwarej *et al.* (2002) and Iatroscan measurements are presented. The questions to be addressed are:

- a. What is the gross composition (wt. %) of the saturate, aromatic, resin, and asphaltene fractions in the different crude oils?
- b. What is the asphaltene content in oil (mg/g) from Iatroscan versus gravimetric method?
- c. Does biodegradation affect the asphaltene content?
- d. Does source affect the asphaltene content?
- e. Which is most accurate, Iatroscan or gravimetric?

5.2 Methods

Quantification of SARA fractions of thirty-six suites of non-degraded and degraded crude oils from varying locations around the world was performed with standard oil (North Sea oil) and the distribution generated in percentage weight of the oil. The samples include:

- a. Fourteen crude oils from Niger Delta, Nigeria.
- b. Ten oils from United Kingdom.
- c. Two oils from Middle East.
- d. Eight from North America and
- e. Two oils were from the Serbia region.

The samples were prepared as described in chapter 3, section 3.3.1 and 3.3.2. The SARA fractions of the oil were estimated as in Karlsen and Larter (1991) using Iatroscan (TLC-FID). The generated data (%) of the total asphaltene component in crude oil from Iatroscan were converted to (mg/g) using equations 5.1 – 5.14.

5.3 Data interpretation

The typical TLC-FID chromatograms of the crude oil fractions: saturated hydrocarbons, aromatic hydrocarbons, resins and asphaltenes used in Iatroscan calibration may differ significantly from each other with respect to density and composition. As a result, it is necessary to have a calibration standard (North Sea oil) that is chemically similar to the samples being analysed. Thus, analytical precision was calculated in each case of the crude oil fractions using equations shown below.

$$w_t \text{ (mg)} = w \text{ (mg)} * v \text{ (\mu L)} / V \text{ (\mu L)} \quad \text{Eq. 5.1}$$

where: w_t = weight of oil used for Iatroscan (mg), w = total weight of oil sample (mg), v = volume of oil sample used for Iatroscan (μL) and V = total volume of oil (μL).

Considering the weight of the oil (μg) used in μg the equation 5.1 can be written as:

$$w_w \text{ (\mu g)} = w_t * 1000 \quad \text{Eq. 5.2}$$

However, a correction constant can be obtained from each of the components from the standard North Sea oil as:

$$\text{Response component } R_c = p_a / (R_f * w_w) \quad \text{Eq. 5.3}$$

where R_c = response component, R_f = response component, and w_w = weight of oil used and p_a is the peak area of the four components in oil sample generated from Iatroscan. Each of the response components is estimated with respect to the response factor as follows:

$$R_{c(sat)} = p_{a(sat)} / (0.57 * w_w) \quad \text{Eq. 5.4}$$

$$R_{c(Aro)} = p_{a(Aro)} / (0.36 * w_w) \quad \text{Eq. 5.5}$$

$$R_{c(resin)} = p_{a(resin)} / (0.06 * w_w) \quad \text{Eq. 5.6}$$

$$R_{c(Asp)} = p_{a(Asp)} / (0.02 * w_w) \quad \text{Eq. 5.5}$$

where $R_{c(sat)}$, $R_{c(Aro)}$, $R_{c(resin)}$ and $R_{c(Asp)}$, are components of saturates, aromatics, resins and asphaltenes respectively. $p_{a(sat)}$, $p_{a(Aro)}$, $p_{a(resin)}$, and $p_{a(Asp)}$ are the peak areas of saturate $R_{f(sat)}$, aromatic $R_{f(aro)}$, $R_{f(resin)}$, and asphaltene $R_{f(Asp)}$ components respectively while 0.57, 0.36, 0.06 and 0.02 are the respective response factors of the saturate, aromatic, resin and asphaltene components of the standard (North Sea oil).

From Eq. 5.3, the derived equations Eq. 5.4 – 5.7 of the percentage of the four components can be written as in Bharati *et al.* (1994).

$$\text{Comp (sat)} = R_f(sat) * 100 / (R_f(sat) + R_f(aro) + R_f(resin) + R_f(Asp)) \quad \text{Eq. 5.8}$$

$$\text{Comp (Aro)} = R_f(Aro) * 100 / (R_f(sat) + R_f(aro) + R_f(resin) + R_f(Asp)) \quad \text{Eq. 5.9}$$

$$\text{Comp (Resin)} = R_f(Resin) * 100 / (R_f(sat) + R_f(aro) + R_f(resin) + R_f(Asp)) \quad \text{Eq. 5.10}$$

$$\text{Comp (Asp)} = R_f(Asp) * 100 / (R_f(sat) + R_f(aro) + R_f(resin) + R_f(Asp)) \quad \text{Eq. 5.11}$$

where Comp (sat), Comp (Aro), Comp (resin) and Comp (Asp) are percentage composition of saturates, aromatics, resins and asphaltenes respectively generated from

the Iatroscan. However, the total asphaltene parameters in the crude oil were converted to mg/g using:

$$\text{Comp (Asp)} = [w_A(\text{mg})/w_0(\text{mg})] \quad \text{Eq. 5.12}$$

where Comp (Asp) = weight (%) of asphaltene fraction as measured by Iatroscan (see section 3.3.1)

w_A = weight of asphaltene recovered from Iatroscan procedure (mg)

w_0 = weight of oil sample (mg)

Then the parameter of our experiment is written as:

$$w_A = w_0(\text{mg}) * A(\%) \quad \text{Eq. 5.13}$$

$$w_A = w_A(\text{mg}) * w_0(\text{g}) \quad \text{Eq. 5.14}$$

5.4 Results and discussion

5.4.1 Iatroscan measurement of asphaltenes

In this section, the gross percentage compositions of the oils were obtained from calculating arithmetic means and standard deviations of repeated peaks areas for the saturate, aromatic, resins and asphaltene fractions of crude oil for 36 replicate analyses from the standard S-III rods run of Iatroscan procedure from Equations (5.8 – 5.11). The statistical results obtained from the Iatroscan method is shown in Appendix 5.1. However, the results obtained from Iatroscan of the total asphaltene content in oil (mg/g) were then converted applying Eq. 5.12. Furthermore, total asphaltene content of Iatroscan results, were compared with those obtained from asphaltene content of gravimetric method from the same crude oil as section 5.4.2.

5.4.1.1 Nigerian oil

The SARA gross compositions of the representative Nigerian crude oils are shown in Figure 5.1. The saturated hydrocarbons comprised 48.27 (\pm 6.12) – 80.76 (\pm 15.93) wt. % of the gross composition of the oil, aromatic hydrocarbons 14.35 (\pm 9.92) – 33.87 (\pm 1.79) wt. %, and resins 3.02 (\pm 4.15) – 18.83 (\pm 5.34) wt. % and asphaltenes 0.09 (\pm 0.10) – 5.01 \pm (3.90) wt. % presented as Table 5.1. As illustrated in Figure 5.1 the gross compositions of the Nigerian crude oils were poor in asphaltenes compared to richer aromatic hydrocarbons.

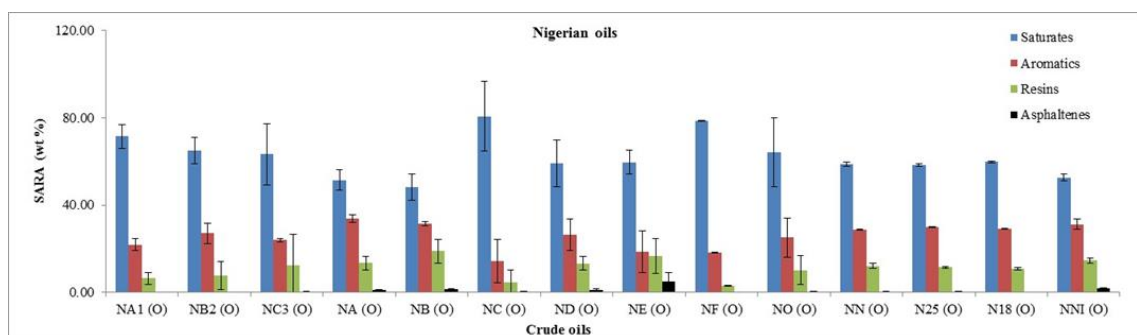


Figure 5.1: Percentage distribution of SARA fractions from the Nigerian oils with values reported as means, with error bars \pm one SD, see table 5.1.

Table 5.1: Variation in gross composition (wt. %) for Nigerian crude oils calculated from Iatroscan analysis.

Sample	Biodegradation level	Saturates		Aromatics		Resins		Asphaltenes	
		(wt. %)	SD	(wt. %)	SD	(wt. %)	SD	(wt. %)	SD
NA1 (O)	1	71.58	± 5.47	21.87	± 2.68	6.42	± 2.76	0.13	± 0.04
NB2 (O)	1	64.91	± 6.15	27.15	± 4.66	7.84	± 6.45	0.09	± 0.10
NC3 (O)	1	63.27	± 14.18	23.91	± 0.71	12.52	± 14.00	0.3	± 0.20
NA (O)	6	51.51	± 4.72	33.87	± 1.79	13.44	± 3.04	1.17	± 0.14
NB (O)	6	48.27	± 6.12	31.34	± 1.04	18.83	± 5.34	1.56	± 0.17
NC (O)	6	80.76	± 15.93	14.35	± 9.92	4.56	± 5.77	0.32	± 0.25
ND (O)	1	59.24	± 10.73	26.3	± 7.18	13.29	± 3.20	1.16	± 0.55
NE (O)	1	59.70	± 5.31	18.58	± 9.61	16.71	± 7.90	5.01	± 3.90
NF (O)	1	78.57	± 0.15	18.27	± 0.06	3.02	± 0.08	0.14	± 0.00
NO (O)	6	64.29	± 15.71	25.15	± 9.03	10.09	± 6.62	0.47	± 0.11
NN (O)	3	58.86	± 0.92	28.74	± 0.37	12.08	± 1.17	0.32	± 0.18
N25 (O)	3	58.3	± 0.50	29.91	± 0.10	11.47	± 0.50	0.33	± 0.10
N18 (O)	3	59.79	± 0.33	29.24	± 0.25	10.81	± 0.53	0.16	± 0.04
NN1 (O)	1	52.71	± 1.56	31.13	± 2.39	14.52	± 1.19	1.65	± 0.20

SD = Standard deviation

5.4.1.2 United Kingdom oils

The distributions of the SARA fractions of the oils from United Kingdom are shown in Figure 5.2. The saturated hydrocarbons comprised 43.60 (± 2.71) – 73.80 (± 17.31) wt. %, of the gross composition of the oil, aromatic hydrocarbons 11.43 (± 2.23) – 35.25 (± 0.11) wt. %, and resins 6.61 (± 1.60) – 30.74 (± 2.59) wt. % and asphaltenes 0.63 (± 0.11) – 6.01 (± 0.89) wt. % as presented in Table 5.2. The compositions show slightly richer asphaltenes compared to Nigerian oils (Figure 5.2).

Table 5.2: Variation in gross composition (wt. %) for United Kingdom crude oils calculated from Iatroscan analysis.

Sample	Biodegradation level	Saturates		Aromatics		Resins		Asphaltenes	
		(wt. %)	SD	(wt. %)	SD	(wt. %)	SD	(wt. %)	SD
UKB (O)	5	73.80	± 17.31	18.28	± 10.04	7.29	± 6.78	0.63	± 0.11
UK88 (O)	3	53.62	± 1.27	30.78	± 0.82	11.40	± 0.61	4.20	± 0.21
UK85 (O)	3	55.61	± 1.41	25.34	± 1.82	16.06	± 2.18	2.99	± 0.65
UK66 (O)	5	80.10	± 3.76	11.43	± 2.23	6.61	± 1.60	1.87	± 0.06
UK65 (O)	3	54.17	± 1.27	26.69	± 0.29	13.13	± 0.67	6.01	± 0.89
UK80 (O)	5	54.17	± 1.16	26.69	± 2.76	13.13	± 3.04	4.49	± 1.52
UK34 (O)	3	43.60	± 2.71	35.23	± 0.11	18.47	± 2.58	2.69	± 1.06
UK11 (O)	1	49.55	± 2.45	17.94	± 1.03	30.74	± 2.59	1.77	± 0.23
UK01 (O)	1	54.06	± 2.93	33.87	± 1.86	10.39	± 2.70	1.68	± 0.91
UK05 (O)	1	52.86	± 1.74	34.81	± 2.12	10.63	± 1.61	1.70	± 0.54

SD – Standard deviation

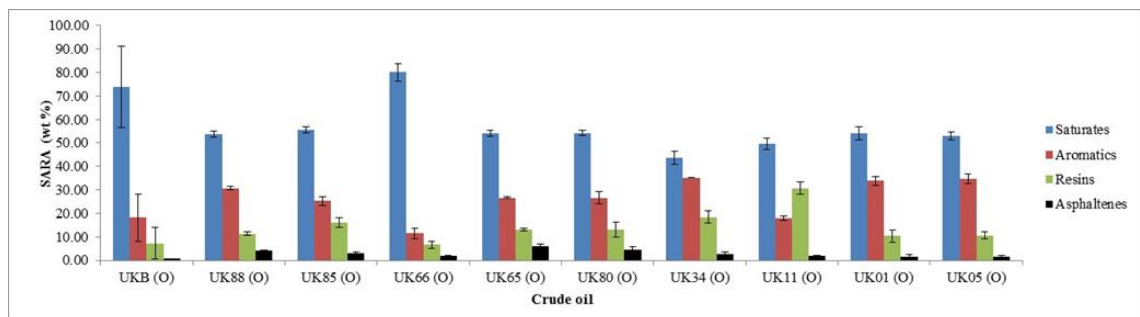


Figure 5.2: Percentage distribution of SARA fractions for the United Kingdom crude oils with values reported as means, with error bars +/- one SD, see table 5.2.

5.4.1.3 Middle East oils

The gross compositions of the representative crude oils from Middle East are shown in Figure 5.3. The oils are highly variable in the distributions of SARA fractions. However they are dominated by saturated hydrocarbons. The saturated hydrocarbons varies from 75.69 (± 23.29) – 78.61 (± 26.29) wt. %, aromatic hydrocarbons vary from 16.17 (± 20.86) – 20.47 (± 20.32) wt. %, resins vary from 3.37 (± 2.06) – 4.73 (± 5.88) wt. % and asphaltene vary from 0.39 (± 0.10) – 0.47 (± 0.37) wt. % as presented in Table 5.3.

Table 5.3: Variation in gross composition (wt. %) for Middle East crude oils calculated from Iatroscan analysis.

Sample	Biodegradation level	Saturates (wt. %)	SD	Aromatics (wt. %)	SD	Resins (wt. %)	SD	Asphaltenes (wt. %)	SD
ME39 (O)	1	75.69	± 23.29	20.47	± 20.86	3.37	± 2.06	0.47	± 0.37
ME43 (O)	1	78.71	± 26.29	16.17	± 20.32	4.73	± 5.88	0.39	± 0.10

SD – Standard deviation

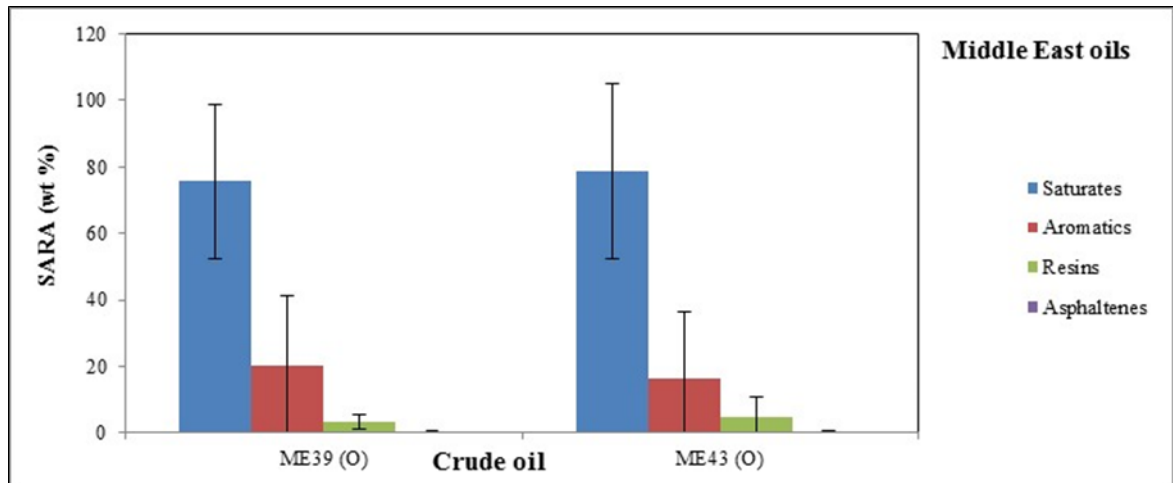


Figure 5.3: Percentage distribution of SARA fractions from the Middle East oils with values reported as means, with error bars +/- one SD, see table 5.3.

5.4.1.4 North American oils

The gross compositions of the representative North American crude oils are shown in Figure 5.4. The oils are highly variable in the distributions of the SARA fractions. However they are dominated by saturated hydrocarbons, where they varies from 21.69 (± 0.67) – 92.19 (± 0.53) wt. %, aromatic hydrocarbons vary from 6.98 (± 0.02) – 48.14 (± 2.93) wt. %, resins vary from 0.63 (± 0.50) – 45.65 (± 3.58) wt. % and asphaltene vary from 0.21 (± 0.02) – 13.72 (± 1.40) wt. % as presented in Table 5.4.

Table 5.4: Variation in gross composition (wt. %) for North American crude oils calculated from Iatroscan analysis.

Sample	Biodegradation level	Saturates		Aromatics		Resins		Asphaltenes	
		(wt. %)	SD	(wt. %)	SD	(wt. %)	SD	(wt. %)	SD
NA72 (O)	1	58.65	± 4.58	30.50	± 4.80	10.45	± 0.36	0.40	± 0.11
NA73 (O)	1	50.23	± 1.02	23.81	± 1.66	23.82	± 0.49	2.14	± 1.02
NA74 (O)	1	55.75	± 3.99	28.38	± 0.78	15.11	± 3.98	0.77	± 0.77
NA75 (O)	1	55.99	± 2.06	29.61	± 2.37	14.14	± 0.71	0.26	± 0.07
NA79 (O)	3	92.19	± 0.53	6.98	± 0.02	0.63	± 0.50	0.21	± 0.02
NA61 (O)	1	21.49	± 0.67	48.14	± 2.93	21.92	± 2.03	8.45	± 0.77
NA76 (O)	1	22.95	± 0.16	17.69	± 4.76	45.65	± 3.58	13.72	± 1.40
NAC (O)	6	35.59	± 19.97	37.42	± 14.91	22.83	± 4.31	4.16	± 0.82

SD – Standard deviation

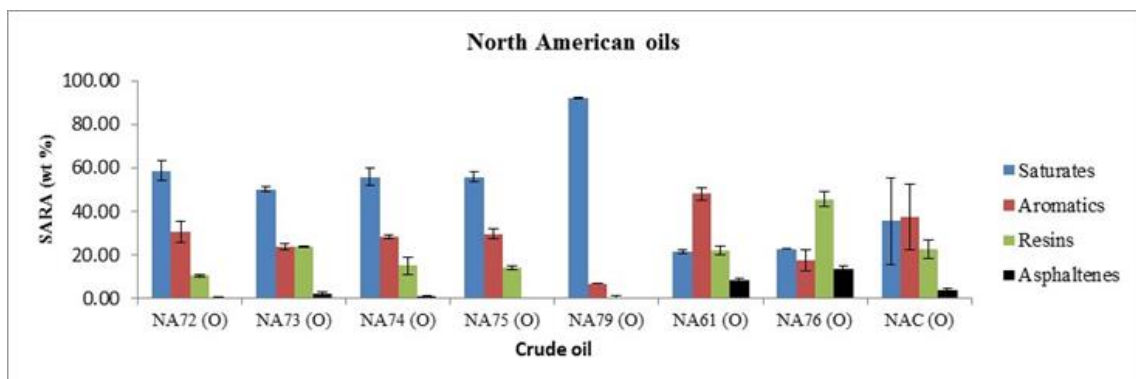


Figure 5.4: Percentage distribution of SARA fractions from the North American oils with values reported as means, with error bars +/- one SD, see table 5.4.

5.4.1.5 Serbian oils

The gross compositions of Iatroscan analysis from the two representative oil samples from Serbia are shown in Figure 5.5. The composition of saturated hydrocarbons varies from 52.84 (± 2.93) – 67.80 (± 2.10) wt. %, aromatic hydrocarbons vary from 20.98 (± 0.74) – 23.57 (± 1.48) wt. %, resins vary from 9.63 (± 1.32) – 16.44 (± 4.71) wt. % and asphaltene vary from 1.59 (± 0.21) – 7.15 (± 0.60) wt. % as presented in Table 5.5.

Table 5.5: Variation in gross composition (wt. %) for Serbian crude oils calculated from Iatroscan analysis.

Sample	Biodegradation level	Saturates		Aromatics		Resins		Asphaltenes	
		(wt. %)	SD	(wt. %)	SD	(wt. %)	SD	(wt. %)	SD
SN1 (O)	6	52.84	± 2.93	23.57	± 1.48	16.44	± 4.71	7.15	± 0.60
SN2 (O)	1	67.80	± 2.10	20.98	± 0.74	9.63	± 1.32	1.59	± 0.21

SD – Standard deviation

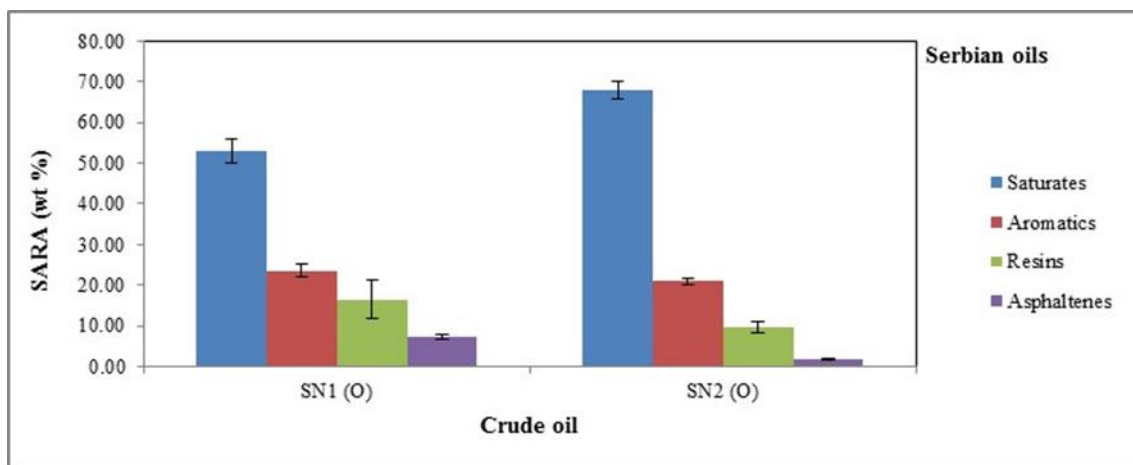


Figure 5.5: Percentage distribution of SARA fractions from the Serbian oils with values reported as means, with error bars +/- one SD, see table 5.5.

5.4.2 Calibration measurement of asphaltenes

In this study, for the purposes of calibration measurement, 19 crude oil samples were obtained and used in the Iatroscan analysis (Appendix 4.0). The calculated contents in mg/g of the asphaltene fraction recovered from gravimetric procedure of the oils are reported as mean \pm one standard deviation (Appendix 5.0).

5.4.2.1 Nigeria oils

Table 5.6 shows the results of Iatroscan analysis and gravimetric procedure of total asphaltene content recovered from Nigerian oils. A comparison of both quantified cases (Figure 5.6), gives a lower yields of asphaltenes for gravimetric. However, plotting Iatroscan TLC-FID versus gravimetric procedure, gives a coefficient of determination (i.e. percentage value of the square of correlation coefficient, R^2) of 93% (Figure 5.7).

Table 5.6: Differences in the asphaltene values of the Nigerian crude oils in the gravimetric method versus Iatroscan method.

Sample	Biodegradation level	Gravimetric		Iatroscan	
		(mg/g)	SD	(mg/g)	SD
NA (O)	6	1.65	\pm 0.24	11.72	\pm 0.14
NB (O)	6	1.11	\pm 0.49	15.62	\pm 0.17
NC (O)	6	2.53	\pm 1.44	3.21	\pm 0.25
ND (O)	1	1.90	\pm 0.96	11.58	\pm 0.55

SD – Standard deviation

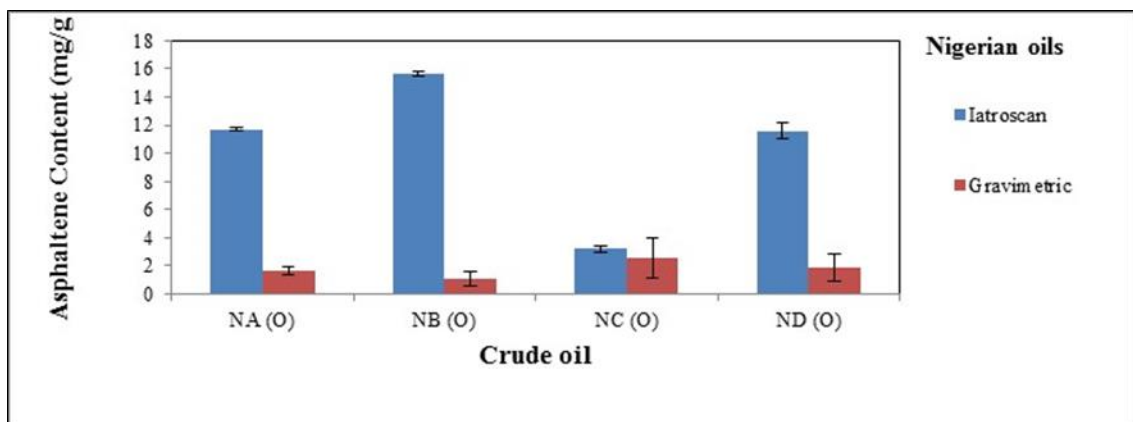


Figure 5.6: Weight of asphaltene content (mg/g) recovered from the Nigerian oils with values reported as means, with error bars +/- one SD, see table 5.6.

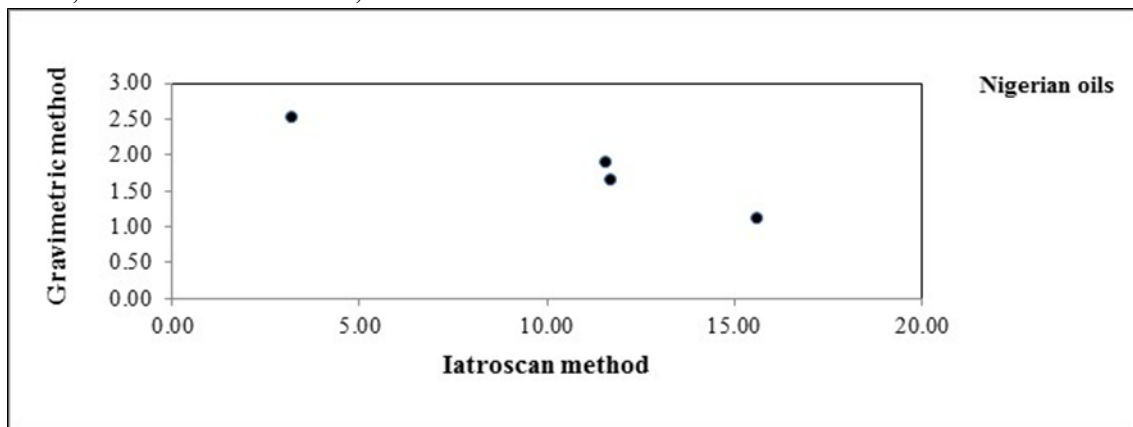


Figure 5.7: Correlation of asphaltene content (mg/g) recovered from Iatroscan versus gravimetric method from the Nigerian oils.

5.4.2.2 United Kingdom oils

Table 5.7 shows the summary of the total amount of asphaltene contents recovered from the 4 selected oils analysed by Iatroscan and gravimetric procedures from the United Kingdom crude oils. Note, Iatroscan TLC-FID has an asphaltene content which exceeds that of gravimetric method excluding the biodegraded oil (Figure 5.8). As both methods are used to determine asphaltene content in oils, a correlation between the two methods is expected. This is confirmed by a strong negative coefficient in Figure 5.9.

Table 5.7: Differences in the asphaltene values of the United Kingdom crude oils in the gravimetric method versus Iatroscan method.

Sample	Biodegradation	Gravimetric		Iatroscan	
		(mg/g)	SD	(mg/g)	SD
UKB (O)	5	28.72	± 0.12	6.26	± 0.11
UK11 (O)	1	8.21	± 3.78	17.68	± 0.23
UK 01 (O)	1	7.03	± 0.11	16.80	± 0.91
UK 05 (O)	1	5.44	± 0.46	17.01	± 0.54

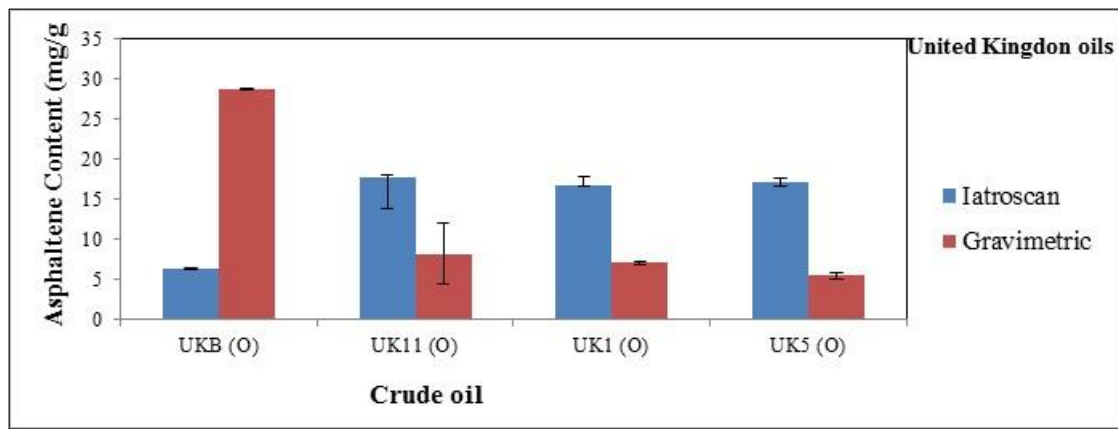


Figure 5.8: Weight of asphaltene content (mg/g) recovered from the United Kingdom oils with values reported as means, with error bars +/- one SD, see table 5.7.

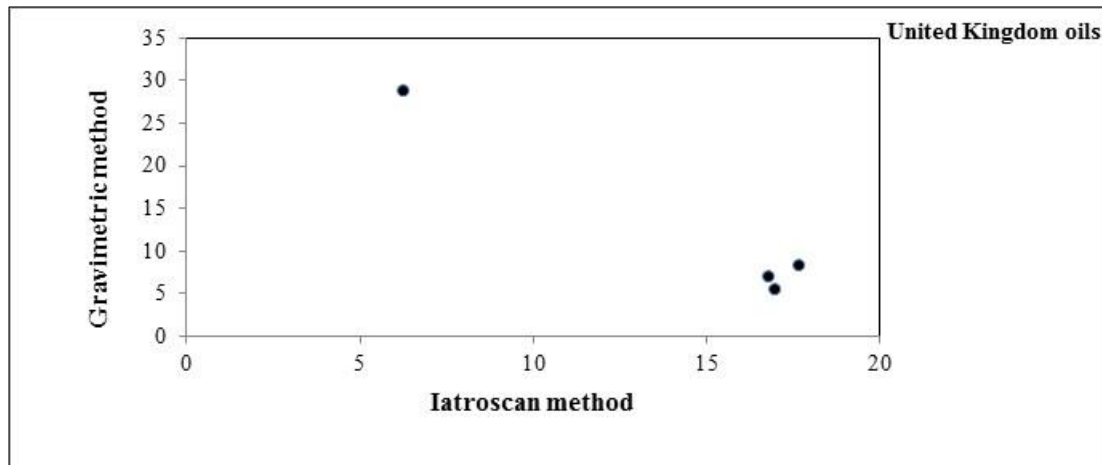


Figure 5.9: Correlation of asphaltene content (mg/g) recovered from Iatroscan versus gravimetric method from the United Kingdom oils.

5.4.2.3 Middle East oils

Table 5.8 shows the results of Iatroscan and gravimetric analyses of representative crude oils from Middle East used in this study. A comparison of both techniques (Figure 5.10), shows a quantified higher absolute yield of asphaltene content from Iatroscan analysis compare to gravimetric analysis.

Table 5.8: Differences in the asphaltene values of the United Kingdom crude oils in the gravimetric method versus Iatroscan method.

Sample	Biodegradation level	Gravimetric (mg/g)	SD	Iatroscan (mg/g)	SD
ME39 (O)	1	16.05	± 3.11	4.70	± 0.37
ME43 (O)	1	22.21	± 0.53	3.92	± 0.10

SD = Standard deviation

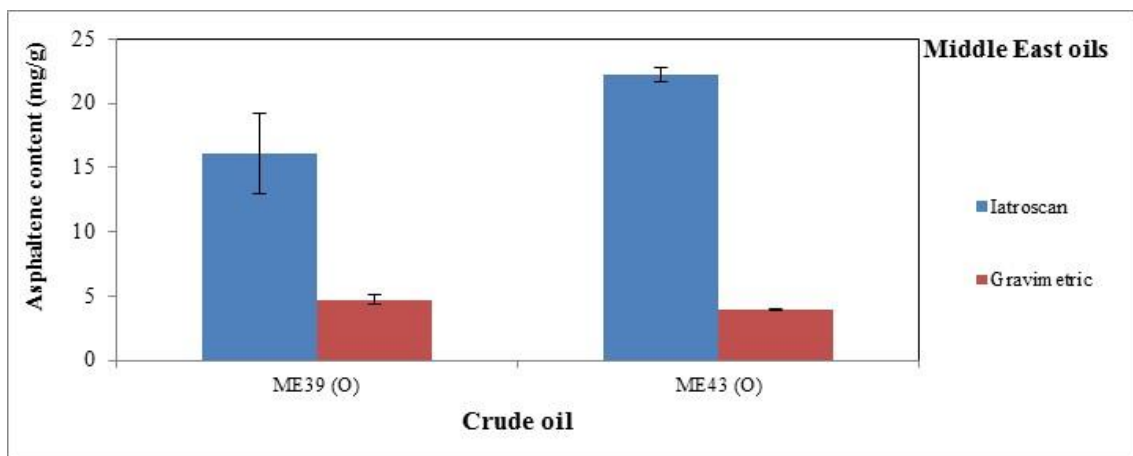


Figure 5.10: Weight of asphaltene content (mg/g) recovered from the Middle East oils with values reported as means, with error bars +/- one SD, see table 5.8.

5.4.2.4 North American oils

Table 5.9 shows the results of gravimetric and Iatroscan method used to determine asphaltene content in the 7 oil samples from North America. A comparison of results of two procedures is shown in Figure 5.11 with standard deviation. In both quantified cases, the North American oils give a coefficient agreement (R^2) of 87% (Figure 5.12). However, sample NA79 (O) and NAC (O) gave a higher yield of asphaltenes (Table 5.9).

Table 5.9: Differences in the asphaltene values of the North American crude oils in the gravimetric method versus Iatroscan method.

Sample	Biodegradation level	Gravimetric		Iatroscan	
		(mg/g)	SD	(mg/g)	SD
NA73 (O)	1	4.19	± 1.98	21.41	± 1.02
NA74 (O)	1	4.07	± 1.36	7.67	± 0.77
NA75 (O)	1	1.73	± 1.19	2.64	± 0.07
NA76 (O)	1	124.36	± 0.57	137.16	± 1.40
NA79 (O)	3	2.79	± 0.14	2.09	± 1.40
NA61 (O)	1	36.34	± 12.45	84.50	± 0.77
NAC (O)	6	50.16	± 0.16	41.65	± 0.82

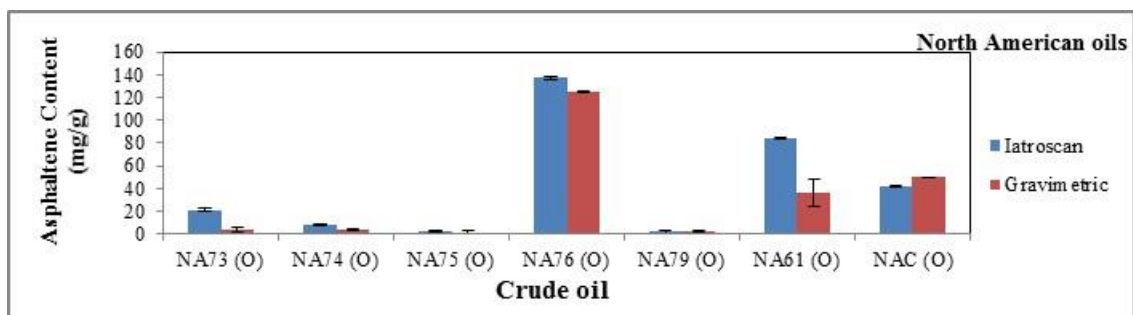


Figure 5.11: Weight of asphaltene content (mg/g) recovered from the North American oils with values reported as means, with error bars +/- one SD, see table 5.9.

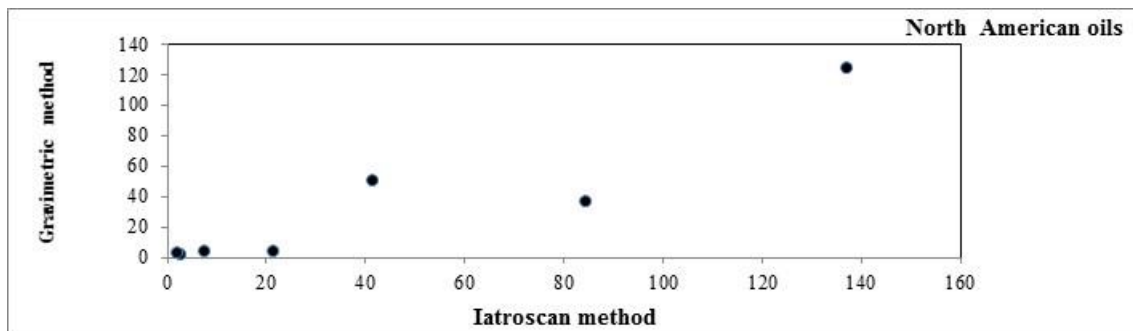


Figure 5.12: Correlation of asphaltene content (mg/g) recovered from Iatroscan versus gravimetric method from the North American oils.

5.4.2.5 Serbian oils

Table 5.10 shows the summary of gravimetric analysis and Iatroscan analysis results from the 2 oil samples from Serbia, while comparison of variable asphaltene yields of both cases are presented in Figure 5.13.

Table 5.10: Differences in the asphaltene values of the Serbian crude oils in the gravimetric method versus Iatroscan method.

Sample	Location	Gravimetric		Iatroscan	
		(mg/g)	SD	(mg/g)	SD
SN1 (O)	6	20.05	± 9.19	71.53	± 0.60
SN2 (O)	1	24.34	± 9.74	15.94	± 0.21

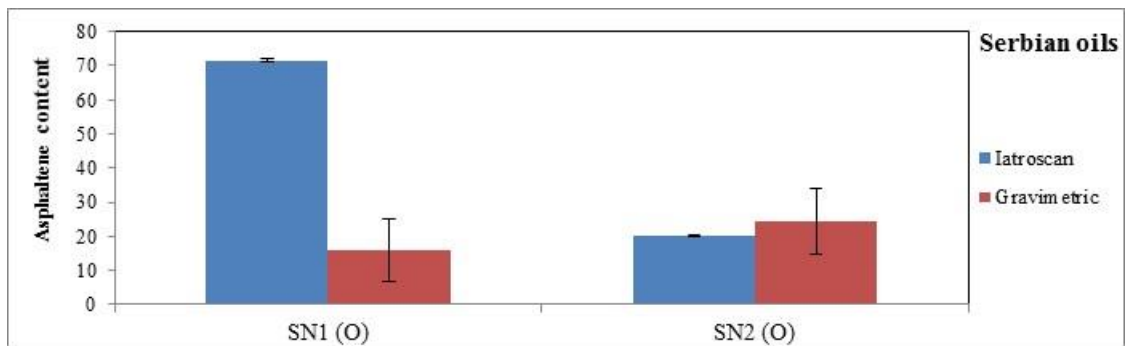


Figure 5.13: Weight of asphaltene content (mg/g) recovered from the Serbian oils with values reported as means, with error bars +/- one SD, see table 5.10.

5.5 Summary and conclusions

Iatroscan TLC-FID analysis was used to characterise crude oils and measurements were compared with gravimetric determinations. The results showed that:

- a. The crude oils in this study showed variable gross compositions (wt. %) with saturated hydrocarbons ranging from 21.49 – 92.19 wt. %, aromatics ranging from 25.62 – 48.14 wt. %, resins ranging from 0.63 – 45.65 wt. % and asphaltenes ranging from 0.09 – 13.72 wt. %.
- b. The range of asphaltene contents determined from both the Iatroscan (2.09 – 137.16 mg/g) and gravimetric (1.11 – 124.36 mg/g) methods were comparable (see Appendices 4.0 and 5.0). However for every non-degraded oil the Iatroscan measured a consistently higher asphaltene content compared to gravimetric analysis whilst for biodegraded oils the gravimetric procedure quantified a higher value consistently for the asphaltenes as compared to the Iatroscan method. Therefore values of the asphaltene content are dependent on the measurement methodology.
- c. It also appears that the asphaltene content is affected by source facies of the oils, as similar terrigenous sources give lower asphaltenes as compared to open marine/ shallow marine Nigerian oils using the same measurement method.
- d. The correlation of Iatroscan method and gravimetric determination appears low when all oils are considered.

Chapter 6 Structural characterisation of asphaltenes by FTIR

6.1 Introduction

Different infrared spectroscopy (IR) techniques have been used to identify functional groups in asphaltenes (Wilt *et al.*, 1998). Absorption FTIR, diffuse reflectance FTIR (DRIFT), attenuated total reflectance (ATR) and photo acoustic (PAS) techniques have been used to obtain chemical information to improve the understanding of petroleum asphaltenes and related organic compounds (Wilt *et al.*, 1998). Due to the extraordinarily complex chemical structure of asphaltenes, the use of FTIR has encountered certain challenges regarding the correct assignment of bands to the various functional groups (Li *et al.*, 2007). Nevertheless, compared to absorption FTIR spectroscopy, ATR-FTIR analysis is a promising alternative to replace absorption FTIR methods because it requires little or no sample preparation, the acquisition of spectra is fast with better detection signals in the 700–900 cm⁻¹ region and offers an acceptable repeatability in samples (Thomasson *et al.*, 2000; Tay and Kazarian, 2009). Furthermore, the ATR-FTIR technique also provides the benefit of no significant spectral distortion over DRIFT, due to scattering when analysing powders, consequently complex mathematical procedures including, Kramers–Krönig transformation to correct spectral distortion is not required. Although, the disadvantage of ATR-FTIR technique is that it lacks mathematical descriptions for quantitative interpretation of the absorption bands from IR spectra that is provided by DRIFT and PAS. The traditional FTIR technique requires the preparation of the potassium bromide (KBr) pellet, which is difficult and time-consuming (Thomasson *et al.*, 2000; Li *et al.*, 2007).

Investigations using the FTIR technique for quantitative (McLean and Kilpatrick, 1997a), and qualitative (McKay *et al.*, 1976) analyses of asphaltenes have been carried out. However, the qualitative investigation usually permits the use of either frequency assignments or intensities related to specific bands for determination of functional groups (McLean and Kilpatrick, 1997a; Mullins and Sheu, 1998). Coelho *et al.* (2006), for example suggested a linear relationship between the frequency ratios (2927 cm⁻¹ and 2957 cm⁻¹) and the ratios of *n*CH₂/*m*CH₃ of the corresponding aliphatic chains of asphaltenes. Where *n* is suggested to reflect the number of alkyl substitution of aromatic molecule and *m* represents the number of branched and side chains for aromatic rings.

Likewise, the $n\text{CH}_2$ is attributed to methyl and $m\text{CH}_3$ methylene groups. Similarly, frequency assignments of 2920 cm^{-1} and 2950 cm^{-1} were assigned to the symmetric stretching frequencies of the methylene groups (Lin and Patrick Ritz, 1993; Calemma *et al.*, 1995; Groenzin and Mullins, 2000). The technique reported by these authors to define the ratio of $n\text{CH}_2/m\text{CH}_3$ of aliphatic chains, usually described a method, where ratios are calculated from the area of bands from IR spectra of a series of linear or branched alkanes to infer both aliphatic chain length and the degree of branching groups within the asphaltene structures. Consequently, the basic interpretation derived from the $n\text{CH}_2/m\text{CH}_3$ ratio, shows that the increasing ratio is probably attributable to longer aliphatic chains bonding to aromatics rings with least amount of branching structure. In previous FTIR study of carbonaceous samples obtained by ATR-FTIR analysis (Castro and Vazquez, 2009; Tay and Kazarian, 2009), reported the results for high refractive index materials, such as crude oils. Both these studies show that the ATR-FTIR technique can provide crucial information on the molecular structure of asphaltenes containing multiple functionalities such as aromatic, aliphatic, carbonyl and hydroxyl groups.

This chapter is generally aimed at applying ATR-FTIR analysis together with a multivariate statistical analysis to study the composition and molecular structure of asphaltenes extracted from crude oils, so as to further the understanding of petroleum. Hence the objectives of the study were the following:

- a. To investigate the various functional groups in the asphaltenes,
- b. To compare and contrast asphaltenes from different locations,
- c. To characterise the possible chemical structure of the asphaltenes,
- d. To classify the asphaltenes on the basis of functional families.

6.2 Methods

6.2.1 Sample preparation

Sixteen representative crude oils were chosen to form a sample set of oils differing from physical properties; weakly biodegraded (PM scale 1), moderate (PM scale 3) and heavily biodegraded (PM scale 5 - 6) asphaltene rich oils from various locations around the world. The samples selected included, *n*-hexane extracted asphaltene fractions from

Nigeria, United Kingdom, Middle East, Serbia and North American crude oils. Initially, the crude oils undergo fractionation as previously described in Chapter 3, section 3.3.2, 3.3.2.1 and 3.3.2.2 and subsequently purified as described in section 3.3.7 and retained for FTIR analysis. The studied samples are presented (in Table 6.1).

Table 6.1: List of samples used for the FTIR study

Sample	Location	PM scale	Asphaltene content (wt. %)	Likely source
NA(A)	Nigeria	6	1.17	Terrigenous/Marine shale
NC(A)	Nigeria	6	0.32	Terrigenous/Marine shale
ND(A)	Nigeria	1	1.16	Terrigenous/Marine shale
NN(A)	Nigeria	3	0.32	Marine/Marine shale
UK88(A)	United Kingdom	3	4.20	Terrigenous /Marine shale
UK11(A)	United Kingdom	1	1.77	Open marine/Marine shale
UK01(A)	United Kingdom	1	1.68	Open marine/Marine shale
UK05(A)	United Kingdom	1	1.70	Open marine/Marine shale
ME39(A)	Middle East	1	0.47	Marine/Marine + lacustrine shale
ME43(A)	Middle East	1	0.39	Marine/Marine + lacustrine shale
SN1(A)	Serbia	5	7.15	Shallow marine/Marine shale
SN2(A)	Serbia	1	1.59	Shallow marine/Marine shale
NA61(A)	North America	1	8.45	Open marine/Marine shale
NA76(A)	North America	1	13.72	Shallow marine/Marine shale
NA79(A)	North America	3	0.21	Open marine/Marine shale
NAC (A)	North America	6	4.16	Shallow marine/Lacustrine shale

6.2.2 Analytical procedure

Following a literature survey, experiments were conducted on (i) absorption FTIR using KBr pellets and (ii) ATR-FTIR using asphaltene grains to test the suitability of the analytical procedure that addresses the respective objectives stated in section 6.1. An asphaltene sample from Table 6.1 was selected for FTIR study. Based on the results of the study as shown in Figure 6.2, ATR-FTIR spectra of the asphaltene (NA61(A))from non-degraded North American crude oil show similar pattern with that of absorption FTIR. However, the ATR-FTIR, displayed better detection signal bands in the 700–900 cm⁻¹ region of asphaltene as shown in Figure 6.2.

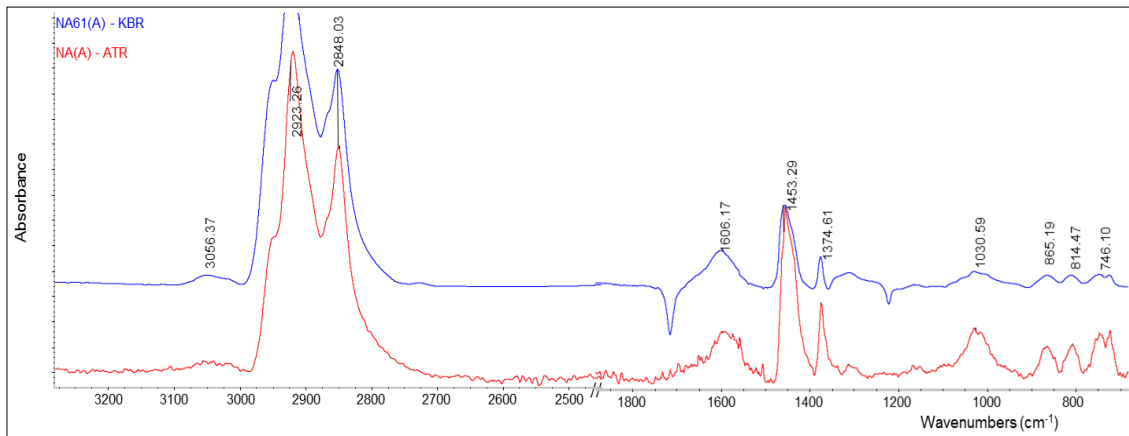


Figure 6.2: FTIR spectra obtained with traditional FTIR-KBr compared with ATR-FTIR of the infrared spectra bands of asphaltene (NA61) from North America.

6.2.3 Infrared analysis

The FTIR analyses were conducted in absorbance mode as described previously in Chapter 3, section 3.3.3. The acquired spectral bands of asphaltenes from the ATR-FTIR measurements were integrated numerically using OMNIC 6.1 software and principal component analysis (PCA). Consequently, OMNIC 6.1 was applied to extract more precisely various functional groups in the asphaltene structure by correcting the baseline across the entire spectrum using line segments between adjacent points to produce a new baseline point and possible changes within the structure were identified. Furthermore, the characteristics of ATR-FTIR spectra bands obtained from infrared (IR) of the different asphaltenes related to stretching, bending and rocking vibrations has been validated by comparison with previous studies (Mullins and Sheu, 1998; Abbas *et al.*, 2008). The PCA statistical tool allowed the determination of outliers and consequently physicochemical properties of the genetic affinities of the functional families of the asphaltenes. Prior to the classification, the tool normalised all the spectra to the respective maximum absorbance, so as to discriminate the effect of their associated concentration profile.

Table 6.2: General features of the infrared spectral bands from FTIR spectrum of asphaltenes from Scotti and Montanari (1998) in Mullins and Sheu (1998).

Wavelength (cm ⁻¹)	Functional group assignments
3100 -3640	O-H, N-H stretch
3000 -3100	aromatic C-H stretch
2780 -3000	aliphatic C-H stretch
1640 -1800	carbonyl C=O stretch
1620 -1590	aromatic C-C stretch
915 -852	aromatic C-H oop def (1 adj H on aromatic ring)
760 -730	aromatic C-H oop def (4 adj H on aromatic ring)

Symbols used in the table: oop (out-of-plane), def (deformation), adj= adjacent.

Table 6.3: Band assignments from FTIR (Abbas *et al.*, 2008).

Wavenumber (cm ⁻¹)	Type of vibration	Intensity	Functional group
3550 -3230	O-H str vib	m-s	Hydrogen-bonded O-H (intermolecular)
3080 -3010	=C-H str vib	m	=C-H (aromatic)
2975 -2950	C-H str vib asym	m-s	-CH ₃ "
2940 -2915	C-H str vib asym	m-s	-CH ₂ "
2870 -2840	C-H str vib sym	m	-CH ₂ "
2885 -2865	C-H str vib sym	m	-CH ₃ "
1720 -1690	C=O str vib	vs	Ketones
1655 -1635	C=O str vib	vs	Polycyclic quinones
1625 -1590	"C=C str vib"	v	Ring -C=C-
1525 -1470	"C=C str vib"	v	Ring -C=C-
1465 -1440	C-H def vib sym	m	"CH ₃ "
1390 -1370	C-H def vib asym	m-s	C-CH ₃
1310 -1210	C-O str vib	m	-O-Aryl
1260 -1180	O-H def and C-O str vib comb	s	O-H and C-O (phenol)
1160, 1075	=C-H in-plane def vib	m	Aromatic =C-H (substituted benzenes)
1070 -1030	S=O str vib	vs	S=O, sulfoxide
1050 -1025	C-O str vib	s	Ar-O-CH ₂ -O-Ar
940 -920	C-H def	v	Ar-O-CH ₂ -O-Ar
900 -830	=C-H oop def vib(1H)	m-s	Aromatic =C-H
850 -810	=C-H oop def vib(2H)	w-m	Aromatic =C-H
815 -785	=C-H oop def vib(3H)	w	Aromatic =C-H
760 - 730	=C-H oop def vib(3H)		Aromatic =C-H
770 -735	=C-H oop def vib(4H)	s	Aromatic =C-H
725 - 720	(CH ₂) rocking	s	Aliphatic (CH ₂) _n
720 - 680	=C-H oop def vib	s	Aromatic =C-H

Symbols used in the table: str (stretching), vib (vibration), asym (asymmetric), sym (symmetric), def (deformation), comb (combination), oop (out-of-plane), w (very weak), m (medium), s (strong), v (variable).

6.3 Results and discussion

6.3.1 Spectral analysis of asphaltene

In order to characterise the chemical properties, three distinctive regions were chosen to allow the identification of functional groups that belong to asphaltenes in the oils. The regions including (a) $3640 - 2780 \text{ cm}^{-1}$ (b) $1800 - 915 \text{ cm}^{-1}$ region and (c) $900 - 650 \text{ cm}^{-1}$. The results of processed spectra detected these regions (Figure 6.2). These characteristic peaks could be assigned to various functional groups of different hydrocarbons (aliphatic, aromatic and alicyclic). The spectra of the asphaltene contributions were identified by comparing spectra with previously published studies (Scotti and Montanari, 1998; Abbas *et al.*, 2008).

a) Assignment of $3640 - 2780 \text{ cm}^{-1}$ region

In this region, three characteristic bands normally assigned to the hydroxyl group region $3100 - 3640 \text{ cm}^{-1}$, aromatic stretching region $3000 - 3100 \text{ cm}^{-1}$ and aliphatic stretching region $3000 - 2780 \text{ cm}^{-1}$ were measured and various chemical functional group ratios calculated. However, two regions from the asphaltene fractions exhibited intense and sharp bands, which might be classified as follows: The most intense absorption band appears in $2700 - 3000 \text{ cm}^{-1}$ the saturated aliphatic species C–H stretch in CH_x at 2915 and 2975 cm^{-1} which is useful in characterising the carbon– and hydrogen– containing species (C–H stretching) of alkyl (Scotti and Montanari, 1998) and the very weak absorption bands that could be definitely attributed to aromatic species stretching in the ($3000 - 3100 \text{ cm}^{-1}$) region.

b) Assignment of $1800 - 915 \text{ cm}^{-1}$ region

This region, typically consist of two sets of absorption bands; with one set carboxyl/carbonyl group region near (1700 cm^{-1}) and the other near 1500 cm^{-1} , which are consistent with aromatic compounds. However, the absorption bands may occur as single band, which is assigned to symmetric carbonyl $\text{C}=\text{O}$ functional group (carbonyl compound) or appear split of the C–C aromatic group in COO^- group, as an asymmetric doublet (Scotti and Montanari, 1998). In this region ($1800 - 915 \text{ cm}^{-1}$),

represents carbonyl groups, including ketones, aldehydes, esters, and amides (Castro and Vazquez, 2009).

c) Assignment of 900 – 650 cm⁻¹ region

This region of the ATR-FTIR spectra, observed three bands that were assigned to aromatic out-of-plane region having one isolated aromatic hydrogen atom at 900 – 730 cm⁻¹, two or three adjacent aromatic hydrogen atoms per ring in the range of 850 – 730 cm⁻¹, and the presence of four aromatics that corresponds to 4 adjacent hydrogen atoms at 760 – 735 cm⁻¹ on the aromatic ring system (Scotti and Montanari, 1998; Walker and Mastalerz, 2004; Abbas *et al.*, 2008).

6.3.2 Functional characteristics of asphaltenes

The following section describes the characteristic features observed in the spectra of the studied asphaltenes, using ATR-FTIR, and calculated FTIR indices are presented in Figures(6.2- 6.6) and Table (6.4).

6.3.2.1 Nigerian oils

The ATR-FTIR spectra of representative asphaltenes from Nigerian oils are presented in Figure 6.2. The IR signals show some similarities and differences between the higher maturity (NA(A), NC(C)) and lower maturity (ND(A), NN(A)) oils. The following spectra bands have been observed for the asphaltenes: a minor broad band at 3000 – 3100 cm⁻¹ (aromatic C=C bond stretching) due to the presence of complex aromatic compounds and a prominent aliphatic stretching region (at 3000 – 2780 cm⁻¹), with dominant peaks at 2919 and 2842 cm⁻¹. The carbonyl band is detected at around 1700 cm⁻¹ while the stretching of multiple carbon to carbon bonds are near 1600 cm⁻¹. The C–C deformation peak corresponding to –CH₃ is at 1336 cm⁻¹ and (–CH₂) at 1444 cm⁻¹. The out-of-plane region 900 – 650 cm⁻¹ is detected near 724, 813 and 863 cm⁻¹ that indicates the presence of aromatics. The main difference between the higher maturity and lower maturity crude oils is in the region (1800 – 650 cm⁻¹). The spectra of asphaltenes from higher maturity oils is characterised by no anhydride bands, higher absorption bands at 1582 (aromatic C=C stretching mode), 1455(C–H def vib sym), and 1375 (C–H def vib asym) cm⁻¹ (Figure 6.2), while the anhydride band at 1706 cm⁻¹, due

to the stretching mode of carbonyl C=O groups, was detected in the spectra of asphaltenes from less mature oils.

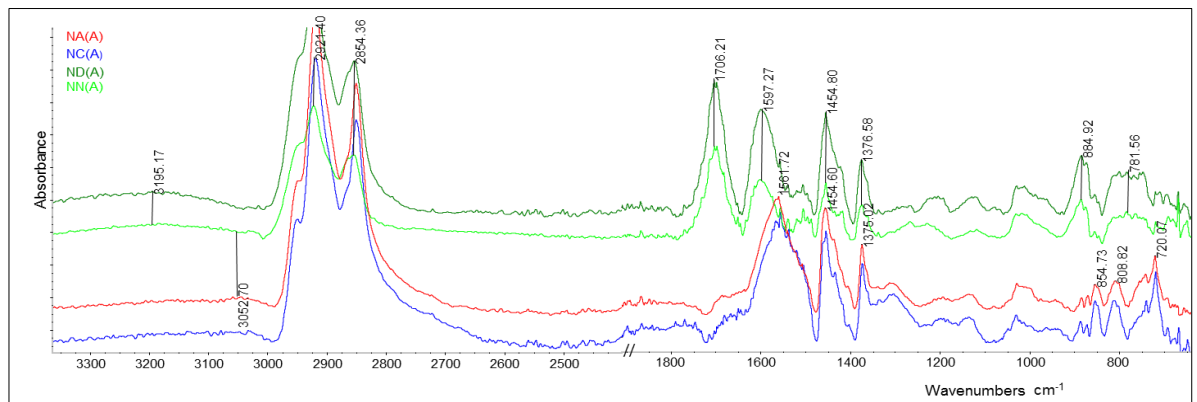


Figure 6.2: Infrared spectra of representative asphaltene fractions from Nigerian crude oils.

6.3.2.2 United Kingdom oils

The ATR-FTIR spectra of asphaltene samples from United Kingdom oils appear relatively similar (Figure 6.3). The spectral bands clearly reveal the presence of hydroxyl group band with a peak at 3054 cm⁻¹, which indicates the presence of –NH₂ and –OH groups and often considered important for asphaltene aggregation via H bond (Ascanius *et al.*, 2004). There is a distinct aromatic band in the aromatic stretching region 3000 – 3100 cm⁻¹ and a prominent aliphatic stretching region 3000 – 2780 cm⁻¹, with dominant peaks at 2918 and 2847 cm⁻¹. In the carbonyl (C=C) band range, due to anhydride, ester, carboxylic acid and ketone groups are observed at 1694, 1591, 1453, 1374 cm⁻¹ respectively. The out-of-plane region 900 – 650 cm⁻¹ is detected near 865, 799 and 750 cm⁻¹ that indicates the presence of aromatics.

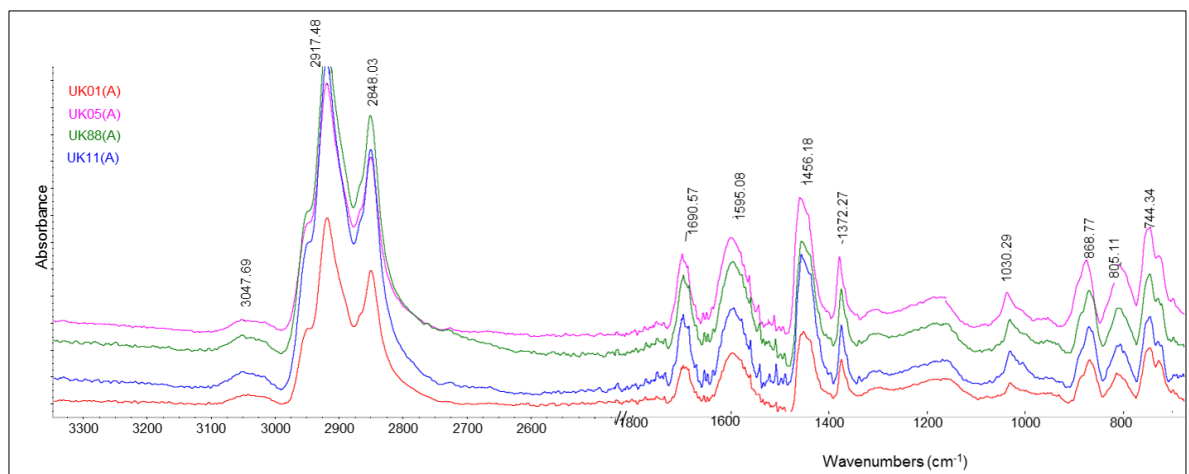


Figure 6.3: Infrared spectra of representative asphaltene fractions from United Kingdom crude oils.

6.3.2.3 Middle East oils

The presented spectra of both asphaltenes from the Middle East oils has revealed similar bands (Figure 6.4). The spectra is characterised by a weak hydroxyl group band with a peak at 3058 cm^{-1} . There is prominent aliphatic stretching region $3000 - 2780\text{ cm}^{-1}$, with dominant peak at 2918 and 2850 cm^{-1} . The carboxylic acid peak at 1450 cm^{-1} (Figure 6.4) is the dominant of the carbonyl ($\text{C}=\text{C}$) band range, that was observed at 1689 , 1595 , 1559 and 1376 cm^{-1} . Also detected was the broad band at 1140 cm^{-1} that indicates the presence of sulphoxides. The out-of-plane region $900 - 650\text{ cm}^{-1}$ is detected at 863 , 806 and 745 cm^{-1} indicating the presence of aromatic C–H deformation bonds.

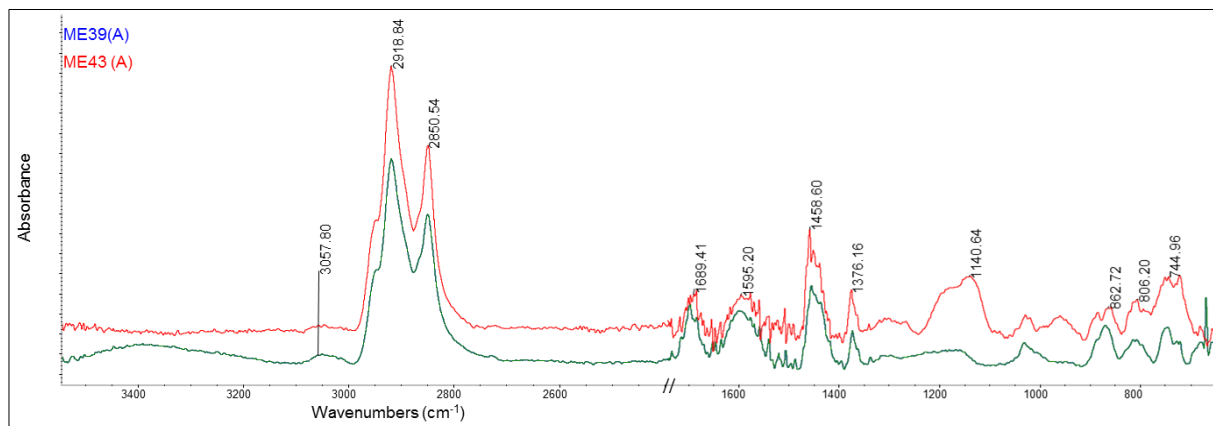


Figure 6.4: Infrared spectra of ME39(A) and ME43(A) asphaltene fractions from Middle East crude oils.

6.3.2.4 North American oils

The ATR-FTIR spectra of asphaltenes from North American oils has revealed similar bands (Figure 6.5). The absorption band at 3040 cm^{-1} is due to the vibrations of the ($\text{C}=\text{C}$) bonds in the aromatic rings. The region $3000 - 3100\text{ cm}^{-1}$ corresponds to molecules with $-\text{NH}$ or $-\text{OH}$ groups in the asphaltenes. The prominent absorption bands of aliphatic C–H stretching region $3000 - 2780\text{ cm}^{-1}$, are at 2919 and 2885 cm^{-1} indicates the presence of alkyl. The absorption bands at 1689 , 1595 , 1559 and 1376 cm^{-1} , due to the $\text{C}=\text{O}$ stretching modes of aromatic hydrocarbons, were identified. The spectra of asphaltenes from North American oils are characterised by the absence of an anhydride band, absorption of bands at 1596 (aromatic $\text{C}=\text{C}$ stretching region), higher absorption of bands 1456 ($\text{C}-\text{H}$ def vib sym), and 1372 ($\text{C}-\text{H}$ def vib asym) cm^{-1} (Figure 6.5). The absorption at 1034 cm^{-1} , point to the presence of the sulphoxide group.

The out-of-plane region have been identified in these asphaltenes at (869, 801 and 745 cm^{-1}).

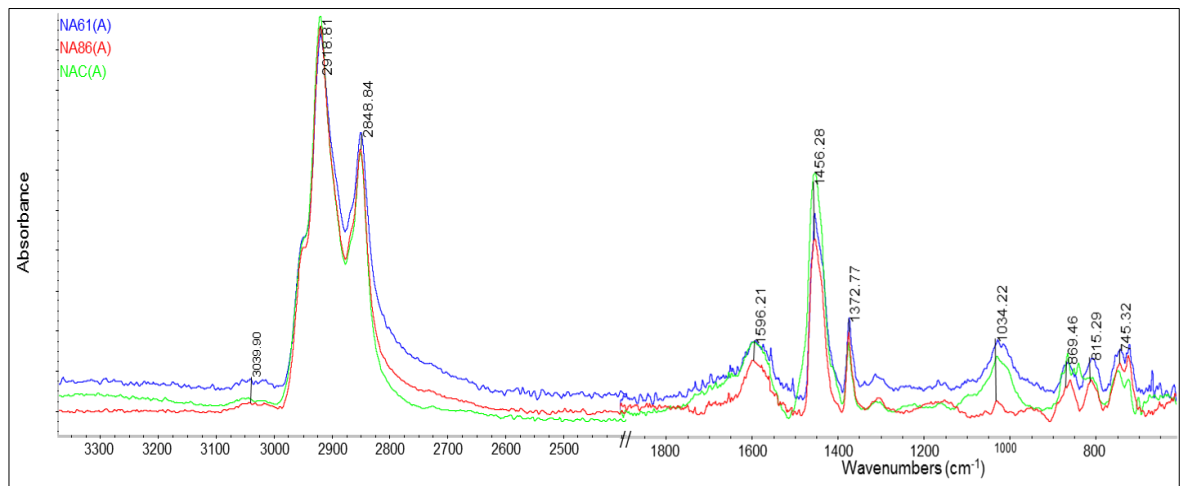


Figure 6.5: Infrared spectra of representative asphaltene fractions from the North American crude oils.

6.3.2.5 Serbian oils

The ATR-FTIR spectra of the two (2) asphaltenes from Serbian oils has revealed similar spectra bands (Figure 6.5). The absorption band at 3047 cm^{-1} is due to the vibrations of the (C=C) bonds in the aromatic rings was observed in the region $3000 - 3100 \text{ cm}^{-1}$. The prominent absorption bands of aliphatic C–H stretching region ($3000 - 2780 \text{ cm}^{-1}$), are at (2914 and 2864 cm^{-1}), indicates the presence of alkyl groups.

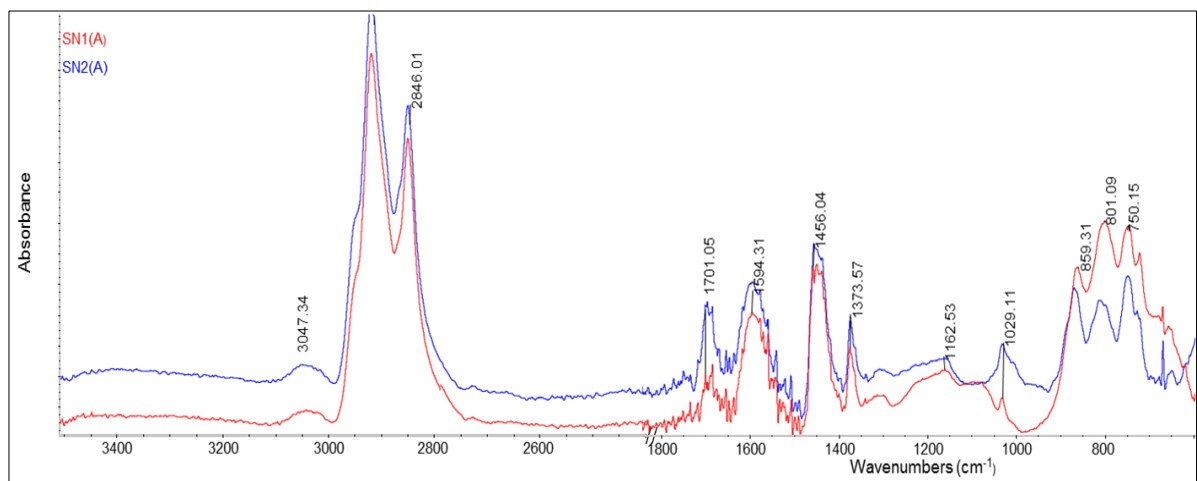


Figure 6.6: Infrared spectra of SN1(A) and SN2(A) asphaltene fractions from Serbian crude oils.

The absorption bands at 1701 , 1594 , 1456 and 1374 cm^{-1} , due to the C=O stretching modes of aromatic hydrocarbons, were identified. Also bands at 1162 and 1029 cm^{-1} were detected and are typical for C–O–C stretching of ethers due to the presence of the

sulphoxide groups (Orrego-Ruiz *et al.*, 2011). The out-of-plane region have been identified in these asphaltenes from Serbia at (859, 801 and 750 cm⁻¹).

6.3.3 Structural characteristics of asphaltenes

In the present study, only the relatively prominent and stable peaks were used and calculations were based on the ratios of integrated characteristic absorption peak areas that are associated with selected functional groups. These ratios, including aromaticity (AR1 and AR2, see Table 6.5), degree of condensation (DoC1 and DoC2, see Table 6.5), chain length, chain length factor (A factor and C factor, see Table 6.5) which are presented in Tables 6.4 and 6.5. The A and C factors are generally used in describing kerogen type and level of maturation. Hence, an increase in the “A” factor indicates a strong hydrocarbon-generating potential, whilst a continuous decrease in the “C” factor (ratio of oxygenated groups to C=C stretching groups) indicates maturation level (Iglesias *et al.*, 1995).

6.3.3.1 Nigerian oils

The variations between asphaltenes from different stages of biodegradation of oils are noted, however in ATR-FTIR calculated ratios. The results of all considered structural relationships and ratios for asphaltenes from the Nigerian oils are presented in Tables 6.4 and 6.5 respectively. In asphaltene samples NA(A) and NC(A) from heavy biodegraded oils showed significant similar AR1 values (0.32 and 0.36 respectively), however the asphaltene (ND) from the weakly biodegraded oil, is slightly higher (0.49). The CH₂/CH₃ can be used to assess both longer aliphatic chain lengths and degree of branching (Lin and Patrick Ritz, 1993). The methyl and methylene CH₂/CH₃ ratio calculated from aliphatic stretching region, shows that the parameter increases slightly for asphaltenes of heavy biodegraded oil than for asphaltenes of weak biodegraded oils (0.53 and 0.44 respectively). Therefore, asphaltene fractions NA(A) may probably be attributed to longer alkyl chain lengths and less alkyl branching, while ND(A) may have shorter alkyl chain lengths and more alkyl branching structures. Another difference appears in the degree of condensation of aromatic rings (DoC1 and DoC 2 ratios) generally indicates increases maturity (Iglesias *et al.*, 1995; Ibarra *et al.*, 1996). Therefore, DoC1 and DoC2 normally have similar trend and the condensation of

aromatic domains increased with maturity. These ratios, calculated in the asphaltenes from Nigerian oils in the aromatic stretching and aromatic out-of-plane deformation stretching regions resulted in a progressively rising DoC value (Table 6.4). These ratios are significantly higher for asphaltenes of higher matured oils than less matured oils range (DoC1; 0.00 - 0.17) and (DoC2; 0.00 - 1.08). The “A” factor and “C” factor generally suggests the hydrocarbon-generating potentials and maturation level (Iglesias *et al.*, 1995). The “A” factor, in Nigerian asphaltenes are displayed in Table 6.4. The observed decreased of “A” factor value in asphaltenes from Nigeria oils, indicates the maturation level of the samples, which has been previously confirmed in Chapter 5, section 5.2.1.5.

6.3.3.2 United Kingdom oils

The ATR-FTIR ratios, calculated from the integrated spectra of the asphaltenes from the United Kingdom oils is presented in Table 6.4. It is clear that, UK88(A) has the highest aromaticity “AR1”, followed by the UK11(A) and UK01(A) (0.17 - 0.10 respectively). The ratio of CH₂/CH₃ in the aliphatic stretching regions is significantly similar for all analysed asphaltenes range from (0.48 - 0.51). The higher ratio of CH₂/CH₃ reflects longer alkyl chain lengths and less-branched aliphatic structures. Therefore, asphaltene fractions UK88(A) may be attributed to longer alkyl chain lengths and less alkyl branching, while UK11(A) may have shorter alkyl chain lengths and more alkyl branching structures. These DoC1 and DoC2 ratios, calculated in the aromatic stretching and aromatic out-of-plane deformation stretching regions are similar (DoC1; 0.03 - 0.09) as shown in Table 6.2. Hence, observed similar values suggest the same maturity level for all of the oils as previously confirmed in Chapter 5, section 5.2.1.5.

6.3.3.3 Middle East oils

The ATR-FTIR ratios presented in Table 6.4 are calculated from the integrated spectra of the asphaltenes from the Middle East, ME43(A) exhibited the lowest CH₂/CH₃ ratio and ‘A’ factor, reflecting shorter aliphatic branching structures and highest hydrocarbon-generating potential. In contrast, asphaltene ME39(A), showed the highest aromaticity and lowest hydrocarbon-generating potential. Variations of the quantitative

ratios of the integrated characteristic absorption areas differ between ME43(A) and ME39(A). Consequently, in the degree of condensation of aromatic rings (DoC1) ratio calculated in the aromatic stretching and aromatic out-of-plane deformation stretching regions differs significantly (DoC1; 0.17 and 0.03 respectively). Hence, the observed values suggest higher matured ME39(A) compared to ME43(A).

6.3.3.4 North American oils

The ATR-FTIR ratios calculated from the integrated spectra of asphaltenes from the North American oils are presented in Table 6.2. The aromaticity ratio of asphaltenes of the heavy biodegraded oils from North America (NA79(A) and NAC(A)), is higher than for (NA61(A) and NA76(A)) of weak biodegraded oil (AR1; 0.66 - 0.85 and 0.24 – 0.18 respectively). These results suggest that the asphaltenes of heavy biodegraded oils contain aliphatic structures that are longer and less-branched aliphatic structures. In contrast, the asphaltenes of weak biodegraded oils have lower CH₂/CH₃ ratios, signifying shorter and more-branched aliphatic structures. Another difference appears in the degree of condensation of aromatic rings (DoC1 and DoC 2) ratios. These ratios, calculated in the aromatic stretching and aromatic out-of-plane deformation stretching regions for the asphaltenes of heavy biodegraded and weak biodegraded oils differs (DoC1; 0.14 – 0.16 and 0.06 – 0.25) and (DoC2; 0.49 – 0.66 and 1.39 – 1.41 respectively). The observed values suggest the different maturation level among the asphaltenes.

6.3.3.5 Serbian oils

The ATR-FTIR ratios calculated from the integrated spectra of asphaltenes from the Serbian oils are presented in Table 6.2. The aromaticity ratio of asphaltene SN1(A) of heavy biodegraded oil from Serbia, is lower than for SN2(A) of weak biodegraded oil (AR1; 0.21 and 0.27 respectively). The ratio of CH₂/CH₃ in the aliphatic stretching region, is higher for SN1(A) sample than for SN2(A) sample (0.34 and 0.24, respectively). These results suggest that SN1(A) contain aliphatic structures that are long and less-branched aliphatic structures. In contrast, SN2(A) have lower CH₂/CH₃ ratios, signifying short and more-branched aliphatic structures. Another difference appears in the degree of condensation of aromatic rings (DoC1 and DoC 2) ratios.

These ratios, calculated in the aromatic stretching and aromatic out-of-plane deformation stretching regions differs significantly (DoC1; 0.02 and 0.14) and (DoC2; 0.67 and 1.01) respectively. Hence, the observed DoC suggests that asphaltene SN1(A) is from more mature oil than asphaltene SN2(A).

Table 6.4: Structural relationships derived from the analysis of the ATR-FTIR spectra*

Sample	Location	AR1	AR2	DOC1	DOC2	CH ₂ /CH ₃	A factor	DoS	C
NA(A)	Nigeria	0.32	0.00	0.13	0.29	0.53	0.98	2.68	0.48
NC(A)	Nigeria	0.36	0.17	0.17	1.08	0.54	0.98	0.26	0.54
ND(A)	Nigeria	0.49	0.04	0.00	0.00	0.44	1.00	1.16	0.51
NN(A)	Nigeria	2.47	0.00	0.01	0.00	0.30	0.48	1.75	1.59
UK88(A)	United Kingdom	0.49	0.01	0.03	0.07	0.49	0.88	0.76	0.69
UK11(A)	United Kingdom	0.17	0.05	0.09	0.92	0.51	0.95	0.72	0.23
UK01(A)	United Kingdom	0.37	0.08	0.04	0.55	0.50	0.88	0.50	0.39
UK05(A)	United Kingdom	0.45	0.06	0.03	0.35	0.48	0.85	0.64	0.30
ME39(A)	Middle East	0.34	0.08	0.03	0.47	0.41	0.85	0.91	0.28
ME43(A)	Middle East	0.24	0.13	0.17	1.94	0.35	0.94	0.58	0.42
SN1(A)	Serbia	0.21	0.07	0.02	0.67	0.44	0.91	1.27	0.34
SN2(A)	Serbia	0.27	0.06	0.14	1.01	0.60	0.95	0.49	0.24
NA61(A)	North America	0.24	0.05	0.80	1.41	0.47	1.00	0.28	0.80
NA76(A)	North America	0.18	0.03	0.02	1.39	0.38	0.98	0.43	1.21
NA79(A)	North America	0.66	0.21	0.01	0.49	0.38	0.69	0.43	0.51
NAC(A)	North America	0.85	0.14	0.02	0.66	0.42	0.83	2.53	0.60

Calculated as defined in Table 6.5

Table 6.5: Ratios calculated from the ATR-FTIR spectra (Walker and Mastalerz, 2004; Chen *et al.*, 2012).

Index	Parameter	Index calculation	Band region (cm ⁻¹)
Aromaticity	AR1	CH _{ar} stretching/CH _{al} stretching CH _{ar} out-of-plane deformation/CH _{al} stretching	(3000-3100)/(2800-3000) (700-900)/(2800-3000)
Aromaticity	AR2		
Degree of condensation of aromatic rings	DOC1	CH _{ar} stretching/C=C stretching CH _{ar} out-of-plane deformation/C=C stretching	(3000-3100)/1600 (700-900)/1600
Degree of condensation of aromatic rings	DOC2		
Chain length factor	CH ₂ /CH ₃	C-H stretching vib sym/C-H str vib asym CH _{al} stretching/(CH _{al} stretching + C=C)	(2900-2940)/(2940-3000) (2800-3000)/[(2800-3000) + 1600]
Hydrocarbon generating potential	A factor		
Oxygen functionality	O	(C=C) _{al} /CH _{al} stretching	(1470-1500)/(2800-3000)

6.3.4 Chemometric analysis of spectroscopic data

From previous sections it has been shown that although asphaltenes are influenced by biodegradation processes, in general asphaltenes from oils that have common source facies exhibit similar functional characteristics. However, the use of chemometric tools, structural relationships derived from the analysis of the ATR-FTIR spectra can be explored for the potential of identifying similarities and differences amongst the asphaltenes. Consequently, chemometric analysis of ATR-FTIR data for the asphaltenes was carried out through multivariate methods, including principal component analysis (PCA) and Cluster analysis to detect samples according to their proximity in the principal components (PC1 and PC2): the closer the samples have similar characteristics and that are different from samples of other groups. The Minitab 16.0 statistical software was used to generate the PCA (loading and score plots), dendrogram and other relevant data. The input variables, including aromaticity, degree of condensation of aromatic rings, chain length factor and hydrocarbon generating potential are presented in Table 6.4.

The results of the PCA show the whole multivariate data is reduced to about 5 important PCs accounting for 96.35% of the variance in the whole data (Table 6.6). However, PC1 and PC2 together account for 77.04% of the variance. The loading of the various input variables on PC1 show the most important contributors to this component are biodegradation in the negative axis. On the hand, the most contributors to PC1 consist of the aromaticity, degree of condensation of aromatic rings, chain length factor and hydrocarbon generating potential.

The score plots constructed on the basis of the PC1, (56.57%) versus PC2, (20.27%) shows the relationship between samples with reference to the plane of PC1-PC2 (Figures 6.7 and 6.8). As shown in the score plots (Figure 6.8), the axis regroup in the positive part, asphaltenes of weakly biodegraded oils (as cluster 2; ND(A), UK11(A), NA61(A), ME39(A), ME43(A), UK01(A), UK01(A), NA76(A) samples) and the negative zone is essentially characterised by the presence of asphaltenes of moderately

or heavily biodegraded oils (cluster 3; NN(A), UK88(A), NA79(A) and cluster 1; NA(A), NC(A), NAC(A), SN1(A), SN2(A)).

Furthermore, improvement in discriminating the asphaltenes is achieved using the cluster analysis, as shown by the dendrogram (Figure 6.9 and Table 6.7). Thus, classified the asphaltenes into three main groupings of which cluster (1) represents asphaltenes (NA(A), NC(A), NAC(A), SN1(A) and SN2(A)) that are grouped together in a near identical chemical composition of which their level of similarity > 80% of the oils and cluster (2) represents (ND(A), UK11(A), NA61(A), ME39(A), ME43(A), UK01(A), UK01(A), NA76(A) samples), with their level of similarity >91% of the oils and consists exclusively of asphaltenes from weakly biodegraded oils. Cluster (3) represents asphaltenes (NN(A), UK88(A) and NA79(A)), with similarity > 61%. As previously observed in Figure 6.8, both asphaltenes (NN(A) and NA79(A)) are from moderately biodegraded oils with negative scores on PC1 - PC2 and asphaltene UK88(A) from weakly biodegraded oil has positive scores on PC1 - PC2.

The multivariate analysis reveal similarities influenced by biodegradation, maturation effects and characteristic chemical compositions from infrared regions on asphaltenes of different regions.

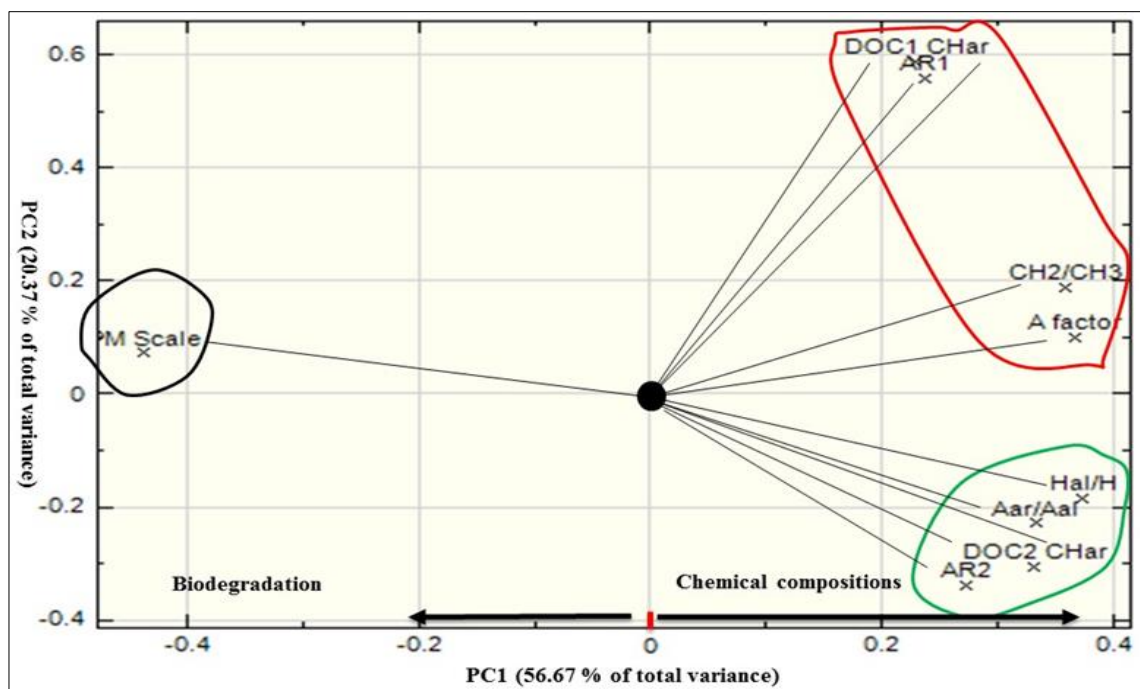


Figure 6.7: Loading plots showing the relationship between studied asphaltene samples in terms of PC1 (56.67% of total variables) versus PC2 (20.37% of total variables) analysis of multivariate data analysis.

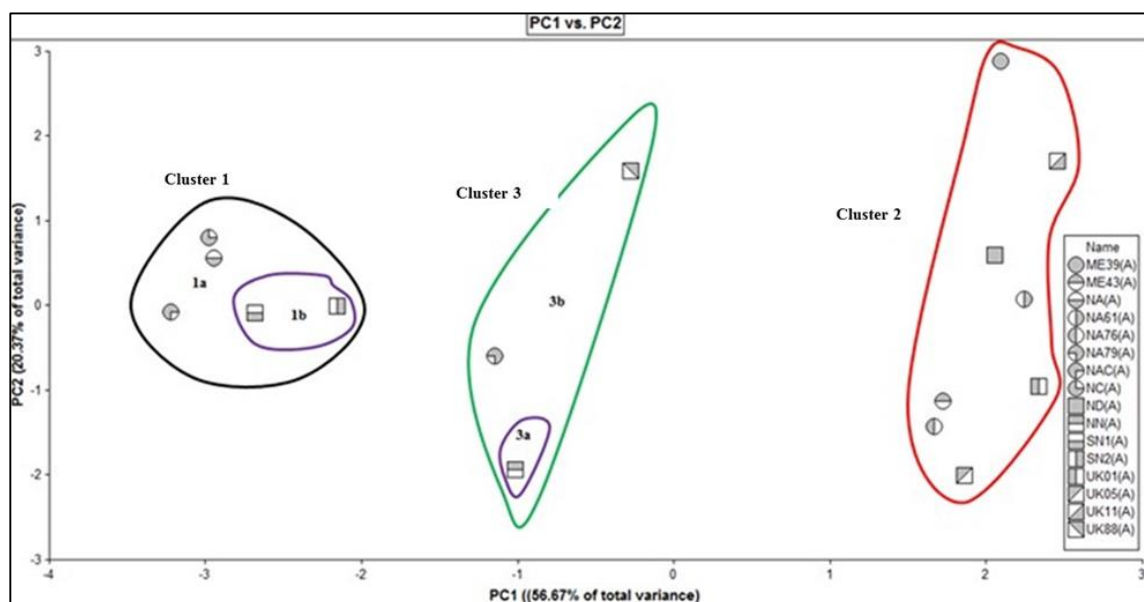


Figure 6.8: Score plots showing the relationship between studied asphaltene samples in terms of PC1 (56.67% of total variables) versus PC2 (20.37% of total variables) analysis of multivariate data analysis.

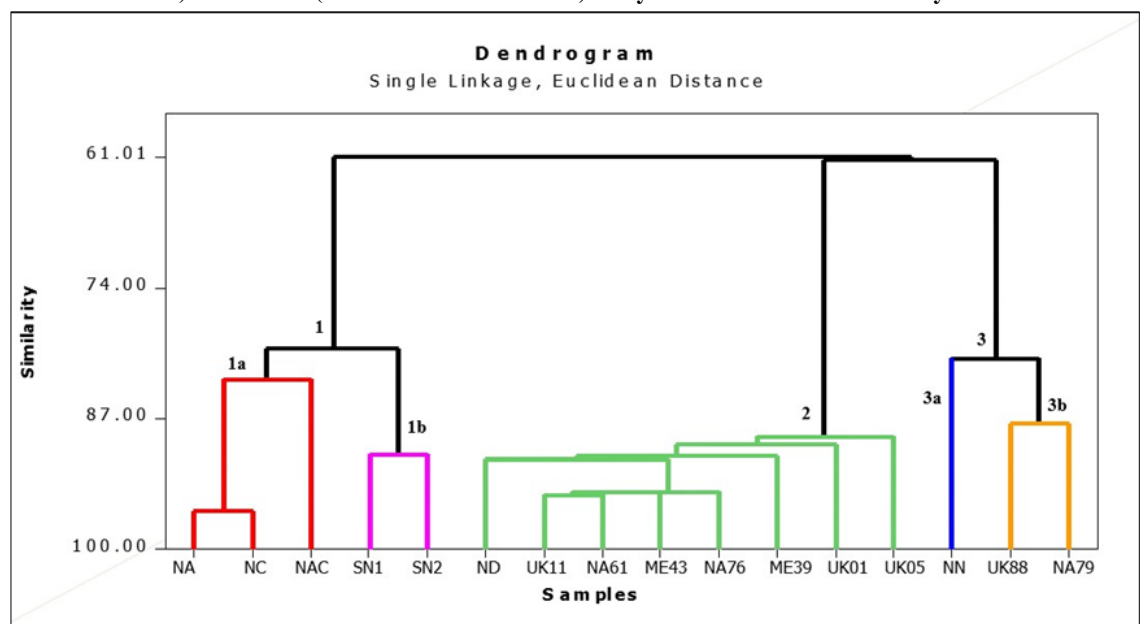


Figure 6.9: Dendrogram showing cluster analysis of structural relationships derived from the analysis of the FTIR spectra.

Table 6.6: Cluster analysis of observations for absorption spectra of quantitative ratios, standardised variables, squared Euclidean distance, linkage and amalgamated steps.

Step	Number of clusters	Similarity level	Distance level	Clusters joined	New clusters	In new clusters
1	15	96.35	0.19	1	2	2
2	14	94.91	0.26	6	13	2
3	13	94.46	0.03	6	10	3
4	12	94.33	0.29	6	14	4
5	11	91.28	0.45	3	6	5
6	10	90.72	0.48	3	9	6
7	9	90.68	0.48	11	12	2
8	8	89.63	0.54	3	7	7
9	7	88.91	0.58	3	8	8
10	6	87.97	0.62	5	15	2
11	5	83.23	0.87	1	16	3
12	4	81.33	0.97	4	5	3
13	3	80.09	1.03	1	11	5
14	2	61.32	2.01	3	4	11
15	1	61.01	2.02	1	11	16

Table 6.7: Final partition of number of clusters

Clusters	Number of observations	Within clusters sum of squares	Average distance from centroid	Maximum distance from centroid
1	3	0.63	0.43	0.64
2	8	1.59	0.42	0.66
3	1	0.00	0.00	0.00
4	2	0.20	0.31	0.31
5	2	0.12	0.14	0.24

6.4 Summary and conclusions

The ATR-FTIR spectroscopy and chemometric analyses of asphaltenes provide valuable information about the molecular structures of asphaltenes isolated from crude oils from various locations, including Nigeria, United Kingdom, North America, the Middle East and Serbia.

- a. In general, characteristic band regions indicate important functionalities observed in the ATR-FTIR spectra of the studied asphaltenes; including mainly saturated aliphatic and aromatic structures. Other bands are characteristic of carbon-oxygen functionalities including anhydride, esters, carboxylic acids and ketones. The oxygenated functionalities in the form of the sulfoxide group are also significantly.
- b. Comparison of asphaltenes of different locations indicated that the key diagnostic band at 1706 cm^{-1} , due to the stretching mode of carbonyl C=O groups, was detected in the spectrum of asphaltenes from United Kingdom, Middle East, Serbian and lightly biodegraded Nigerian oils, but was absent in all North American and heavily biodegraded Nigerian oils.
- c. The structural parameters; CH_2/CH_3 ratio and ‘A’ factor reveal the longest aliphatic chain length and highest hydrocarbon-generating potential amongst all the asphaltenes. This however was observed to be maturity and degradation dependent. Hence, the ‘A’ factor of the asphaltenes decreases with increasing maturity and in contrast CH_2/CH_3 ratio increases with maturity and biodegradation.
- d. The multivariate analysis provides an alternative way for classifying asphaltene group-types on the based on their chemical characteristics (which were probably influenced by their source organofacies, amongst other things) in each sample type. The variability of the spectroscopic data coupled with principal components capture two components (PC1 and PC2) explain 78.84% of the total variance in the asphaltene within the data set.

Chapter 7 Characterisation of bound biomarkers of asphaltenes released by ruthenium ion catalysed oxidation (RICO)

7.1 Introduction

RICO has been used in a number of studies on crude oils (Mojelsky *et al.*, 1992; Trifilieff *et al.*, 1992; Peng *et al.*, 1999b; Peng *et al.*, 1999c; Strausz *et al.*, 1999a; Strausz *et al.*, 1999b; Ma *et al.*, 2008) as well as coals (Stock and Tse, 1983; Blanc and Albrecht, 1991; Muhammad and Abbott, 2012). In a RICO study of asphaltenes in petroleum, Strausz *et al.* (1999a) also found a host of biomarkers bound on α -aromatic ring compounds, which includes both acyclic (*n*-alkyl and iso-alkyl) and cyclic (hopanoids, steroids etc). However, the alkyl groups (*n*-alkyl and iso-alkyl) are the dominant components of the oxygenated functionalities that are also present as ester and ether and carbon-carbon bonds to the aromatic cores of the asphaltenes (Peng *et al.*, 1999c; Strausz *et al.*, 1999a). Consequently, the changes in the relative abundance of certain biomarker isomers (biomarker maturity ratios) of hopanes from hopanoic acids have been investigated and the maturity profiles of the homohopanes and the hopanoic acids are suggested to be comparable from natural heating of organic-rich sediments and laboratory pyrolysis experiments (Bennett and Abbott, 1999).

RICO has been used by petroleum geochemists for correlation studies, such as; assessments of genetic relationships, biodegradation, maturity and other important geochemical parameters with aim of decreasing exploration risks (Peng *et al.*, 1999b; Ma *et al.*, 2008; Silva *et al.*, 2008). Therefore, the main aim of this chapter is to investigate asphaltene bound on biomarkers from biodegraded and non-biodegraded oils from different locations with RICO, in order to obtain information on the structural variability of the asphaltenes. Hence, the objectives were the following:

- a. To characterise the aliphatic moieties in asphaltenes from different sources and regional locations.
- b. To compare and contrast the biomarker distributions, such as those of hopanes and steranes in maltenes with their corresponding asphaltenes (hopanoic and steranoic acids) released during RICO treatment.

- c. To investigate the thermal maturation parameters from the effect of RICO products.
- d. To investigate biodegradation pathways and source information obtained from biomarkers bounded on the asphaltenes.
- e. To evaluate the importance of bound biomarkers of asphaltenes released by RICO treatment and established the genetic affinities of such variables among asphaltenes and maltenes.

7.2 Methods

7.2.1 Sample preparation

Sixteen crude oil samples, including thirteen crude oils consisting of a range of oils at different biodegradation levels) and three coal samples were sampled to cover different regional locations, source facies and depositional environments (see Table 7.1). In the present study, also used were corresponding sixteen asphaltene fractions from oils and coal extracts listed in Table 7.1. However, to justify that the acid-containing fractions of the RICO products have no significant input from free maltenes, corresponding samples were chosen and then compared.

Table 7.1: List of the samples used in the RICO analysis of the asphaltenes

New Name	Location	Source facies
NA(A)	Nigeria	Terrigenous/Marine shale
NB(A)	Nigeria	Terrigenous/Marine shale
NC(A)	Nigeria	Terrigenous/Marine shale
ND(A)	Nigeria	Terrigenous/Marine shale
NN(A)	Nigeria	Marine/Marine shale
SN1(A)	Serbia	Shallow marine/Marine shale
SN2(A)	Serbia	Open marine/Marine shale
ME77(A)	Middle East	Marine/Marine + lacustrine shale
NA61(A)	North America	Open marine/Marine shale
NA76(A)	North America	Shallow marine/Marine shale
NA79(A)	North America	Open marine/Marine shale
UK88(A)	United Kingdom	Open marine/Marine shale
UK11(A)	United Kingdom	Open marine/Marine shale
CA3(A)	North Sea coal, UK	Terrigenous/Marine shale
CA4(A)	North Sea coal, UK	Terrigenous/Fluvio deltaic
CA6(A)	North Sea coal, UK	Terrigenous/Marine shale

The asphaltenes were isolated from the crude oils and coal extracts by precipitation as described in Chapter 3, Section 3.3.2.1. The asphaltenes were then cleaned as described in Chapter 3, Section 3.3.2.2 to attain satisfactory purity by removal of co-precipitated resins and possible adsorbed compounds from the isolated asphaltene solids. Furthermore, the cleaned asphaltene was subjected to RICO procedure.

The RICO analysis adopted for this study was carried out as previously described in Chapter 3, Section 3.3.5, and 3.3.5.1. Subsequently, the resulting products were analysed by GC (see section 3.4.1) and GC-MS (see section 3.4.2) as previously described. The GC-MS was operated in the selected ion detection mode (Appendix 3.2).

7.2.2 Identification and quantification of acids

The biomarkers bonded on the asphaltenes of oils and coals after RICO treatment were analysed as methyl esters. However, the derivatised acids were then identified on the bases of their respective mass spectra (comparison with standards), relative retention time in mass chromatograms and comparison with published mass spectra in GCMS distributions (Jaffé *et al.*, 1988; Christie, 1998; Bennett and Abbott, 1999). Consequently, quantification of compound was achieved as previously described by Peng *et al.* (1999c) using peak areas in the mass chromatogram compared to the relative

response factor of a known amount of internal standard ($n\text{C}_{16}\text{d}_{31}$) added to the product. Hence, the amount of ester was calculated assuming equal FID response factors for the standard and the sample constituents by application of the expression Eq. 7.1:

$$C_x = (P_x * W_{Ti}) / (P_s * W_{Ta}) \quad \text{Eq. 7.1}$$

where C_x (mg/g) is the calculated amount of a given ester, P_x is the peak area of the ester, P_s is the peak area of the internal standard, W_{Ta} is the weight of the asphaltene and W_{Ti} is the weight of the internal standard added to the sample. Note that deuterated hexadecanoic ($n\text{C}_{16}\text{d}_{31}$) acid was used as the internal standard and relative response factor of the ester was assumed to be unity. The ester yields (C_x) could then be calculated using the corresponding acid yields, Eq. 7.2:

$$C_n = (C_x * \%C) / (12 * M_c) \quad \text{Eq. 7.2}$$

where C_n represent the amount per 1000C (number carbon atoms in an asphaltene), the percentage weight of carbon in a given asphaltene is $\%C$, the molar mass of carbon is 12 and the molar mass of analyte is M_c . However, the response factors of the esters, including; n -alkanoic acids, α - ω -di- n alkanoic acids, hopanoic and steranoic acid methyl esters were assumed to be corresponding to the same carbon member of n -alkanoic acid methyl esters.

7.2.3 Chemometric multivariate analysis

As part of the data analysis, hierarchical cluster analysis dendrogram (HCA) was conducted for the studied data: including biomarkers bonded on the asphaltenes and corresponding maltones and oils to have a comprehensive view of the genetic affinities of the data set. The HCA is mainly aimed at developing classification system, so as to definesamples that have similar characteristics and that are different from samples of other groups. Consequently, an important statistical tool used in understanding and improving chemical results (Peters and Fowler, 2002; Azevedo *et al.*, 2008). This statistical analysis relies on selected measured variables that reduce the dimensionality of the data to a few important groups, or clusters that best described the homogeneous clusters of cases. In this study, the HCA calculations were performed using computer program from Minitab 16.0 statistical software for hierarchical cluster Euclidean

distance, where each selected parameters of aliphatic hydrocarbon and asphaltene fractions were normalised and used as factors.

7.3 Results and discussion

The oxidation products of the asphaltenes from the organic phase, including linear acids, branched alkanoic acids and cyclic acids, as the previous evidence indicated (Peng *et al.*, 1999c; Anlai *et al.*, 2008; Muhammad and Abbott, 2012). Typically, the linear acids are *n*-alkanoic acids and α - ω -di-*n* alkanoic acids, while the branched alkanoic acids are α -methyl, α -ethyl-, α -propyl *n*-alkanoic acids and cyclic acids are the steranoic, and hopanoic acids methyl esters.

7.3.1 *n*-alkanoic acids

7.3.1.1 *Mass spectral characteristics of n-alkanoic compounds*

The series of *n*-alkanoic acids are by far the most abundant class of the monoacids in the RICO products of the studied asphaltenes. In order to identify the *n*-alkanoic acids by mass spectrometry, it was necessary to establish a typical fragmentation pattern of mass spectra of authentic compound to predict the compounds of which there were no standards, as reported (Christie, 1998). Hence, the mass spectrum of authentic methyl hexadecanoate is a typical example used for identification, shown in Figure 7.1. In this instance, the molecular ion that may distinguish the spectrum from that of the straight-chain analogue and other branched isomers are clearly seen and the important prominent ion is that of ion $[M]^+$ at m/z 270 representing molecular ion from COO group. However, this ion is accompanied by the adduct ion $[M-31]^+$ and $[M-43]^+$ at m/z 231 and m/z 227 respectively. These fragmentation ions at m/z 231 and m/z 227 correspond to the loss of a methoxyl (CH_3O) and C_3 (carbonyl bond), respectively, from the methoxyl group. Hence, during the fragmentation process, the availability of C_3 favourable mechanistic pathways can result in the characteristic McLafferty rearrangement ion at m/z 74 confirming that it is indeed a methyl ester.

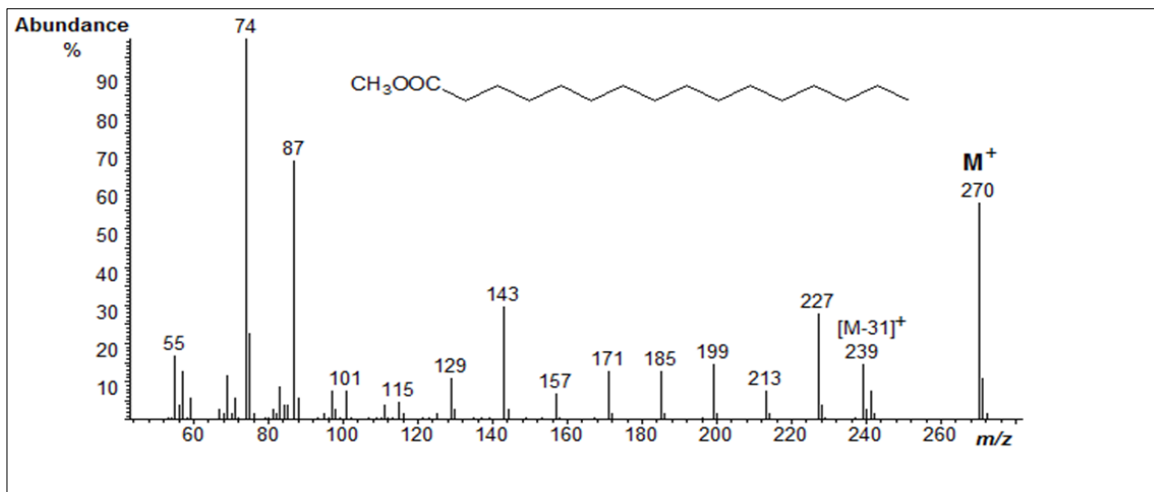


Figure 7.1: The mass spectrum of methyl hexadecanoate used to identify the *n*-alkanoic acids from the RICO products of the methyl esters.

7.3.1.2 Distribution of *n*-alkanoic compounds

The RICO products of the asphaltenes, revealed the presence of series of *n*-alkanoic acids homologous or pseudo homologous series of α - ω -di-*n* alkanoic acids and α -branched alkanoic acids. Figure 7.2 shows the gas chromatograms of the RICO products, in the form of their methyl ester derivatives, released from representative asphaltenes of Nigerian oils with corresponding maltene (bottom). The *n*-alkanoic distribution covers the C₇ - C₃₇ range with a predominance of C₇ - C₁₆ especially C₁₆ acids (Figure 7.2). The presence of short-chain C₈-C₁₄ fraction indicates the presence of short alkyl bridges in the asphaltene. This observation was previously reported to occur in the extractable organic phase of the oxidation products of asphaltenes (Peng *et al.*, 1999c; Strausz *et al.*, 1999b; Ma *et al.*, 2008). It must be noted that the distribution of *n*-alkanoic acids differs significantly, from those reported from maltene distribution and composition of the *n*-alkane series as shown in Figure 7.2. The carbon preference index (CPI_{20 - 30}) of the RICO products of the asphaltenes showed variability in the range of 0.77 -1.19 (Table 7.3).

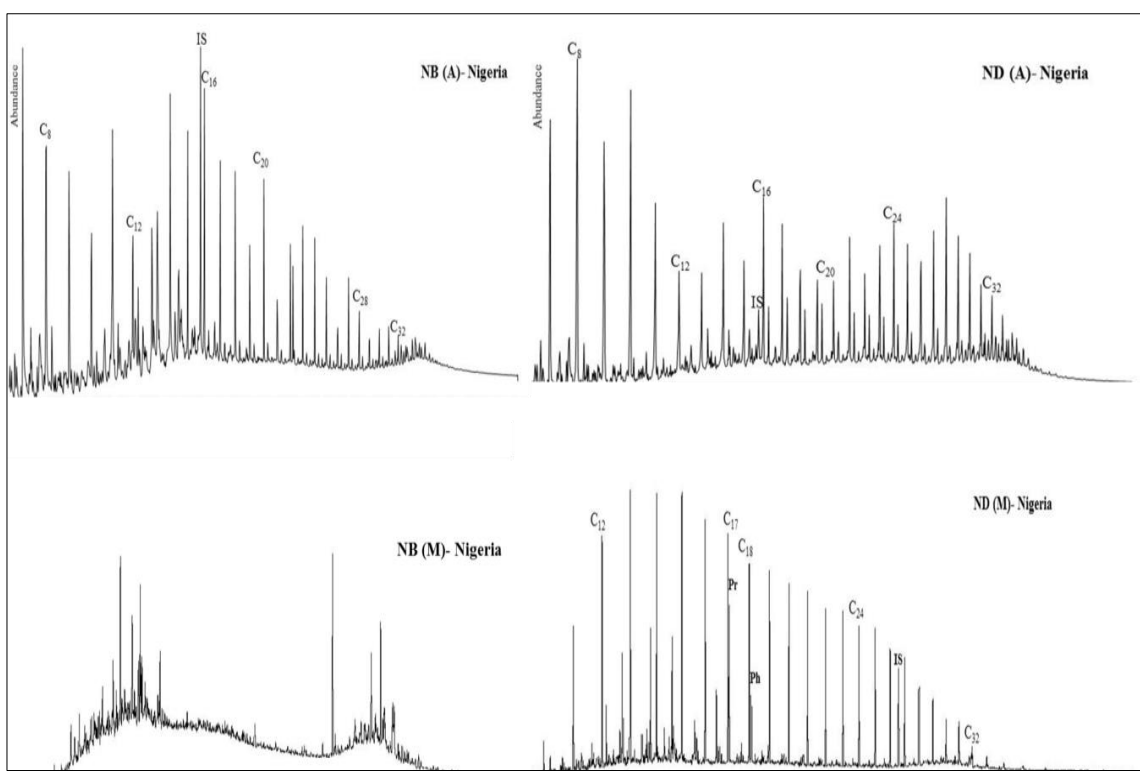


Figure 7.2: GC of *n*-alkanoic acids methyl esters from RICO products of representative asphaltenes of biodegraded and non-biodegraded Nigerian oils (top) with correspondent *n*-alkanes on maltenes (bottom). The numbers above the peak are the carbon numbers in the acid portion of the esters.

7.3.2 $\alpha\text{-}\omega\text{-di-}n$ alkanoic acids

The resulting $\alpha\text{-}\omega\text{-di-}n$ alkanoic acids containing carbon numbers ranging from C₉– C₃₆ can be identified in the organic phase of the RICO products (Figure 7.3). The $\alpha\text{-}\omega\text{-di-}n$ alkanoic acids were identifiable through a major ion at *m/z* 98 mass chromatogram of the RICO products as shown in Figure 7.3.

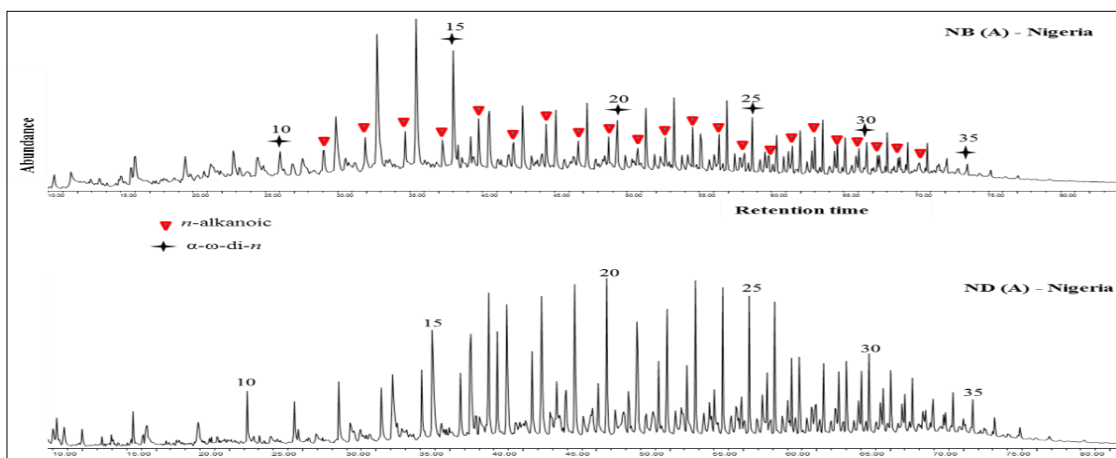


Figure 7.3: GC-MS *m/z* 98 ion chromatograms of $\alpha\text{-}\omega\text{-di-}n$ alkanoic acids of organic phase of RICO products of representative asphaltenes from Nigeria. The identified numbers above the peaks are the carbon numbers in the acid portion of the esters.

7.3.3 α -branched alkanoic acids

The distributions of the α -methyl, α -ethyl-, and α -propyl *n*-alkanoic acids were identified in the organic phase of the RICO products, with *m/z* 88, 102, 106 mass chromatograms respectively (Figure 7.4). The concentration drops off monotonically with increasing chain length.

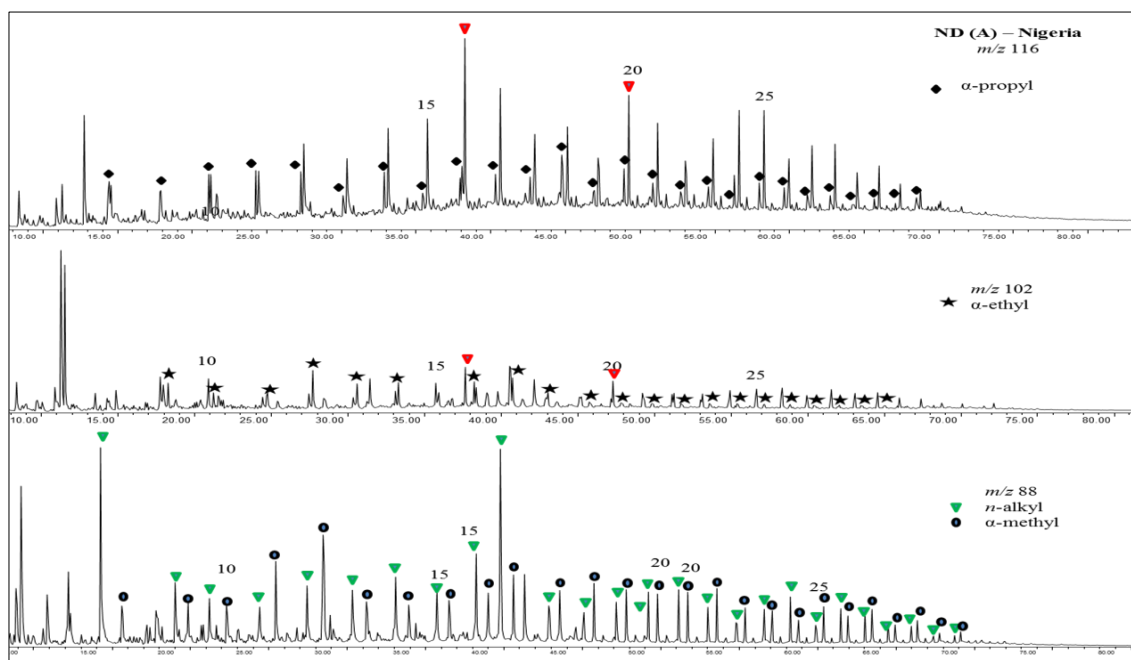


Figure 7.4: GC-MS chromatograms of *n*-alkanoic acid for asphaltene ND (A) from Nigeria. The numbers above the peaks are the carbon numbers on the acid portion of the esters.

7.3.4 Cyclic acids

7.3.4.1 Hopanoic acids

The hopanoic acids are present in C₃₀ - C₃₂ range, and were easily identified by molecular ions at *m/z* 191/235 of the methyl esters in the case of C₃₀ acid, *m/z* 191/249 for C₃₁ and *m/z* 191/263 for C₃₂ homologous series (Jaffé *et al.*, 1988; Bennett and Abbott, 1999; Rodrigues *et al.*, 2000). The mass chromatograms of the characteristic fragment ions of the C₃₀ - C₃₂ isomers of the hopanoic acids for the representative samples from Nigeria is shown in Figure 7.5, with peak identification given in Table 7.2. However, three diastereomeric series 17 α (H),21 β (H) and 17 β (H),21 β (H) hopane skeleton and 17 β (H),21 α (H) of moretane skeleton configurations were identified. The C₃₃-C₃₅ hopanoic acids are either absent or present in negligible measures and thus, the present study focused on the important C₃₀-C₃₂ homologues. It is interesting to note

that, the pair of diastereoisomers (22R and 22S) $17\alpha(\text{H}),21\beta(\text{H})$ and $17\beta(\text{H}),21\alpha(\text{H})$ - of C_{30} and C_{31} hopanoic acids were dominant than those of the C_{32} homologues pair of $17\beta(\text{H}),21\beta(\text{H})$ configuration and the resulting parameters are given in Table 7.3. The difference between the proportion of 22S relative to 22R- C_{32} of $17(\text{H}),21\beta(\text{H})$, shows lower values for the samples (Figures 7.6 and 7.7). The values for these samples are relatively low, hence supports higher thermal stress of their transformation at position 17 and 21 forming the more stable $17\alpha(\text{H}),21\beta(\text{H})$ and $17\beta(\text{H}),21\alpha(\text{H})$ isomers (Cyr and Strausz, 1984; Jaffé *et al.*, 1988; Bennett and Abbott, 1999).

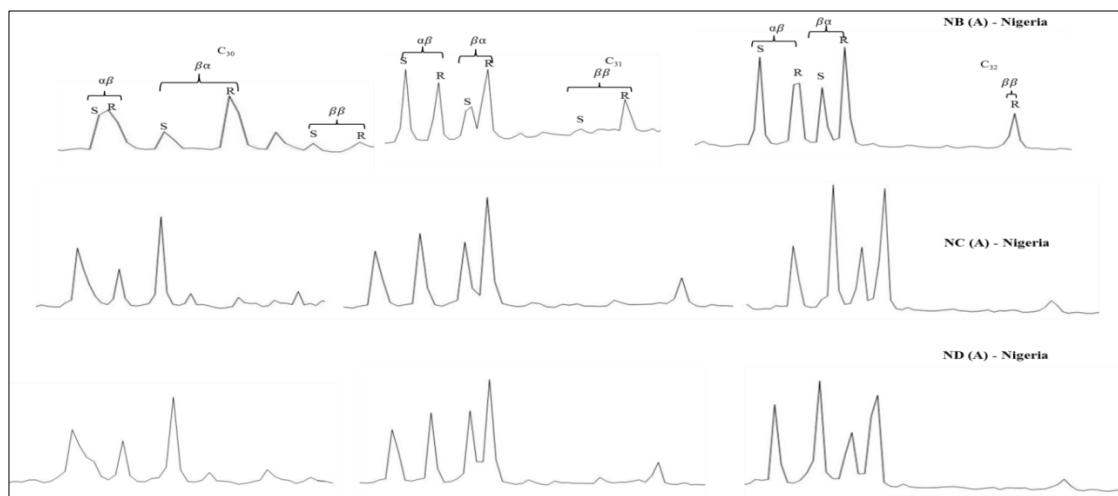


Figure 7.5: Partial mass chromatograms of the C_{30} ($m/z = 235$), C_{31} ($m/z = 249$) and C_{32} ($m/z = 263$) hopanoic acids on asphaltene sample from NB(A), NC(A) biodegraded oils and ND(A) of non-biodegraded oil from Nigeria.

Table 7.2: Structural assignments of steroid alkanoic and hopanoic acid biomarkers present in the asphaltene fraction.

Ion	Peak	Compound
m/z 275	SE1	[5 β (H),14 α (H),17 α (H)-cholestan-3-yl] methanoic acid (20R*)
	SE2	[5 α (H),14 α (H),17 α (H)-cholestan-3-yl] methanoic acid (20R*)
	SE3	[5 β (H),14 α (H),17 α (H)-24-methylcholestan-3-yl] methanoic acid
	SE4	[5 α (H),14 α (H),17 α (H)-24-methylcholestan-3-yl] methanoic acid
	SE5	[5 α (H),14 α (H),17 α (H)-24-methylcholestan-3-yl] methanoic acid
	SE6	[5 α (H),14 α (H),17 α (H)-24-ethylcholestan-3-yl] methanoic acid
m/z 289	SE7	[5 α (H),14 α (H),17 α (H)-24-ethylcholestan-3-yl] methanoic acid
	SE8	2-[5 β (H),14 α (H),17 α (H)-24-cholestan-3-yl] ethanoic acid (20R*)
	SE9	2-[5 α (H),14 α (H),17 α (H)-24-cholestan-3-yl] ethanoic acid (20R*)
	SE10	2-[5 α (H),14 α (H),17 α (H)-24-methylcholestan-3-yl] ethanoic acid
	SE11	2-[5 α (H),14 α (H),17 α (H)-24-methylcholestan-3-yl] ethanoic acid
	SE12	2-[5 α (H),14 α (H),17 α (H)-24-ethylcholestan-3-yl] ethanoic acid
	SE13	2-[5 α (H),14 α (H),17 α (H)-24-ethylcholestan-3-yl] ethanoic acid
m/z 235	HA 1	17 α (H), 21 β (H)-hopanoic acid 22S
	HA 2	17 α (H), 21 β (H)-hopanoic acid 22R
	HA 3	17 β (H), 21 α (H)-moretanoic acid 22S
	HA 4	17 β (H), 21 α (H)-moretanoic acid 22R
	HA5	17 β (H), 21 β (H)-hopanoic acid 22S
	HA6	17 β (H), 21 β (H)-hopanoic acid 22R
m/z 249	HA7	17 α (H), 21 β (H)-30-homohopanoic acid 22S
	HA8	17 α (H), 21 β (H)-30-homohopanoic acid 22R
	HA9	17 β (H), 21 α (H)-30-homomoretanoic acid 22S
	HA10	17 β (H), 21 α (H)-30-homomoretanoic acid 22R
	HA11	17 β (H), 21 β (H)-30-homohopanoic acid 22S
	HA12	17 β (H), 21 β (H)-30-homohopanoic acid 22R
m/z 263	HA13	17 α (H), 21 β (H)-30,31-bishomohopanoic acid 22S
	HA14	17 α (H), 21 β (H)-30,31-bishomohopanoic acid 22R
	HA15	17 β (H), 21 α (H)-30,31-bishomomoretanoic acid 22S
	HA16	17 β (H), 21 α (H)-30,31-bishomomoretanoic acid 22R
	HA17	17 β (H), 21 β (H)-30,31-bishomohopanoic acid 22S
	HA18	17 β (H), 21 β (H)-30,31-bishomohopanoic acid 22R

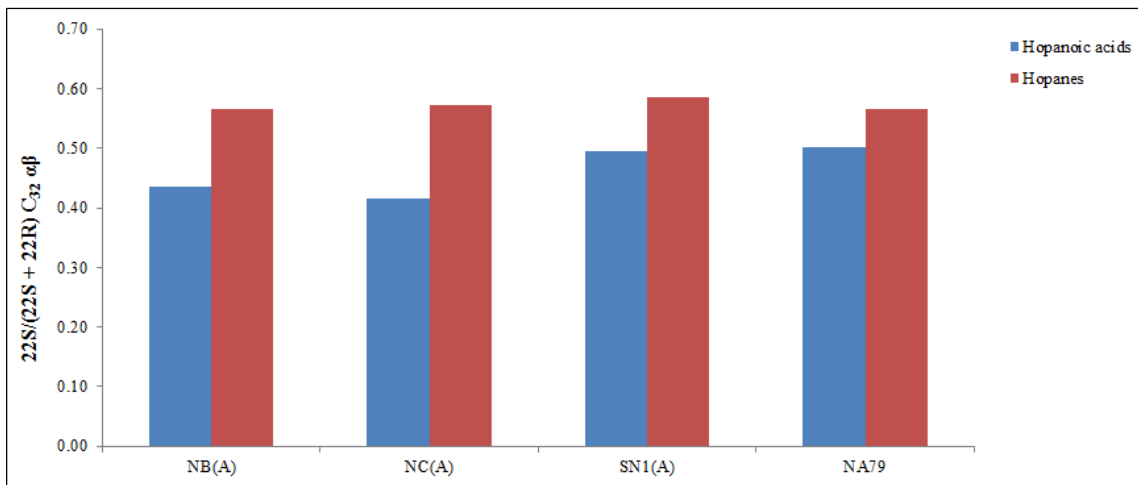


Figure 7.6 Bar charts showing a comparison of $22S/(22S + 22R) C_{32}\alpha\beta$ maturity parameter values for maltene-derived hopanes and the asphaltene-derived hopanoic acid RICO products from biodegraded oils (see table 7.3).

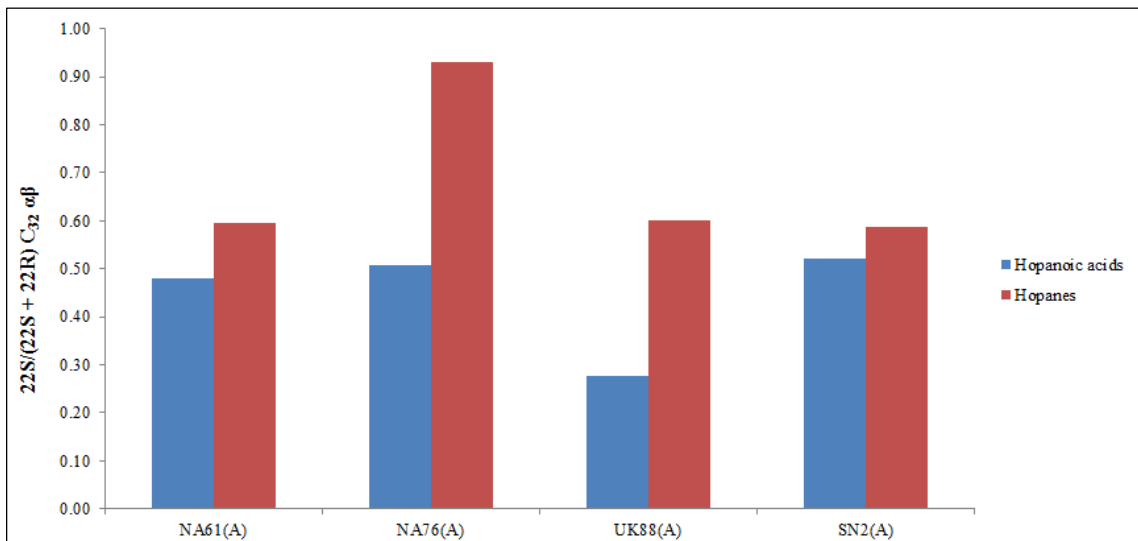


Figure 7.7 Bar charts showing a comparison of $22S/(22S + 22R) C_{32}\alpha\beta$ maturity parameter values for maltene-derived hopanes and the asphaltene-derived hopanoic acid RICO products from non-biodegraded oils (see table 7.3).

Table 7.3: Parameters calculated on the basis of distribution and abundance of hopanoic, steranoic and *n*-alkanoic acids in the asphaltene fraction.

Sample	Location	22S	20S	Sterane (%)			CPI
		$\frac{22S}{22S + 22R}$ $C_{32}\alpha\beta$	$\frac{20S}{20S + 20R}$ $C_{29}\alpha\alpha\alpha R$	$C_{28}\alpha\alpha\alpha R$	$C_{29}\alpha\alpha\alpha R$	$C_{30}\alpha\alpha\alpha R$	
NA(A)	Nigeria	0.39/0.58	0.16/0.64	28.95/30.05	26.90/27.05	44.14/42.89	1.09/nd
NB(A)	Nigeria	0.43/0.57	0.24/0.34	28.62/24.98	27.46/57.89	43.92/17.12	1.00/nd
NC(A)	Nigeria	0.42/0.57	0.07/0.42	32.04/25.88	30.04/37.93	37.92/36.19	1.11/nd
ND(A)	Nigeria	0.46/0.57	0.14/0.63	21.39/26.49	28.32/24.80	50.29/48.71	1.02/1.11
NN(A)	Nigeria	0.40/0.58	0.14/0.51	20.01/30.68	30.95/27.48	49.04/41.84	1.11/1.31
SN1(A)	Serbia	0.52/0.59	0.34/0.78	29.62/24.44	28.62/22.16	41.76/53.40	0.86/nd
SN2(A)	Serbia	0.52/0.59	0.41/0.65	32.54/33.68	33.49/30.15	33.97/36.17	0.79/1.21
ME77(A)	Middle East	0.19/0.58	0.46/0.63	28.91/47.29	27.91/16.79	43.17/35.91	1.16/0.97
NA61(A)	North America	0.48/0.60	0.27/0.54	37.56/34.23	23.85/24.79	38.60/40.99	1.02/0.96
NA76(A)	North America	0.51/0.93	0.29/0.59	40.09/35.70	24.44/24.57	35.46/39.72	0.93/1.04
NA79(A)	North America	0.50/0.57	0.20/0.57	29.31/36.12	26.39/21.52	44.30/42.36	1.19/1.66
UK88(A)	United Kingdom	0.28/0.60	0.39/0.61	34.93/35.37	36.35/26.40	28.72/38.22	0.81/1.00
UK11(A)	United Kingdom	0.51/0.59	0.32/0.61	44.94/30.70	21.39/21.52	33.67/47.77	0.85/0.90
CA3(A)	United Kingdom	0.46/0.58	0.36/0.75	10.11/34.25	31.23/18.95	58.66/46.80	0.77/1.26
CA4(A)	United Kingdom	0.46/0.59	0.32/0.75	9.94/42.69	40.80/13.96	49.26/43.36	1.11/1.12
CA6(A)	United Kingdom	0.26/0.55	0.32/0.58	5.73/38.73	29.72/17.34	64.55/43.93	1.01/1.37

The values on the left of "/" are parameters from compounds bound on the asphaltenes and the right values of "/" are the parameters corresponding maltenes of the whole oil; CPI₂₀₋₃₀ = 0.5x[(C₂₁-C₂₉)(odd)/(C₂₀-C₂₈)(even) + (C₂₁-C₂₉)(odd)/(C₂₂-C₃₀)(even)].

7.3.4.2 Steranoic acid acids

Two series of bound steroid acids with the carboxylic acid distributions were released from the oxidation products of the representative asphaltenes shown in Figure 7.8. The ion chromatogram *m/z* 275 and *m/z* 289 of the methyl ester derivatives of the carboxylic acids were used to revealed the presence of a series of ring-C aromatic steroid with a methanoic and ethanoic acid group, respectively attached to ring A. These acids occur as a series of 3β-carboxylic acids (C₂₈ - C₃₀) and 4-methylsterane carboxylic acids (C₂₉ - C₃₁) with their chromatographic profiles shown in Figure 7.8 and peak identification in Table 7.2. The series of similar distribution was previously reported to occur in oxidation products but not identical to sterane of maltane fraction of oil (Peng *et al.*, 1997).

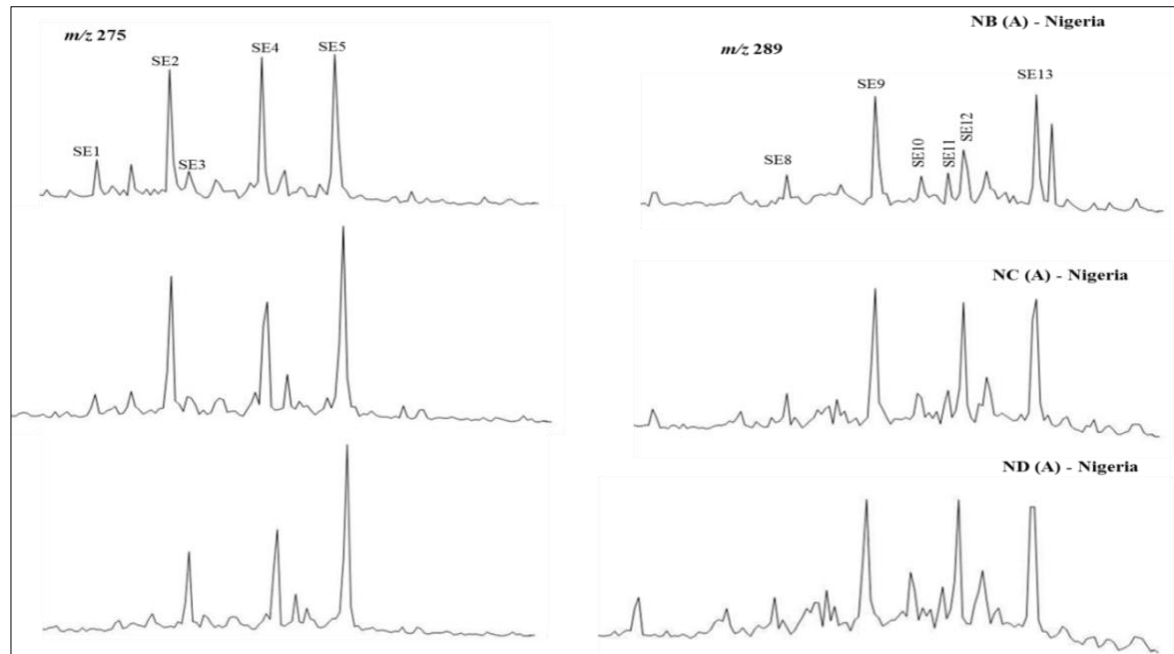


Figure 7.8: Partial mass chromatograms of the $m/z = 275$ and $m/z = 289$ of the steranoic and 4-methylstaronoic acids methyl esters of RICO products of asphaltenes from NB(A), NC(A) biodegraded oils and ND(A) of non-biodegraded Nigeria oils. (Refer to Table 7.2 for legend).

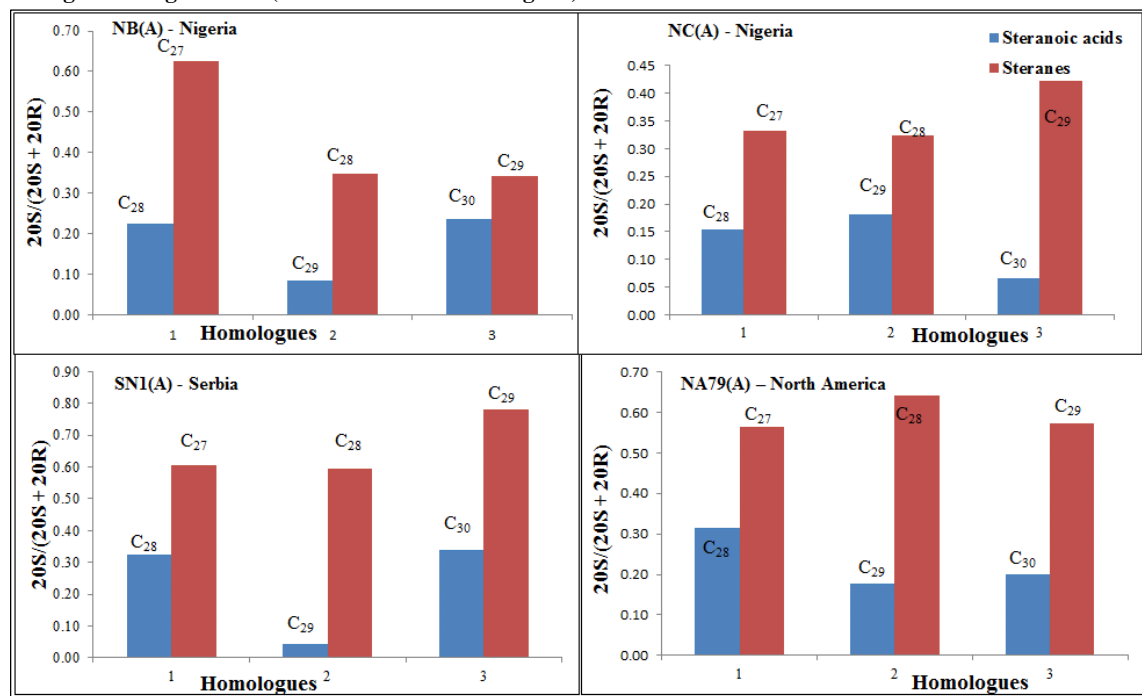


Figure 7.9: Bar charts showing comparison of $20S/(20S + 20R)$ values for asphaltene-derived steranoic acid RICO products and the maltene-derived steranes from biodegraded oils. The C_{27} $20\alpha\alpha\alpha R$ sterane in saturated hydrocarbon fraction of maltene corresponds to C_{28} $20\alpha\alpha\alpha R$ sterane carboxylic acids.

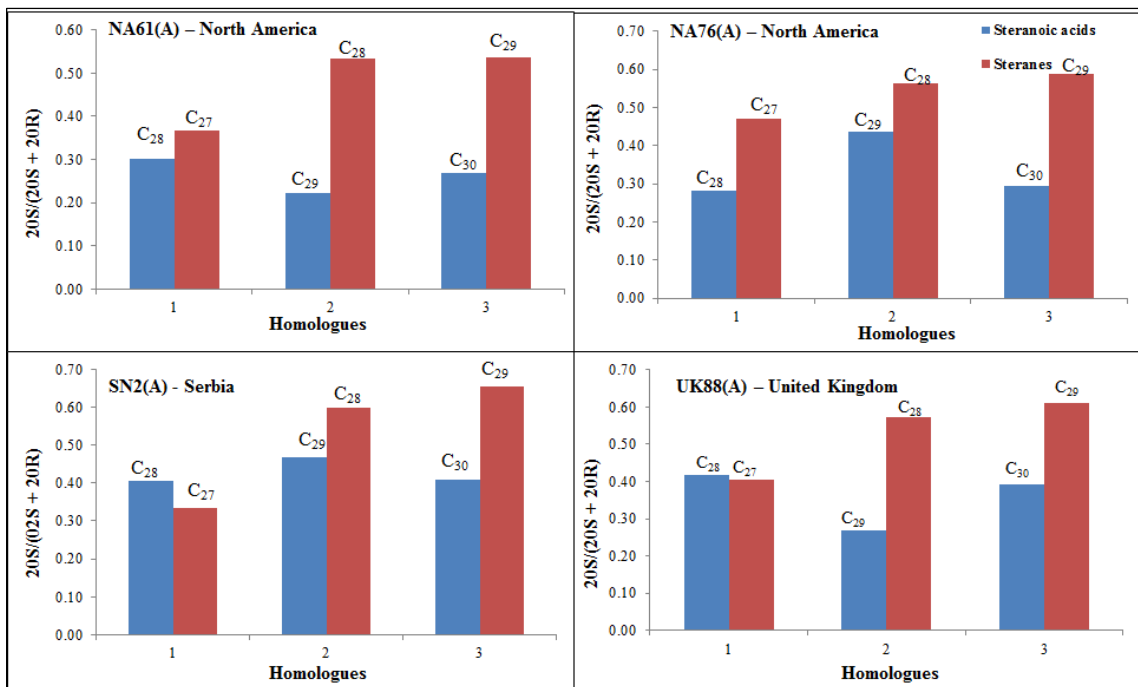


Figure 7.10: Bar charts showing comparison of $20S/(20S + 20R)$ values for asphaltene-derived steranoic acid RICO products and the maltene-derived steranes from non-biodegraded oils. The C_{27} 20 $\alpha\alpha\alpha R$ sterane in saturated hydrocarbon fraction of maltene corresponds to C_{28} 20 $\alpha\alpha\alpha R$ sterane carboxylic acids.

7.3.5 Effect of thermal maturation on asphaltene biomarkers

The isomeric distribution of hopanoic acids (Meredith *et al.*, 2000) and incorporated carboxylic acids from the migration pathway can be used to describe the maturity of the rocks through which an oil had migrated (Jaffé and Gallardo, 1993). Thus, results from maturity parameters (Table 7.3), such as $C_{30}\alpha\beta/(\alpha\beta + \beta\alpha)$, $C_{31}S/(S + R)$, $C_{32}S/(S+R)$, generally indicate maturity level. The results are consistent with previous evaluation that bound biomarkers of hopanoic acids should have lower maturity level compared to those of corresponding crude oil maltenes (Pelet *et al.*, 1986; Peng *et al.*, 1997; Liao and Geng, 2002). It is noteworthy that the thermal maturities molecular parameters of the biomarkers (Table 7.3) in the hopanes from the maltenes show strikingly different molecular distributions from the hopanoic acids released from asphaltenes following RICO treatment (Table 7.3). The epimeric ratio at C-22 in C_{32} , 17 α , 21 $\beta(H)$ for the maltenes has values (0.55 – 0.93) generally close to equilibrium range value indicating a thermally mature state, while those of asphaltenes (0.19 – 0.51) are considerably below the equilibrium level, indicating significant thermal immaturity (Peters *et al.*, 2005a). Hence, the asphaltenes are less mature than their aliphatic hydrocarbon counterparts. It is not clear why this is the case but may likely be related to the

isomerisation of the bound biomarkers being protected from secondary alterations (Jaffé and Gallardo, 1993).

This is also true of the assessment of the maturity of $\alpha\beta\beta / (\alpha\beta\beta + \alpha\alpha\alpha)$ for C₂₉ $\alpha\alpha\alpha$ and C₃₀ $\alpha\alpha\alpha$ isomerisation ratios calculated from the bound biomarkers compared with their maltene counterparts (Table 7.3). The maturation changes of the thermally dependent stereoisomerisations in asphaltenes are less compared to stereoisomerisations of hydrocarbon fractions equivalent.

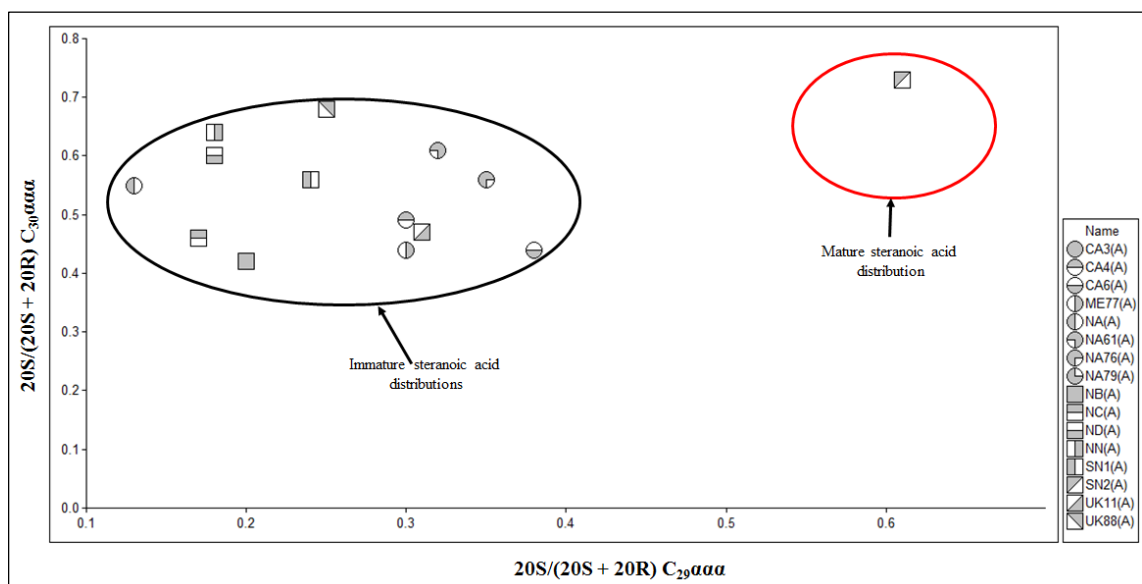


Figure 7.11: Distributions in steranoic acids from asphaltene-derived acid RICO products of C₂₉ vs. C₃₀ 20S/(20S + 20R) maturity parameters (see Table 7.3).

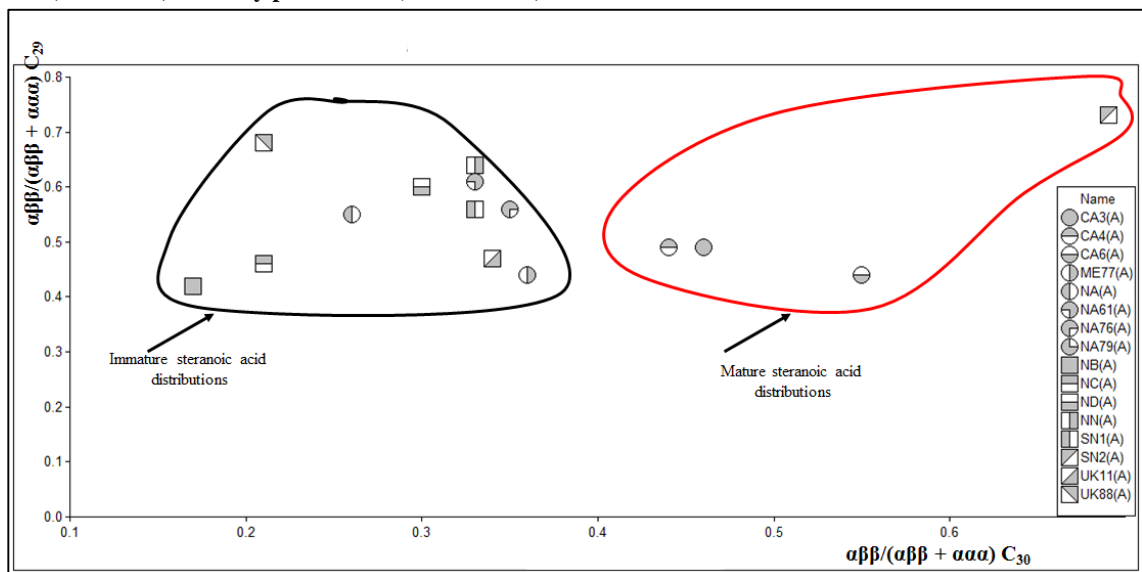


Figure 7.12: Distributions in steranoic acids from asphaltene-derived acids RICO product of C₂₉ vs. C₃₀ $\alpha\beta\beta / (\alpha\beta\beta + \alpha\alpha\alpha)$ maturity parameters (see Table 7.3).

7.3.6 Effect of biodegradation on asphaltene biomarkers

The RICO products and corresponding *n*-alkane data obtained from the selected samples in this study show differences in terms of their biodegradation histories (Figure 7.1). The distribution of *n*-alkanoic acid methyl ester, suggests that the easiest biodegraded *n*-alkane bonded on aromatic ring in asphaltene macromolecular network had little or no microbiological degradation effect on the alkyl side chain bonded on the asphaltenes. The RICO products of the studied asphaltenes show similar degree of biodegradation, confirmed by the presence of large amounts of *n*-alkanoic acid methyl ester. In contrast, *n*-alkanes from their corresponding aliphatic maltene fractions (e.g. NB (M), NC (D), SN1 (M), NA79 (M)) samples, display various baseline hump of *n*-alkanes, branch alkanes and isoprenoids, hence believed to have been exposed to significant microbiological degradation. In general, crude oil samples show characteristic distributions of regular sterane C₂₇>C₂₈>C₂₉(22 $\alpha\alpha\alpha$) that reflect biodegradation (Peters *et al.*, 2005b). However, we observed the dominance of C₂₉ regular sterane (Table 7.3 and Figure 7.8), which may have resulted from the degradation of the lower homologs (C₂₇ and C₂₈). The investigated samples from this class of biomarker suggested C₂₈>C₂₉<C₃₀ for sterane carboxylic acids in the RICO products, probably biodegraded oils and C₂₈<C₂₉< C₃₀ for non-degraded oils.

7.3.7 Effect of source parameters on asphaltene biomarker

There have been many studies using the distribution of C₂₇, C₂₈ and C₂₉ regular steranes to determine oils from different source or organofacies of the same source rock, e.g. Peters *et al.* (2005b). In this study, the percentage distribution of C₂₇, C₂₈ and C₂₉ regular steranoic acids have been plotted in a ternary diagram into groups defined by depositional environments (Figures 7.13 and 7.14). Furthermore, since the distribution of C₂₈, C₂₉ and C₃₀ steranoic carboxylic biomarker acids correspond to that of their free steranes C₂₇, C₂₈ and C₂₉ counterpart of maltene of oils (Rodrigues *et al.*, 2000), the saturated hydrocarbon fractions of these fractions were compared with those of asphaltenes (Figures 7.13 and 7.14). The ternary plots show disagreement with their counterparts of steranoic acids from the asphaltene fraction. The biomarker pattern observed from the steranoic acids presumably reflect the original distribution of steranoic acids after expulsion from the source rock and the maltene source might have

been incorporated on its secondary migration route. This result lend to support the view that asphaltenes represent parts of kerogens during the formation of oil (Cassani and Eglinton, 1986).

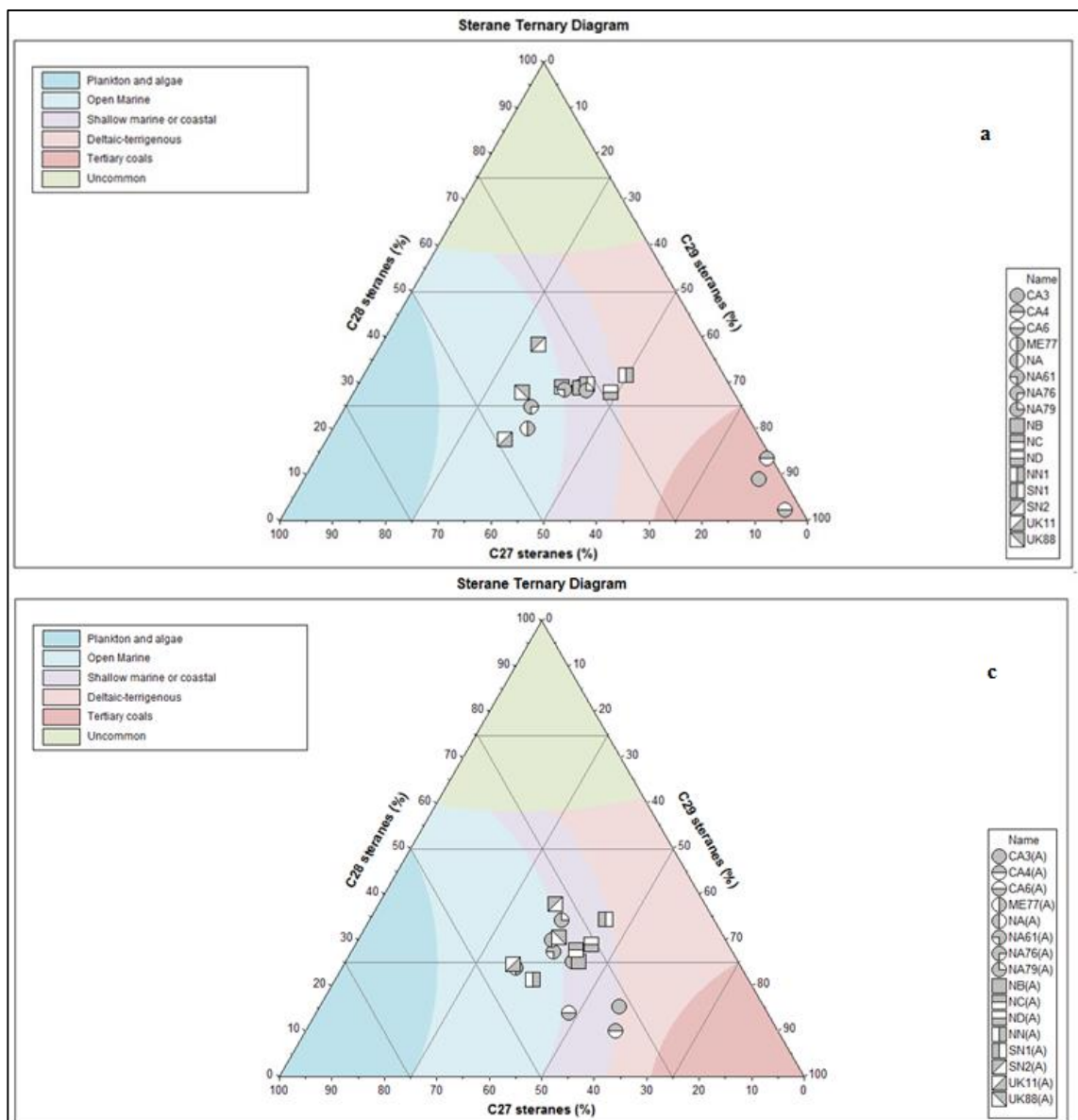


Figure 7.13: Ternary diagram of $C_{28} - C_{30}\alpha\alpha\alpha(R)$ of steranoic acid distributions from asphaltene fractions of asphaltene (a) corresponding to maltene (c), suggesting likely depositional environment. (After IGI's p: 3.5 geochemical interpretation software).

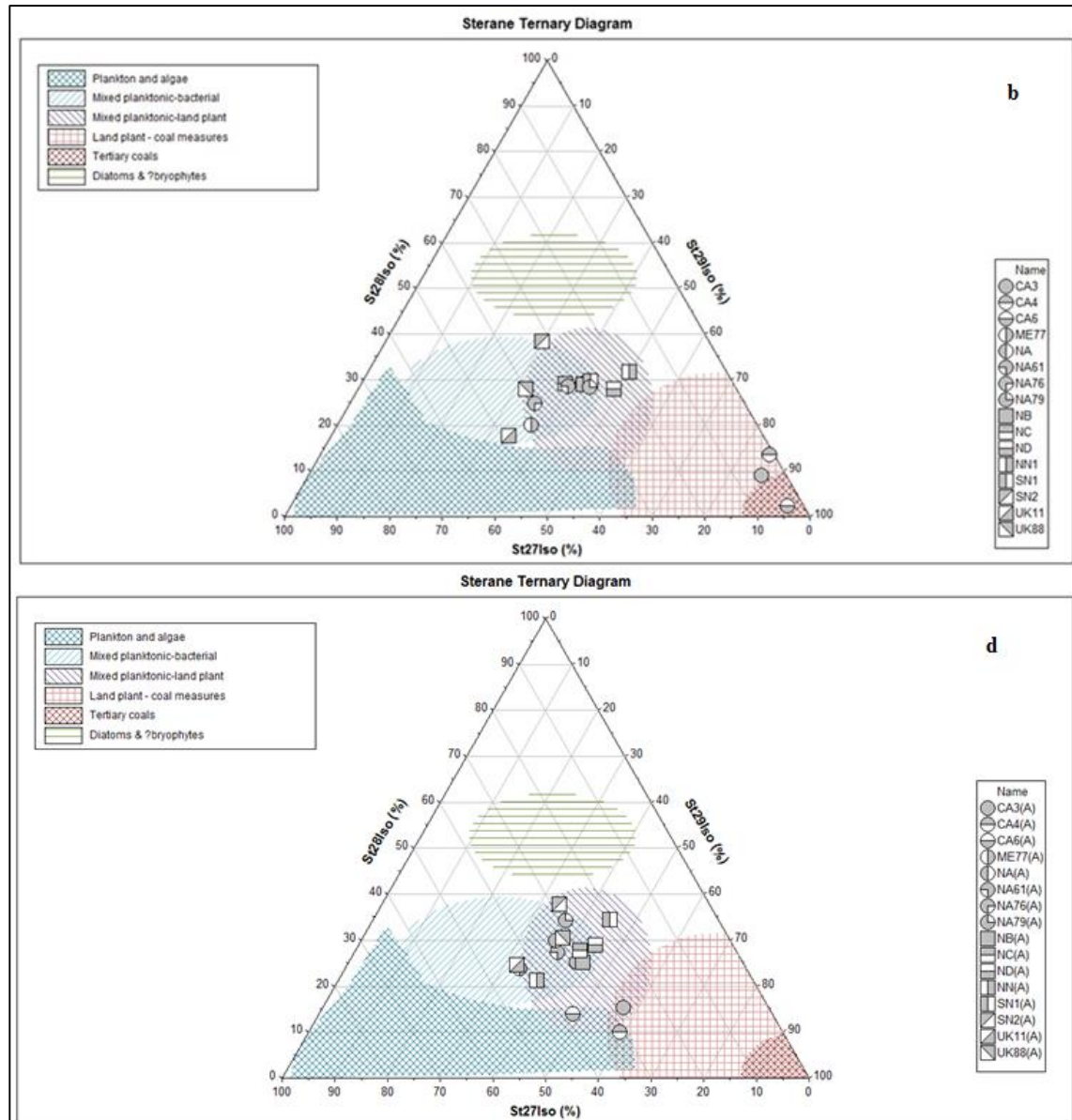


Figure 7.14: Ternary diagram of C₂₈ – C₃₀aaa (R) of steranoic acid distributions from asphaltene fractions of asphaltene (b) corresponding to maltene (d), suggesting likely facies source. (After IGI's p: 3.5 geochemical interpretation software).

7.3.8 Comparative biomarker analysis of the studied maltene and bound asphaltenes.

An attempt was made to correlate asphaltenes that exhibited similar molecular characteristics. PCA applied to the dataset (Table 7.3) resulted with two significant PC's (PC1 and PC2) accounting for 62.38% of the total variance in the data. Loading and score plots constructed on the basis of PC1 versus PC2 show the contribution of each variable related to PC1 and PC2 (Figure 7.15) and the genetic relationship among the asphaltenes again in the plane of PC1 and PC2 (Figure 7.16).

As shown in the score plots (Figure 7.16), three distinct asphaltene clusters along the PC1 are recognised: Cluster 1 (8 asphaltenes from Nigerian and North American oils), cluster 2 (7 asphaltenes from Serbian, United Kingdom and Middle East oils) and cluster 3 (3 asphaltenes from North Sea coals). When the distribution of molecular parameters in Figure 7.15 is interpreted, PC1 appear to be mostly influenced to source organic facies. In Figure 7.15, PC1 is characterised by marine organic matter designated by % C₂₈ that are enriched in the cluster 1 asphaltenes whilst at the left hand side of the PC1 axis, PC1 is characterised by terrestrial organic matter inferred by % C₃₀ that are enriched in the cluster 3 asphaltenes. However, cluster 2 is characterised by increasing diatom input designated by C₂₉ $\alpha\alpha\alpha$, C₃₀ $\alpha\beta\beta$ ($\alpha\beta\beta + \alpha\alpha\alpha$) and C₃₀ $\alpha\alpha\alpha$ S(S + R). Along the PC2, the asphaltene clusters are clearly divided into cluster 2 (7 asphaltenes including from, Nigeria, Serbia, United Kingdom and Middle East oils) and cluster 3 (4 asphaltenes from North Sea coals). PC2 displays negatively correlation variable of higher % C₃₀ ratio, and Cluster 1 C₂₈ $\alpha\alpha\alpha$, C₃₀ $\alpha\beta\beta$ ($\alpha\beta\beta + \alpha\alpha\alpha$) and C₃₀ $\alpha\alpha\alpha$ S(S + R) ratios. It can therefore be expected that PC2 is sensitive to source facies by higher % C₃₀ and increasing angiosperm.

On the hand, the HCA applied to dataset (Table 7.3) resulted with the first four PC's accounting for about 94% of the total variance in the data. The dendrogram correlate excellently with the scores plot showing significant heterogeneity with three clusters similarities. Cluster 1 consist of asphaltenes (Nigerian and North American oils), have 94.76% similarity level while Cluster 2 consist of asphaltenes (Serbian, United Kingdom and Middle East oils), have 81.19% similarity level (Table 7.3) and Cluster 3 consist of asphaltenes (North Sea coals). Cluster 1 consist of asphaltenes (NA, ND, NN & NB) from marine (+ lacustrine) shale sourced Nigerian oils and asphaltenes (NA76, NA79, NA61 & NAC) from marine shale sourced North American oils. However, cluster 2 consists of mixture of asphaltenes from two different geological locations and sources. The heterogeneity of the cluster shows the two asphaltenes (SN1 & SN2) from marine (+ lacustrine) shale sourced Serbian oils and asphaltenes (UK88, UK11) from marine (+ lacustrine) shale sourced United Kingdom oils. Cluster 3 consists exclusively of asphaltenes (CA3, CA4 & CA6) from fluvio/deltaic (coal) sourced North Sea coals. The significance of the difference is shown from the distance between cluster centroids (0.00 – 2.19) is highest wherever it is involved (Table 7.4). Since, the studied North Sea

coals were generally deposited under oxic and dysoxic conditions, the difference could be reflected on level of maturity the coals were generated.

Table 7.3: Cluster Analysis of Observations for biomarkers from RICO analysis

Step	Number of clusters	Similarity level	Distance level	Clusters joined	New clusters	In new clusters
1	15	87.890	0.88	4 5	4	2
2	14	83.980	1.16	1 4	1	3
3	13	77.370	1.63	1 2	1	4
4	12	77.030	1.66	1 11	1	5
5	11	75.730	1.75	1 10	1	6
6	10	75.620	1.76	6 12	6	2
7	9	68.660	2.27	1 9	1	7
8	8	68.230	2.3	1 6	1	9
9	7	66.730	2.41	1 7	1	10
10	6	66.38	2.43	1 3	1	11
11	5	65.58	2.49	1 13	1	12
12	4	62.78	2.69	14 15	14	2
13	3	59.21	2.95	14 16	14	3
14	2	56.57	3.14	1 8	1	13
15	1	35.95	4.63	1 14	1	16

Table 7.4: Final partition of biomarkers from RICO analysis

Clusters	Number of observations	Within clusters sum of squares	Average distance from centroid	Maximum distance from centroid
1	3	1.33	0.66	0.79
2	4	8.81	1.46	1.90
3	5	15.98	1.76	2.19
4	1	0.00	0.00	0.00
5	3	8.29	1.66	1.76

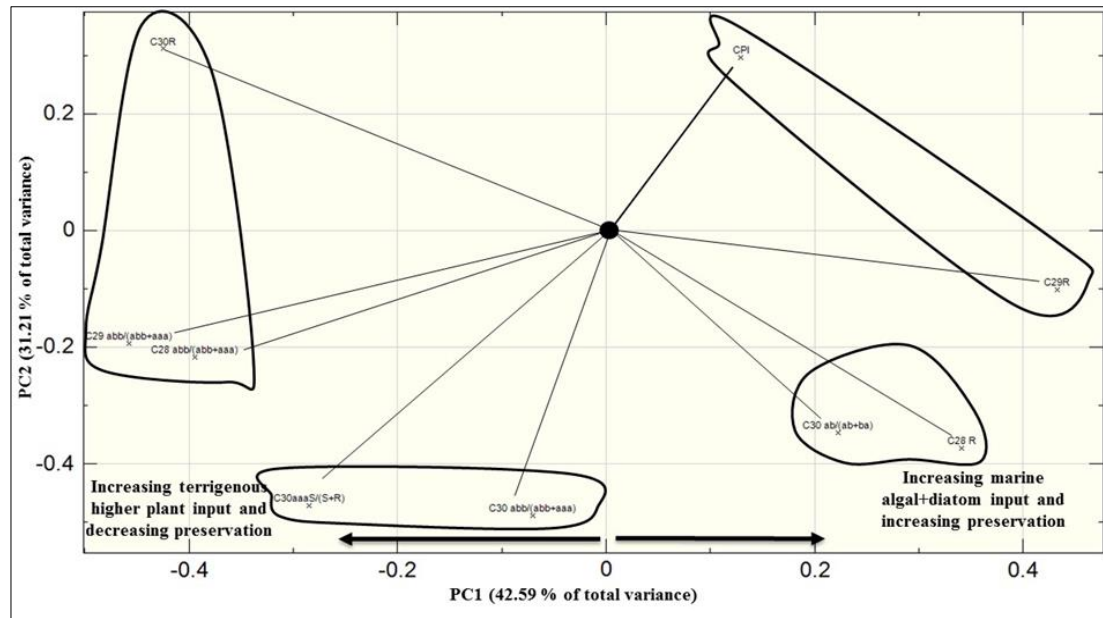


Figure 7.15: A loadings plot showing the relationship between different biomarker parameters in terms of PC1 versus PC2 analysis of multivariate RICO data analysis.

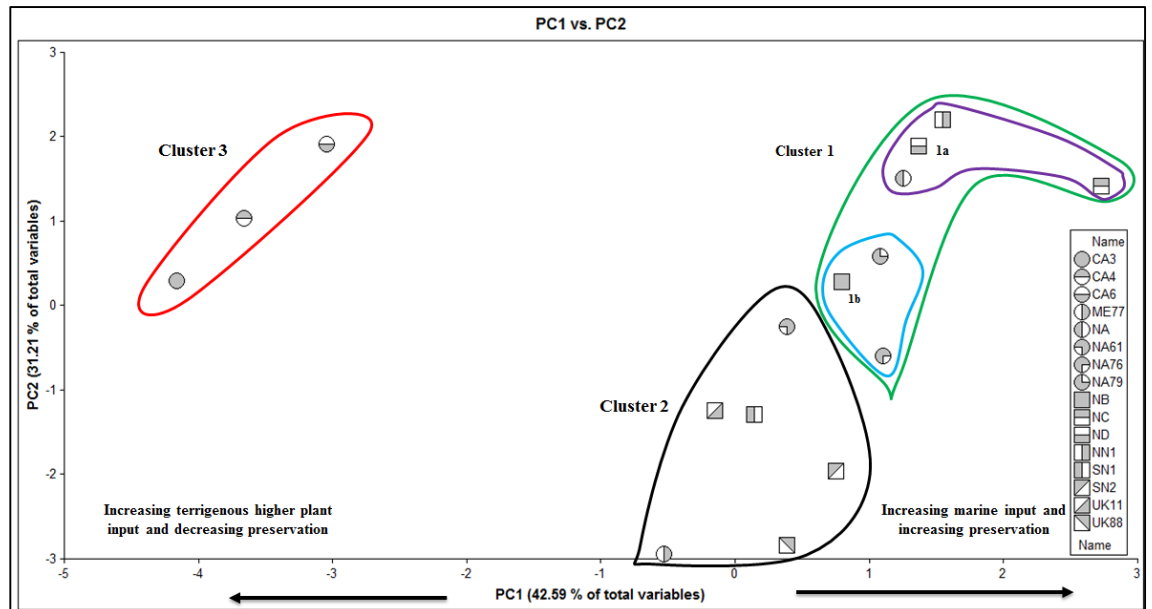


Figure 7.16: A scores plot showing the relationship between studied oil and coal samples in terms of PC1 versus PC2 from a principal component analysis of biomarkers from RICO analysis.

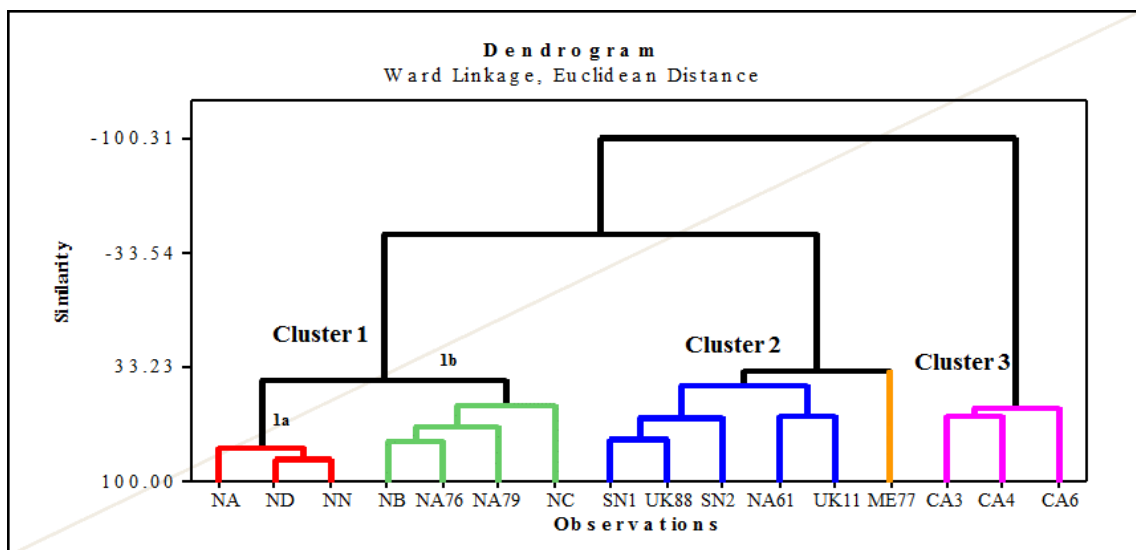


Figure 7.17: Principal component analysis results showing similarity of the samples based on biomarkers from RICO treatment of asphaltene.

7.4 Summary and conclusions

Bound biomarker compounds generated from oxidation products of sixteen asphaltenes from various locations, sources and depositional environments, were assessed. The following interpretations were based on the results (see data in Table 7.3):

- a. The RICO products revealed a clear difference in the distributions of *n*-alkanoic acid methyl ester compared to their corresponding maltenes. The aliphatic moieties in the asphaltenes are dominated by *n*-alkyl distributions.
- b. Comparison of the molecular distributions of the hopanes - hopanoids in the asphaltenes, revealed the existence of carbon number shifts between the series. The hopanoic fractions showed the presence of three diastereomeric series ($17\alpha(H),21\beta(H)$ and $17\beta(H),21\beta(H)$ hopane skeleton and $17\beta(H),21\alpha(H)$), whilst the maltene fractions contain only two series ($17\alpha(H),21\beta(H)$ and $17\beta(H),21\alpha(H)$) epimers with sidechain $22S$ - and $22R$ -configurations.
- c. The thermal maturity parameters calculated from the bound biomarkers of the asphaltene fractions are consistent with low maturity distribution amongst all oils.
- d. The RICO products of the asphaltenes showed that alkyl and hopanoids moieties are not exposed to microbiological degradation. Hence, bound biomarker ratios obtained from the asphaltenes may be considered as relatively reliable parameters for the oils.
- e. Successful application of chemometric analysis by principal components help to correlate a better distinction and classification of the data and consequently of the locations.

Chapter 8 The ultrasonic characterisation of asphaltene nanoaggregation in petroleum

8.1 Introduction

The petroleum industry is an example where several analytical techniques including ultrasonic (Andreatta *et al.*, 2005a; Mullins *et al.*, 2007; Mullins, 2010), small-angle neutron scattering (Gawrys and Kilpatrick, 2005) centrifugation (Mostowfi *et al.*, 2008; Indo *et al.*, 2009), and conductivity (Sheu, 1998; Andreatta *et al.*, 2005a) have studied the tendency of asphaltenes to self-associate and form molecular aggregates. Among these, centrifugation studies have shown that there is some uncertainty where the exact critical nanoaggregate concentration of asphaltene (CNAC) can be identified (Mostowfi *et al.*, 2008). Whereas, other studies such as conductivity measurements have provided evidence of CNAC, which is in agreement with high-Q ultrasonics study due to aggregation in organic solvents (Mullins, 2011).

Ultrasound resonance spectroscopy is one of the emerging technologies that have been investigated by numerous researchers (Seifert and Moldowan, 1979; McClements, 1991; Povey, 1997; Andreatta *et al.*, 2005a; Holmes *et al.*, 2011; Abbott and Povey, 2012; Mullins *et al.*, 2012b; Parker and Povey, 2012). The ultrasound spectroscopy measurement provides precise frequencies and bandwidths for a series of resonances from which velocity of sound and attenuation data are recorded. Generally, this is a non-destructive technique that is applied to probe a wide range of materials, including many that are optically opaque, and provides accurate, fast, reliable and high quality information at low cost (Povey, 1997). Other applications, include the flow dynamics and composition of oils, the oil content and droplet size of emulsions and the solid fat content of partially crystalline emulsions (McClements and Povey, 1992).

The use of ultrasonic spectroscopy for characterizing asphaltene has been established by (Andreatta *et al.*, 2005a; Mullins *et al.*, 2012b). However, most work to date has focused on the asphaltene as a function of toluene solution, for example the preparation of asphaltene concentration to show the existence of asphaltene nanoaggregates along with structures of other length scales (Sheu, 2002). A high-Q ultrasonic measurement is believed to have led to the development of a simple molecular aggregations model (Yen

model or the Yen-Mullins model). The reported model found that asphaltenes in toluene and known surfactants comprises of monomers and nanoaggregates. The challenge of understanding the fundamental dynamics of asphaltene aggregation as a function of the crude oil composition is enormous. Hence, this work aims to fill this knowledge gap and builds on an earlier high quality factor (high-Q) ultrasonics study that was used to demonstrate asphaltene nanoaggregation (Andreatta *et al.*, 2005a).

Andreatta *et al.* (2005a), have shown that asphaltenes exhibit a critical nanoaggregate concentration (CNAC) at room temperature in the range of 50 – 150 mg/L in toluene, depending upon the asphaltene. The authors illustrated the state of colloidal aggregation using the micelle phase equilibrium model, comprising monomer and nanoaggregate. In the study by Andreatta *et al.* (2005a), high resolution ultrasonic spectroscopy was performed on asphaltenes from Kuwaiti crude oils (UG8 and BG5) as well as known surfactants: sodium dodecyl sulphate (SDS), hexade-cyltrimethylammonium bromide ($C_{16}TAB$), polyoxyethylene 23 lauryl ether (Brij 35; $C_{12}E_{23}$), and polyoxyethylene sorbitan monooleate (Tween 80), purity > 99%. In order to validate the model for aggregation in asphaltene solutions, the following were considered: (a) standard surfactants and (b) mathematical model (Andreatta *et al.*, 2005a). The standard surfactants were used to detect the formation of critical micelle concentration (CMC) and both the surfactants and asphaltenes are considered to be nonionic surfactants that undergo micelle formation. The mathematical model (equations) provides the micelle phase equilibrium model for standard surfactant and asphaltene data. From the mathematical model, at low concentrations the aggregation transition is accompanied by change in the gradient of the speed of sound as a function of asphaltene concentration.

In our study, high-precision ultrasound resonance spectroscopy by the Resoscan-Research system is used directly to probe the asphaltene bulk properties to understand the formation of aggregation in crude oils. The instrument simultaneously measures both the velocity and attenuation of sound of a given sample as described in Chapter 3, section 3.4.4. In order to elucidate the essential dynamics of asphaltene aggregation, the objectives were based on the following,

- a. To characterise the velocity of sound (or attenuation of sound) as a function of the concentration of asphaltene.

- b. To extract the CNAC from the velocity of sound and attenuation data.
- c. To compare and contrast the CNACs, such as those of ultrasonic velocity and attenuation of sound from asphaltenes of different geological locations.
- d. To calculate the error in the CNAC value that has not been calculated in earlier research.
- e. To calculate the error in the measured CNAC value; this was not performed in the study by Andreatta et al. (2005a).

8.2 Theory

8.2.1 Sound and ultrasonic sound wave

Sound is a travelling wave which is an oscillation of pressure transmitted through a solid, liquid, or gas. However, the propagation of sound is dependent on physical, chemical and biological properties of material through which it propagates (Povey, 1997). Consequently, as the wave of compression and rarefaction (e.g. auditory sound, seismic waves) passes through the homogeneous medium, particles oscillate elastically about their equilibrium points as illustrated in Figure 8.1. Hence, the speed of sound can be determined from Urick equation as:

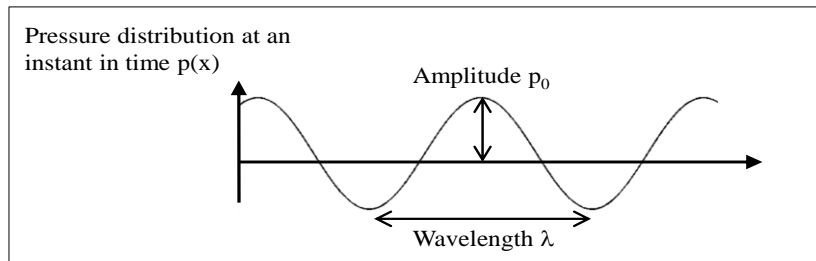


Figure 8.1: Schematic diagram of longitudinal ultrasonic waves.

$$u = \frac{1}{\sqrt{k\rho}} \quad \text{Eq. 8.1}$$

where ρ is the density of the medium and k is its compressibility. The compressibility is a measure of how easily the system is compressed under a force (gases have large compressibilities and solids have low compressibilities), and is given mathematically as

$$k = \frac{1}{u} \frac{dV}{dp}, \quad \text{Eq. 8.2}$$

where V is the volume of the fluid and p is the pressure.

An ultrasonic wave is an oscillating sound wave which has a frequency greater than 20 kilo-Hertz. However, this frequency is greater than the upper limit of the human hearing range. Its application to study asphaltene in toluene solution is associated with the characteristics of elastic constant, density, composition and microstructure of a phase-equilibrium system (Andreatta et al., 2005a). However, as ultrasonic wave can travel through materials in different forms, e.g. shear waves, surface waves and compressional waves are frequently used as non-destructive probes of material concentrations and structural properties (McClements, 1991). Consequently, compressional wave passes through a polydisperse medium by successive compressions and expansions (Figure 8.1), leaving the physical properties of the material unaltered. The use of ultrasonic wave to study materials, mostly measure velocity and attenuation parameters that is associated with the physical properties of the material.

8.2.2 Speed of sound in homogenous liquid

The pure homogenous liquids possess no discontinuity and as such do not scatter ultrasound waves. In this system, Urick equation (Equation 8.1) represents the simple ultrasonic properties and volume of the liquid.

As the wave propagates through the medium, its energy will be dissipated to the surrounding, causing a reduction in the wave amplitude. This is termed attenuation. In a homogeneous liquid, there are two main contributions to the sound attenuation. *Viscous losses* arise due to the inherent viscosity of the liquid, which causes dissipation of energy whenever there is relative motion within the liquid. *Thermal losses* arise since the compression/rarefaction of the medium causes local heating (relative to the background temperature); these local regions act as heat sources, and dissipate energy into the surroundings via heat conduction.

The effect of attenuation is to cause the amplitude of sound wave to decrease as it propagates (Figure 8.2). Considering motion along x we can write the variation of pressure in an ideal, non-attenuating medium as

$$p(x, t) = p_0 \exp[i(\kappa x - \omega t)] \quad \text{Eq. 8.3}$$

where $\kappa = 2\pi/\lambda$ is the wavenumber and $\omega = 2\pi f$ is the angular frequency of the wave, and p_0 is the initial wave amplitude.

In an attenuating medium, this becomes modified as

$$p(x, t) = p_0 \exp(-\alpha x) \exp[i(\kappa x - \omega t)]. \quad \text{Eq. 8.4}$$

In other words, the amplitude decays exponentially with distance. The rate of this decay in amplitude is specified by the attenuation coefficient, α (McClements, 1991; Povey, 1997). The unit of attenuation is often express as decibels per meter (dB m^{-1}), where 1Np is equivalent to 8.686 dB (McClements, 1991).

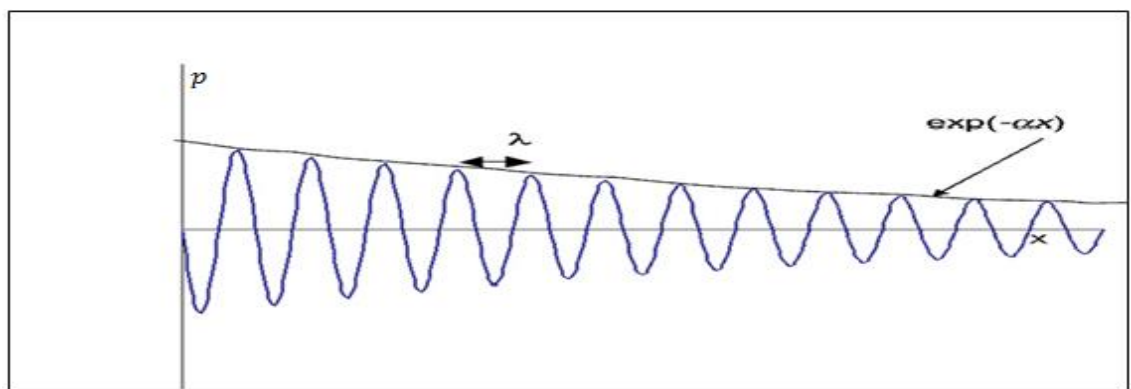


Figure 8.2: Schematic diagram of attenuation of sound. The pressure of the wave decreases exponentially with distance travelled x .

8.2.3 Speed of sound in asphaltene solution

Generally, for dilute solutions, the velocity of sound and the solution density can be expressed as a function of the concentration of the solute. Here we describe the model employed by Andreatta et al (2005a) for modelling the variation of the speed of sound of a solution with its concentration, including the process of aggregation at some critical concentration. This model begins by modelling the solution density and compressibility in terms of the asphaltene concentration; this can then be related to the speed of sound in the solution via Eq. 8.1.

The asphaltene molecules exist in either monomeric or aggregate forms, or a combination of both. The total mass of asphaltenes w is the sum of the mass in monomeric form w_1 and the mass in nanoaggregate form w_{NA} , i.e.:

$$w = w_1 + w_{NA}. \quad \text{Eq. 8.7}$$

The total volume of the solution can be expressed as the sum of the apparent volumes of the solvent, monomers and nanoaggregates:

$$V = w_0 v_0 + w_1 w v_1 + w_{NA} v_{NA}, \quad \text{Eq. 8.8}$$

where w_0 is the mass of the solvent, v_0 is the specific volume of the solvent, v_1 is the apparent specific volume of monomers and v_{NA} is the apparent specific volume of the nanoaggregates.

The mass of the asphaltene solution can be written as:

$$\rho V = w_0 + w_1 + w_{NA}. \quad \text{Eq. 8.9}$$

The density of the asphaltene solution is then expressed as:

$$\rho = \rho_0 + (1 - v_1 \rho_0) c_1 + (1 - v_{NA} \rho_0) c_{NA} \quad \text{Eq. 8.10}$$

where ρ_0 is the density of the solvent, c_1 is the mass concentration of the monomeric form and c_{NA} is the mass concentration of the asphaltene in the aggregate form. The total mass concentration of asphaltene is equal to $c = c_1 + c_{NA}$.

If we assume that the phase-equilibrium model for asphaltene is valid here, then:

$$c_1 = c \text{ and } c_{NA} = 0 \text{ (for } c < cnac\text{)}$$

$$c_1 = cnac \text{ and } c_{NA} = c - cnac \text{ (for } c > cnac\text{)}$$

where $cnac$ is the numerical value of the CNAC. The density of the solution, both above and below the aggregation concentration, follows as:

$$\rho = \rho_0 + (1 - v_1 \rho_0) c. \quad (\text{for } c < cnac) \quad \text{Eq. 8.11}$$

$$\rho = \rho_0 + (v_{NA} - v_1) \rho_0 cnac + (1 - v_{NA} \rho_0) c \quad (\text{for } c > cnac) \quad \text{Eq. 8.12}$$

Having developed expressions for the solution density as a function of concentration, we turn to address the adiabatic compressibility. The adiabatic compressibility of the solution k_s (at constant entropy S) is related to density according to:

$$k_s = \frac{1}{\rho} \left(\frac{\partial \rho}{\partial P} \right)_S . \quad \text{Eq. 8.13}$$

Differentiating Eq. (8.10) gives:

$$\begin{aligned} \left(\frac{\partial \rho}{\partial P} \right)_S &= \left(\frac{\partial \rho_0}{\partial P} \right)_S + \left(\frac{(1 - v_1 \rho_0)}{\partial P} \right)_S c_1 + (1 - v_1 \rho_0) \left(\frac{\partial c_1}{\partial P} \right)_S + \\ &\quad \left(\frac{\partial (1 - v_{NA} \rho_0)}{\partial P} \right)_S c_{NA} + (1 - v_{NA} \rho_0) \left(\frac{\partial c_{NA}}{\partial P} \right)_S . \end{aligned} \quad \text{Eq. 8.14}$$

We assume that the concentration of monomers c_1 and the concentration of nanoaggregates c_{NA} changes with pressure only through changes in the solution volume. Then it follows that:

$$\left(\frac{\partial c_1}{\partial P} \right)_S = c_1 k \quad \text{Eq. 8.15}$$

$$\left(\frac{\partial c_{NA}}{\partial P} \right)_S = c_{NA} k \quad \text{Eq. 8.16}$$

The adiabatic compressibility of the solvent is given by:

$$k_0 = \frac{1}{\rho_0} \left(\frac{\partial \rho_0}{\partial P} \right)_S \quad \text{Eq. 8.17}$$

The apparent adiabatic compressibility of the asphaltene monomers is:

$$k_1 = -\frac{1}{v_1} \left(\frac{\partial v_1}{\partial P} \right)_S \quad \text{Eq. 8.18}$$

Similarly, the apparent adiabatic compressibility of the nanoaggregates is defined by:

$$k_{NA} = -\frac{1}{v_{NA}} \left(\frac{\partial v_{NA}}{\partial P} \right)_S \quad \text{Eq. 8.19}$$

With these definitions, and using Eq. 8.14 we can write:

$$\begin{aligned} \rho k &= \rho_0 k_0 + k[(1 - v_1 \rho_0)c_1 + (1 - v_{NA} \rho_0)c_{NA}] + \rho_0 c_1 v_1 (k_1 - k_0) + \\ &\quad \rho_0 c_{NA} v_{NA} (k_{NA} - k_0), \end{aligned} \quad \text{Eq. 2.20}$$

$$k = k_0 + (k_1 - k_0)v_1 c_1 + (k_{NA} - k_0)v_{NA} c_{NA}. \quad \text{Eq. 2.21}$$

Recall that Eq. 8.1 gives the speed of sound as a function of the density and compressibility of the medium. Substituting in our expressions for the density and compressibility of the solution, and taking the limit of dilute solutions ($c_1 \ll 1$ and $c_{NA} \ll 1$) we arrive at the following expression for the solution speed of sound:

$$u = u_0 + \frac{u_0}{2} \left[v_1 \left(2 - \frac{k_1}{k_0} \right) - v_0 \right] c_1 + \frac{u_0}{2} \left[v_{NA} \left(2 - \frac{k_{NA}}{k_0} \right) - v_0 \right] c_{NA}. \quad \text{Eq. 8.22}$$

This tells us that, for $c < cnac$:

$$u = u_0 + \frac{u_0}{2} \left[v_1 \left(2 - \frac{k_1}{k_0} \right) - v_0 \right] c, \quad \text{Eq. 8.23}$$

and for $c > cnac$:

$$\begin{aligned} u = u_0 + \frac{u_0}{2} \left[v_1 \left(2 - \frac{k_1}{k_0} \right) - v_{NA} \left(2 - \frac{k_{NA}}{k_0} \right) \right] cnac + \\ \frac{u_0}{2} \left[v_{NA} \left(2 - \frac{k_{NA}}{k_0} \right) - v_0 \right] c. \end{aligned} \quad \text{Eq. 8.24}$$

We see that both above and below the CNAC, the speed of sound varies linearly with the total asphaltene concentration c . But, importantly, the gradient of this relationship is different either side of the CNAC. This tells us that if we plot the solution speed of sound versus asphaltene concentration we expect two straight lines, with the transition between these behaviours occurring at the CNAC. This is the principle we will use to identify the CNAC.

8.2.4 Attenuation of sound in asphaltene solution

The above section describes a physical model for how we expect the speed of sound to vary as concentration is changed through an aggregation process. A similar model for attenuation is challenging, due to the necessity to account for the multitude of contributions to the attenuation in a suspension. Nonetheless, we can examine the variation of attenuation empirically. Below and above the CNAC, the physical characteristics of the liquid are different (below we have a solution, above we have a suspension), and so we would expect the attenuation to change discontinuously at the CNAC. We will see that this is indeed the case, and that the attenuation appears to scale

linearly with concentration either side of the CNAC, similar to the speed of sound. As such, we will empirically proceed to determine the CNAC from the attenuation data by fitting to two straight lines and identifying their crossing point, as detailed below for the speed of sound data. While it would be interesting to determine more precisely the actual functional form of the attenuation either side of the CNAC, this is beyond the scope of this work which is focussed on identifying the CNAC.

8.3 Methods

The asphaltenes used in this study were three crude oil asphaltenes (SN1, SN2 and NA61) from different regional locations, source facies and depositional environments. They were prepared as described in Chapter Three, section 3.3.2., 3.3.2.1, 3.3.2.2 and 3.3.7. Ultrasonic spectroscopy was carried out on the asphaltenes in toluene as described in section 3.4.4.

In order to determine the mean CNAC value more accurately, it was necessary to fit the data to two connected straight lines (the CNAC then being associated with the point of intercept of these two lines). Then, by considering the error in these two straight line fits, it was possible to estimate the error of the CNAC itself. We will describe these methods below.

8.3.1 Fitting to two straight lines and the mean CNAC

To extract the CNAC we need to fit our speed of sound and attenuation data to two straight lines. Here we describe this methodology. For generality, we consider some general data $y(x)$ which approximates two straight lines, as shown in Figure 8.3, and seek to find the crossing point of the data subsets, denoted x_{cross} . To find the optimum fit to two connected straight lines, it is necessary to divide the data into two subsets, one representing the data below the critical point, one representing the data above the critical point. Then each subset can be independently fit to a straight line; the success of each straight line fit is provided by the R^2 -coefficient. However, the choice of how and where to divide the data requires some care. Here we define this division as being when the sum of the R^2 -coefficients is maximised, in other words, we vary the boundary between the two subsets of the data until the best combined fit is achieved.

Each data subset is then fit to a straight line using the least squares method. This provides a mean fit function for each subset, \hat{y}_1 and \hat{y}_2 , where the 1 and 2 subscripts refer to the lower and upper data subsets. That is,

$$\hat{y}_1 = \hat{a}_1 + \hat{\beta}_1 x, \quad \text{for } x < x_{\text{cross}} \quad \text{Eq. 8.25}$$

$$\hat{y}_2 = \hat{a}_2 + \hat{\beta}_2 x, \quad \text{for } x > x_{\text{cross}} \quad \text{Eq. 8.26}$$

Here \hat{a}_1 and \hat{a}_2 are the best-fit y -intercepts, and $\hat{\beta}_1$ and $\hat{\beta}_2$ are the best-fit gradients, of these straight lines. The best-fit mean CNAC crossing point is then the intercept between these two lines of best fit. At this crossing point, $\hat{y}_1 = \hat{y}_2$. Setting this and rearranging for x leads to an expression for the x -position of the crossing point,

$$x_{\text{cross}} = \frac{\alpha_1 - \alpha_2}{\beta_2 - \beta_1}. \quad \text{Eq. 8.27}$$

In our curves of sound velocity and sound attenuation, this coincides with the best-fit CNAC.

8.3.2 Error analysis

In order to estimate the accuracy of the determined mean CNAC for asphaltenes in toluene solutions in the range $\sim 0.006 - 2.3$ g/L concentration, SigmaPlot 11.0 software packages was used to ascertain the statistical uncertainty limit for the intercepts and gradients as illustrated in Figure 8.3.

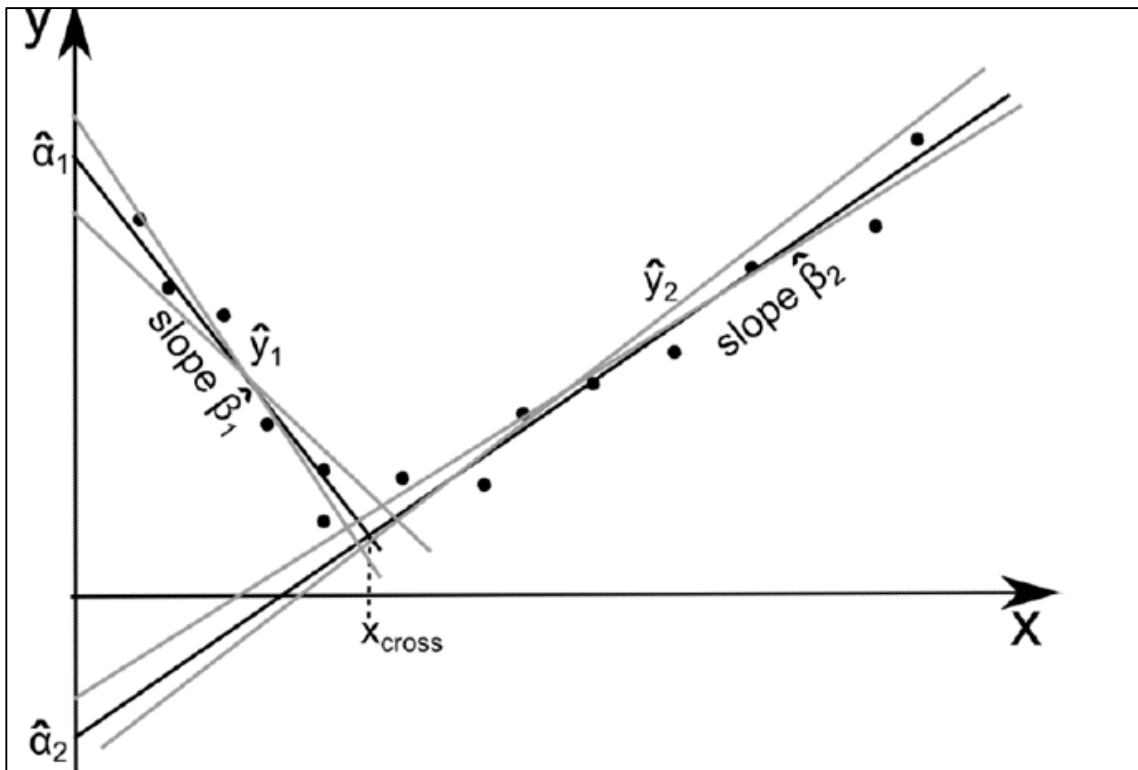


Figure 8.3: Schematic illustration of the fitting of the data to two straight lines. The black lines, $\hat{y}_{1,i}$ and $\hat{y}_{2,i}$, are the two lines of best fit. The grey lines represent the extreme fits, within error tolerances. The axes here represent generalised variables x and y - in our work y corresponds to either velocity of sound or sound attenuation and x represents asphaltene concentration.

An important distinction between this study and the Andreatta study is the calculation of the CNAC error. The best fit CNAC above is the crossing point of the lines of best fit x_{cross} . However, the fits have errors associated with them. This allows us to establish the statistical error associated with x_{cross} and hence the CNAC as follows. For the line of best fit for each subset of the data, the statistical uncertainty of the intercept and gradient was calculated using the SigmaPlot 11.0 software package. In other words, the y -intercept and gradient for each straight line fit lies within a range. Consideration of the extreme values provides a bound on the possible straight line fits, such as those shown in Figure 8.3 (grey lines). From these extreme fits, we deduce the range in the crossing points, i.e. the CNAC.

We wish to compare the CNAC from different oil samples, and it is important to establish whether any numerical difference is statistically significant. A 2-sample t-test was applied on the CNAC values with errors, so as to determine the statistical difference between the mean CNACs. This test quantifies how significant is the

difference between two means. The produced p-value must be greater than 0.05 for the mean to define the group to be statistically significant different.

8.4 Results and discussion

8.4.1 The effects of asphaltene concentration on ultrasonic velocity of sound

Figures 8.4 – 8.6 show the variation of the speed of sound for the asphaltene solution as a function of concentration (all at 25 °C), for the three different oils NA61, SN1 and SN2. The chosen subsets of data below and above the CNAC are shown by blue cycles and red cycles, respectively. The line of best fit for each subset (solid line) is superimposed. The data agrees well with the expected form of two connected straight lines.

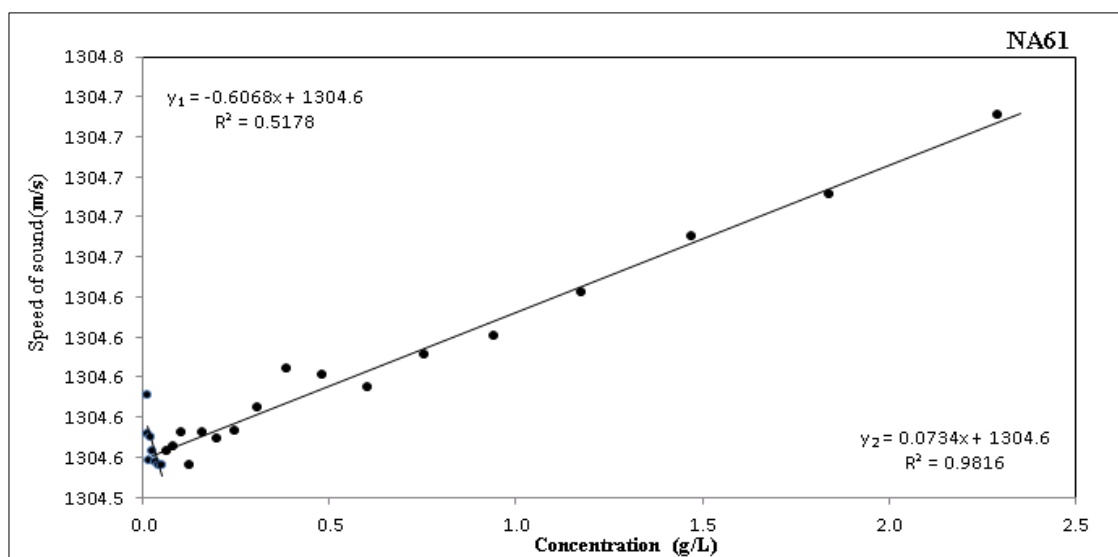


Figure 8.4: Measured velocity of sound versus concentration of asphaltene (NA61) in toluene (NA61) at 25 °C.

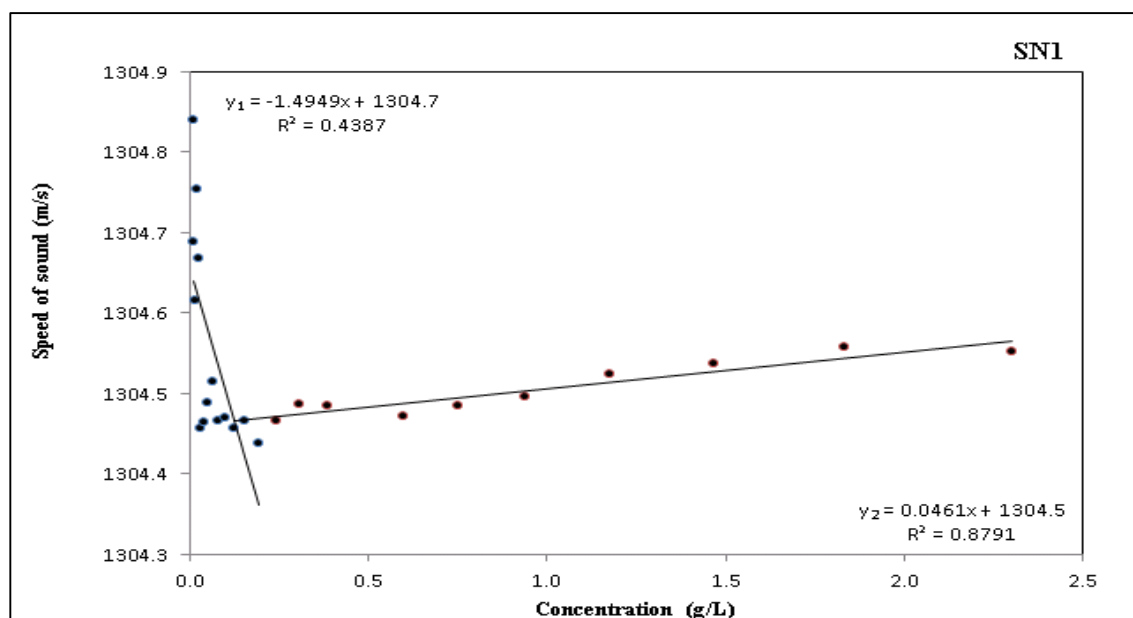


Figure 8.5: Measured velocity of sound versus concentration of asphaltene (SN1) in toluene at 25 °C.

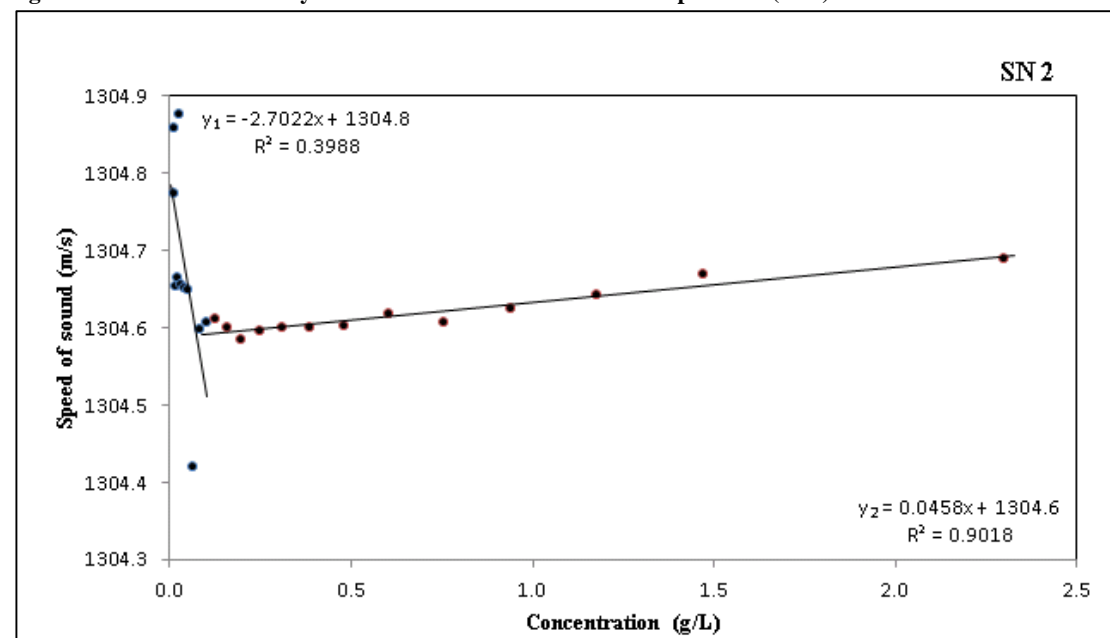


Figure 8.6: Measured velocity of sound versus concentration of asphaltene (SN2) in toluene at 25 °C.

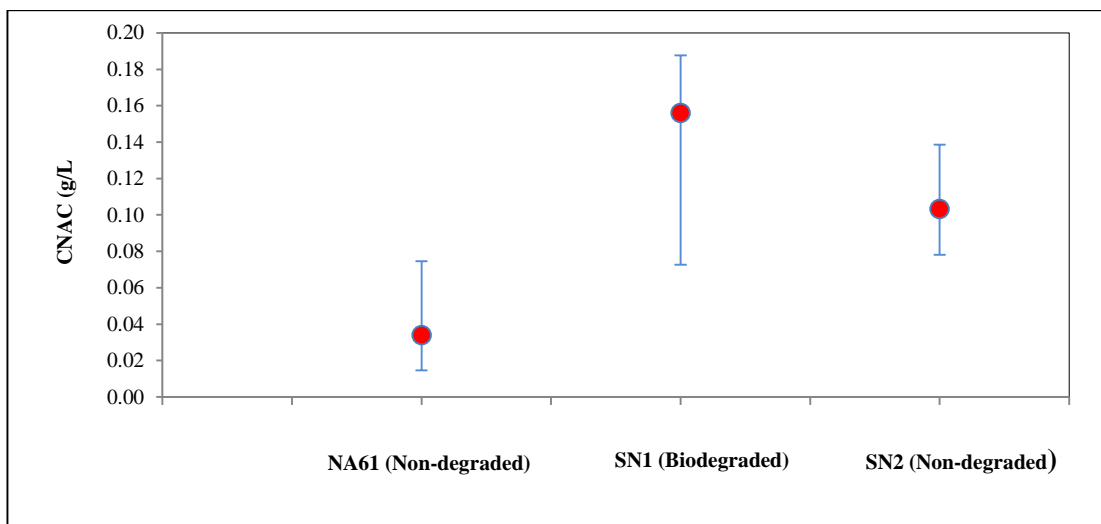


Figure 8.7: Statistical uncertainties of CNAC's of studied asphaltenes in toluene at 25 °C calculated from ultrasonic velocity of sound.

Table 8.1: Experimentally determined CNAC with statistical uncertainties in velocity of sound for asphaltenes in toluene at 25 °C.

Sample	Mean CNAC (g/L)	"+"	"-"	Upper CNAC (g/L)	Lower CNAC (g/L)
North American (Non-degraded)	0.03	0.04	0.02	0.08	0.02
Serbian (biodegraded)	0.16	0.03	0.08	0.19	0.07
Serbian (Non-degraded)	0.10	0.04	0.03	0.14	0.08

The mean CNAC, and their errors, are depicted in Figure 8.7 and tabulated in Table 8.1. The CNAC varies across the 3 samples (SN1, SN2 and NA61), over the range $\sim 0.03 - 0.16$ g/L (Table 8.1). A similar trend of CNAC has been observed by others for asphaltenes in toluene solution (Andreatta et al., 2005b; Mullins, 2010). According to these authors, asphaltenes in toluene solution exhibit CNACs at $\sim 0.05 - 0.15$ g/L. The mean CNAC of asphaltenes (SN1 & SN2) have a significant difference from 0.10 – 0.16 g/L respectively, with $p = 0.13$. This p -value indicates that this difference is statistical significant, and suggests that asphaltenes of different compositions exhibit CNACs with some variability in the exact value. The asphaltenes from the non-degraded oils (NA61 & SN2) are not significantly different, suggesting a similar CNAC covers across the non-degraded oils ($p = 0.02$).

8.4.2 The effects of asphaltene concentration on attenuation of sound

The corresponding results for the sound attenuation as a function of concentration are shown in Figures 8.8 – 8.11 and Table 8.2.

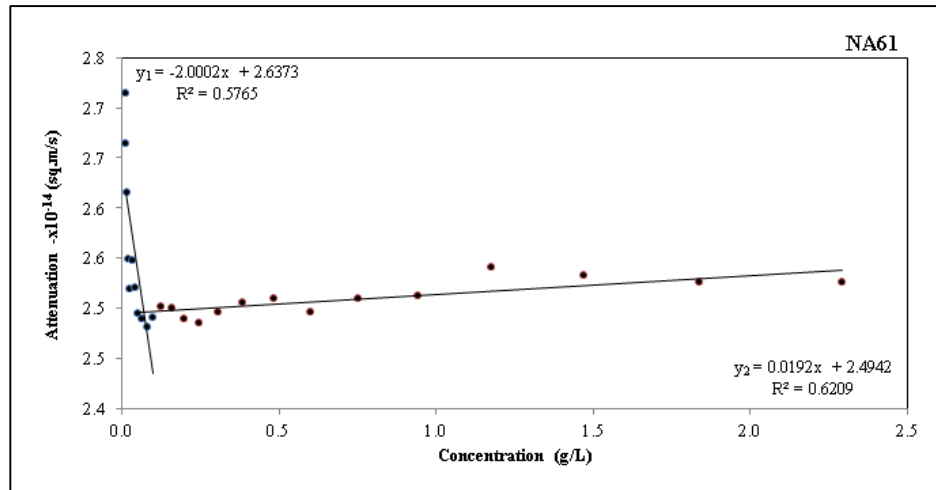


Figure 8.8: Measured attenuation of sound versus concentration of asphaltene (NA61) in toluene at 25 °C.

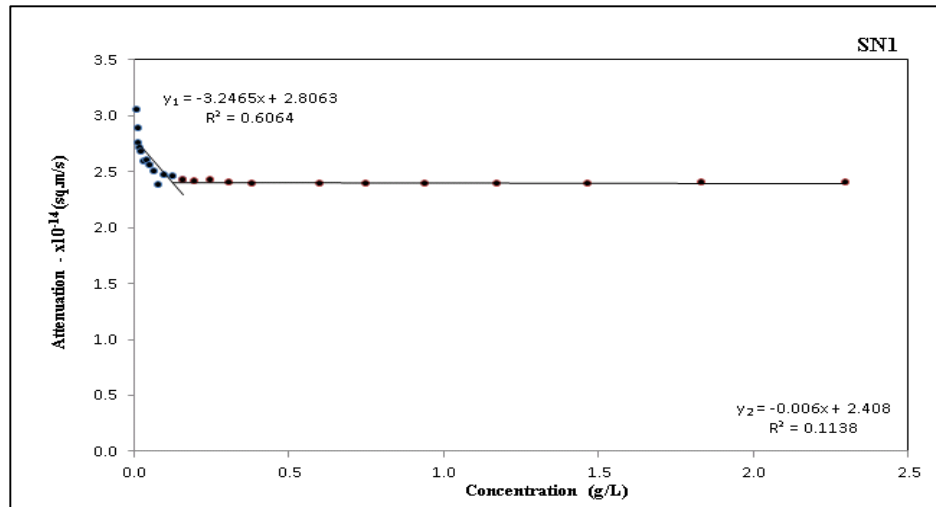


Figure 8.9: Measured attenuation of sound versus concentration of asphaltene (SN1) in toluene at 25 °C.

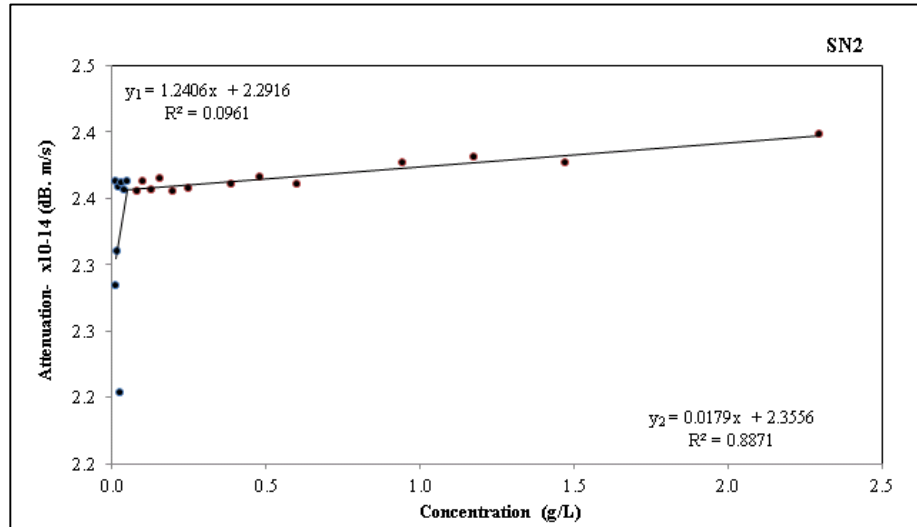


Figure 8.10: Measured attenuation of sound versus concentration of asphaltene (SN2) in toluene at 25 °C.

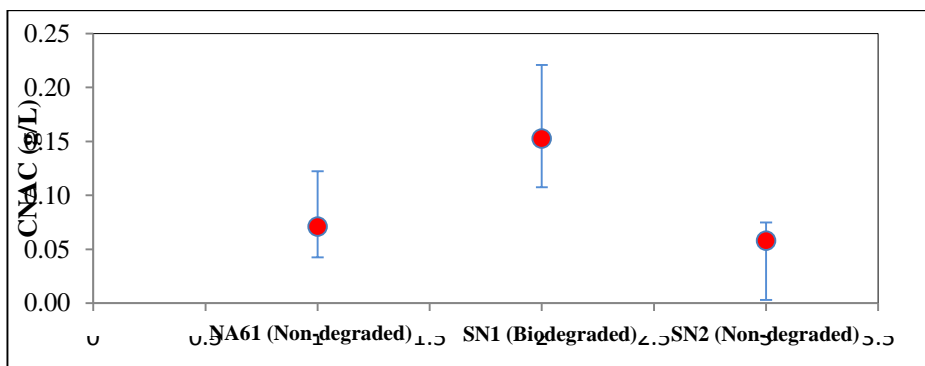


Figure 8.11: Statistical uncertainties of CNAC's of studied asphaltenes in toluene at 25 °C calculated from attenuation of sound.

Table 8.2: Experimentally determined CNAC with statistical uncertainties in attenuation of sound for asphaltenes in toluene at 25 °C.

Sample	Mean CNAC (g/L)	"+"	"+"	Upper CNAC (g/L)	Lower CNAC (g/L)
North American (Non-degraded)	0.07	0.05	0.03	0.12	0.02
Serbian (biodegraded)	0.15	0.07	0.05	0.22	0.11
Serbian (Non-degraded)	0.06	0.02	0.06	0.04	0.03

The attenuation data also fits well to two connected straight lines, although it should be emphasized that we offer no physical explanation for this appearance. We proceed to empirically identify the CNAC as the crossing point of these two fitted straight lines. The CNAC of the studied samples (SN1, SN2 and NA61), range from ~0.06 – 0.15g/L (Table 8.2). The asphaltenes from the non-biodegraded oils (SN2 & NA61) are significantly similar with CNAC value of ~0.06 – 0.07 g/L respectively ($p = 0.156$) whilst the asphaltene from the biodegraded oil (SN1) is significantly different with CNAC value of 0.15g/L ($p = 0.156$). These values support the values derived from the sound data.

8.4.3 Comparative analysis of ultrasonic velocity and attenuation of sound to petroleum asphaltenes of different compositions

As discussed in Sections 8.1.1 and 8.1.2 ultrasound spectroscopy is sensitive to detect the presence of aggregation in asphaltene/toluene system. Examples of its application for the purpose of this study have generated sound velocity and attenuation shown in Figures (8.4 – 8.11). There is a steady decrease in velocity as concentration increases to a point (sudden break in the velocity of curve), wherein the velocity increases as the

asphaltene molecules aggregate into cluster to form larger clusters. The velocity of sound from the studied asphaltenes, irrespective of their sources, exhibits a similar behaviour (Figure 8.4 – 8.6). This behaviour is similar to observation of Andreatta et al. (2005a). These authors conducted a series of stepwise dissolution of asphaltene solids in toluene system as well as known surfactants. Consequently, measurements of these concentrations revealed that asphaltenes are non-ionic surfactants that form nanoaggregates and exhibit CNACs.

In addition, the attenuation data do exhibit similar behaviour to velocity data for all studied asphaltene in toluene samples. The clear break in SN1 asphaltene curve (Figure 8.6) is in contrast to the behaviour of SN2 asphaltene in toluene using velocity of sound (Figure 8.10). It will be difficult to confuse the behaviour since SN2 increases the attenuation of sound compared to velocity of sound. It should be pointed out that attenuation of sound data from the measurement of asphaltene in toluene solution at 25 °C do exhibit similar break in curve to velocity data that represents CNAC. The data of velocity and attenuation of sound from asphaltene of non-biodegraded oil has been shown (Table 8.3) to be much low concentrations ($C \leq 0.03 - 0.10 \text{ g/L}$) whilst higher concentrations ($C \leq 0.15 - 0.16 \text{ g/L}$) for asphaltene of degraded oil.

Table 8.3: Comparison of experimentally determined CNAC with statistical uncertainties in toluene using attenuation and velocity of sound for asphaltenes in toluene at 25 °C

Sample	Mean CNAC (g/L)	"+"	"-"	Upper CNAC (g/L)	Lower CNAC (g/L)
NA61 (Non-degraded)	0.07/0.03	0.05/0.04	0.03/0.02	0.12/0.08	0.02/0.02
SN1 (biodegraded)	0.15/0.16	0.07/0.03	0.05/0.08	0.22/0.08	0.11/0.07
SN2 (Non-degraded)	0.06/0.10	0.02/0.04	0.06/0.03	0.04/0.14	0.03/0.08

The values on the right of "/" are mean CNACs estimated using attenuation of sound, the left of "/" are the CNACs from ultrasonic velocity of sound on the asphaltene-toluene system; "+" and "-" are the estimated standard errors.

8.5 Summary and conclusions

High-precision ultrasound spectroscopy was used to assess asphaltene aggregates in toluene. The ultrasound data clearly show a change in the aggregation profile of asphaltenes at 25 °C, in the range of approximately 0.03 – 0.16 g/L. These data are consistent with formation of nanoaggregates at the previously reported CNAC of approx. 0.10 g/L. Our results provide further evidence that substantial aggregation is taking place in regions of low concentrations ($C \leq 0.03$ g/L) for primary molecular aggregation formations in non-degraded oils and higher concentrations ($C \leq 0.16$ g/L) for biodegraded oil. Asphaltene nanoaggregates of biodegraded oils showed an increase in the CNAC from both sound velocity and attenuation compared to those of the non-degraded oils, indicating that the molecular composition of crude oils may be correlated with the asphaltene aggregation process. This result is consistent with recent studies which indicate that asphaltenes can self-associate in solution to give rise to, more or less, extended aggregates (Andreatta et al., 2005a; Betancourt et al., 2008; Mullins, 2010).

The CNAC derived from the attenuation data yields good agreement with the velocity data, which indicates that the phase-equilibrium theory fits well for both measurements at room temperature. Furthermore, since the interaction of asphaltene particles is sensitive to the effects of concentration, the theory can best be associated with components of a hydrocarbon system. Consequently, attenuation sound data has considerable potential to corroborate previous finds regarding CNAC, it is nevertheless very compelling that very substantial aggregation is taking place in the corresponding concentration range.

Importantly, the statistical uncertainty in the CNAC value measured from both the velocity and attenuation of sound data shows significant difference between asphaltenes of biodegraded to non-biodegraded oils.

Chapter 9 Conclusions and Future Work

9.1 General conclusions

The oils analysed in this study consist of varying levels of biodegradation ranging from 1 to 6 on the Peters and Moldowan (PM) biodegradation scale.

The studied biomarkers suggest that the oils were sourced from facies containing either terrigenous organic matter deposited under oxic-suboxic conditions, marine organic matter deposited under anoxic conditions or a mixed contribution of terrestrial and marine sources. The thermal maturities of the oils were assessed using both the distributions of the saturated and the aromatic biomarkers. There was a wide range of values for the thermal maturity parameters of the oils ranging from immature to highly mature.

The Iatroscan technique tends to measure a consistently higher asphaltene content in most oils as compared to the gravimetric procedure whilst for biodegraded oils the gravimetric procedure quantified a higher value consistently for the asphaltenes as compared to the Iatroscan method. The reasons for this are unknown, but it could be that biodegraded asphaltenes have a different chemical composition to that of undegraded asphaltenes.

The attenuated total reflectance (ATR) FTIR analysis of the asphaltenes revealed that the asphaltenes consist predominantly of aliphatic moieties bound to aromatic structures. Furthermore, minor components of hydroxyl, ether, ester, carboxyl, sulphoxide and ketone groups are also present. However, irrespective of source facies and location, carboxyl groups were detected in asphaltenes from weakly biodegraded oils and absent in all asphaltenes from heavily biodegraded oils.

The biomarkers of the maltenes show different distributions compared to those of the asphaltenes, e.g. the $17\beta(H),21\beta(H)$ hopanes are absent from the maltenes whereas the asphaltene RICO products of hopanoids revealed all three series $17\alpha(H),21\beta(H)$, $17\beta(H),21\beta(H)$ and $17\beta(H),21\alpha(H)$ of hopane skeleton configurations. The maturity parameters of the hopane distributions of the maltenes and oils were observed to show apparent higher levels of thermal maturity compared to those of the respective asphaltenes that show lower levels of thermal maturity. The composition of the steroids in the asphaltenes includes C_{28} - C_{30} regular steranes and C_{29} - C_{31} steranoic acids which

were observed to consist of the $5\alpha(\text{H}),7\alpha(\text{H}),17\alpha(\text{H})$ with 20S and 20R configurations. The maturity parameters of the chemically bound biomarkers are also consistent with apparent lower maturity amongst all oils compared to the corresponding sterane in the maltene hydrocarbon fraction. The most likely explanation is that isomerisation of the bound biomarkers is inhibited due to steric effects afforded by the protective nature of the asphaltene matrix (Jaffe and Gardinali, 1990).

The critical nanoaggregate concentration of asphaltenes (CNAC) in toluene solution was measured using high-precision ultrasound resonance spectroscopy. According to the Mullins model (Mullins, 2010), the CNAC represents the concentration at which the asphaltene changes from being in monomeric form (for concentrations below the CNAC) to a nanoaggregate of approximately 8 asphaltene monomers molecules. Using the mathematical model proposed by Andreatta et al (2005a), the CNAC is identified as the intersection of two straight line when the speed of sound is plotted as a function of asphaltene concentration. The attenuation of sound versus concentration shows a similar behaviour, allowing a second, albeit empirical approach to determine the CNAC. The measured CNAC values, lie between $\sim 0.03 - 0.16 \text{ g/L}$ were comparable with previously measured CNAC values by Andreatta et al. (2005a). Furthermore, the CNAC of non-degraded and biodegraded oils is found to be statistically significantly different. The CNAC of asphaltenes from the non-biodegraded oils starts to associate at $\sim 0.03 - 0.10 \text{ g/L}$ and from a biodegraded oil at $\sim 0.16 \text{ g/L}$. These results indicate that biodegradation influences the aggregation properties of the asphaltenes.

9.2 Future work

The application of organic geochemical techniques and high-precision ultrasound resonance spectroscopy in this study has potential to improve our understanding of both the biomarkers and the aggregation properties of asphaltenes. The mechanisms responsible for aggregation of asphaltenes in whole oils is another long term goal that must be quantified. Recent studies (Mullins *et al.*, 2012a) have shown the concentration of formation and most significantly, the link between laboratory species and those that exist in crude oils, especially in the oil reservoirs. Future studies should consider the feasibility of investigating the following:

- a. Iatroscan and gravimetric studies have highlighted the difficulties in quantifying asphaltene contents in crude oils, it is proposed that it may be feasible to use ATR-FTIR spectroscopy to quantify in-situ asphaltenes in whole oils. The method has been demonstrated to reliably characterize and obtain information at a microscopic level of crude oil asphaltenes without having to precipitate the asphaltenes out of the oil with aliphatic organic solvents (Welte *et al.*, 1982; Gabrienko *et al.*, 2014). The ATR-FTIR spectroscopy can measure the asphaltene content by applying the focal plane array (FPA) detector in the vicinity of the diamond crystal to probe a relatively thin layer of crude oil. Consequently, the detector allows recording of up to several thousand individual infrared spectra simultaneously of the crude oil. Future studies could investigate the possibility that ATR-FTIR spectra could be used to quantify the asphaltene content in an oil.
- b. There are some compounds in acid fractions of the RICO products of oil asphaltenes that have not been identified. There is therefore the need to further investigate these products as these could improve the understanding of the nature of precursor molecules in asphaltenes.
- c. Ultrasonic spectroscopy of asphaltenes from more crude oils (biodegraded and non-biodegraded samples) from various sources should be acquired and analysed from regional locations to identify the significant differences that exist between asphaltenes of the biodegraded and non-degraded oils. This is necessary as the technique used to characterise the asphaltene aggregation in this study did not consider the potential that

various potential sources can provide an improved understanding of asphaltene aggregation state in petroleum.

d. Aggregation can also be further investigated over higher concentrations of up to 10.0 g/L in crude oils to increase the information regarding the balance of association/disassociation of aggregates as a function of concentration. In addition, a log-log scale should be plotted at the lower concentrations to see if asphaltene in crude oil exhibits a power law, which is a function of the continuous phase together with the suspended particles, operating at low concentrations.

e. Ultrasound may be used to determine the size of the scattering particles from the acoustic spectrum including the changing size of asphaltene particles during aggregation. This method uses attenuation as a function of frequency to measure the size distribution of the dispersed phase.

REFERENCES

- Abbas, O., Rebufa, C., Dupuy, N., Permanyer, A. and Kister, J. (2008) 'Assessing petroleum oils biodegradation by chemometric analysis of spectroscopic data', *Talanta*, 75(4), pp. 857-71.
- Abbott, G.D., Bashir, F.Z. and Sugden, M.A. (2001) *Kerogen-bound and free hopanoic acids in the messel oil shale kerogen* (8) (1520-636X).
- Abbott, G.D. and Povey, M.J.W. (2012) 'The acoustic spectroscopy of asphaltene aggregation in petroleum', *IOP Conf. Series: Materials Science and Engineering*, 42.
- Abbott, G.D., Wang, G.Y., Eglinton, T.I., Home, A.K. and Petch, G.S. (1990) 'The kinetics of sterane biological marker release and degradation processes during the hydrous pyrolysis of vitrinite kerogen', *Geochimica et Cosmochimica Acta*, 54(9), pp. 2451-2461.
- Acevedo, S., Escobar, G., Ranaudo, M.A., Piñate, J., Amorín, A., Díaz, M. and Silva, P. (1997) 'Observations about the Structure and Dispersion of Petroleum Asphaltenes Aggregates Obtained from Dialysis Fractionation and Characterization†', *Energy & Fuels*, 11(4), pp. 774-778.
- Acevedo, S., Ranaudo, M.A., Escobar, G., Gutiérrez, L. and Ortega, P. (1995) 'Adsorption of asphaltenes and resins on organic and inorganic substrates and their correlation with precipitation problems in production well tubing', *Fuel*, 74(4), pp. 595-598.
- Alboudwarej, H., Beck, J., Svrcek, W.Y., Yarranton, H.W. and Akbarzadeh, K. (2002) 'Sensitivity of Asphaltene Properties to Separation Techniques', *Energy & Fuels*, 16(2), pp. 462-469.
- Ali Mansoori, G. (1997) 'Modeling of asphaltene and other heavy organic depositions', *Journal of Petroleum Science and Engineering*, 17(1-2), pp. 101-111.
- Andersen, S.I. and Birdi, K.S. (1991) 'Aggregation of asphaltenes as determined by calorimetry', *Journal of Colloid and Interface Science*, 142(2), pp. 497-502.
- Andersen, S.I. and Christensen, S.D. (1999) 'The Critical Micelle Concentration of Asphaltenes As Measured by Calorimetry', *Energy & Fuels*, 14(1), pp. 38-42.
- Andersen, S.I. and Speight, J.G. (2001) 'Petroleum resins: Separation, character, and role in petroleum', *Petroleum Science and Technology*, 19(1-2), pp. 1-34.
- Andreatta, G., Bostrom, N. and Mullins, O.C. (2005a) 'High-Q ultrasonic determination of the critical nanoaggregate concentration of asphaltenes and the critical micelle concentration of standard surfactants', *Langmuir*, 21(7), pp. 2728-2736.

- Andreatta, G., Goncalves, C.C., Buffin, G., Bostrom, N., Quintella, C.M., Arteaga-Larios, F., Pérez, E. and Mullins, O.C. (2005b) 'Nanoaggregates and Structure–Function Relations in Asphaltenes†', *Energy & Fuels*, 19(4), pp. 1282-1289.
- Anlai, M., Shuichang, Z. and Dajiang, Z. (2008) 'Ruthenium-ion-catalyzed oxidation of asphaltenes of heavy oils in Lunan and Tahe oilfields in Tarim basin, NW China', *Organic Geochemistry*, 39, pp. 1502 - 1511.
- Ascanius, B.E., Garcia, D.M. and Andersen, S.I. (2004) 'Analysis of Asphaltenes Subfractionated by N-Methyl-2-pyrrolidone', *Energy & Fuels*, 18(6), pp. 1827-1831.
- Azevedo, D.A., Tamanqueira, J.B., Dias, J.C.M., Carmo, A.P.B., Landau, L. and Gonçalves, F.T.T. (2008) 'Multivariate statistical analysis of diamondoid and biomarker data from Brazilian basin oil samples', *Fuel*, 87(10–11), pp. 2122-2130.
- Bada, G., Horváth, F., Dövényi, P., Szafián, P., Windhoffer, G. and Cloetingh, S. (2007) 'Present-day stress field and tectonic inversion in the Pannonian basin', *Global and Planetary Change*, 58(1–4), pp. 165-180.
- Badre, S., Carla Goncalves, C., Norinaga, K., Gustavson, G. and Mullins, O.C. (2006) 'Molecular size and weight of asphaltene and asphaltene solubility fractions from coals, crude oils and bitumen', *Fuel*, 85(1), pp. 1-11.
- Barakat, A.O., Scholz-Böttcher, B.M. and Rullkötter, J. (2012) 'Ruthenium tetroxide oxidation of immature sulfur-rich kerogens from the Nördlinger Ries (southern Germany)', *Fuel*, 96(0), pp. 176-184.
- Behar, F., Pelet, R. and Roucache, J. (1984) 'Geochemistry of asphaltenes', *Organic Geochemistry*, 6, pp. 587 - 595.
- Behar, F.H. and Albrecht, P. (1984) 'Correlations between carboxylic acids and hydrocarbons in several crude oils. Alteration by biodegradation', *Organic Geochemistry*, 6(0), pp. 597-604.
- Bennett, B. and Abbott, G.D. (1999) 'A natural pyrolysis experiment — hopanes from hopanoic acids?', *Organic Geochemistry*, 30(12), pp. 1509-1516.
- Bennett, B. and Larter, S.R. (2008) 'Biodegradation scales: Applications and limitations', *Organic Geochemistry*, 39(8), pp. 1222-1228.
- Bharati, S., Patience, R., Mills, N. and Hanesand, T. (1997) 'A new North Sea oil-based standard for Iatroscan analysis', *Organic Geochemistry*, 26(1–2), pp. 49-57.
- Bharati, S., Røstum, G.A. and Løberg, R. (1994) 'Calibration and standardization of Iatroscan (TLC-FID) using standards derived from crude oils', *Organic Geochemistry*, 22(3–5), pp. 835-862.
- Bishop, A.N. and Abbott, G.D. (1993) 'The interrelationship of biological marker maturity parameters and molecular yields during contact metamorphism', *Geochimica et Cosmochimica Acta*, 57(15), pp. 3661-3668.

Bissada, K.K., Katz, B.J., Barnicle, S.C. and Schunk, D.J. (1988) *Origin of hydrocarbons in Gulf of Mexico basin: A reappraisal.*

Blanc, P. and Albrecht, P. (1991) 'Parameters of "Macromaturity" (PMM): novel rank and type related indices from chemical degradation of macromolecular network of coals', *Organic Geochemistry*, 17(6), pp. 913-918.

Boduszynski, M.M. (1988) 'Composition of heavy petroleums. 2. Molecular characterization', *Energy & Fuels*, 2(5), pp. 597-613.

Branco, V.A.G., Ali Mansoori, G.A., Xavier, G.C., Parker, S.J. and Manafi, H. (2001) 'Asphaltene flocculation and collapse from petroleum fluids', *Petroleum Science & Engineering*, 32, pp. 217– 230.

Brandt, H.C.A., Hendriks, E.M., Michels, M.A.J. and Visser, F. (1995) 'Thermodynamic Modeling of Asphaltene Stacking', *The Journal of Physical Chemistry*, 99(26), pp. 10430-10432.

Bray, E.E. and Evans, E.D. (1961) 'Distribution of n-paraffins as a clue to recognition of source beds', *Geochimica et Cosmochimica Acta*, 22(1), pp. 2-15.

Buckley, J.S. (1999) 'Predicting the Onset of Asphaltene Precipitation from Refractive Index Measurements', *Energy & Fuels*, 13(2), pp. 328-332.

Buckley, J.S., Hirasaki, G.J., Liu, Y., Von Drasek, S., Wang, J.-X. and Gill, B.S. (1998) 'Asphaltene precipitation and solvent properties of crude oils', *Petroleum Science Technology*, 16, pp. 251 - 285.

Calemma, V., Iwanski, P., Nali, M., Scotti, R. and Montanari, L. (1995) 'Structural Characterization of Asphaltenes of Different Origins', *Energy & Fuels*, 9(2), pp. 225-230.

Calemma, V., Iwanski, P., Nali, M., Scotti, R. and Montanari, L. (1999) 'Structural characterization of asphaltenes of different origins', *Energy & Fuels*, 9, pp. 225 - 230.

Calemma, V., Rausa, R., D'Antona, P. and Montanari, L. (1998) 'Characterization of Asphaltenes Molecular Structure', *Energy & Fuel*, 12, pp. 422 - 428.

Callejas, M.A. and Martínez, M.T. (2000) 'Hydroprocessing of a Maya Residue. 1. Intrinsic Kinetics of Asphaltene Removal Reactions', *Energy & Fuels*, 14(6), pp. 1304-1308.

Carnahan, N.F., Salager, J.-L., Antón, R. and Dávila, A. (1999) 'Properties of Resins Extracted from Boscan Crude Oil and Their Effect on the Stability of Asphaltenes in Boscan and Hamaca Crude Oils', *Energy & Fuels*, 13(2), pp. 309-314.

Cassani, F. and Eglinton, G. (1986) 'Organic geochemistry of Venezuelan extra-heavy oils: 1. Pyrolysis of asphaltenes: A technique for the correlation and maturity evaluation of crude oils', *Chemical Geology*, 56(3-4), pp. 167-183.

Castro, L.V. and Vazquez, F. (2009) 'Fractionation and Characterization of Mexican Crude Oils', *Energy & Fuels*, 23(3), pp. 1603-1609.

Chen, Y., Mastalerz, M. and Schimmelmann, A. (2012) 'Characterization of chemical functional groups in macerals across different coal ranks via micro-FTIR spectroscopy', *International Journal of Coal Geology*, 104(0), pp. 22-33.

Christie, W.W. (1998) 'Gas chromatography-mass spectrometry methods for structural analysis of fatty acids', *Lipids*, 33(4), pp. 343-353.

Coelho, R., Hovell, I., Monte, M., Middea, A. and Souza, A. (2006) 'Characterisation of aliphatic chains in vacuum residues (VRs) of asphaltenes and resins using molecular modelling and FTIR techniques', *Fuel processing technology*, 87(4), pp. 325-333.

Cyr, T.D. and Strausz, O.P. (1984) 'Bound carboxylic acids in the Alberta oil sands', *Organic Geochemistry*, 7(2), pp. 127-140.

Dewey, J.F. and Burke, K. (1974) 'Hot Spots and Continental Break-up: Implications for Collisional Orogeny', *Geology*, 2(2), pp. 57-60.

Didyk, B.M., Simoneit, B.R., Brassell, S.C. and Eglinton, G. (1978) 'Organic geochemical indicators of palaeoenvironmental conditions of sedimentation', *Nature*, 272(5650), pp. 216-222.

Dow, W.G. (1977) 'Kerogen studies and geological interpretations', *Journal of Geochemical Exploration*, 7(0), pp. 79-99.

EIA, U.E.I.A.-. (2012) *Nigeria Energy Report: Downstream*.

Ekweozor, C.M. (1984) 'Tricyclic terpenoid derivatives from chemical degradation reactions of asphaltenes', *Organic Geochemistry*, 6(0), pp. 51-61.

Ekweozor, C.M. and Daukoru, C.M. (1994) 'Northern delta depobelt portion of the Akata-Agbada(!) petroleum system, Niger Delta, Nigeria, in The Petroleum system-from source to trap.', *AAPG Memoir*, 60, pp. 599-613.

Ekweozor, C.M., Okogun, J.I., Ekong, D.E.U. and Maxwell, J.R. (1979) 'Preliminary organic geochemical studies of samples from the Niger delta (Nigeria) I. Analyses of crude oils for triterpanes', *Chemical Geology*, 27(1-2), pp. 11-28.

Ekweozor, C.M. and Strausz, O.P. (1982) '18,19-bisnor-13 β H,14 α H-cheilanthane: A novel degraded tricyclic sesterterpenoid-type hydrocarbon from the Athabasca oil sands', *Tetrahedron Letters*, 23(27), pp. 2711-2714.

Ekweozor, C.M. and Telnaes, N. (1990) 'Oleanane parameter: Verification by quantitative study of the biomarker occurrence in sediments of the Niger delta', *Organic Geochemistry*, 16(1-3), pp. 401-413.

- Ekweozor, C.M. and Udo, O.T. (1988) 'The oleananes: Origin, maturation and limits of occurrence in Southern Nigeria sedimentary basins', *Organic Geochemistry*, 13(1–3), pp. 131-140.
- Fails, T.G. (1990) 'The Northern Gulf Coast Basin: a classic petroleum province', *Geological Society, London, Special Publications*, 50(1), pp. 221-248.
- Fan, T. and Buckley, J.S. (2002) 'Rapid and Accurate SARA Analysis of Medium Gravity Crude Oils', *Energy & Fuels*, 16(6), pp. 1571-1575.
- Gawrys, K.L. and Kilpatrick, P.K. (2005) 'Asphaltenic aggregates are polydisperse oblate cylinders', *Journal of Colloid and Interface Science*, 288(2), pp. 325-334.
- Gray, M.R., Tykwinski, R.R., Stryker, J.M. and Tan, X. (2011) 'Supramolecular Assembly Model for Aggregation of Petroleum Asphaltenes', *Energy & Fuels*, 25(7), pp. 3125-3134.
- Groenzin, H. and Mullins, O.C. (1999) 'Asphaltene Molecular Size and Structure', *The Journal of Physical Chemistry A*, 103(50), pp. 11237-11245.
- Groenzin, H. and Mullins, O.C. (2000) 'Molecular size and structure of asphaltenes from various sources', *Energy & Fuels*, 14 pp. 677 – 684.
- Gürgey, K. (2003) 'Correlation, alteration, and origin of hydrocarbons in the GCA, Bahar, and Gum Adasi fields, western South Caspian Basin: geochemical and multivariate statistical assessments', *Marine and Petroleum Geology*, 20(10), pp. 1119-1139.
- Hakimi, M.H., Abdullah, W.H. and Shalaby, M.R. (2011) 'Organic geochemical characteristics of crude oils from the Masila Basin, eastern Yemen', *Organic Geochemistry*, 42(5), pp. 465-476.
- Hammami, A. and Ratulowski, J. (2007) *Precipitation and deposition of asphaltenes in production systems: A flow assurance overview*. Springer.
- Hayward, R.D., Martin, C.A.L., Harrison, D., Van Dort, G., Guthrie, S. and Padgett, N. (2003) 'The Flora Field, Blocks 31/26a, 31/26c, UK North Sea', *Geological Society, London, Memoirs*, 20(1), pp. 549-555.
- Head, I.M., Jones, D.M. and Larter, S.R. (2003) 'Biological activity in the deep subsurface and the origin of heavy oil', *Nature*, 426(6964), pp. 344-352.
- Herod, A.A. (2010) 'Limitations of mass spectrometric methods for the characterization of polydisperse materials', *Rapid Communications in Mass Spectrometry*, 24(17), pp. 2507-2519.
- Holmes, M.J., Parker, N.G. and Povey, M.J.W. (2011) 'Temperature dependence of bulk viscosity in water using acoustic spectroscopy', *Journal of Physics: Conference Series*, 269(1), p. 012011.

Hortal, A.R., Hurtado, P., Martínez-Haya, B. and Mullins, O.C. (2007) 'Molecular-Weight Distributions of Coal and Petroleum Asphaltenes from Laser Desorption/Ionization Experiments', *Energy & Fuels*, 21(5), pp. 2863-2868.

Hu, G. (1991) 'Geochemical characterization of steranes and terpanes in certain oils from terrestrial facies within the South China Sea', *Journal of Southeast Asian Earth Sciences*, 5(1–4), pp. 241-247.

Huang, W.-Y. and Meinschein, W.G. (1979) 'Sterols as ecological indicators', *Geochimica et Cosmochimica Acta*, 43(5), pp. 739-745.

Hughes, W.B., Holba, A.G. and Dzou, L.I.P. (1995) 'The ratios of dibenzothiophene to phenanthrene and pristane to phytane as indicators of depositional environment and lithology of petroleum source rocks', *Geochimica et Cosmochimica Acta*, 59(17), pp. 3581-3598.

Hunt, J.M. (1996) *Petroleum Geochemistry and Geology*. Second edn. New York: W. H. Freeman and Company.

Ibarra, J., Muñoz, E. and Moliner, R. (1996) 'FTIR study of the evolution of coal structure during the coalification process', *Organic Geochemistry*, 24(6–7), pp. 725-735.

IGI (2004) *The program for integrated geochemical interpretation, p:IGI -The P:IGI geochemical Manual*. United Kingdom: IGI Ltd.

Iglesias, M.J., Jimenez, A., Laggoun-Defarge, F. and Suarez-Ruiz, I. (1995) 'FTIR Study of Pure Vitrains and Associated Coals', *Energy & Fuels*, 9(3), pp. 458-466.

Indo, K., Ratulowski, J., Dindoruk, B., Gao, J., Zuo, J. and Mullins, O.C. (2009) 'Asphaltene Nanoaggregates Measured in a Live Crude Oil by Centrifugation', *Energy & Fuels*, 23(9), pp. 4460-4469.

Jaffé, R., Albrecht, P. and Oudin, J.L. (1988) 'Carboxylic acids as indicators of oil migration: II. Case of the Mahakam Delta, Indonesia', *Geochimica et Cosmochimica Acta*, 52(11), pp. 2599-2607.

Jaffé, R. and Gallardo, M.T. (1993) 'Application of carboxylic acid biomarkers as indicators of biodegradation and migration of crude oils from the Maracaibo Basin, Western Venezuela', *Organic Geochemistry*, 20(7), pp. 973-984.

Jaffe, R. and Gardinali, P.R. (1990) 'Generation and maturation of carboxylic acids in ancient sediments from the Maracaibo Basin, Venezuela', *Organic Geochemistry*, 16(1–3), pp. 211-218.

Jiang, C., Larter, S.R., Noke, K.J. and Snowdon, L.R. (2008) 'TLC–FID (Iatroscan) analysis of heavy oil and tar sand samples', *Organic Geochemistry*, 39(8), pp. 1210-1214.

Kanaly, R.A. and Harayama, S. (2000) 'Biodegradation of High-Molecular-Weight Polycyclic Aromatic Hydrocarbons by Bacteria', *Journal of Bacteriology*, 182(8), pp. 2059-2067.

Karlsen, D.A. and Larter, S.R. (1991) 'Analysis of petroleum fractions by TLC-FID: applications to petroleum reservoir description', *Organic Geochemistry*, 17(5), pp. 603-617.

Kennicutt II, M.C., McDonald, T.J., Comet, P.A., Denoux, G.J. and Brooks, J.M. (1992) 'The origins of petroleum in the northern Gulf of Mexico', *Geochimica et Cosmochimica Acta*, 56(3), pp. 1259-1280.

Kidena, K., Murata, S. and Nomura, M. (2008) 'A newly proposed view on coal molecular structure integrating two concepts: Two phase and uniphase models', *Fuel Processing Technology*, 89(4), pp. 424-433.

Killops, S. and Killops, V. (2005) *Introduction to organic geochemistry*. 2nd edn. UK: Blackwell Publishing company.

Killops, S.D., Funnell, R.H., Suggate, R.P., Sykes, R., Peters, K.E., Walters, C., Woolhouse, A.D., Weston, R.J. and Boudou, J.P. (1998) 'Predicting generation and expulsion of paraffinic oil from vitrinite-rich coals', *Organic Geochemistry*, 29(1-3), pp. 1-21.

Killops, S.D. and Killops, V.J. (1994) *An introduction to organic geochemistry*. England: Longman Scientific & Technical.

Kunka, J.M., Williams, G., Cullen, B., Boyd-Gorst, J., Dyer, G.R., Garnham, J.A., Warnock, A., Wardell, J., Davis, A. and Lynes, P. (2003) 'The Nelson Field, Blocks 22/11, 22/61, 22/7, 22/12a, UK North Sea', *Geological Society, London, Memoirs*, 20(1), pp. 617-646.

Larter, S., Huang, H., Adams, J., Bennett, B. and Snowdon, L.R. (2012) 'A practical biodegradation scale for use in reservoir geochemical studies of biodegraded oils', *Organic Geochemistry*, 45(0), pp. 66-76.

Lehne, E. and Dieckmann, V. (2010) 'Improved understanding of mixed oil in Nigeria based on pyrolysis of asphaltenes.', *Organic Geochemistry* 41, pp. 661 - 674.

León, O., Rogel, E., Espidel, J. and Torres, G. (1999) 'Asphaltenes: Structural Characterization, Self-Association, and Stability Behavior', *Energy & Fuels*, 14(1), pp. 6-10.

Leontaritis, K.J. and Ali Mansoori, G. (1988) 'Asphaltene deposition: a survey of field experiences and research approaches', *Journal of Petroleum Science and Engineering*, 1(3), pp. 229-239.

Li, Z., Fredericks, P.M., Rintoul, L. and Ward, C.R. (2007) 'Application of attenuated total reflectance micro-Fourier transform infrared (ATR-FTIR) spectroscopy to the

study of coal macerals: Examples from the Bowen Basin, Australia', *International Journal of Coal Geology*, 70(1–3), pp. 87-94.

Liao, Z. and Geng, A. (2002) 'Characterization of nC₇-soluble fractions of the products from mild oxidation of asphaltenes', *Organic Geochemistry*, 33(12), pp. 1477-1486.

Liao, Z., Geng, A., Graciaa, A., Creux, P., Chrostowska, A. and Zhang, Y. (2006) 'Saturated hydrocarbons occluded inside asphaltene structures and their geochemical significance, as exemplified by two Venezuelan oils', *Organic Geochemistry*, 37(3), pp. 291-303.

Lin, R. and Patrick Ritz, G. (1993) 'Studying individual macerals using i.r. microspectrometry, and implications on oil versus gas/condensate proneness and "low-rank" generation', *Organic Geochemistry*, 20(6), pp. 695-706.

Love, G.D., Snape, C.E., Carr, A.D. and Houghton, R.C. (1995) 'Release of covalently-bound alkane biomarkers in high yields from kerogen via catalytic hydrolysis', *Organic Geochemistry*, 23(10), pp. 981-986.

Lu, X., Kalman, B. and Redelius, P. (2008) 'A new test method for determination of wax content in crude oils, residues and bitumens', *Fuel*, 87(8–9), pp. 1543-1551.

Ma, A., Zhang, S. and Zhang, D. (2008) 'Ruthenium-ion-catalyzed oxidation of asphaltenes of heavy oils in Lunnan and Tahe oilfields in Tarim Basin, NW China', *Organic Geochemistry*, 39(11), pp. 1502-1511.

Mackenzie, A.S. (1984) *Advances in Petroleum Geochemistry*. London: Academic Press.

Mackenzie, A.S., Hoffmann, C.F. and Maxwell, J.R. (1981) 'Molecular parameters of maturation in the Toarcian shales, Paris Basin, France—III. Changes in aromatic steroid hydrocarbons', *Geochimica et Cosmochimica Acta*, 45(8), pp. 1345-1355.

Mackenzie, A.S., Patience, R.L., Maxwell, J.R., Vandenbroucke, M. and Durand, B. (1980) 'Molecular parameters of maturation in the Toarcian shales, Paris Basin, France—I. Changes in the configurations of acyclic isoprenoid alkanes, steranes and triterpanes', *Geochimica et Cosmochimica Acta*, 44(11), pp. 1709-1721.

Mansoori, G.A., Vazquez, D. and Shariaty-Niassar, M. (2007) 'Polydispersity of heavy organics in crude oils and their role in oil well fouling', *Journal of Petroleum Science and Engineering*, 58(3–4), pp. 375-390.

McClements, D.J. (1991) 'Ultrasonic characterisation of emulsions and suspensions', *Advances in Colloid and Interface Science*, 37(1–2), pp. 33-72.

McClements, D.J. and Povey, M.J.W. (1992) 'Ultrasonic analysis of edible fats and oils', *Ultrasonics*, 30(6), pp. 383-388.

McKay, J.F., Weber, J.H. and Latham, D.R. (1976) 'Characterization of nitrogen bases in high-boiling petroleum distillates', *Analytical Chemistry*, 48(6), pp. 891-898.

McLean, J.D. and Kilpatrick, P.K. (1997a) 'Comparison of Precipitation and Extrography in the Fractionation of Crude Oil Residua', *Energy & Fuels*, 11(3), pp. 570-585.

McLean, J.D. and Kilpatrick, P.K. (1997b) 'Effects of Asphaltene Solvency on Stability of Water-in-Crude-Oil Emulsions', *Journal of Colloid and Interface Science*, 189(2), pp. 242-253.

Meredith, W., Kelland, S.J. and Jones, D.M. (2000) 'Influence of biodegradation on crude oil acidity and carboxylic acid composition', *Organic Geochemistry*, 31(11), pp. 1059-1073.

Mojelsky, T.W., Ignasiak, T.M., Frakman, Z., McIntyre, D.D., Lown, E.M., Montgomery, D.S. and Strausz, O.P. (1992) 'Structural features of Alberta oil sand bitumen and heavy oil asphaltenes', *Energy & Fuels*, 6(1), pp. 83-96.

Moldowan, J.M., Lee, C.Y., Watt, D.S., Jegannathan, A., Slougui, N.-E. and Gallegos, E.J. (1991) 'Analysis and occurrence of C₂₆-steranes in petroleum and source rocks', *Geochimica et Cosmochimica Acta*, 55(4), pp. 1065-1081.

Moldowan, J.M., Sundararaman, P. and Schoell, M. (1986) 'Sensitivity of biomarker properties to depositional environment and/or source input in the Lower Toarcian of SW-Germany', *Organic Geochemistry*, 10(4-6), pp. 915-926.

Mostowfi, F., Indo, K., Mullins, O.C. and McFarlane, R. (2008) 'Asphaltene Nanoaggregates Studied by Centrifugation†', *Energy & Fuels*, 23(3), pp. 1194-1200.

Mrkić, S., Stojanović, K., Kostić, A., Nytoft, H.P. and Šajnović, A. (2011) 'Organic geochemistry of Miocene source rocks from the Banat Depression (SE Pannonian Basin, Serbia)', *Organic Geochemistry*, 42(6), pp. 655-677.

Muhammad, A.B. and Abbott, G.D. (2012) 'The thermal evolution of asphaltene-bound biomarkers from coals of different rank: A potential information resource during coal biodegradation', *International Journal of Coal Geology*, (0).

Mullins, O.C. (2010) 'The Modified Yen Model', *Energy & Fuels*, 24, pp. 2179-2207.

Mullins, O.C. (2011) 'The Asphaltenes', *Annual Review of Analytical Chemistry*, 4(1), pp. 393-418.

Mullins, O.C., Betancourt, S.S., Cribbs, M.E., Dubost, F.X., Creek, J.L., Andrews, A.B. and Venkataraman, L. (2007) 'The Colloidal Structure of Crude Oil and the Structure of Oil Reservoirs', *Energy & Fuels*, 21(5), pp. 2785-2794.

Mullins, O.C., Sabbah, H., Eyssautier, J., Pomerantz, A.E., Barré, L., Andrews, A.B., Ruiz-Morales, Y., Mostowfi, F., McFarlane, R., Goual, L., Lepkowicz, R., Cooper, T., Orbulescu, J., Leblanc, R.M., Edwards, J. and Zare, R.N. (2012a) 'Advances in Asphaltene Science and the Yen–Mullins Model', *Energy & Fuels*, 26(7), pp. 3986-4003.

Mullins, O.C., Seifert, D.J., Zuo, J.Y. and Zeybek, M. (2012b) 'Clusters of Asphaltene Nanoaggregates Observed in Oilfield Reservoirs', *Energy & Fuels*, 27(4), pp. 1752-1761.

Mullins, O.C. and Sheu, E. (1998) *Structures and Dynamics of Asphaltenes*. New York: Plenum Press.

Murgich, J., Abanero, J.A. and Strausz, O.P. (1999) 'Molecular Recognition in Aggregates Formed by Asphaltene and Resin Molecules from the Athabasca Oil Sand', *Energy & Fuels*, 13(2), pp. 278-286.

Murgich, J., Rodríguez, J.M. and Aray, Y. (2006) 'Molecular recognition and molecular mechanics of micelles of some model asphaltenes and resins', *Energy & Fuel*, 10, pp. 68 - 76.

Neto, F.R.A., Restle, A., Connan, J., Albrecht, P. and Ourisson, G. (1982) 'Novel tricyclic terpanes (C19, C20) in sediments and petroleums', *Tetrahedron Letters*, 23(19), pp. 2027-2030.

Orrego-Ruiz, J.A., Guzmán, A., Molina, D. and Mejía-Ospino, E. (2011) 'Mid-infrared Attenuated Total Reflectance (MIR-ATR) Predictive Models for Asphaltene Contents in Vacuum Residua: Asphaltene Structure–Functionality Correlations Based on Partial Least-Squares Regression (PLS-R)', *Energy & Fuels*, 25(8), pp. 3678-3686.

Parker, N.G. and Povey, M.J.W. (2012) 'Ultrasonic study of the gelation of gelatin: Phase diagram, hysteresis and kinetics', *Food Hydrocolloids*, 26(1), pp. 99-107.

Peakman, T.M., Haven, H.L.T., Rechka, J.R., De Leeuw, J.W. and Maxwell, J.R. (1989) 'Occurrence of (20R)- and (20S)- $\Delta 8(14)$ and $\Delta 14$ 5 α (H)-sterenes and the origin of 5 α (H),14 β (H),17 β (H)-steranes in an immature sediment', *Geochimica et Cosmochimica Acta*, 53(8), pp. 2001-2009.

Pelet, R., Behar, F. and Monin, J.C. (1986) 'Resins and asphaltenes in the generation and migration of petroleum', *Organic Geochemistry*, 10(1–3), pp. 481-498.

Peng, P., Fu, J., Sheng, G., Morales-Izquierdo, A., Lown, E.M. and Strausz, O.P. (1999a) 'Ruthenium-ions-catalyzed oxidation of an immature asphaltene: Structural features and biomarker distribution', *Energy and Fuels*, 13(2), pp. 266-277.

Peng, P., Morales-Izquierdo, A., Lown, E.M. and Strausz, O.P. (1999b) 'Chemical structure and biomarker content of Jinghan asphaltenes and kerogens', *Energy & Fuels*, 13(2), pp. 248-265.

Peng, P.a., Fu, J., Sheng, G., Morales-Izquierdo, A., Lown, E.M. and Strausz, O.P. (1999c) 'Ruthenium-Ions-Catalyzed Oxidation of an Immature Asphaltene: Structural Features and Biomarker Distribution', *Energy & Fuels*, 13(2), pp. 266-277.

Peng, P.a., Morales-Izquierdo, A., Hogg, A. and Strausz, O.P. (1997) 'Molecular Structure of Athabasca Asphaltene: Sulfide, Ether, and Ester Linkages', *Energy & Fuels*, 11(6), pp. 1171-1187.

Peng, P.a., Sheng, G., Fu, J. and Yan, Y. (1998) 'Biological markers in 1.7 billion year old rock from the Tuanshanzi Formation, Jixian strata section, North China', *Organic Geochemistry*, 29(5–7), pp. 1321-1329.

Peters, K.E. and Fowler, M.G. (2002) 'Applications of petroleum geochemistry to exploration and reservoir management', *Organic Geochemistry*, 33(1), pp. 5-36.

Peters, K.E. and Moldowan, J.M. (1991) 'Effects of source, thermal maturity, and biodegradation on the distribution and isomerization of homohopanes in petroleum', *Organic Geochemistry*, 17(1), pp. 47-61.

Peters, K.E., Moldowan, J.M., McCaffrey, M.A. and Fago, F.J. (1996) 'Selective biodegradation of extended hopanes to 25-norhopanes in petroleum reservoirs. Insights from molecular mechanics', *Organic Geochemistry*, 24(8–9), pp. 765-783.

Peters, K.E., Moldowan, J.M. and Sundararaman, P. (1990) 'Effects of hydrous pyrolysis on biomarker thermal maturity parameters: Monterey Phosphatic and Siliceous members', *Organic Geochemistry*, 15(3), pp. 249-265.

Peters, K.E., Scheuerman, G.L., Lee, C.Y., Moldowan, J.M., Reynolds, R.N. and Pena, M.M. (1992) 'Effects of refinery processes on biological markers', *Energy & Fuels*, 6(5), pp. 560-577.

Peters, K.E., Walters, C. and Moldowan, J.M. (2005a) *The biomarker guide: Biomarkers and isotope in the environment and human history*. 2nd edn. Cambridge, UK: Cambridge University Press.

Peters, K.E., Walters, C.C. and Moldowan, J.M. (2005b) 'The Biomarker guide: Biomarkers and isotopes in the environment and human history', in 2 edn. New York: Cambridge university press.

Petrov, A.A. (1984) *Petroleum hydrocarbons*. Berlin: Springer-Verlag.

Philp, R.P. and Gilbert, T.D. (1986) 'Biomarker distributions in Australian oils predominantly derived from terrigenous source material', *Organic Geochemistry*, 10(1–3), pp. 73-84.

Pinnock, S.J. and Clitheroe, A.R.J. (1997) 'The Captain Field, UK North Sea; appraisal and development of a viscous oil accumulation', *Petroleum Geoscience*, 3(4), pp. 305-312.

Pinnock, S.J., Clitheroe, A.R.J. and Rose, P.T.S. (2003) 'The Captain Field, Block 13/22a, UK North Sea', *Geological Society, London, Memoirs*, 20(1), pp. 431-441.

Pollard, S.J., Hrudey, S.E., Fuhr, B.J., Alex, R.F., Holloway, L.R. and Tosto, F. (1992) 'Hydrocarbon wastes at petroleum- and creosote-contaminated sites: rapid characterization of component classes by thin-layer chromatography with flame ionization detection', *Environmental Science & Technology*, 26(12), pp. 2528-2534.

Povey, M.J. (1997) *Ultrasonic techniques for fluids characterisation*. San Diego: Academic Press.

Priyanto, S., Mansoori, G.A. and Suwono, A. (2001) 'Measurement of property relationships of nano-structure micelles and coacervates of asphaltene in a pure solvent', *Chemical Engineering Science*, 56(24), pp. 6933-6939.

Radke, M. (1988) 'Application of aromatic compounds as maturity indicators in source rocks and crude oils', *Marine and Petroleum Geology*, 5(3), pp. 224-236.

Radke, M., Leythaeuser, D. and Teichmüller, M. (1984) 'Relationship between rank and composition of aromatic hydrocarbons for coals of different origins', *Organic Geochemistry*, 6(0), pp. 423-430.

Radke, M., Welte, D.H. and Willsch, H. (1982a) 'Geochemical study on a well in the Western Canada Basin: relation of the aromatic distribution pattern to maturity of organic matter', *Geochimica et Cosmochimica Acta*, 46(1), pp. 1-10.

Radke, M., Welte, D.H. and Willsch, H. (1986) 'Maturity parameters based on aromatic hydrocarbons: Influence of the organic matter type', *Organic Geochemistry*, 10(1-3), pp. 51-63.

Radke, M., Willsch, H., Leythaeuser, D. and Teichmüller, M. (1982b) 'Aromatic components of coal: relation of distribution pattern to rank', *Geochimica et Cosmochimica Acta*, 46(10), pp. 1831-1848.

Reijers, T. (2011) 'Stratigraphy and sedimentology of the Niger Delta', *Geologos*, 17(3), pp. 133-162.

Requejo, A.G. (1994) 'Maturation of petroleum source rocks—II. Quantitative changes in extractable hydrocarbon content and composition associated with hydrocarbon generation', *Organic Geochemistry*, 21(1), pp. 91-105.

ResoScanTM (2007) *ResoScanTM -System Operations Manual*. Germany TF Instruments GmbH.

Rodrigues, D.C., Koike, L., Reis, F.d.A.M., Alves, H.P., Chang, H.K., Trindade, L.A. and Marsaioli, A.J. (2000) 'Carboxylic acids of marine evaporitic oils from Sergipe-Alagoas Basin, Brazil', *Organic Geochemistry*, 31(11), pp. 1209-1222.

Rohmer, M., Bisseret, P. and Neunlist, S. (1992) 'The hopanoids, prokaryotic triterpenoids and precursors of ubiquitous molecular fossils', in Moldowan, J.M., Albrecht, P., Philp, R. P (ed.) *Biological Markers in Sediments and Petroleum*. Englewood Cliffs, New Jersey: Prentice Hall, pp. 1-17.

Ross, A.S., Farrimond, P., Eedmann, M. and Larter S. R. (2010) 'Geochemical compositional gradients in a mixed oil reservoir indicative of ongoing biodegradation', *Organic Chemistry*, 41, pp. 307 - 320.

Rubinstein, I., Spyckerelle, C. and Strausz, O.P. (1979) 'Pyrolysis of asphaltenes: a source of geochemical information', *Geochimica et Cosmochimica Acta*, 43(1), pp. 1-6.

Samuel, O.J., Cornford, C., Jones, M., Adekeye, O.A. and Akande, S.O. (2009) 'Improved understanding of the petroleum systems of the Niger Delta Basin, Nigeria', *Organic Geochemistry*, 40(4), pp. 461-483.

Sarmah, M.K., Borthakur, A. and Dutta, A. (2010) 'Pyrolysis of petroleum asphaltenes from different geological origins and use of methylnaphthalenes and methylphenanthrenes as maturity indicators for asphaltenes', *Materials Science*, 33, pp. 509 - 515.

Scotti, R. and Montanari, L. (1998) 'Molecular structure and intermolecular interaction of asphaltenes by FT-IR, NMR, EPR', in Mullins, O.C. and Sheu, E.Y. (eds.) *Structures and dynamics of asphaltenes*. New York: Plenum, p. pp. 438.

Seifert, W. and Moldowan, J. (1978) 'Applications of steranes, terpanes and monoaromatics to the maturation, migration and source of crude oils', *Geochimica et Cosmochimica Acta*, 42(1), pp. 77-95.

Seifert, W.K. and Michael Moldowan, J. (1979) 'The effect of biodegradation on steranes and terpanes in crude oils', *Geochimica et Cosmochimica Acta*, 43(1), pp. 111-126.

Seifert, W.K. and Moldowan, J.M. (1979) 'Effect of biodegradation on steranes and terpanes in crude oils', *Geochimica Et Cosmochimica Acta*, 43(1), pp. 111-126.

Selley, R.C. (1985) *Elements of petroleum geology*. Second edn. New York: W. H. Freeman and Company.

Sheu, E.Y. (1998) 'Structures and Dynamics of Asphaltenes', in Mullins and O. C., S. (eds.) *Structures and Dynamics of Asphaltenes*. New York: Plenum Press, p. pp. 115-144.

Sheu, E.Y. (2002) 'Petroleum asphaltenes properties, characterization and Issues', *Energy & Fuels*, 16, pp. 74 - 82.

Silva, T.F., Azevedo, D.A., Rangel, M.D., Fontes, R.A. and Neto, F.R.A. (2008) 'Effect of biodegradation on biomarkers released from asphaltenes', *Organic Geochemistry*, 39(8), pp. 1249-1257.

Sinninghe Damsté, J.S., Kenig, F., Koopmans, M.P., Köster, J., Schouten, S., Hayes, J.M. and de Leeuw, J.W. (1995) 'Evidence for gammacerane as an indicator of water column stratification', *Geochimica et Cosmochimica Acta*, 59(9), pp. 1895-1900.

Šolević, T., Stojanović, K., Bojesen-Koefoed, J., Nytoft, H.P., Jovančićević, B. and Vitorović, D. (2008) 'Origin of oils in the Velebit oil-gas field, SE Pannonian Basin, Serbia – Source rocks characterization based on biological marker distributions', *Organic Geochemistry*, 39(1), pp. 118-134.

- Sonibare, O., Alimi, H., Jarvie, D. and Ehinola, O.A. (2008) 'Origin and occurrence of crude oil in the Niger delta, Nigeria', *Journal of Petroleum Science and Engineering*, 61(2–4), pp. 99-107.
- Sonibare, O.O., Snape, C.E., Meredith, W., Uguna, C.N. and Love, G.D. (2009) 'Geochemical characterisation of heavily biodegraded tar sand bitumens by catalytic hydropyrolysis', *Journal of Analytical and Applied Pyrolysis*, 86(1), pp. 135-140.
- Speight, J.G. (ed.) (1984) *The chemical nature of petroleum of asphaltenes. In characterization of heavy crude oils and petroleum residues*. Paris: Edition Technip
- Speight, J.G. (1991) *The chemistry and technology of petroleum*. Second edn. New York: Marcel Dekker.
- Speight, J.G. (1999) 'The chemical and physical structure of petroleum: effects on recovery operations', *Journal of Petroleum Science and Engineering*, 22(1–3), pp. 3-15.
- Speight, J.G. (2004) 'Petroleum asphaltenes, Part 1. Asphaltenes, resins and the structure of petroleum', *Oil & Gas Science and Technology - IFP*, 59, pp. 467 - 477.
- Speight, J.G. and Moschopedis, S.E. (1981) 'On the molecular nature of petroleum asphaltenes', in Bunger, J. W. and Li, N. C (eds) *Chemistry of Asphaltenes*. Washington D. C', *American Chemical society*, pp. 1 - 15.
- Stock, L.M. and Tse, K.T. (1983) 'Ruthenium tetroxide catalysed oxidation of illinois no.6 coal and some representative hydrocarbons', *Fuel*, 62(8), pp. 974-976.
- Stojanović, K., Jovančićević, B., Šajnović, A., Sabo, T.J., Vitorović, D., Schwarzbauer, J. and Golovko, A. (2009) 'Pyrolysis and Pt(IV)- and Ru(III)-ion catalyzed pyrolysis of asphaltenes in organic geochemical investigation of a biodegraded crude oil (Gaj, Serbia)', *Fuel*, 88(2), pp. 287-296.
- Stout, S.A., Liu, B., Millner, G.C., Hamlin, D. and Healey, E. (2007) 'Use of Chemical Fingerprinting to Establish the Presence of Spilled Crude Oil in a Residential Area Following Hurricane Katrina, St. Bernard Parish, Louisiana', *Environmental Science & Technology*, 41(21), pp. 7242-7251.
- Strausz, O.P., Mojelsky, T.W., Faraji, F., Lown, E.M. and Peng, P.a. (1999a) 'Additional Structural Details on Athabasca Asphaltene and Their Ramifications', *Energy & Fuels*, 13(2), pp. 207-227.
- Strausz, O.P., Mojelsky, T.W. and Lown, E.M. (1992a) 'The molecular structure of asphaltene: an unfolding story', *Fuel*, 71(12), pp. 1355-1363.
- Strausz, O.P., Mojelsky, T.W. and Lown, E.M. (1992b) 'The molecular structure of asphaltene: an unfolding story', *Fuel*, 71, pp. 1355 - 1363.
- Strausz, O.P., Mojelsky, T.W. and Lown, E.M. (1999b) 'Structural features of Boscan and Duri asphaltenes', *Energy & Fuels*, 13, pp. 228 - 247.

Sugden, M.A. and Abbott, G.D. (2002) 'The stereochemistry of bound and extractable pentacyclic triterpenoids during closed system pyrolysis', *Organic Geochemistry*, 33(12), pp. 1515-1521.

Sumitomo Corporation (2009) *Share sale of Petro Summit Investment UK Ltd* (Accessed: 29 Jul).

Tay, H., F. and Kazarian, G., S. (2009) 'Study of Petroleum Heat-exchanger Deposits with ATR-FTIR Spectroscopic Imaging', *Energy & Fuels*, 23, pp. 4059–4067.

ten Haven, H.L., de Leeuw, J.W., Rullkötter, J. and Damste, J.S.S. (1987) 'Restricted utility of the pristane/phytane ratio as a palaeoenvironmental indicator', *Nature*, 330(6149), pp. 641-643.

The Scottish Government (2009) *Opportunities for CO₂ Storage around Scotland - an integrated strategic research study*. Available at: <http://www.scotland.gov.uk/Publications/2009/04/28114540/6> (Accessed: 29 Jul).

Thomasson, J., Coin, C., Kahraman, H. and Fredericks, P.M. (2000) 'Attenuated total reflectance infrared microspectroscopy of coal', *Fuel*, 79(6), pp. 685-691.

Tissot, B.P. and Welte, D.H. (1984) *Petroleum formation and occurrence*. Berlin: Springer-Verlag.

TOTAL (2006) *Deep Water Development: The ultimate frontier*.

Trifilieff, S., Sieskind, O. and Albrecht, P. (1992) 'Biological markers in petroleum asphaltenes: possible mode of incorporation', in Moldowan, J.M., Albrecht, P. and Philp, R.P. (eds.) *Biological markers in sediments and petroleum*. New Jersey: Prentice Hall, pp. 350 - 369.

Vazquez, D. and Mansoori, G.A. (2000) 'Identification and measurement of petroleum precipitates', *Journal of Petroleum Science and Engineering*, 26(1–4), pp. 49-55.

Volkman, J.K., Alexander, R., Kagi, R.I., Rowland, S.J. and Sheppard, P.N. (1984) 'Biodegradation of aromatic hydrocarbons in crude oils from the Barrow Sub-basin of Western Australia', *Organic Geochemistry*, 6(0), pp. 619-632.

Walker, R. and Mastalerz, M. (2004) 'Functional group and individual maceral chemistry of high volatile bituminous coals from southern Indiana: controls on coking', *International Journal of Coal Geology*, 58(3), pp. 181-191.

Wang, J.X. and Buckley, J.S. (2001) 'A Two-Component Solubility Model of the Onset of Asphaltene Flocculation in Crude Oils', *Energy & Fuels*, 15(5), pp. 1004-1012.

Welte, D.H. (1972) 'Petroleum exploration and organic geochemistry', *Journal of Geochemical Exploration*, 1(1), pp. 117-136.

- Welte, D.H., Kratochvil, H., Rullkötter, J., Ladwein, H. and Schaefer, R.G. (1982) 'Organic geochemistry of crude oils from the Vienna Basin and an assessment of their origin', *Chemical Geology*, 35(1–2), pp. 33-68.
- Whelan, J.K., Kennicutt II, M.C., Brooks, J.M., Schumacher, D. and Eglington, L.B. (1994) 'Organic geochemical indicators of dynamic fluid flow processes in petroleum basins', *Organic Geochemistry*, 22(3–5), pp. 587-615.
- White, N., Thompson, M. and Barwise, T. (2003) 'Understanding the thermal evolution of deep-water continental margins', *Nature*, 426(6964), pp. 334-343.
- Whyatt, M., Bowen, J.M. and Rhodes, D.N. (1992) 'The Nelson Field: a successful application of a development geoseismic model in North Sea exploration', *Geological Society, London, Special Publications*, 67(1), pp. 283-305.
- Wilhelms, A. and Larter, S.R. (1984) 'Origin of tar mats in petroleum reservoirs. Part I: introduction and case studies', *Marine & Petroleum Geology*, 11, pp. 418 - 441.
- Wilhelms, A. and Larter, S.R. (1994) 'Origin of tar mats in petroleum reservoirs. Part II: formation mechanisms for tar mats', *Marine and Petroleum Geology*, 11(4), pp. 442-456.
- Wilt, B.K., Welch, W.T. and Rankin, J.G. (1998) 'Determination of Asphaltenes in Petroleum Crude Oils by Fourier Transform Infrared Spectroscopy', *Energy & Fuels*, 12(5), pp. 1008-1012.
- Xiong, Y. and Geng, A. (2000) 'Carbon isotope composition of individual n-alkane in asphaltenen pyrolysates of biodegraded crude oils from the Liaohe Basin, China', *Organic Chemistry*, 31, pp. 1441 - 1449.
- Xu, G., Zhang, D. and Wang, P. (2003) 'Using biomarker bonded on the asphaltenes for biodegrade oil-source correlation', *Chinese Science Bulletin*, 48, pp. 300 - 304.
- Yen, T.F., Erdman, J.G. and Pollack, S.S. (1961) 'Investigation of the Structure of Petroleum Asphaltenes by X-Ray Diffraction', *Analytical Chemistry*, 33(11), pp. 1587-1594.
- Yen, T.F., Wu, W.H. and Chilingar, G.V. (1984) 'A study of the structure of petroleum asphaltenes and related substances by infrared spectroscopy', *Energy Sources, Part A: Recovery, Utilization, and Environmental Effects*, 7, pp. 203 – 235.

APPENDIX

Appendix 1.0: Study samples and locations

No	Sample name	Sample type	Location
1	NA1	Oil	Nigeria
2	NB2	Oil	Nigeria
3	NC3	Oil	Nigeria
4	NA	Oil	Nigeria
5	NB	Oil	Nigeria
6	NC	Oil	Nigeria
7	ND	Oil	Nigeria
8	NE	Oil	Nigeria
9	NF	Oil	Nigeria
10	NO	Oil	Nigeria
11	NN	Oil	Nigeria
12	N25	Oil	Nigeria
13	N18	Oil	Nigeria
14	NNI	Oil	Nigeria
15	NA41	Oil	Nigeria
16	UKB	Oil	United Kingdom
18	UK88	Oil	United Kingdom
19	UK85	Oil	United Kingdom
20	UK66	Oil	United Kingdom
21	UK65	Oil	United Kingdom
22	UK80	Oil	United Kingdom
23	UK34	Oil	United Kingdom
24	UK11	Oil	United Kingdom
25	UK01	Oil	United Kingdom
26	UK05	Oil	United Kingdom
27	ME12	Oil	Middle East
28	UKV	Oil	United Kingdom
29	ME77	Oil	Middle East
30	ME39	Oil	Middle East
31	ME43	Oil	Middle East
32	SN1	Oil	Serbia
33	SN2	Oil	Serbia
34	NA72	Oil	North America
35	NA73	Oil	North America
36	NA74	Oil	North America
37	NA75	Oil	North America
38	NA79	Oil	North America
39	NA61	Oil	North America
40	NA76	Oil	North America
41	NAC	Oil	North America
42	CA3	Coal	North Sea, UK
43	CA4	Coal	North Sea, UK
44	CA6	Coal	North Sea, UK

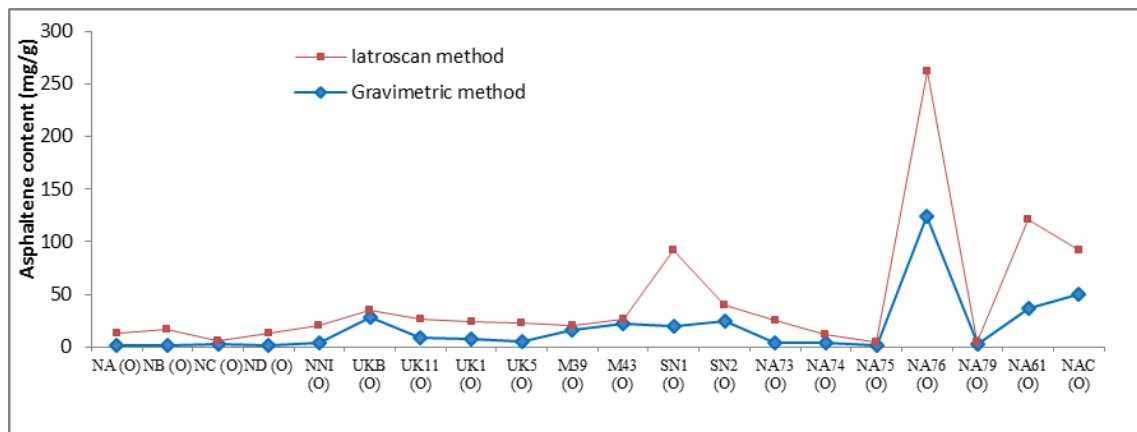
Appendix 2.0: Monitored ions (*m/z*) in selected ion and full scan modes

Aliphatic HC	Aromatic HC	AMFAMES 2	AMFAMESIM
Fatty acid methyl esters			
83	85	74	74
85	91	77	77
91	105	88	88
97	112	91	98
98	118	98	191
123	119	102	217
142	125	105	275
163	128	116	289
177	133	130	303
183	134	163	470
191	142	177	484
193	148	191	498
205	154	205	
215	156	217	
217	162	221	
218	166	231	
219	168	235	
231	170	245	
233	176	249	
245	178	260	
253	180	263	
257	182	275	
259	184	276	
260	189	277	
271	190	279	
274	191	289	
318	192	291	
330	198	303	
365	202	305	
367	204	319	
386	206	337	
412	212	395	
	219	430	
	220	444	
	228	458	
	230	470	
	231	472	
	233	484	
	234	498	
	242	512	
	244		
	245		
	248		
	252		
	253		
	267		
	546		

Appendix 3.0: Selected biomarker data for principal components analysis for the oils and coals

Sample	Pr/Ph	Pr/nC17	Ph/nC18	CPI	Preg	0S(20S+20R)S(20S+20R)	C27aaa	C28aaa	C29aaa	MPI-1	MPI-2	DBT/PHEN	Ts/(Ts+Tm)	29Ts/29Tm	HomoHop	Hop(35/34)	Hop32(S/R)	
						C29aaa	C29 $\alpha\beta$											
NA1(O)	4.59	0.92	0.22	1.13	7.01	0.28	0.44	14.05	20.90	65.05	0.61	0.62	0.12	0.40	0.15	0.29	0.40	0.58
NB2(O)	4.38	1.14	0.29	0.95	8.94	0.30	0.50	17.15	21.12	61.73	0.82	0.81	0.11	0.43	0.16	0.30	0.41	0.58
NC3(O)	4.29	1.00	0.26	1.12	8.58	0.28	0.53	19.33	22.37	58.31	0.75	0.75	0.11	0.42	0.15	0.29	0.37	0.58
NA(O)	1.02	1.57	0.97	nd	12.89	0.36	0.54	30.98	26.45	42.58	0.77	0.87	0.09	0.49	0.29	0.40	0.43	0.56
NB(O)	nd	nd	nd	nd	11.00	0.35	0.48	29.94	26.12	43.95	0.79	0.79	0.07	0.50	0.27	0.42	0.39	0.58
NC(O)	nd	nd	nd	nd	14.51	0.43	0.51	29.52	27.77	42.71	0.93	0.93	0.10	0.50	0.34	0.41	0.49	0.57
ND(O)	2.36	0.81	0.39	1.16	13.84	0.33	0.46	27.16	26.13	46.71	0.93	0.96	0.12	0.46	0.23	0.36	0.40	0.57
NE(O)	2.52	0.44	0.19	1.09	9.98	0.33	0.43	25.75	23.80	50.44	0.81	0.81	0.13	0.47	0.16	0.34	0.40	0.58
NF(O)	2.18	0.46	0.24	0.78	9.02	0.31	0.41	29.11	25.07	45.82	0.84	0.84	0.12	0.43	0.16	0.34	0.37	0.57
NO(O)	1.32	8.47	25.55	nd	19.59	0.55	0.42	46.51	14.86	38.63	0.61	0.66	0.04	0.56	0.32	0.62	0.55	0.57
NN(O)	2.35	2.92	1.40	nd	15.20	0.37	0.36	40.19	22.90	36.92	1.00	1.01	0.07	0.44	0.22	0.31	0.44	0.60
N25(O)	2.01	13.14	6.31	nd	11.69	0.36	0.39	32.26	26.11	41.63	0.76	0.69	0.02	0.42	0.17	0.34	0.42	0.56
N18(O)	1.96	27.89	11.79	nd	12.97	0.37	0.41	29.93	29.69	40.38	0.79	0.69	0.01	0.42	0.15	0.35	0.41	0.57
NNI(O)	2.84	3.32	1.41	nd	11.87	0.38	0.41	31.44	27.53	41.02	0.97	0.97	0.11	0.41	0.18	0.35	0.41	0.58
NN41(O)	2.13	5.60	2.35	1.04	12.64	0.35	0.38	31.16	29.20	39.64	0.82	0.77	0.03	0.39	0.03	0.32	0.37	0.58
UKB(O)	1.11	13.08	28.85	nd	17.20	0.55	0.46	47.53	16.13	36.33	0.64	0.65	0.03	0.57	0.29	0.61	0.56	0.58
UK88(O)	1.10	0.52	0.57	0.95	18.24	0.50	0.50	34.12	24.83	41.05	0.47	0.48	0.47	0.53	0.28	0.60	0.55	0.60
UK85(O)	1.58	0.96	0.70	1.05	8.59	0.47	0.43	29.49	24.95	45.57	0.23	0.25	nd	0.86	0.22	0.56	0.48	0.62
UK66(O)	1.25	0.42	0.39	0.99	22.69	0.52	0.46	56.05	17.10	26.85	nd	nd	nd	0.67	0.35	0.57	0.48	0.58
UK65(O)	1.27	0.50	0.47	1.00	20.11	0.54	0.50	46.73	18.94	34.33	0.11	0.15	nd	0.50	0.53	0.56	0.35	0.57
UK80(O)	nd	nd	nd	nd	18.97	0.53	0.46	45.18	22.05	32.76	nd	nd	nd	0.66	0.82	0.70	0.56	0.58
UK34(O)	1.33	0.82	0.68	1.06	23.00	0.51	0.48	47.53	18.45	34.01	nd	nd	nd	0.51	0.40	0.57	0.58	0.62
UK11(O)	0.76	0.24	0.37	0.97	15.24	0.52	0.45	47.58	16.73	35.69	0.43	0.44	0.97	0.60	0.30	0.64	0.55	0.56
UK01(O)	0.78	0.31	0.45	0.93	18.47	0.57	0.48	48.06	18.65	33.29	0.38	0.37	1.21	0.73	0.49	0.69	0.61	0.58
UK05(O)	0.72	0.30	0.46	0.94	21.78	0.55	0.49	50.65	16.36	32.99	0.40	0.40	1.24	0.76	0.51	0.70	0.51	0.58
UKV(O)	nd	nd	nd	nd	18.22	0.56	0.45	49.16	19.21	31.62	0.59	0.62	0.03	0.56	0.36	0.53	0.38	0.58
NA72(O)	0.95	1.09	1.34	nd	20.20	0.50	0.44	36.64	23.91	39.45	0.68	0.70	0.94	0.42	0.14	0.52	0.51	0.59
NA73(O)	7.76	0.75	0.12	1.01	20.23	0.52	0.45	32.79	25.03	42.17	0.64	0.65	0.85	0.43	0.15	0.54	0.57	0.59
NA74(O)	1.10	0.46	0.52	1.00	20.14	0.51	0.44	29.34	26.12	44.54	0.64	0.65	0.87	0.44	0.14	0.49	0.50	0.59
NA75(O)	1.01	1.18	1.54	nd	20.25	0.52	0.45	32.71	23.05	44.24	0.65	0.69	0.90	0.43	0.15	0.53	0.67	0.59
NA79(O)	1.24	1.39	1.62	nd	22.67	0.54	0.47	32.82	25.61	41.58	nd	nd	nd	0.36	0.13	0.63	0.52	0.61
NA61(O)	1.02	0.43	0.52	nd	17.16	0.52	0.41	34.96	25.62	39.43	0.57	0.57	1.45	0.31	0.11	0.53	0.58	0.61
NA76(O)	1.05	0.44	0.52	1.16	19.33	0.53	0.47	35.78	24.42	39.80	0.60	0.62	0.98	0.29	0.04	0.49	0.53	0.93
NAC(O)	0.35	1.91	0.25	nd	29.03	0.46	0.36	44.49	16.02	39.49	0.64	0.63	0.04	0.21	0.18	0.50	0.58	0.59
ME77(O)	0.54	0.2	0.42	1.08	29.59	0.52	0.44	47.19	16.56	36.26	0.58	0.65	1.00	0.20	0.07	0.44	0.57	0.60
ME39(O)	0.76	0.18	0.26	0.97	28.55	0.54	0.50	52.82	8.34	38.85	0.57	0.67	1.16	0.91	0.60	0.61	0.55	0.59
ME43(O)	0.72	0.23	0.36	1.01	12.84	0.53	0.45	37.10	12.04	50.87	0.51	0.56	0.93	0.55	0.22	0.64	0.49	0.59
ME12(O)	0.89	0.66	1.74	1.04	7.25	0.53	0.51	50.82	16.76	32.42	0.14	0.24	nd	0.59	0.37	0.53	0.47	0.65
SN1(O)	1.51	3.04	2.34	nd	5.01	0.44	0.60	24.44	22.16	53.40	0.08	0.11	0.04	0.50	0.19	0.37	0.39	0.59
SN2(O)	1.44	0.56	0.41	1.47	16.82	0.47	0.58	31.64	31.05	37.31	0.51	0.53	0.11	0.46	0.21	0.53	0.41	0.59
CA3(C)	2.44	0.53	0.27	nd	23.72	0.35	0.43	30.79	19.70	49.51	0.65	0.70	0.01	0.37	0.20	0.45	0.35	0.58
CA4(C)	4.36	0.74	0.20	1.01	6.99	0.38	0.47	40.98	14.15	44.87	0.52	0.56	0.01	0.06	0.04	0.46	0.33	0.60
CA6(C)	2.48	0.64	0.33	nd	22.55	0.39	0.36	38.28	17.47	44.25	0.60	0.64	0.05	0.27	0.19	0.43	0.44	0.56

Appendix 4.0: Comparison of weight of asphaltene content (mg/g) recovered from Iatroscan and gravimetric methods.



Appendix 5.0: Calculated contents in mg/g of the asphaltene fraction recovered from gravimetric procedure of the oils as mean \pm one standard error.

Sample	Location	GRAVIMETRIC		IATROSCAN	
		(mg/g)	SD	(mg/g)	SD
NA (O)	Nigeria	1.65	\pm 0.24	11.72	\pm 0.14
NB (O)	Nigeria	1.11	\pm 0.49	15.62	\pm 0.17
NC (O)	Nigeria	2.53	\pm 1.44	3.21	\pm 0.25
ND (O)	Nigeria	1.9	\pm 0.96	11.58	\pm 0.55
UKB (O)	United Kingdom	28.72	\pm 0.12	6.26	\pm 0.11
UK11 (O)	United Kingdom	8.21	\pm 3.78	17.68	\pm 0.23
UK 01 (O)	United Kingdom	7.03	\pm 0.11	16.8	\pm 0.91
UK 05 (O)	United Kingdom	5.44	\pm 0.46	17.01	\pm 0.54
ME39 (O)	Middle East	16.05	\pm 3.11	4.70	\pm 0.37
ME43 (O)	Middle East	22.21	\pm 0.53	3.92	\pm 0.10
SN1 (O)	Serbia	20.05	\pm 9.19	71.53	\pm 0.60
SN2 (O)	Serbia	24.34	\pm 9.74	15.94	\pm 0.21
NA73 (O)	North America	4.19	\pm 1.98	21.41	\pm 1.02
NA74 (O)	North America	4.07	\pm 1.36	7.67	\pm 0.77
NA75 (O)	North America	1.73	\pm 1.19	2.64	\pm 0.07
NA76 (O)	North America	124.36	\pm 0.57	137.16	\pm 1.40
NA79 (O)	North America	2.79	\pm 0.14	2.09	\pm 1.40
NA61 (O)	North America	36.34	\pm 12.45	84.50	\pm 0.77
NAC (O)	North America	50.16	\pm 0.16	41.65	\pm 0.82